PREDICTION OF CHILLING TIMES OF FOODS

A thesis presented in partial fulfilment of the requirement
for the degree of Doctor of Philosophy in Process
and Environmental Technology at
Massey University

ZHANG LIN, B.E. (Tsinghua)

ABSTRACT

Chilling is one of the most important branches of food preservation under low temperature as it retains, more closely than any other means, the "fresh" quality and appearance of the food. No simple method to predict chilling times for a wide range of geometric shapes without major disadvantages was found in the literature. Investigation via a set of test problems showed that for each available method, there were ranges of conditions under which accuracy of prediction reduced significantly. This justified development and testing of a new method. A theoretical and experimental study of methods for predicting the chilling times of both regularly and irregularly shaped foods was carried out.

Using the sphere as a reference shape and based on the first term of the series analytical solution, empirical mathematical expressions for extending the existing concept of equivalent heat transfer dimensionality E to take account of the effect of geometry on unsteady state heat conduction processes, which has been successfully applied in freezing time prediction, were derived. These cover a wide range of heat transfer environmental conditions and multi-dimensional regular and irregular geometries. Empirical formulae for the lag factor, L, as a function of object geometric shape were also developed for the thermal centre and mass-average temperatures.

Guidelines to define object geometry for irregular shapes were established. The recommended dimensional measurement approach uses actual measurements of the three dimensions of an irregular geometry to define the dimensional ratios for an equivalent ellipsoid. The neglect of sharp protrusions and of hollows in taking measurements is recommended.

Experimental chilling data for foods found in the literature, were limited in usefulness for model testing because the experimental conditions were usually not sufficiently accurately measured, described or controlled. Therefore, a comprehensive set of 3879 analytical solution simulations, 351 finite element method procedures and 165 experiments of chilling processes were made over a wide range of conditions. The chilling experiments were carried out using sixteen different two- and three-dimensional irregularly shaped objects made of Tylose, a food analogue, or of Cheddar cheese. Experiments for bricks of Cheddar cheese with uniformly distributed voids were also conducted because of the scarcity of published experimental data for chilling of products with voids.

For regular geometries (short cylinder, squat cylinder, infinite rectangular rod, rectangular brick, oblate and prolate spheroids), and across a wide range of conditions and product shape ratios the methodology predicted chilling times to within -7.6 to 5.6% of the theoretical solutions for the thermal centre position and ±9.4% for the mass-average condition. For many commonly encountered conditions the lack of fit was considered acceptably low when likely data uncertainties are taken into account.

When the guidelines for defining an equivalent ellipsoid and the simple method were tested, the 95% confidence interval of the percentage difference comparing predictions with the experimentally measured chilling times for thermal centre temperatures of two-dimensional irregular geometries was -3.1 to 14.4%. For three-dimensional irregular geometries, the equivalent interval was -6.4 to 11.6%. No experimental testing of predicted mass-average temperatures was carried out. The simple prediction method failed to match the experimental data in a similar manner to the finite element method. Lack of fit was probably more due to experimental error than errors in the form of geometric approximation and the prediction method itself.

In situations where the product contains significant uniformly distributed voids, either the simple empirical prediction method or any relevant analytical solution can be applied if an "equivalent thermal conductivity" is defined. Keey's method, with a distribution factor dependent on voidage fraction, is recommended for calculating the equivalent thermal conductivity on the basis of best fit to experimental data but ranges of applicability require further investigation. It could not be established whether natural convection in the voids was a significant enhancer of the cooling rate.

In many industrial applications, data such as heat transfer coefficients and thermal properties are difficult to estimate, and non-uniformity of chilling conditions is difficult to avoid. The overall accuracy of predictions in such applications is unlikely to be significantly increased through further reduction in the inherent inaccuracy of the proposed methodologies. The methodologies are therefore suitable for routine industrial use.

ACKNOWLEDGEMENTS

The author would like to acknowledge the following persons for advice and assistance during the course of this project:

Professor Andrew C. Cleland, Department of Food Technology, Massey University, Chief Supervisor;

Associate Professor Donald J. Cleland, Department of Process and Environmental Technology, Massey University, Supervisor;

Dr. George F. Serrallach, Department of Process and Environmental Technology, Massey University, Supervisor.

The author would like to acknowledge the following persons for technical assistance during the experimental phase of the project:

Mr. John Alger, Mr. Wayne Mallett, Mr. Don McLean and Mr. Bruce Collins, Department of Process and Environmental Technology, Massey University;

Mr. Byron McKillop, Department of Food Technology, Massey University.

The author would like to thank family and friends for their continual support and helpfulness.

The author would also like to thank Huiting for her moral support and for proof reading.

TABLE OF CONTENTS

ABSTRACT ii

ACKNOWLEDGEMENTS iv

TABLE OF CONTENTS v

LIST OF FIGURES ix

LIST OF TABLES xiv

1 INTRODUCTION 1

2. LITERATURE REVIEW 2

2.1 Problem Definition and Formulation 2

2.1.1 Unsteady State Heat Conduction 2

2.1.2 Boundary Conditions 4

2.1.3 Initial Conditions 6

2.2 Solutions for Problems Involving Chilling Time Prediction 7

2.2.1 Solutions for Problems with a Convection-Only Heat Transfer Environment 7

2.2.1.1 Analytical Solutions 7

2.2.1.2 Numerical Solutions 10

2.2.1.3 Empirical Solutions 15

2.2.1.4 Solutions for Problems in a Time-Varying, Convection only Heat Transfer Environment 22

2.2.2 Solutions for Problems with Simultaneous Convection and Evaporation .. 23

2.2.2.1 Numerical Solutions 23

2.2.2.2 Empirical Solutions 26

2.3 Published Data Suitable for Testing Methodologies 28

2.3.1 Thermal Properties 30

2.3.2 Heat Transfer Coefficients 30

3. PRELIMINARY CONSIDERATIONS 31

4. DEVELOPMENT OF A NEW GENERAL EMPIRICAL METHOD 33

4.1 Introduction 33

4.2 Proposed Form of the New Method 33

4.3 Geometric Definitions 36

4.4 Creation of Database for the Regular Geometries 38

4.5 Formulation of the Equivalent Heat Transfer Dimensionality, and the Lag Factors for the Thermal Centre and the Mass-Average Temperatures 40

4.5.1 Formulation of the Equivalent Heat Transfer Dimensionality, Denoted E . 40

4.5.1.1 Formulation of the Equivalent Heat Transfer Dimensionality at $Bi = 0$ 40

4.5.1.2 Formulation of the Equivalent Heat Transfer Dimensionality for $Bi \rightarrow \infty$ 41

4.5.1.3 Formulation of the Equivalent Heat Transfer Dimensionality at any Biot number 45

4.5.2 Formulation of the Lag Factor for the Thermal Centre, Denoted L_c 46

4.5.2.1 Formulation of the Lag Factor at $Bi = 0$, Denoted L_0 47

4.5.2.2 Formulation of the Lag Factor at $Bi \rightarrow \infty$, Denoted L_∞ 47

4.5.2.3 Formulation of the Lag Factor at any Biot Number 47

4.5.3 Formulation of the Lag Factor for the Mass-Average Temperature, Denoted L_m 48

4.6 Testing the New Formulae for Regular Shapes 49

4.7 Comparison with Existing Chilling Time Prediction Methods 49

4.8 Summary of the Proposed Method 51

5. EXPERIMENTAL PROCEDURE AND DATA COLLECTION 55

5.1 The Equipment 55

5.2 Experimental Error 56

5.3 Choice of Chilling Material 57

5.4 Temperature Measurement and Control 59

5.5 Chilling of Two-Dimensional Irregular Shapes 60

5.5.1 The Test Samples 60
5.5.2 Dimension Measurement and Control 61
5.5.3 Measurement and Control of Surface Heat Transfer Coefficients 62
5.5.4 Analysis of Heat Transfer in Two-Dimensional Irregular Shapes 64
5.6 Chilling of Three-Dimensional Irregular Shapes 66
5.6.1 The Test Samples 66
5.6.2 Dimension Measurement and Control 68
5.6.3 Measurement and Control of Surface Heat Transfer Coefficients 68
5.6.4 Analysis of Heat Transfer in Three-Dimensional Irregular Shapes 69
5.6.5 Summary 70

6. EXPERIMENTAL DESIGN AND RESULTS 83
6.1 Treatment of the Effect of Geometry 84
6.2 Chilling of Two-Dimensional Irregular Shapes 87
6.3 Chilling of Three-Dimensional Irregular Shapes 91
6.4 Prediction of Chilling Times for Two-Dimensional Irregular Shapes by the Proposed Method 93
6.5 Prediction of Chilling Times for Three-Dimensional Irregular Shapes by the Proposed Method 94
6.6 Discussion and Conclusions 95

7. CHILLING OF OBJECTS WITH UNIFORMLY DISTRIBUTED VOIDS 116
7.1 Introduction 116
7.2 Variables Considered Important 116
7.3 Approach Undertaken 116
7.4 Experimental Methods 117
7.4.1 The Test Samples 117
7.4.2 Dimension Measurement and Control 118
7.4.3 Measurement and Control of Surface Heat Transfer Coefficients 118
7.4.4 Analysis of Heat Transfer in Rectangular Bricks with Uniformly Distributed Voids 119
7.5 Experimental Design 120

8. PREDICTION METHODS TO ACCOUNT FOR UNIFORMLY DISTRIBUTED VOIDS 127

8.1 Introduction 127

8.2 Determination of the Equivalent Thermal Conductivity from the Experimental Data 127

8.3 Existing Equivalent Thermal Conductivity Models 129

8.4 Results from Application 133

8.5 Summary 137

9 CONCLUSIONS 152

NOMENCLATURE 154

REFERENCES 155

APPENDIX A: MANUAL OF A GENERALLY APPLICABLE METHOD FOR CHILLING TIME PREDICTION A-1

APPENDIX B: CHILLING TIME PREDICTION PROGRAMME . . . . . DISKETTE I & II

APPENDIX C: CHILLING TIME ANALYTICAL SOLUTION PROGRAMME . . . . . DISKETTE II

LIST OF FIGURES

Figure 4.1 Plot of ln Y vs Fo during a chilling process 34

Figure 4.2 Plot of error arising from use of eqn. (4.30) vs log (β_1) for an infinite rectangular rod 44

Figure 4.3. Plot of L_c vs log (β_1) for an infinite rectangular rod 46

Figure 5.1 Schematic diagram of the air environmental tunnel 75

Figure 5.2 Schematic diagram of the brine immersion tank 75

Figure 5.3 The sample rotator used in the brine immersion tank 76

Figure 5.4 The sample oscillator and the two-dimensional irregularly shaped sample I_c used in the air environmental tunnel 76

Figure 5.5 The sample oscillator and the three-dimensional irregularly shaped sample I_t used in the air tunnel 77

Figure 5.6 Cross-section and finite element method grid for the two-dimensional irregularly shaped sample E_a 77

Figure 5.7 Cross-section and finite element method grid for the two-dimensional irregularly shaped sample E_b 78

Figure 5.8 Cross-section and finite element method grid for the two-dimensional irregularly shaped sample E_c 78

Figure 5.9 Cross-section and finite element method grid for the two-dimensional irregularly shaped sample E_d 79

Figure 5.10 Cross-section and finite element method grid for the two-dimensional irregularly shaped sample I_a 79

Figure 5.11 Cross-section and finite element method grid for the two-dimensional irregularly shaped sample I_b 80

Figure 5.12 Cross-section and finite element method grid for the two-dimensional irregularly shaped sample I_c 80

Figure 5.13 Schematic diagram showing the arrangement of the polystyrene foam caps for two-dimensional samples 81

Figure 5.14 Schematic diagram showing the method of thermocouple insertion and position within the moulded multi-dimensional samples (not to scale)81

Figure 5.15 The three-dimensional irregularly shaped samples 82

Figure 5.16 Schematic diagram of box corner types 82

Figure 6.1 Temperature/time profile for chilling of the Tylose two-dimensional irregular shape E_a during Run E_a1 97

Figure 6.2 Temperature/time profile for chilling of the Tylose two-dimensional irregular shape E_b during Run E_b5 97

Figure 6.3 Temperature/time profile for chilling of the Tylose two-dimensional irregular shape E_c during Run E_c1 98

Figure 6.4 Temperature/time profile for chilling of the Tylose two-dimensional irregular shape E_d during Run E_d7 98

Figure 6.5 Temperature/time profile for chilling of the Tylose two-dimensional irregular shape I_a during Run I_a5 99

Figure 6.6 Temperature/time profile for chilling of the Tylose two-dimensional irregular shape I_b during Run I_b2 99

Figure 6.7 Temperature/time profile for chilling of the Tylose two-dimensional irregular shape I_c during Run I_c3 100

Figure 6.8 Plot of M_{exp} versus M_{FEM} for Tylose two-dimensional irregular shapes 100

Figure 6.9 Plot of $L_{c\ exp}$ versus $L_{c\ FEM}$ for Tylose two-dimensional irregular shapes 101

Figure 6.10 Errors arising from displacement of the thermocouple from the thermal centre 101

Figure 6.11 Temperature/time profile for chilling of the Tylose three-dimensional irregular shape I_p during Run I_p3 102

Figure 6.12 Temperature/time profile for chilling of the Tylose three-dimensional irregular shape I_q during Run I_q1 102

Figure 6.13 Temperature/time profile for chilling of the Tylose three-dimensional irregular shape I_r during Run I_r1 103

Figure 6.14 Temperature/time profile for chilling of the Tylose three-dimensional irregular shape I_s during Run I_s3 103

Figure 6.15 Temperature/time profile for chilling of the Tylose three-dimensional irregular shape I_t during Run I_t1 104

Figure 6.16 Temperature/time profile for chilling of the Tylose three-dimensional irregular shape S_a during Run S_a3 104

Figure 6.17 Temperature/time profile for chilling of the Tylose three-dimensional irregular shape S_b during Run S_b1 105

Figure 6.18 Temperature/time profile for chilling of the Tylose three-dimensional irregular shape S_c during Run S_c1 105

Figure 6.19 Temperature/time profile for chilling of the Tylose three-dimensional irregular shape S_d during Run S_d1 106

Figure 6.20 Examples of measurement of object geometry 106

Figure 8.1 Data analysis procedure used to find k_e and $L_{c\ model}$ 128

Figure 8.2 Plot of f, the distribution factor in Keey's method determined from experimental k_e data vs Bi 144

Figure 8.3 Normal probability plot to determine data outliers for the approach of Keey (1) 144

Figure 8.4 Normal probability plot to determine data outliers for the approach of Keey (2) 145

Figure 8.5 Normal probability plot to determine data outliers for the approach of Keey (3) 145

Figure 8.6 Plot of mean differences between the predictions of Keey (1) and the experimental data for k_e versus ratio of ($L_{c\ exp}$ / $L_{c\ model}$) 146

Figure 8.7 Plot of mean differences between the predictions of Keey (2) and the experimental data for k_e versus ratio of ($L_{c\ exp}$ / $L_{c\ model}$) 146

Figure 8.8 Plot of mean differences between the predictions of Keey (3) and the experimental data for k_e versus ratio of ($L_{c\ exp}$ / $L_{c\ model}$) 147

Figure 8.9 Plot of differences between the predictions of k_e by the Keey (1) approach and experimental k_e values versus Biot number 147

Figure 8.10 Plot of differences between the predictions of k_e by the Keey (2) approach and experimental k_e values versus Biot number 148

Figure 8.11 Plot of differences between the predictions of k_e by the Keey (3) approach and experimental k_e values versus Biot number 148

Figure 8.12 Plot of differences between the predictions of k_e by the Keey (1) approach and experimental k_e values versus voidage fraction 149

Figure 8.13 Plot of differences between the predictions of k_e by the Keey (2) approach and experimental k_e values versus voidage fraction 149

Figure 8.14 Plot of differences between the predictions of k_e by the Keey (3) approach and experimental k_e values versus voidage fraction 150

Figure 8.15 Plot of differences between the predictions of k_e by the Keey (2) approach and experimental k_e values versus box size 150

Figure 8.16 Plot of differences between the predictions of k_e by the Keey (2) approach and experimental k_e values versus particle size 151

Figure 8.17 Plot of differences between the predictions of k_e by the Keey (2) approach and experimental k_e values versus particle size/box size 151

LIST OF TABLES

Table 4.1 Values of geometric parameters P_1 P_2 and P_3 45

Table 4.2 Values of geometric parameters γ_1, γ_2 and λ 48

Table 4.3 Percentage errors in predicted chilling times to selected thermal centre temperatures ($1 \leq \beta \leq 4$, $0.1 \leq Bi \leq 10$, $0.05 \leq Y_c \leq 0.55$) 50

Table 4.4 Percentage errors in predicted chilling times to selected mass-average temperatures. ($1 \leq \beta \leq 4$, $0.1 \leq Bi \leq 10$, Y_m corresponding to $0.05 \leq Y_c \leq 0.55$) 50

Table 4.5 Percentage Differences in Predicted Times for Different Empirical Methods Against Analytical (*) or Numerical (°) Solutions 54

Table 5.1 Thermal Properties of Chilling Test Materials 59

Table 5.2 Experimental Conditions for Cylinders 71

Table 5.3 Experimental Conditions for Tylose Bricks 74

Table 5.4 Experimental Data for Cheddar Cheese Bricks 74

Table 6.1 Geometric Parameters of Two-Dimensional Samples 107

Table 6.2 Geometric Parameters of Three-Dimensional Samples 107

Table 6.3 Experimental Data and Finite Element Predictions for Chilling of Two-Dimensional Irregular Shapes 108

Table 6.4 Percentage Differences Between Experimental and Calculated Chilling Times for Two-Dimensional Irregular Shapes (Cumulative Results for Y_c = 0.50, 0.25, 0.10) 110

Table 6.5 Percentage Differences Between Experimental and Calculated Chilling Times for Two-Dimensional Irregular Shapes when Y_c = 0.50 110

Table 6.6 Percentage Differences Between Experimental and Calculated Chilling Times for Two-Dimensional Irregular Shapes when Y_c = 0.25 111

Table 6.7 Percentage Differences Between Experimental and Calculated Chilling Times for Two-Dimensional Irregular Shapes when Y_c = 0.10 111

Table 6.8 Comparison of Percentage Errors in Predicted Times by Different Methods for Shape I_c with and without Excision of Protrusions 112

Table 6.9 Correlations in Percentage Errors Between Finite Element Calculations and Other Approaches for Two-Dimensional Irregular Shapes 112

Table 6.10 Experimental Data for Chilling of Three-Dimensional Irregular Shapes 113

Table 6.11 Mean Percentage Differences in Analytically Predicted Chilling Time for the Equivalent Brick Model for Shape I_p Using the Conservation of Area-Volume Approach 113

Table 6.12 Summary of Percentage Differences Between Experimental and Proposed Method Predicted Chilling Times for Two-Dimensional Irregular Shapes 114

Table 6.13 Percentage Differences Between Experimental Results and Chilling Times Predicted by the Proposed Method for Three-Dimensional Shapes 115

Table 7.1 Geometric Measurements of the Rectangular Bricks Used in Voidage Experiments 122

Table 7.2 Correlation Coefficients Between Variables Used in Voidage Experiments 122

Table 7.3 Experimental Data for the Cheddar Cheese Bricks with Uniformly Distributed Voids 123

Table 8.1 Percentage Error in Predicted Thermal Conductivities for Objects with Uniformly Distributed Voids Using Various Approaches 138

Table 8.2 Curve-fit Coefficients Used in Eqn (8.24) for the Different Versions of Keey's Method 143

1. INTRODUCTION

Although there is a wide variety of means for food preservation, low temperature is one of the most important. Further, chilling is one of the most important branches of food preservation under low temperature as it retains, more closely than any other means, the "fresh" quality and appearance of the food. This is especially true for many New Zealand food industries, particularly the horticultural industry which is heavily dependent on export of chilled produce to distant markets. On one hand, rapid chilling under carefully controlled conditions usually helps minimise both quality loss (due mainly to respiration processes) and product weight loss, (which not only constitutes a direct loss in revenues when the produce is sold, also contributes to quality loss). On the other hand, accurate chiller design, which depends on a reliable method for chilling time prediction, will reduce the costs to New Zealand of producing chilled food for export, and hence the benefit from selling such produce overseas will increase.

Because of the importance of food chilling there has been considerable amount of research into the changes in physical, chemical and biological properties that occur in the process, and how the changes affect the organoleptic appeal of the food. The major emphasis in this field of research has been on finding a set of chilling conditions that minimises damage to the food product. Another important area of the research is gathering of data for the design of chilling equipment.

If accurate prediction of chilling under a wide range of conditions and geometries can be achieved by a simple method, and the method could be easily applied by industrial practitioners, more accurate design of chilling equipment for foodstuff could result. Therefore the present research into prediction of chilling times by simple methods and the effect of product shape on chilling rate is justified.

2. LITERATURE REVIEW

This chapter consists of two parts: a physical description of chilling leading to a mathematical formulation, and a review of attempts to derive prediction methods for chilling times.

2.1 Problem Definition and Formulation

In practical processes for chilling solids, there are four main modes of heat transfer. Within the object the only mode usually assumed to occur is heat conduction; and on the surface of the object there may be one or more of convection, radiation and evaporation.

The product may be irregular in shape, or in some cases it approximates a simple, regular geometrical shape. It may be homogeneous in composition, but more often it is not. There may be air or gas voids within the product in which convection occurs, and there can be substantial variations between supposedly similar product items. All these factors make prediction of the temperature/time history in an object undergoing chilling difficult. Therefore the only practical approach is to make simplifying assumptions (Gaffney *et al.* 1985, Cleland 1990).

2.1.1 Unsteady State Heat Conduction

The first assumption that is almost invariably made is that heat transfer internal to the product is only by conduction. If voids are present, their effect on the heat transfer is then expressed in heat conduction terms as "effective" thermal properties such as thermal conductivity, density and specific heat capacity. Therefore the problem of predicting the time for a material to be chilled to a certain temperature under a given set of conditions is classed physically as heat conduction. This situation is described by the partial differential equation of heat conduction, subject to boundary conditions and initial conditions according to the particular circumstances:

$$\rho(T)\,c(T)\frac{\partial T}{\partial t} = \frac{\partial}{\partial x}\left[k(T)\frac{\partial T}{\partial x}\right] + \frac{\partial}{\partial y}\left[k(T)\frac{\partial T}{\partial y}\right] + \frac{\partial}{\partial z}\left[k(T)\frac{\partial T}{\partial z}\right] + Q \qquad (2.1)$$

where T = temperature (°C)

t = time (s)

k = thermal conductivity (W $m^{-1}K^{-1}$)

ρ = density (kg m^{-3})

c = specific heat capacity (J $kg^{-1}K^{-1}$)

x = displacement in x coordinate (m)

y = displacement in y coordinate (m)

z = displacement in z coordinate (m)

Q = internal heat generation (W)

In common chilling processes, the major form of internal heat generation is often respiration within fruit and vegetables. However, there are few industrial situations in which the heat of respiration significantly slows the chilling process (Gaffney *et al.* 1985). The thermal properties of agricultural and horticultural produce generally do not vary significantly in the temperature range important for chilling so the small variations in properties can usually be adequately managed by using mean values. Since heterogeneity can only be effectively handled by numerical methods, it is common for foodstuff to be assumed to be homogeneous. Therefore, $\rho(T)$, $k(T)$ and $c(T)$ are usually treated as constants. The simplified formulation of eqn (2.1) can then be written as:

$$\frac{\partial T}{\partial t} = \frac{k}{\rho c}\left[\frac{\partial^2 T}{\partial x^2} + \frac{\partial^2 T}{\partial y^2} + \frac{\partial^2 T}{\partial z^2}\right] + \frac{Q}{\rho c} \qquad (2.2)$$

For a sphere or infinite cylinder it is more common to use the polar coordinates to describe the heat conduction process in one direction and this description can also be extended to the infinite slab:

$$r^{(N-1)}\rho\, c\frac{\partial T}{\partial t} = \frac{\partial}{\partial r}\left[r^{(N-1)}k\frac{\partial T}{\partial r}\right] + r^{(N-1)}Q \qquad (2.3)$$

where N = number of dimension of an object (N = 1 for an infinite slab, N = 2 for an infinite cylinder, and N = 3 for a sphere)

r = displacement along the radius from the object centre (m)

Other important cases involving regular geometry are the finite cylinder, infinite rectangular rod and rectangular brick shapes. Eqn (2.1) to (2.3) can only apply in a defined physical region. Because of the difficulty in describing the shapes, formulations for irregular shapes are very difficult to derive in precise mathematical expressions.

2.1.2 Boundary Conditions

There are traditionally differentiated five kinds of boundary condition of importance in heat transfer problems that apply at the surface of a solid object, usually called the first, second, third and fourth kinds of boundary condition and the symmetry boundary condition. The first kind of boundary condition is also known as a defined surface temperature:

$$T_s = T_a \quad \text{for} \quad t > 0 \tag{2.4}$$

where T_s = surface temperature (°C)

T_a = ambient medium temperature (°C)

The second kind of boundary condition is a fixed rate of heat flow to the surface. For the case of a planar boundary at $x = 0$, this becomes:

$$\phi = -kA\left[\frac{\partial T}{\partial x}\right]_{x=0} \tag{2.5}$$

where A = surface area (m^2)

ϕ = heat flow to surface(W)

The third kind of boundary condition is where the heat transfer coefficient is a known function of position and time; this boundary condition is also known as the convection case and as Newton's law of cooling. For a surface at $x = 0$:

$$h(T_a - T_s) = -\left[k\frac{\partial T}{\partial x}\right]_{x=0} \quad \text{for } t > 0 \tag{2.6}$$

where h = surface heat transfer coefficient (W $m^{-2}K^{-1}$)

The fourth kind of boundary condition is where the surface temperature is an arbitrary function of time:

$$T_s = f(t) \qquad \text{for} \quad t > 0 \tag{2.7}$$

The symmetry boundary condition is the case that applies to either a perfectly insulated surface or to an axis of symmetry, for example:

$$\left[\frac{\partial T}{\partial x}\right]_{x=0} = 0 \tag{2.8}$$

The first kind of boundary condition can be treated as a special case of either the third kind (by setting $h = \infty$), or of the fourth kind (where $f(t) = T_a$). As there are always resistances to heat transfer, h is never infinite in practical problems. The symmetry case also can be regarded as a special case of the third kind (by setting $h = 0$). The second and fourth kinds have few practical applications so the third kind of boundary condition is by far the most important in chilling practice.

In situations in which convection is involved, both radiation and evaporation can also be significant. The boundary condition in these cases is defined by an extension of the third kind:

$$\phi = \phi_{conv} + \phi_{rad} + \phi_{evap} = -kA\left[\frac{\partial T}{\partial x}\right]_{x=0} \tag{2.9}$$

where ϕ = sum of heat flows to the surface (W)

The convection heat flow is defined by :

$$\phi_{conv} = h_{conv} A (T_a - T_s) \tag{2.10}$$

where h_{conv} = heat transfer coefficient for convection (W $m^{-2}K^{-1}$)

The radiation heat flow can be defined by:

$$\phi_{rad} = F_{12} A \sigma [(T_a + 273.15)^4 - (T_s + 273.15)^4] \tag{2.11}$$

where σ = Stefan-Boltzmann constant (W $m^{-2}K^{-4}$)

F_{12} = radiation view factor

or expressed in a practically-convenient pseudo-convection form as:

$$\phi_{rad} = h_{rad} A (T_a - T_s) \tag{2.12}$$

$$h_{rad} = F_{12} \sigma (T_a + T_s + 546.30)[(T_a + 273.15)^2 + (T_s + 273.15)^2] \tag{2.13}$$

In situations where simultaneous convection and radiation occur, and provided the air and radiation heat source or sink are at the same temperature (which is the case in some practical applications), eqn (2.6) can be applied by setting $h = (h_{conv} + h_{rad})$.

The evaporative heat transfer for use in eqn (2.9) is defined by :

$$\phi_{evap} = u A (p_a - p_s) l \tag{2.14}$$

where u = mass transfer coefficient (s m^{-1})

p_a = partial pressure of water vapour in the surrounding air (Pa)

p_s = partial pressure of water vapour in the boundary layer over the product surface (Pa)

l = latent heat of evaporation (J kg^{-1})

By using well-known relationships, the evaporative heat transfer is also defined by:

$$\phi_{evap} = k_g A (p_{wa} H_r - p_{ws} a_w) l \tag{2.15}$$

where p_{wa} = vapour pressure of water at the air temperature (Pa)

H_r = relative humidity of the surrounding air

p_{ws} = vapour pressure of water at the surface temperature (Pa)

a_w = water activity of the product surface

2.1.3 **Initial Conditions**

The initial condition for a chilling process defines the temperature distribution in the object prior to the start of the process. There are two cases:

(1) uniform initial condition:

$T = T_i$ at all places in the object at $t = 0$ (2.16)

(2) non-uniform initial condition :

$T = f(x,y,z)$ at $t = 0$ (2.17)

2.2 Solutions for Problems Involving Chilling Time Prediction

There are two main approaches towards developing chilling time prediction methods; one is to seek a method that applies to a specific kind of product with specified conditions, the other is to develop a versatile method that applies to objects of all shapes under normal heat transfer conditions. Because of the huge variety of such products and conditions which exist in industrial practice, there is little general benefit to be gained from the first approach. Most methods of interest found in literature belong to the second approach, and they can be further classified into three categories:

1. analytical solutions;
2. numerical solutions; and
3. empirical solutions.

Within these three categories, methods are further classified into three groups according to different assumptions about modes of heat transfer at the surface of the objects:

(i) convection, but no evaporation and radiation, occurs at the surfaces of the object;

(ii) both convection and radiation occur at the surface of the objects.

These divisions are used in the discussion of published chilling time prediction methods. Useful reviews which cover many prediction methods have been published by Gaffney *et al.* (1985), and more recently, Cleland (1990).

2.2.1 Solutions for Problems with a Convection-Only Heat Transfer Environment

2.2.1.1 Analytical Solutions

Almost all analytically derived methods are based on the hypothesis of homogeneous materials, constant thermal properties, constant ambient conditions and a uniform initial condition.

For regular shapes with the above assumptions, solutions are available for first and third kinds of boundary condition. The solution is a series that predicts the object temperature as a function of time. Reverse-calculation of chilling time to reach a certain temperature may have to be iterative if more than one term in the appropriate series solution is significant. The inherent prediction method uncertainty is zero if the hypothesis, on which the derivation is based, is met. Carslaw & Jaeger (1959) state the methods for the regular shapes including the infinite slab, infinite cylinder, sphere, infinite rectangular rod, rectangular brick and finite cylinder. Four dimensionless numbers are used:

$$Fo = \frac{k\,t}{\rho\,c\,R^2} \tag{2.18}$$

where Fo = Fourier number

$$Y = \frac{T - T_a}{T_i - T_a} \tag{2.19}$$

where Y = fractional unaccomplished temperature change for any position in the object;

$$Y_m = \frac{T_m - T_a}{T_i - T_a} \tag{2.20}$$

where Y_m = fractional unaccomplished temperature change based on mass average temperature

$$Bi = \frac{h\,R}{k} \tag{2.21}$$

where Bi = Biot number

The solutions for the infinite slab are:

$$Y = \sum_{i=1}^{\infty} \frac{2\,Bi\cos(\omega_i x/R)}{Bi(Bi+1)+\omega_i^2}\exp(-\omega_i^2 Fo) \tag{2.22}$$

$$Y_m = \sum_{i=1}^{\infty} \frac{2\,Bi^2}{\omega_i^2[Bi(Bi+1)+\omega_i^2]}\exp(-\omega_i^2 Fo) \tag{2.23}$$

where the values of ω are the roots of:

$$\omega \tan \omega = Bi \tag{2.24}$$

The infinite cylinder cases are:

$$Y = \sum_{i=1}^{\infty} \frac{2Bi\,J_0(\omega_i r/R)}{(\omega_i^2 + Bi^2)J_0(\omega_i)} \exp(-\omega_i^2 Fo) \tag{2.25}$$

$$Y_m = \sum_{i=1}^{\infty} \frac{4Bi^2}{\omega_i^2(\omega_i^2 + Bi^2)} \exp(-\omega_i^2 Fo) \tag{2.26}$$

where the values of ω are the roots of:

$$\omega J_1(\omega) - Bi\,J_0(\omega) = 0 \tag{2.27}$$

and J_0 and J_1 are zero- and first-order Bessel's functions respectively

The sphere case for Y at positions other than the centre is:

$$Y = \sum_{i=1}^{\infty} \frac{2Bi\,R[\omega_i^2 + (Bi - 1)^2]\sin(\omega_i r/R)\sin(\omega_i)}{r\,\omega_i^2[\omega_i^2 + Bi(Bi - 1)]} \exp(-\omega_i^2 Fo) \tag{2.28}$$

where the values of ω are the roots of:

$$\omega \cot\omega + (Bi - 1) = 0 \tag{2.29}$$

The sphere case for the centre position is:

$$Y_c = \sum_{i=1}^{\infty} \frac{2Bi[\omega_i^2 + (Bi - 1)^2]\sin(\omega_i)}{\omega_i[\omega_i^2 + Bi(Bi - 1)]} \exp(-\omega_i^2 Fo) \tag{2.30}$$

where Y_c = fractional unaccomplished temperature change based on centre temperature;

$$Y_c = \frac{T_c - T_a}{T_i - T_a} \tag{2.31}$$

where T_c = object thermal centre temperature (°C),

and the mass average temperature in the sphere is given by:

$$Y_m = \sum_{i=1}^{\infty} \frac{6Bi^2}{\omega_i^2[\omega_i^2 + Bi(Bi - 1)]} \exp(-\omega_i^2 Fo) \tag{2.32}$$

Temperatures at a particular point in a multidimensional regular shape are given using the product solution of Newman (1936):

$$Y = Y_x \cdot Y_y \cdot Y_z \tag{2.33}$$

where Y_x, Y_y and Y_z are the Y values for the x, y and z directions eqn (2.22) respectively in a rectangular coordinates, or

$$Y = Y_r \cdot Y_x \tag{2.34}$$

where Y_r and Y_x are the Y values for the radial direction (eqn (2.25)) and for the direction parallel to the cylindrical axis respectively in cylindrical coordinates. The product rule also applies for mass average temperature, and where there are different surface heat transfer coefficients on different surfaces of an object provided the coefficient is the same on parallel surfaces (Carslaw & Jaeger 1959). Based on theory of Newman (1936), Langston (1982) illustrated the way to applied the charts of Gröber *et al.* (1961) for one-dimensional regularly shaped geometries to multi-dimensional regularly shaped geometries.

McLachlan (1945) developed the equation which governs heat conduction in elliptical plates and cylinders in which the effect of heat transfer from the ends can be neglected. An exact solution to this equation was developed by Kirkpatrick & Stokey (1959) for the case in which the ellipses were initially at a uniform temperature, the boundary condition was of the first kind ($h \rightarrow \infty$) and there was constant thermal diffusivity. However the method is difficult to use because it requires substantial computation, practical only by computer.

2.2.1.2 Numerical Solutions

Although many numerical methods found in literature were primarily intended for freezing time prediction, most of them can be used for chilling. As stated earlier, because the thermal properties of many foodstuffs vary only slightly with temperature during the chilling process, the model of heat conduction with constant properties can be used instead of that for variable properties, thus simplifying the mathematics. When thermophysical properties are time invariant and the heat transfer processes are linear, finite difference or finite element space discretration methods, the most often used methods, effectively reduce transient multidimensional heat transfer problems into a set

of first-order differential equations. For chilling, all existing schemes of both finite difference method and finite element method perform well provided space and time steps are properly chosen and data input are accurate. A good overview of prediction of chilling time by numerical methods was presented by Cleland (1990).

Finite Difference Method

The finite difference method is easily applied to regularly shaped objects, but it is much more difficult to apply the method to a irregularly shaped object because of its use of rectangular grids. A recent comprehensive introduction to the method was given by Cleland (1990). Commonly used schemes were introduced in detail.

A finite difference model was developed by Wadsworth & Spadaro (1969, 1970) to describe the transient temperature distribution in sweetpotatoes during immersion heating. An alternating-direction-implicit technique, which involved the alternate use of two different finite difference analogues to the partial differential equation over a double time step, was applied to a general two-dimensional irregular geometry. Good prediction of experimental data for heating of sweetpotato was achieved by the method when temperature dependent thermal diffusivity was incorporated.

Fleming (1970) used a two-dimensional alternating direction implicit scheme with irregular grid to predict temperature/time profiles during freezing of a lamb leg and chilling of a beef hindquarter. Both shapes were irregular and modelled in two dimensions. Diagonal boundary elements had been permitted to provide flexibility in region description, so that the geometric approximation provided a good fit to the original shape. In the case of the lamb leg the computed bone temperature was in good agreement with the experimental results, but the calculated maximum freezing time was some 25% longer than the experimental results for four carcasses. No experimental validation was reported for the beef hindquarter. By using the same approach, a finite difference scheme and a computer programme for two-dimensional irregular geometries which can handle inhomogeneous materials was developed by Fleming (1971a, 1971b).

An explicit finite difference scheme was used by James & Swain (1983) to model the rate of heat flow, both from and through slab-shaped beef samples with position-dependent thermal properties and with various thickness of fat whilst undergoing chilling. No measurements were reported.

Temperature/time predictions by a modified Crank-Nicolson scheme for situations with the convection heat transfer environment were reported by Fikiin & Fikiin (1989). The objectives were the determination of the temperature field and the duration of the non-steady process of cooling solid objects (foodstuffs). The general solution obtained was applied to a wide variety of shapes representative of foodstuffs. Excellent agreement with experimental results in hydrocooling of fish were achieved. Further development of the method was reported by Fikiin (1992), who included heterogeneous product composition. Non-uniform surface conditions and an initial condition expressing a spatial unevenness of the temperature were applied for objects of different shape. Various multi-dimensional objects were studied by using a theory of multi-dimensional temperature fields to reduce the problem to one-dimensional. The initial temperature distribution, the ambient fluid temperature and the internal heat generation were considered arbitrary functions of space and time respectively. An effective algorithm for numerical simulation software was proposed. The grid complexity of this approach could hinder industrial applications of the method.

A finite difference scheme was discussed by Tucker & Holdsworth (1991), who used energy balances to account for different heat transfer rates through various surfaces of a food container. This heat transfer model has particular application to packaged food in semi-rigid plastic containers and glass jars. Details of the finite difference scheme used was not given.

Heat conduction during cooking of foodstuff with heterogeneous thermal properties was simulated by Califano & Zaritzky (1993), mainly for irregular shapes. Boundary-fitted grids were implemented using a control volume formulation. The control volume method, introduced in detail by Patankar (1980), can overcome problems of geometric irregularity. This technique consists of finding a numerical coordinate

transformation which fits a regular finite difference grid to the domain of integration. The model was experimentally verified for cooking of irregularly shaped pieces of beef containing a uneven distribution of fat. Relative errors were found to be less than 2%.

Finite Element Method

Based on different mathematics to the finite difference method, the finite element method can be used for handling both regular and irregular shapes. Since the implementation of finite element method needs much more grid and data preparation and computation power, it is usually more difficult to implement than the finite difference method. However, it is favoured for irregular shapes.

The finite element method was formulated by Cleland *et al.* (1984) for the solution of three dimensional heat transfer problems in objects of arbitrary geometry with variable thermal properties. The accuracy of the method was tested against available analytical solutions and against experimental data for freezing of regular shapes. The method gave comparable predictions to finite difference methods for similar problems and precision was more limited by the data uncertainty rather than by the numerical approximation inherent in the method. The flexibility of the method allowed application to a wide variety of situations. Rates of chilling of foodstuffs or other objects of any shape under any type of heat transfer environment could be predicted, and heterogeneous composition could be considered in the predictions.

de Baerdemaeker *et al.* (1977) used a two-dimensional axisymmetric finite element scheme (giving a three-dimensional model) for the calculation of heat transfer in chilling of a pear. They showed how the method could easily accommodate a wide variety of shapes, thermal properties and boundary conditions within a single programme. No experimental verification was reported.

Jiang *et al.* (1987) modelled chilling of broccoli stalks. A two-dimensional axisymmetric grid containing 202 nodes was used to represent the three-dimensional object. Experimentally determined thermal properties were used to enable simulation

of the temperature field of the stalk in a chilling process. Details of the grid used were not given but plotted results showed excellent agreement with experiments.

A finite element method was used by Pan & Bhowmik (1991) for predicting the temperature distribution in mature green tomatoes represented by realistic axisymmetric shapes. The predicted temperatures agreed with the experimental values within 1°C for an ambient temperature of 12°C and an initial temperature of 20°C.

van Gerwen *et al.* (1991) described the development and application of computer models for the simulation of carcass chilling processes. Carcass models for pig, calf, turkey and chicken were developed. With these models, carcass temperatures, heat removal and weight losses could be simulated. Details of the grids were not given but plotted results showed excellent agreement between predicted and experimental temperature/time profiles.

Other Numerical Methods

An application of the z-transfer function method to predict time-temperature history for foodstuffs of irregular shapes during chilling and cold storage was presented by Sanz *et al.* (1986). This application was based on obtaining the temperature z-transfer function coefficients by means of an experimental method and scaling the results from one chilling trial to a different temperature/time regime, provided other conditions (especially the surface heat transfer coefficient) remained the same. These coefficients were used to predict the time-temperature history of a homogeneous object and the results were compared with analytical and numerical solutions. Results showed moderate agreement with experimental data.

Seem *et al.* (1989) presented a method for approximating the exact analytical solution for multi-dimensional rectangular shapes to a set of first-order differential equations when the inputs were modelled by a continuous, piecewise linear curve. Plotted results showed that the method presented was more efficient than Euler, Crank-Nicolson, or other classical integration techniques.

2.2.1.3 Empirical Solutions

Empirical methods have been developed because 1) for irregular shapes, no exact analytical solutions exist for a boundary condition of the third kind; 2) for regular shapes, the analytical solutions are too complex, *eg.*, often more than one term in the series is significant.

General Empirical Solutions

Methods Developed for Prediction of Chilling Times

Due to the huge variety of irregular shapes that exist in agricultural and horticultural produce there is little general benefit to be gained from shape-specific prediction methods. Therefore the major attention has been focused on ways of extending the analytical solutions for regular shapes to irregular shapes in an empirical, but general fashion.

In all chilling processes, after an initial lag, the temperature at the thermal centre decreases in a exponential manner (Cleland 1990). In the case of the slab, cylinder and sphere the exponential fall corresponds to only one term in the series analytical solution being significant. Interest is often restricted to just the slowest cooling position in the object and to the mass-average temperature. The general form of the solution then became:

$$Y_c = \frac{T_c - T_a}{T_i - T_a} = L_c \exp\left(-\frac{2.303\,t}{j}\right) \tag{2.35}$$

$$Y_m = \frac{T_m - T_a}{T_i - T_a} = L_m \exp\left(-\frac{2.303\,t}{j}\right) \tag{2.36}$$

where L_c = lag factor for the thermal centre temperatures

L_m = lag factor for the mass-average temperatures

j = time for a 90% reduction in Y (s)

An alternative, but totally equivalent approach is to use the half-life time $t_{0.5}$ rather than j, so that eqns (2.35) and (2.36) are rewritten as:

$$Y_c = \frac{T_c - T_a}{T_i - T_a} = L_c \exp\left(-\frac{0.693\,t}{t_{0.5}}\right) \tag{2.37}$$

$$Y_m = \frac{T_m - T_a}{T_i - T_a} = L_m \exp\left(-\frac{0.693\,t}{t_{0.5}}\right) \tag{2.38}$$

where $t_{0.5}$ = half-life time(s) = $0.3010\,j$

Most chilling processes proceed for sufficiently long times so that the exponential fall in centre temperature becomes well-established. Hence eqns (2.35) to (2.38) can be used as a generally applicable prediction method for irregularly shaped objects of homogeneous composition cooled with the third kind of boundary condition. Values of j, $t_{0.5}$, L_c and L_m are function of Biot number and geometric shape. For infinite slabs, infinite cylinders and spheres, they can be calculated from the analytical solutions. Relevant charts and tables have been published by Pflug *et al.* (1965).

Earle and Fleming (1967) measured temperature at the deepest part of the legs of lamb and mutton carcasses during chilling and freezing under various conditions. Chilling and freezing rates were calculated from analytical solution using as a theoretical model, a so-called equivalent cylinder, to represent the deepest part of the leg. The cylinder of meat had a diameter appropriate to the weight and grade of the carcass, and was of infinite length. The concept of an equivalent cylinder could be seen as a shape factor. Rate of chilling and freezing could be predicted if the heat transfer conditions were known. Of nine chilling trials, the largest error of eight calculated results was less than 10%. The disadvantage of this approach is that some experimental work to relate equivalent cylinder size to carcass size was needed before any prediction could be made.

Fikiin & Fikiina (1971) curve-fitted the analytical solutions given earlier to establish a relationship between Biot number, Fourier number and temperature field during the chilling of foodstuffs of different shapes. This provided a simple mathematical formula for determining the chilling time for foodstuffs:

$$t = 3600 \frac{V}{AR} \frac{CR^2}{k} \left[\left(\frac{2.3}{Bi} + 0.8 \right) \ln \frac{T_i - T_a}{T - T_a} + 0.12 \right] \quad (2.39)$$

where R = characteristic dimension (half thickness) (m)

V = volume of an object (m^3)

The factor used to take account of shape is the ratio *V/AR*, irrespective of the Biot number though *V/AR* is only exact at $Bi = 0$ for slabs, infinite cylinders and spheres. Values of the shape factor *V/AR* were quoted by Fikiin (1983) for a number of shapes, plus some food products; apples, pears, and hind-quarters of beef and pork. There are also two earlier methods of the same general type: Baehr (1953) whose method applies to only the basic regular shapes, and that of Rutov (1958) which could be applied to irregularly shaped objects only if a shape factor is incorporated. In testing for 256 experimental tests Fikiin found that his method was accurate within 9.1% compared to 10.3% for the Rutov method and 12.8% for the Baehr method.

A set of experimental formulae was obtained by Hayakawa (1971) for estimating the entire portion of transient temperature profile curve for either convective or conductive food products of regular shape during the initial cooling stage by refrigeration. These formulae were derived by analyzing a number of temperature profile curves obtained by experiments. In these formulae, experimental constants, j and L values, were used to accurately estimate the entire portion of the curve. By using the derived formulae, a new procedure was developed for the estimation of heat processes of canned food. A number of heating and cooling curves of food, which were obtained through experimentation, were used to evaluate the accuracies of the developed and of existing procedures for the process calculation. This evaluation shows that the heat processes can be estimated more accurately by the proposed procedure than by any previously existing procedures.

A large and comprehensive study involving theoretical and experimental work with irregular shapes was carried out by Smith & Nelson plus co-workers (Clary *et al.* 1968, 1971, Smith *et al.* 1967, 1968, 1971, Smith & Nelson 1969). The objectives of the study were to derive a model and a parameter G to denote the geometry of a

irregular shape. The method was based on the first term of the infinite series solution for the sphere (eqn (2.30)). An ellipsoidal model was used to approximate the irregular shapes. The minimum half-thickness of the object and model was used as the characteristic length, R. Dimensionless ratios β_1 and β_2 were used to define the lengths of the semimajor axes, in relation to R, of the two ellipses that defined the general ellipsoid. Orthogonal areas of planes of R were set equal for the model and the irregular shape to calculate β_1 and β_2. A geometry index G was defined in terms of the parameters β_1 and β_2 and predicted for the ellipsoidal model by the following equation:

$$G = \frac{1}{4} + \frac{3}{8\beta_1^2} + \frac{3}{8\beta_2^2} \tag{2.40}$$

A unified system of charts and graphs was presented for use over a wide range of conditions and different geometric shapes. Experimental temperature distributions were used to relate the location of the mass average temperature to the geometry index G. Experiments were also conducted to test the validity of using the geometry index G in predicting internal temperature for the ellipsoidal model and irregular shapes. The results covered only a restricted range of conditions but suggested that the prediction method uncertainty was small compared to error in the experiments and in thermal property data. A possible shortcoming of the method is that the geometry index G is not Biot number dependent, being derived for the case $Bi \rightarrow \infty$ (in contrast, Fikiin's method was derived for $Bi \rightarrow 0$). Instead of deriving a Biot number dependent shape factor, the authors used a pseudo-Biot number to account for the effect of Bi on G. Another shortcoming is that the nomograph for evaluating elements of the equation can introduce large interpretative errors when $Bi > 5$. This includes part of the important practical Biot range. Interpretations of the other charts can also introduce some uncertainty. Hayakawa & Villalobos (1989) proposed regression formulae to implement the method without charts, but the formulae are still difficult to implement because of their multiple expressions and complexity. Using Smith *et al.*'s method, Güemes *et al.* (1989) successfully determined the effective surface heat transfer coefficients during air precooling of strawberries.

Cleland & Earle (1982) presented a simple method for prediction of temperature/ time relationships in solids undergoing heating or cooling. Half-life time was used to represent the time taken for Y to be halved. A parameter E (equivalent heat transfer dimensionality) was developed to describe the effect of geometry, and was made Biot number dependent:

$$E = 1 + W_1 + W_2 \tag{2.41}$$

$$\text{where } W_1 = \left(\frac{Bi}{Bi + 0.1}\right)\frac{1}{\beta_1^2} + \left(\frac{0.1}{Bi + 0.1}\right)\frac{1}{\beta_1} \tag{2.42}$$

$$W_2 = \left(\frac{Bi}{Bi + 0.1}\right)\frac{1}{\beta_2^2} + \left(\frac{0.1}{Bi + 0.1}\right)\frac{1}{\beta_2} \tag{2.43}$$

The two shape factor $ß_1$ and $ß_2$ were the ratios of the longer two dimensions to the shortest. For oval, cylindrical and rectangular shapes the predictions were based on the analytical solutions for sphere, cylinder and slab respectively. An alignment chart was provided for finding the centre temperature of a shape as a function of time and the external heat transfer conditions. The method accuracy was assessed for a wide range of regular and irregular shapes, and for a variety of cooling conditions. The 95% confidence bounds were ±12%. The method was restricted to chilling time prediction for the thermal centre position in an object. It was not a unified system because of the three different reference shapes.

Cuesta *et al.* (1990) proposed a general graphical method to predict both the thermal centre and mass average temperatures based on the exponential half-chilling times in three basic regular shapes (infinite slab, infinite cylinder and sphere). For this purpose, two diagrams were constructed to depict these dimensionless times, plus the prime root of the Λ transcendental equation and other useful variables for the indirect approximate calculation of thermophysical parameters. For irregular shapes, the method had to be applied in conjunction with other methods, *e.g.* Cleland & Earle (1982), Fikiin (1983), etc. It can deal with only a narrow range of fractional unaccomplished temperature change based on mass-average temperature ($Y_{ma} < 0.25$) yet the error was still significant at about ±10%.

SHAPE FACTORS DEVELOPED FOR PREDICTION OF FREEZING TIMES THAT MAY HAVE APPLICABILITY TO CHILLING

To take account the effect of object geometries on freezing times, a number of shape factors have been developed. Amongst them some were considered possibly applicable to chilling.

By assuming that the freezing front is similar in shape to the surface object, a formula was derived by Pham (1991) for the shape factors of ellipses and ellipsoids undergoing freezing. The formula agreed well with numerical solutions at Biot number of infinity but disagreed by up to 17% for intermediate Biot numbers. A curve-fitting expression was incorporated that agreed with the numerical results to within 6%. Comparing with the author's previous works on geometric factor (Pham 1984, 1985, 1986), the new version has higher accuracy.

In the work of Hossain *et al.* (1992a, 1992b, 1992c), analytical solutions for phase change for regular shapes and semi-analytical solutions for two- and three-dimensional shapes were utilised to derive formulae for a geometric factor that describes the effect of product shape on freezing and thawing times. These formulae depend only on the Biot number and simple parameters that describe object geometry. The accuracy of these formulae was demonstrated by comparisons with both large sets of experimental food freezing and thawing data and numerically calculated data. The formulae out-perform all geometric factors previously proposed for freezing yet are simple to use.

Product Specific Empirical Solutions

The disadvantages of this approach are that some experimental work is required before any prediction can be made; and that the application of any set of formulae is limited to only one specific type of product.

The chilling rate of avocados in commercial operation as a function of different factors was investigated by Haas & Felsenstein (1985). The separate influence of each of the following factors on the chilling rate was established: the approach air velocity, the free flow area on the carton walls perpendicular to the air direction and the number of carton layers stacked in the direction of air flow. For each test the correlation between the dimensionless temperature and the chilling time was determined and the effective heat transfer coefficient was calculated. Tests with full size pallet were carried out and results similar to those in the laboratory scale tests were achieved.

Experimental data for chilling rates of beef carcasses were obtained in a carcass chiller by Schneider *et al.* (1982). The chilling rates were modeled as a function of carcass weight, thickness of fat covering on the carcass, and location of the carcass within the cooler by curve-fitting the experimental data.

Stermer *et al.* (1984,1986) studied hydrocooling of beef hearts, kidneys, livers and tongues. Temperatures in the centre of the thickest portion of each organ during chilling were monitored. A least squares regression analysis of the heat transfer equation was performed to provide chilling models. A heating or cooling rate modulus provided an indicator of rate of chilling.

Wade (1984) treated individual fruit pieces as spheres and pallets of carton as infinite slabs. Chilling rate was defined in term of the seven- eighths chilling time, S, and the lag factor, L, which was an empirical measure of the thermal properties of the produce.

Dincer *et al.* (1992) reported that when freshly harvested apricot, plums and peaches in crates were hydrocooled, the cooling parameters: lag factor and half life time for the centre positions and cooling coefficient were found to vary with crate load.

2.2.1.4 Solutions for Problems in a Time-Varying, Convection only Heat Transfer Environment

Approximate Analytical Solutions

A procedure was developed by Hayakawa (1971) for predicting the transient temperature of a solid food exposed to time variable ambient temperatures. Duhamel's theorem was applied to the curve-fitted formulae used for calculating the temperature of food product subjected to a step changes in ambient temperature. The formulae contained two constants: j, the slope index of the heating or chilling curve of a food product; and L, the intercept coefficient of the heat or chilling curve. With the procedure developed transient temperature could be estimated without regard to the geometric shape of the food product provided the j and L values were known. A table was presented to reduce computations involved in the procedure. Sample calculations were given for an orange, a fresh carrot and a canned food product.

Numerical Solutions

FINITE DIFFERENCE METHOD

Lovett (1988) used the Lees slab scheme for modelling chilling of sides of beef (assuming slab-like geometry). The beef side or meat carton was modelled as a one-dimensional meat slab convectively cooled at both surfaces. Evaporative heat loss was assumed to be zero. The predictions were considered adequate taking into account data uncertainties. A programme based on the theory runs on small personal computers and requires less than one minute for a 24 hour chilling or freezing prediction.

FINITE ELEMENT METHOD

The finite element method was applied to two time-dependent axisymmetric problems in food products by de Baerdemaeker *et al.* (1977); the heating of a homogenous material in a cylindrical can and the heating of a chicken leg composed of four different materials. No experimental results were given.

BOUNDARY ELEMENT METHOD

Wrobel & Brebbia (1979, 1981) developed a formulation of the boundary element method for the analysis of axisymmetric transient heat conduction problems. The axisymmetric time-dependent fundamental solution was obtained by directly integrating the three-dimensional heat conduction equation. Due to its complexity, series expansions have to be introduced in order to make possible the analytical evaluation of the time integrals that appeared in the formulation. Several results of numerical analyses were presented, including problems with time-dependent boundary conditions. They demonstrated the feasibility of using boundary elements in space and time to solve axisymmetric heat conduction problems. Graphical results showed good agreement with analytical solutions for problems with the third kind of boundary condition. The method has the advantage of reducing the dimensionality of a problem and hence the computing power and preparation. However, it would be accurate only for shapes with large surface area to volume ratios.

2.2.2 Solutions for Problems with Simultaneous Convection and Evaporation

No exact analytical solutions for such problems were found in the literature.

2.2.2.1 Numerical Solutions

A model for the evaporation of water from a meat surface was presented by Radford *et al.* (1976). It was capable of simulating experimental results obtained in wind-tunnel runs. Diffusion was the mechanism of water transport within the meat, with diffusivity dependent upon temperature and water content of the product. Good agreement between experiments and simulations was achieved.

A comprehensive mathematical model was developed by Hayakawa (1978) to simulate heat transfer and moisture loss from fresh produce of foodstuff being cooled. The model was utilized to examine the influence of several physical parameters on moisture loss as well as transient temperature distribution in an idealized fresh produce. No experimental data were reported.

A computerized procedure was developed by Hayakawa & Succar (1982) for simulating the post harvest cooling and moisture loss of produce. This model was derived on the basis of assuming temperature- and time-variable respiration heat generation and temperature-variable thermophysical property values. The developed procedure was employed to examine influence of five key dimensionless parameters on the cooling rate and moisture loss. These parameters were related to the rates of changes in density and thermal conductivity with changes in produce temperature, surface heat transfer conductance, transpiration rate, and environmental relative humidity. Theoretical results were verified through heat transfer and moisture loss experiments using fresh potatoes and tomatoes. Moderate agreement was shown.

Badari Narayaya & Krishna Murthy (1981) presented a Crank-Nicolson implicit finite difference model to predict temperature/time characteristics of a moist slab-shaped food product subject to the effects of both heat and mass transfer. The model used a heat transfer-based approach to evaporation. Theoretical temperature/time histories were presented in the form of charts in terms of five dimensionless parameters. The experimentation consisted of applying a uniform heat flux on one side of the slab and exposing the other to the ambient where both heat and mass transfer occurred under free convection conditions. The theoretical and experimental thermal histories were matched through a non-linear estimation method to determine the thermal properties. The Lewis relationship was used in conjunction with empirical equations to alter the value of air temperature from the dry bulb temperature to a value approaching the wet bulb temperature. Comparison of predictions with measurements for model food gels showed only moderate agreement.

Abdul Majeed (1982) used a backward (implicit) finite difference scheme to model a continuous liquid film of cold water on a cylinder-shaped product surface with evaporation from the film. Calculated temperature/time histories during chilling of cylindrical food products were presented. The range of parameters for which the process was most effective were identified and correlations between parameters and chilling rate were calculated. Comparisons with chilling data for model food gels showed only moderate agreement.

The one dimensional transient heat conduction equation in spherical coordinates was solved with convective surface boundary condition, during air cooling by Ansari *et al.* (1984). An explicit finite difference scheme was proposed in which, up to half the cooling time, the calculation was made with both heat and mass transfer from the product surface by curve-fitting; thereafter it was continued with heat transfer only. The calculated temperatures for apples and potatoes were compared with the measured values available in the literature, and moderate agreement was observed. The work was extended to cylindrical commodities by Ansari & Afaq (1986). Their numerical calculations involved explicit finite differences for cylinders. The calculated temperature of banana, carrot, cucumber and radish were compared with the measured data and good agreement was observed.

An explicit finite difference scheme was used by James *et al.* (1988). Simultaneous heat and mass transfer were modelled by linking finite difference calculation for diffusion with finite difference calculation for heat conduction. The model assumed that both the heat and mass transfer coefficients remained constant during the process, that there was no heat transfer due to moisture movement within the product, that the product was a semi-infinite slab, that loss of water caused no change in either volume or density of the product, and that vapour pressure had no effect on the latent heat of evaporation. The slab was initially at a uniform temperature equal to that of the ambient air. Heat flow was initiated by evaporative chilling of the exposed surface layer and the progress of both heat and mass movement was simulated. Comparisons with chilling data for models of retail meat displays showed only moderate agreement.

Gaffney *et al.* (1985) summarized existing methods for calculating heat and mass transfer in fruits and vegetables, both individually and in bulk. The authors found out that there was no solution which is best for all situations, therefore it was important to have a general understanding of the factors that should be considered in a solution for a specific product and a set of operating regimes.

Experiments were conducted by Chau *et al.* (1985) to study the temperature responses of oranges in a closed container during chilling. To evaluate the effect of natural convection of the air in the void spaces inside the carton, several experiments were conducted with the cooling source applied to the bottom, the top, or the side of the container. It was found that natural convection had a very significant effect on the cooling rate which was fastest when the cooling source was at the top of the container and slowest when the cooling source was at the bottom. A finite difference model to simulate conduction cooling with the cooling source at the bottom of the carton was developed. It took account of the heat of respiration of the oranges, the heat conduction through the oranges, the moisture loss due to transpiration, the heating effect due to condensation (if any), the heat transfer between the air and the cold plate, and the diffusion of water vapour in the air. Significant differences between predicted and experimental temperature/time profiles were observed.

2.2.2.2 Empirical Solutions

General Empirical Solutions

Srinivasa Murthy *et al.* (1974, 1976) analyzed heat transfer characteristics during chilling of moist food products, taking into account the effects of the evaporation of the moisture film that usually existed on the product surface. The one dimensional transient heat conduction equations for the slab (Srinivasa Murthy *et al.* (1974), cylinder and sphere (Srinivasa Murthy *et al.* (1976) were needed. A backward (implicit) finite difference scheme was used to generate data for plotting on charts which were proposed as a simple prediction method. Comparisons with chilling data for model food gels showed only moderate agreement.

An analysis of the air-chilling characteristics of food products, was presented by Abdul Majeed *et al.* (1980). The coupled effects of heat and moisture transfer at the product surface were taken into account. The one-dimensional heat conduction equation in rectangular, spherical and cylindrical coordinates was solved using backward difference schemes. The variation of product temperature with time was obtained in

dimensionless form in terms of Biot number, wet bulb temperature of ambient air and initial product temperature. Empirical correlations were obtained for the time variation of temperature as a function of the governing parameters. The theoretical predictions yielded only moderate agreement with experimentally determined temperature/time histories.

Pham (1987) used psychrometric principles to predict the direction and maximum possible moisture change (in terms of percentage weight change). Equations and graphical methods were presented and illustrated with examples: for cooling and freezing of meat, product temperature change due to air infiltration or heat conduction during storage, transport by unrefrigerated containers. Good agreement was achieved with experimental data.

Product Specific Empirical Solutions

Levy (1978) reported that during the chilling of a carcass, both its heat losses by convection and by evaporation are governed by the convection heat transfer coefficient h_c. While both phenomena occurred at the same temperature difference ΔT between the surface of the carcass and the cold air, the quantity of heat flux of the former part became $h_c \Delta T$, and the latter part became the product of h_c multiplied by an equivalent temperature difference ΔD which is a function of the vapour pressure differences between the wet surface and the cold air. The diagram for evaluating the relationship between convective and evaporative heat transfer during the chilling of carcasses was developed. The ratio $\Delta D/\Delta T$ could be established from the diagram and the heat loss by convection and evaporation could be calculated for any given value of h_c. Consequently, the anticipated theoretical weight loss of the carcass could be calculated.

James & Bailey (1986) found that air temperature, air velocity, and to a limited extent, relative humidity were the environmental variables that affected the chilling time of beef sides. For any particular side chilling rate would also be a function of weight and fat cover. The relative magnitude of these effects, and their interaction, was discussed.

2.3 Published Data Suitable for Testing Methodologies

For data to be useful for testing of chilling time prediction methods all conditions must be fully defined. Cleland (1990) and Sainsbury (1985) concluded that for the most important situation of a convection heat transfer environment, the following information is necessary:

i) geometric description of the object;
ii) thermal properties or composition of the object;
iii) description of the degree of homogeneity and isotropy of the object;
iv) temperature/time history;
v) reliable surface heat transfer coefficient data;
vi) description of measurement techniques.

Few data found in the literature conform with all these criteria.

Both Cleland and Sainsbury found that while in theory, chilling data in the literature could be used to evaluate an industrial chilling performance problem, their use and accuracy imposed some limitations. The greatest problem was that the project installation under analysis may not conform to the laboratory environment in terms of use of identical packages, stacking pattern and air flow characteristics that prevailed in gathering the original data. That is, the results obtained in the tests apply very specifically to the circumstances tested. The largest problems are the lack of good quality data on surface heat transfer coefficients and the scarcity of thermal diffusivity data for food products.

Data were obtained by Smith *et al.* (1967) to validate their prediction equation for the ellipsoidal model and for the irregular shapes. Experimental temperature distributions were used to relate the location of the mass-average temperature to the geometry index G. Boneless processed ham was used as an example of an irregular shape to test the method. The temperature/time data and geometry analysis were used to find thermal diffusivity. With diffusivity and conductivity known for the processed

ham, temperature/time data obtained during air cooling was used to evaluate surface conductance for specified conditions. Applications of the concept of geometry analysis for irregular shapes, when thermal properties are known, were presented.

Nolan (1987) reported several temperature histories measured at the centre of beef roasts during chilling with cold liquid coolant as obtained at an industrial beef processing factory. Comparison of these temperatures with the two-dimensional solution for an elliptical cylinder (Kirkpatrick and Stokey 1959) subject to forced convection heat transfer problem showed that satisfactory predictions can be made during liquid chilling. Ice/water velocities should be kept in excess of about 0.076 m/s to ensure that minimal surface resistance to heat transfer occurred during chilling of cooked roasts. Ice/water velocity in the order of 0.15 m/s seemed to lead to excellent chilling conditions. In this situation h was sufficiently large that the error introduced by the assumption of infinite surface heat transfer coefficient was small. Based on this mathematical solution, a graphical method was given together with a practical example. The paper implied the assumption of the first kind of boundary condition.

Heat transfer characteristics during air precooling of strawberries were studied by Güemes *et al.* (1989). Effective surface heat transfer coefficients were determined and a *Nu-Re* correlation which included the effect of moisture evaporation was developed. The mean value of film coefficients obtained for strawberries were 16 to 25% higher than those predicted by the correlation of McAdams (1954) for spheres cooled only by convection. Furthermore, a geometry analysis for strawberries was carried out when determining surface heat transfer coefficients. It was concluded that for practical applications strawberries might be acceptably considered as spheres.

2.3.1 **Thermal Properties**

Accurate thermal property data are critical to prediction of chilling times.

The thermal properties required to predict chilling temperature/time profile in foodstuff with heat generation include density, ρ, specific heat capacity, c and thermal conductivity, k. There are many good and relevnt general reviews, such as these of Jowitt *et al.* (1983), Nesvadba (1982), Sweat (1985), Murakami & Okos (1989) and Heldman & Lund (1992). These cover useful data as well as measurement techniques and prediction methods developed for thermal properties.

2.3.2 **Heat Transfer Coefficients**

All three mechanisms of heat transfer, including convection, radiation and evaporation, can occur at the surface of a food product or of a food package. The commonly applied approach to account for them is to find an effective surface heat transfer coefficient which is also commonly assumed to be constant throughout the chilling process and uniform over all the surface. Comprehensive reviews on estimation techniques and useful data were given by Arce & Sweat (1980), Hallstrom *et al.* (1988), Cleland (1990) and ASHRAE (1993).

3. PRELIMINARY CONSIDERATIONS

Chapter 2 reviewed general empirical methods for extending the analytical prediction methods available for simple shapes (infinite slabs, infinite cylinder, spheres) to irregular shapes. Each of previous proposals for a general empirical method has weaknesses under certain circumstances, so that it is desirable to develop an improved generally applicable chilling time prediction method, which meets the following criteria:

i) Better accuracy than available methods;

ii) Applicability to both regular and irregular geometries;

iii) Applicability to both thermal centre and mass-average temperatures;

iv Algebraic equations requiring no graphical aids;

v) Applicability to the most common and practical condition of the heat transfer environment of convection only;

vi) A shape factor which fits all known cases for which there are analytical solutions (infinite slab, infinite cylinder, sphere, infinite rectangular rod, finite cylinder, rectangular brick);

vii) A shape factor which fits all available data for elliptical, ellipsoidal and other irregular geometries.

This method would ideally be designed for later extension to more complex external heat transfer conditions involving radiation and evaporation.

Because of time and resource limitations, a decision was made to confine the first part of the current study to situations where the following eight conditions apply:

1) The object is of a homogeneous and isotropic nature;

2) The thermal properties of the object are constant;

3) The initial temperature of the object is uniform;

4) The process is subject only to convection heat transfer environment (radiation is considered only in a pseudo-convection fashion);

5) The ambient temperature is constant;

6) All points of the surface are subject to the same heat transfer coefficient;

7) No change of phase takes place within the object;

8) No heat generation occurs within the object.

In the second part of the study, means to adapt the method to some situations in which not all the eight conditions above apply will be sought. A common situation is the presence of air or gas voids within the product. These can be internal to product items, *eg* in bakery products, or between product items in a container. They affect the heat transfer, yet in the literature survey no systematic, experimentally based study of their effect on chilling rate was found. A first stage in the study of voidage would be to consider uniform distribution, even though this may not occur in practice. Voids size may be important as it may correlate with the extent of natural convection.

Therefore, the two objectives for the research were to:

I. Develop a new generally applicable chilling time prediction method with specific characteristics described above, and

II. Establish appropriate means to extend this method so that it accurately predicts rates of chilling in situations where the product contains significant uniformly distributed voids.

4. DEVELOPMENT OF A NEW GENERAL EMPIRICAL METHOD

4.1 Introduction

The first objective stated in Chapter 3 was to develop a new generally applicable empirical chilling time prediction method for the convection-only cooling environment, focusing particularly on ways to empirically extend analytical solutions for regular shapes to all other shapes. The results from application of any new prediction method must agree with both the analytical solutions (for regular shapes) and experiments (for irregular shapes) if the method is to be an advancement on those presently available. In this chapter only the limited range of "regular" shapes was considered. Extension of the method to other shapes will be covered in Chapter 6.

Most approaches found in the literature use shape factors, belonging to one of the three categories:

i) derived for $Bi = 0$;

ii) derived for $Bi = \infty$;

iii) derived for all Bi.

For all two- and three-dimensional shapes (other than the infinite cylinder and sphere), the surface is not isothermal with respect to position unless $Bi = 0$ or $Bi = \infty$. Therefore, the true geometric factor for multi-dimensional shapes is in reality dependent on the Biot number. For that reason, the third approach was considered most physically realistic and hence most desirable.

4.2 Proposed Form of the New Method

Due to the practical importance of both the slowest cooling or heating point, and the mean object temperature, consideration must be given to temperature/time profiles for both the thermal centre and mass-average temperatures. In Section 2.3.1.1 the analytical solutions for both thermal centre and mass-average situations were reviewed. These solutions are in the form of infinite series, but as Figure 4.1 shows, often only

one term is significant for values of the fractional unaccomplished temperature change (Y) that arise in practical chilling situations (typically less than about 0.7).

Chuntranuluck *et al.* (1989) considered that whilst there was no need for any new method to cover the regular geometric shapes (because there are analytical series solutions for these), it was desirable to do so, to reduce the calculation complexity and to form a basis of a unified prediction method. The most common technique in seeking a general prediction method has been to use the analytical solution for a simple shape (usually the sphere, but sometimes the infinite slab), and to determine ways to adjust both the slope and intercept of the linear section of plots of ln Y vs Fo such as Figure 4.1 according to product shape. This was the approach adopted here.

The equivalent heat transfer dimensionality, denoted E, is introduced as a measure of how each of the three dimensions of a geometry contribute to heat transfer. It makes the influence of geometric arrangement of an object on practical unsteady state heat conduction processes easier to understand, and it has been successfully applied in freezing time prediction (Hossain *et al.* 1992a, 1992b, 1992c). As a result it has growing worldwide acceptance. However, its numerical values for chilling may not coincide with those for freezing. This is a disadvantage but the advantage of using a known concept were considered sufficient to compensate.

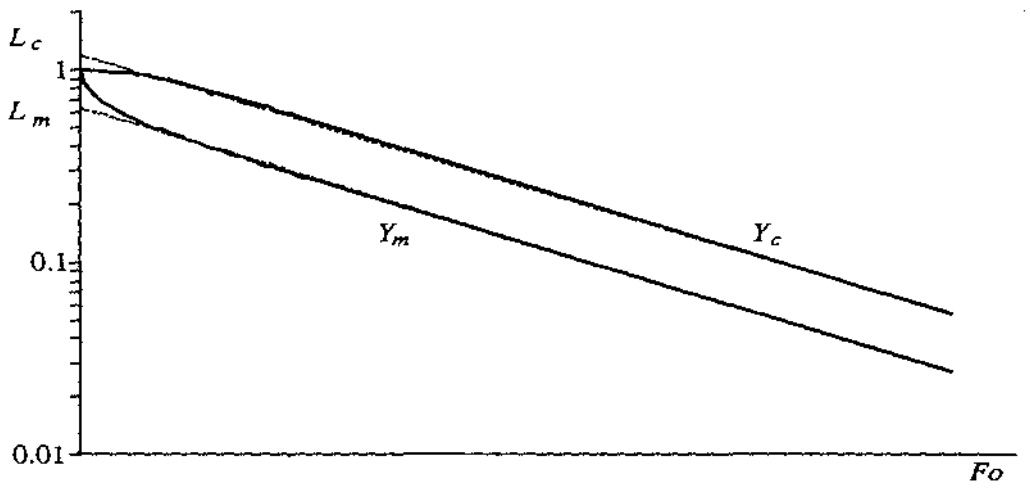

Figure 4.1 Plot of ln Y vs Fo during a chilling process

Being perfectly three-dimensional, the sphere was chosen as the reference shape for all geometric shapes in the formulation of the equivalent heat transfer dimensionality (E), because its E value keeps constant at 3 for the entire range of Biot number. This is in contrast to the use of the slab as reference in freezing but other workers (Smith *et al.* 1967, 1968, Clary *et al.* 1968, Smith & Nelson 1969, and Clary *et al.* 1971) have found the sphere a more appropriate reference than the slab in chilling. Consequently the proposed forms for the new general empirical method were as following:

For the thermal centre position:

$$Y_c = L_c \exp\left(-\frac{\alpha^2 E\, Fo}{E_{sphere}}\right) \tag{4.1}$$

$$Y_c = L_c \exp\left(-\frac{\alpha^2 E\, Fo}{3}\right) \tag{4.2}$$

where E = equivalent heat transfer dimensionality

E_{sphere} = equivalent heat transfer dimensionality for a sphere (= 3)

Fo = Fourier number

L_c = lag factor for the thermal centre temperatures

Y_c = fractional unaccomplished temperature change for the thermal centre

α = first root of the transcendental equation for a sphere (eqn (2.29))

For the mass-average situation:

$$Y_m = L_m \exp\left(-\frac{\alpha^2 E\, Fo}{E_{sphere}}\right) \tag{4.3}$$

$$Y_m = L_m \exp\left(-\frac{\alpha^2 E\, Fo}{3}\right) \tag{4.4}$$

where L_m = lag factor for the mass-average temperature

Y_m = fractional unaccomplished temperature change for the mass-average temperature

The first stage of development of the new generally applicable empirical method was to find expressions for E, L_c and L_m for different geometric shapes and Biot numbers. These should be derived to cover the most practical range of conditions.

Typical values for Y_m and Y_c at process completion are of the order of 0.1 to 0.3, but it would also be advantageous if the method enabled predictions of Y to be made during the process. However, as Figure 4.1 shows, at high Y values the simple model form of eqn (4.2) and (4.4) breaks down. A compromise must then be reached. Upper limits of $Y_c < 0.7$ and $Y_m < 0.55$ were selected. These enable the most important part of the temperature/time history to be predicted accurately, yet do, to some extent extend into the regions where linearity of plots such as Figure 4.1 is not guaranteed.

For higher Y values during the initial "lag period", the method of Hayakawa (1970) can be applied if the proposed shape factors E and L are first used to find the slope and the intercept of the plot of ln Y vs Fo.

4.3 Geometric Definitions

To enable formulation, unambiguous description of geometric shapes is necessary. For any regular shape the geometry is defined by:

D_1 = shortest dimension through the geometric centre of the object (first dimension);

D_2 = shortest dimension through geometric centre of the object taken at right angles to the first dimension (second dimension);

D_3 = dimension through geometric centre of the object at right angles to both the first and second dimensions (third dimension).

The concepts of "characteristic dimension" and "dimensional ratios", widely found in the literature of chilling time prediction, were adopted:

R, the characteristic dimension, is half of the first dimension:

$$R = D_1 / 2 \tag{4.5}$$

$ß_1$, is the ratio of the second shortest dimension (the shortest dimension perpendicular to the first dimension) to the first dimension:

$$ß_1 = D_2 / D_1 \tag{4.6}$$

$ß_2$, is the ratio of the longest dimension (the shortest dimension perpendicular to both the first and the second dimensions) to the first dimension:

$$ß_2 = D_3 / D_1 \tag{4.7}$$

The regularly shaped geometries are then defined as follows:

1) basic shapes:

infinite slab ($ß_1 = ß_2 = \infty$),

infinite cylinder ($ß_1 = 1$, $ß_2 = \infty$), and

sphere ($ß_1 = ß_2 = 1$).

2) intersection of two infinite slabs:

infinite rectangular rod ($ß_1 \geq 1$, $ß_2 = \infty$).

3) intersection of one infinite slab and one infinite cylinder:

finite cylinder, which was further divided into two varieties:

short cylinder (height > diameter, $ß_1 = 1$, $ß_2 > 1$), and

squat cylinder (height $\leq$ diameter, $ß_1 = ß_2$, $ß_1 \geq 1$).

4) intersection of three infinite slabs:

rectangular brick ($ß_1 \geq 1$, $ß_2 \geq ß_1$).

5) infinite ellipse ($ß_1 > 1$, $ß_2 = \infty$), and

6) ellipsoid ($ß_1 \geq 1$, $ß_2 \geq ß_1$) including two special cases:

prolate spheroid ($ß_1 = 1$, $ß_2 > 1$), and

oblate spheroid ($ß_1 = ß_2$, $ß_1 > 1$).

4.4 Creation of Database for the Regular Geometries

Using the analytical solutions for regular shapes with the third kind of boundary condition, calculations were carried out for a wide range of Bi, $ß_1$ and $ß_2$ values. It was found that for practical Y values (0.05 to 0.70 for the thermal centre temperature, and 0.05 to 0.55 for mass-average temperature) plots of the type in Figure 4.1 are sometimes slightly non-linear. As it has been discussed, the ranges considered in the present work were limited to values of Fo that led to Y_c between 0.05 and 0.7. Within these Fo ranges Y_m was typically, but not necessarily between 0.5 and 0.01, but the limits on Fo were set according to the desirable Y_c range and not Y_m.

In many circumstances for Y_c values between 0.7 and 0.05 it cannot be assumed that only one term in the analytical solutions for the second and third dimensions is significant. *e.g.* if Y_c equals 0.054 for a three-dimensional shape, the Y_c values can be 0.2, 0.3 and 0.9 for the first, second and third dimensions respectively. For Y_c of 0.9, it is expected that more than one term is significant. This means that for the regular geometric shapes, the slope and intercept of the best-fit line in the ranges of Y indicated above cannot be theoretically calculated from the one term truncation of the series solution. Instead, they must be determined by plotting the data, and establishing a line of best-fit.

A computer programme implementing the Fourier series analytical solutions for slabs, infinite cylinders, infinite rectangular, rectangular bricks and finite cylinders was developed (Appendix C). The line of $\ln(Y_c)$ vs Fo for each of the regular shapes was plotted using the full analytical solution for that particular shape and taking as many terms as were required to ensure series truncation error was not more than 10^{-5}. Using linear regression lines were of best-fit for data in the ranges $0.05 \le Y_c \le 0.70$ and $0.05 \le Y_m \le 0.55$ established and slope and intercepts found. The intercepts are the expected values of L_c and L_m. The slope of a plot of $\ln(Y_c)$ vs Fo line for the sphere was also calculated, based on only

the first term of the Fourier series. The two slopes were compared and the best-fit E value for the regular shape was then generated:

$$E = \frac{3\,Slope_{shape}}{Slope_{sphere}} \tag{4.8}$$

E values for infinite ellipses and spheroids was found in a similar way. The only difference was that the slopes of the $\ln(Y_c)$ vs Fo line for the ellipse and the spheroids were found using calculations by the finite element method, instead of using an analytical solution. A three-dimensional finite element programme was available, but the computation and grid preparation times to carry out large numbers of calculations were excessive. Therefore a two-dimensional axisymmetric implementation was used to enable some ellipsoids (the prolate and oblate spheroids) to be studied in detail within a reasonable time frame. The two-dimensional programme used was developed by Cleland *et al.* (1987b). The space and time steps were set to be relatively small ($\geq$ 10 space steps from the thermal to the surface and $\geq$ 500 time steps for one run) to minimise approximation errors in the numerical solution.

For each shape, Bi was varied logarithmically in 9 even steps from 0.01 to 100 (*i.e.* 0.01, 0.0316, 0.10, 0.316, 1.00, 3.16, 10.00, 31.6 and 100.00). For the infinite rectangular rod, the infinite ellipse, the squat cylinder and the oblate spheroid, the dimensional ratio $ß_1$ was varied in 13 logarithmically spaced steps from 1 to 10 (1.000, 1.136, 1.292, 1.488, 1.668, 1.896, 2.154, 2.783, 3.594, 4.642, 5.995, 7.743, 10.000). For the short cylinder and the prolate spheroid, the dimensional ratio $ß_2$ was varied in the same fashion to $ß_1$. Both $ß_1$ and $ß_2$ were varied across these logarithmic steps for the rectangular brick.

The result of all the calculations was a large data set of values of E, L_c and L_m which best-fitted plots of ln Y vs Fo within the most critical range of Y. There were two sets of E data, for the thermal centre and mass-average situations. These were very close to each other but not always identical. The E data for the thermal centre were adopted as the data set to be fitted most closely when deriving the new method, but this was an arbitrary decision.

4.5 Formulation of the Equivalent Heat Transfer Dimensionality, and the Lag Factors for the Thermal Centre and the Mass-Average Temperatures

4.5.1 Formulation of the Equivalent Heat Transfer Dimensionality, Denoted *E*

From the form of the analytical solutions, it can be shown that the variations in E, L_c and L_m can be expressed as:

$$E = \text{f (Geometric Shape, } Bi) \tag{4.9}$$

$$L_c = \text{f (Geometric Shape, } Bi) \tag{4.10}$$

$$L_m = \text{f (Geometric Shape, } Bi) \tag{4.11}$$

These relationships were assumed to extend to irregular shapes on an empirical basis. The approach taken was to consider the values that E should take at the two limiting conditions, $Bi = 0$ and $Bi \rightarrow \infty$. These were denoted E_0 and E_∞ respectively. A Bi dependent weighting function would then be used to determine E at other Bi numbers.

4.5.1.1 Formulation of the Equivalent Heat Transfer Dimensionality at $Bi = 0$

It can be analytically proven that the equivalent heat transfer dimensionality E tends to a dimensionless surface area to volume ratio, AR/V, at $Bi = 0$ (Cleland 1990). This ratio can be calculated from geometric considerations as following:

For a finite cylinder, brick or infinite rod:

$$E_0 = 1 + \frac{1}{\beta_1} + \frac{1}{\beta_2} \tag{4.12}$$

For an ellipse using an approximation formula for the surface area:

$$E_0 \approx \left(1 + \frac{1}{\beta_1}\right)\left[1 + \left(\frac{\beta_1 - 1}{2\beta_1 + 2}\right)^2\right] \tag{4.13}$$

(The error introduced by using this approximation is less than 1.0%).

For an ellipsoid ($1 < ß_1 < 10$, $1 < ß_2 < 10$):

$$E_0 \approx \frac{3(\beta_1 + \beta_2 + \beta_1^2(1 + \beta_2) + \beta_2^2(1 + \beta_1))}{2(\beta_1\beta_2(1 + \beta_1 + \beta_2))} - \frac{[(\beta_1 - \beta_2)^2]^{0.4}}{15} \quad (4.14)$$

(The error introduced by using this approximation is not greater than 3.0%). The accuracy of eqn (4.13) and (4.14) were tested, including for the worst cases.

4.5.1.2 Formulation of the Equivalent Heat Transfer Dimensionality for $Bi \rightarrow \infty$

Using the computer-generated data set, E_∞ (assumed to be close to E at $Bi = 100$) values for the infinite slab and infinite cylinder were found to be 0.75 and 1.76 respectively. Considering the analytical solution for the brick shape (which is the product of the analytical solutions for three infinite slabs of characteristic dimensions R, $ß_1R$ and $ß_2R$ respectively, of which the infinite rectangular rod is considered a special case where $ß_2 = \infty$), when $Bi = \infty$ and only the first term in the analytical solution for each of the three dimensions is significant, the analytical solution for the mass-average temperature (eqn (2.23) and 2.34) becomes:

$$Y_m = \left[\frac{2}{\zeta^2}\exp\left(-\zeta^2\frac{kt}{\rho c R^2}\right)\right]\left[\frac{2}{\zeta^2}\exp\left(-\zeta^2\frac{kt}{\rho c(\beta_1 R)^2}\right)\right]\left[\frac{2}{\zeta^2}\exp\left(-\zeta^2\frac{kt}{\rho c(\beta_2 R)^2}\right)\right] \quad (4.15)$$

where ζ is the first root of eqn (2.24). This simplifies to:

$$Y_m = \frac{8}{\zeta^6}\exp\left[-\zeta^2\left(1 + \frac{1}{\beta_1^2} + \frac{1}{\beta_2^2}\right)Fo\right] \quad (4.16)$$

Because by definition,

$$E = \frac{3\,\text{Slope}_{\text{brick}}}{\text{Slope}_{\text{sphere}}} \quad (4.17)$$

this implies,

$$E_{\infty} = \frac{3\zeta_1^2}{\alpha^2}\left(1 + \frac{1}{\beta_1^2} + \frac{1}{\beta_2^2}\right) \tag{4.18}$$

For $Bi = \infty$, $\zeta = \frac{\pi}{2}$ and $\alpha = \pi$. Hence,

$$E_{\infty} = 0.75 + \frac{0.75}{\beta_1^2} + \frac{0.75}{\beta_2^2} \tag{4.19}$$

Under the same assumptions, the analytical solution (eqn (2.26) and (2.34)) for a short cylinder ($\beta_1 = 1$) yields:

$$Y_m = \left[\frac{4}{\xi^2}\exp\left(-\xi^2\frac{kt}{\rho c R^2}\right)\right]\left[\frac{2}{\zeta^2}\exp\left(-\zeta^2\frac{kt}{\rho c(\beta_2 R)^2}\right)\right] \tag{4.20}$$

where ξ is the first root of eqn (2.27). This simplifies to:

$$Y_m = \frac{8}{\zeta^2\xi^2}\exp\left[-\left(\xi^2 + \frac{\zeta^2}{\beta_2^2}\right)Fo\right] \tag{4.21}$$

Because by definition,

$$E = \frac{3\,\text{Slope}_{\text{short cylinder}}}{\text{Slope}_{\text{sphere}}} \tag{4.22}$$

this implies

$$E_{\infty} = \frac{3}{\alpha^2}\left(\xi^2 + \frac{\zeta^2}{\beta_2^2}\right) \tag{4.23}$$

For $Bi = \infty$, $\xi = 2.4048$. Hence,

$$E_{\infty} = 1.76 + \frac{0.75}{\beta_2^2} \tag{4.24}$$

The analytical solution (eqn (2.26) and (2.34) for a squat cylinder ($\beta_1 = \beta_2$) suggests:

$$Y_m = \left[\frac{2}{\zeta^2}\exp\left(-\zeta^2\frac{kt}{\rho c R^2}\right)\right]\left[\frac{4}{\xi^2}\exp\left(-\xi^2\frac{kt}{\rho c(\beta_1 R)^2}\right)\right] \tag{4.25}$$

$$Y_m = \frac{8}{\zeta^2 \xi^2} \exp\left[-\left(\zeta^2 + \frac{\xi^2}{\beta_1^2} \right) Fo \right] \tag{4.26}$$

Because by definition,

$$E_\infty = \frac{3\ \text{Slope}_{\text{squat cylinder}}}{\text{Slope}_{\text{sphere}}} \tag{4.27}$$

this implies

$$E_\infty = \frac{3}{\alpha^2} \left(\zeta^2 + \frac{\xi^2}{\beta_1^2} \right) \tag{4.28}$$

Therefore,

$$E_\infty = 0.75 + \frac{1.76}{\beta_1^2} \tag{4.29}$$

Eqns (4.15), (4.24) and (4.29) are useful starting points, but in themselves may not be accurate across the ranges of Y covered if more than one term in the series solutions for any of the dimensions is significant. Based on eqns (4.15), (4.24) and (4.29) and using analogies to establish the ellipsoid case, preliminary empirical expressions for E_∞ were established:

For the infinite rectangular rod and rectangular brick:

$$E_\infty = 0.75 + \frac{0.75}{\beta_1^2} + \frac{0.75}{\beta_2^2} \tag{4.30}$$

For the finite cylinders and infinite ellipse:

$$E_\infty = 0.75 + \frac{1.01}{\beta_1^2} + \frac{0.75}{\beta_2^2} \tag{4.31}$$

For the oblate and prolate spheroids:

$$E_\infty = 0.75 + \frac{1.01}{\beta_1^2} + \frac{1.24}{\beta_2^2} \tag{4.32}$$

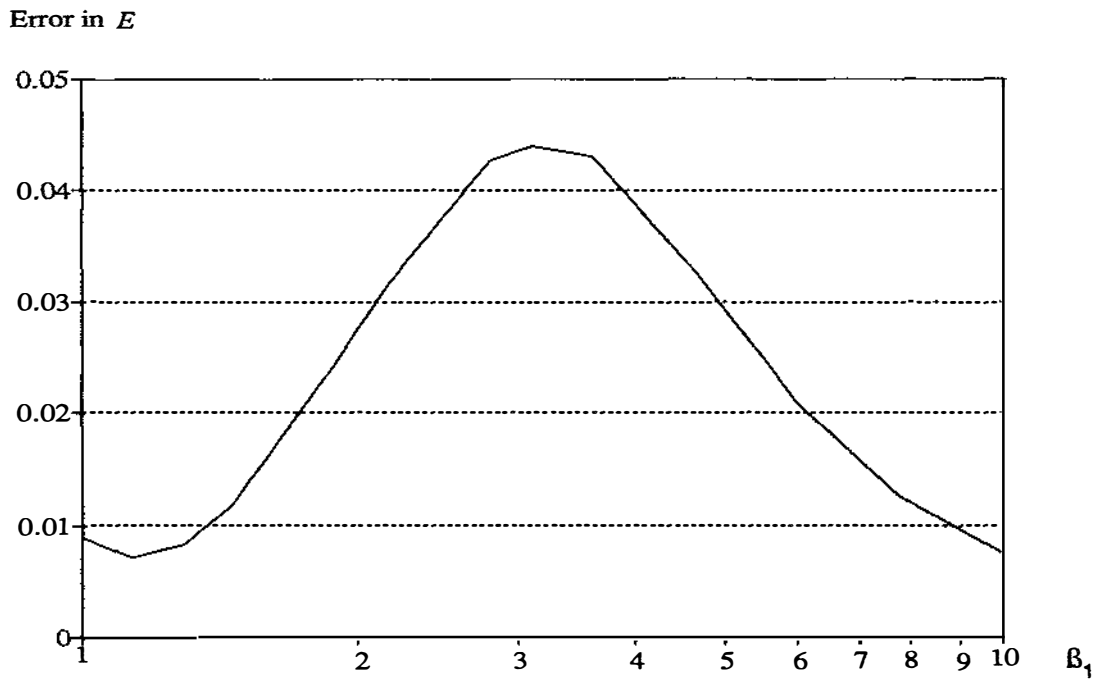

Figure 4.2 Plot of error arising from use of eqn. (4.30) vs log (β_1) for an infinite rectangular rod

The preliminary formulae were tested against the data at Bi = 100 generated by the computer programmes. Discrepancies were found for each shape. Figure 4.2 shows an example of the error that arises from the use of eqn (4.30) for the infinite rectangular rods. It was decided that a correction for this error should be included in the E_∞ formulae. The shape of the error follows the normal distribution function closely with a maximum value at about $\beta_1 = 3$ on a (log β_1) scale and even if β_1 is not put on a log scale the improvement possible was only slightly compromised. Therefore, for simplicity β_1 rather than (log β_1) was applied in regression of the coefficients of the correction function. Non-linear regression was carried out using a statistical package "BMDP" (Dixon *et al.* 1984) to find the parameters. These were then rounded slightly to achieve conveniently sized numbers, thus aiding calculation ease but reducing accuracy only slightly. The final correction factor was added to a generalised form of eqns (4.30) to (4.32):

$$E_\infty = 0.75 + P_1 f(\beta_1) + P_2 f(\beta_2) \tag{4.33}$$

$$f(\beta) = \frac{1}{\beta^2} - 0.01 P_3 \exp\left(\beta - \frac{\beta^2}{6}\right) \tag{4.34}$$

Values of P_1, P_2 and P_3 are stated in Table 4.1.

Table 4.1 Values of geometric parameter P_1 P_2 and P_3

SHAPE	P_1	P_2	P_3
Infinite slab ($ß_1 = ß_2 = \infty$)	0	0	0
Infinite rectangular rod ($ß_1 \geq 1$, $ß_2 = \infty$)	0.75	0	-1
Infinite ellipse ($ß_1 > 1$, $ß_2 = \infty$)	0.75	0	1
Ellipsoid ($ß_1 \geq 1$, $ß_2 \geq ß_1$, $ß_2 > 1$)	1.01	1.24	1
Brick ($ß_1 \geq 1$, $ß_2 \geq ß_1$)	0.75	0.75	-1
Infinite cylinder ($ß_1 = 1$, $ß_2 = \infty$)	1.01	0	0
Squat cylinder ($ß_1 = ß_2$, $ß_1 \geq 1$)	1.01	0.75	-1
Short cylinder ($ß_1 = 1$, $ß_2 \geq 1$)	1.01	0.75	-1
Sphere ($ß_1 = ß_2 = 1$)	1.01	1.24	0

4.5.1.3 Formulation of the Equivalent Heat Transfer Dimensionality at any Biot Number

A weighting function was then needed for finding E at any Bi from known E_0 and E_∞. Whilst studying freezing, McNabb *et al.* (1990) had tried a variational approach using a quadratic temperature approximation with position in a ellipsoid model. This had yielded:

$$E = \frac{Bi/2 + 1}{\dfrac{Bi/2}{1 + 1/ß_1^2 + 1/ß_2^2} + \dfrac{V}{AR}} \tag{4.35}$$

The basic form of this expression can be restated as:

$$E = \frac{Bi^1 + 2}{\dfrac{Bi^1}{E_\infty} + \dfrac{2}{E_0}} \tag{4.36}$$

This form of equation was adopted for chilling and the coefficients in the formula were

calculated by non-linear regression to best-fit all the data for regular (including elliptical and ellipsoidal) shapes. Finally the coefficients were adjusted to the nearest conveniently sized number to aid in hand calculations. This adjustment reduced accuracy only slightly. The resulting formula for E was:

$$E = \frac{Bi^{4/3} + 1.85}{\frac{Bi^{4/3}}{E_\infty} + \frac{1.85}{E_0}} \tag{4.37}$$

As stated earlier, it was assumed that E derived for the thermal centre applies universally within the object including the mass-average temperature/time history.

4.5.2 Formulation of the Lag Factor for the Thermal Centre, Denoted L_c

The approach taken was similar to that for deriving E, *i.e.*, to initially consider the values that L_c should take at the two limiting conditions, $Bi = 0$ and $Bi \rightarrow \infty$. These were denoted L_0 and L_∞ respectively. A Bi dependent weighting function would then be used to determine L_c at other Bi numbers.

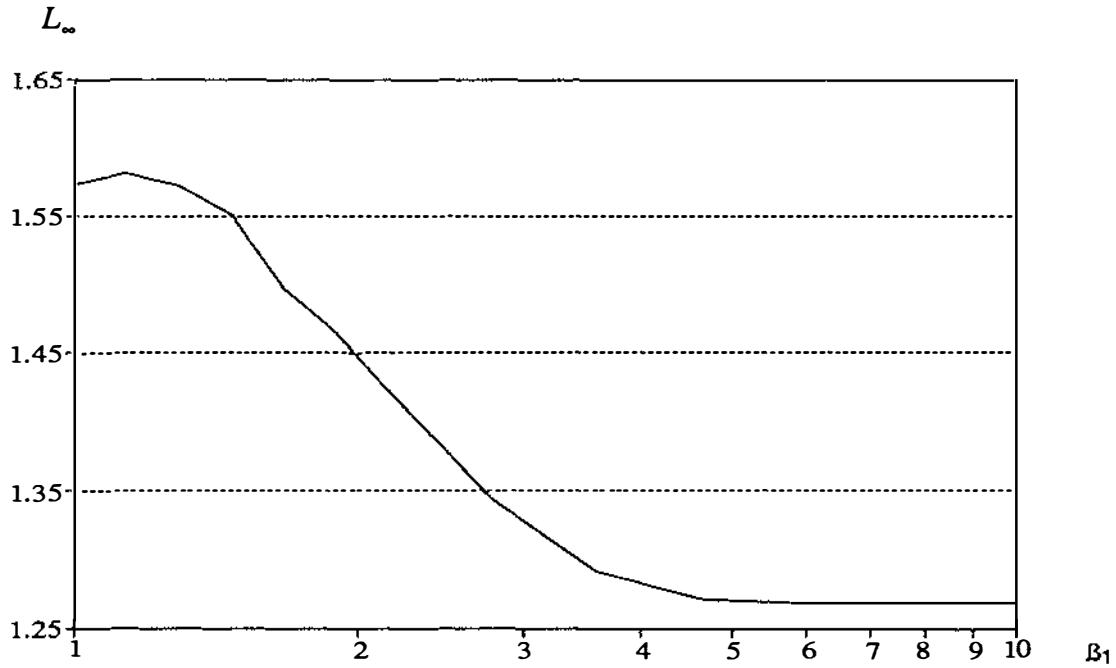

Figure 4.3. Plot of L_c vs log (β_1) for an infinite rectangular rod

4.5.2.1 Formulation of the Lag Factor at $Bi = 0$, Denoted L_0

Subject to the eight conditions stated in Chapter 3 and as $Bi \rightarrow 0$, the heat transfer conditions imply no internal temperature gradient within the object. When the analytical solutions are plotted they result in $L_0 = 1$ for all shapes.

4.5.2.2 Formulation of the Lag Factor at $Bi \rightarrow \infty$, Denoted L_∞

Using the computer-generated data set, the values of L_∞ (assumed to be close to L_c at $Bi = 100$) for the infinite slab, infinite cylinder and sphere were found to be 1.271, 1.576 and 2.001 respectively. Expressions for L_∞ for other shapes were determined empirically. Figure 4.3 shows an example of the shape of L_∞ vs β_1, which approximates a normal distribution function with a maximum value at about $\beta_1 = 1.1$ on a ($\log \beta_1$) scale. However, accuracy was again slightly compromised for simplicity. β_1 rather than ($\log \beta_1$) was applied in regression of the coefficients of the L_∞ expression. Non-linear regression was carried out using the statistical package "BMDP" and a uniform equation applicable to all shapes sought. The resultant expression, chosen as compromise between accuracy and arithmetic complexity from a large set of trial and error analyses was:

$$L_\infty = 1.271 + 0.305 \exp(0.172\gamma_1 - 0.115\gamma_1^2) + 0.425 \exp(0.09\gamma_2 - 0.128\gamma_2^2) \quad (4.38)$$

Values of γ_1 and γ_2 are given in Table 4.2.

4.5.2.3 Formulation of the Lag Factor at any Biot Number

The same mathematical form for the weighting factor as had been used for E was adopted and the coefficients in the formula were determined by non-linear regression using all data for the regular (including elliptical and ellipsoidal) shapes. The results were rounded slightly to aid in hand calculations. This adjustment reduced accuracy only slightly. The resulting formula for L_c was therefore:

Table 4.2 Values of geometric parameters γ_1, γ_2 and λ

SHAPE	N	γ_1	γ_2	λ
Infinite slab ($\beta_1 = \beta_2 = \infty$)	1	∞	∞	1
Infinite rectangular rod ($\beta_1 \geq 1$, $\beta_2 = \infty$)	2	$4\beta_1/\pi$	∞	γ_1
Infinite ellipse ($\beta_1 > 1$, $\beta_2 = \infty$)	2	β_1	∞	γ_1
Ellipsoid ($\beta_1 \geq 1$, $\beta_2 \geq \beta_1$, $\beta_2 > 1$)	3	β_1	β_2	γ_1
Brick ($\beta_1 \geq 1$, $\beta_2 \geq \beta_1$)	3	$4\beta_1/\pi$	$1.5\beta_2$	γ_1
Infinite cylinder ($\beta_1 = 1$, $\beta_2 = \infty$)	2	1	∞	1
Squat cylinder ($\beta_1 = \beta_2$, $\beta_1 \geq 1$)	3	$1.225\beta_1$	$1.225\beta_2$	γ_1
Short cylinder ($\beta_1 = 1$, $\beta_2 \geq 1$)	3	β_1	$1.5\beta_2$	γ_1
Sphere ($\beta_1 = \beta_2 = 1$)	3	1	1	1

$$L_c = \frac{Bi^{1.35} + \dfrac{1}{\lambda}}{\dfrac{Bi^{1.35}}{L_\infty} + \dfrac{1}{\lambda}} \tag{4.39}$$

Values of λ are stated in Table 4.2.

4.5.3 Formulation of the Lag Factor for the Mass-Average Temperature, Denoted L_m

The approach taken for L_m was to apply a modifier to L_c. This was determined by a non-linear regression analysis with coefficient rounding. A variety of expressions were tested, but that adopted as a compromise between accuracy and complexity was:

$$L_m = \mu L_c \tag{4.40}$$

where

$$\mu = [(1.5 + 0.69\,Bi) / (1.5 + Bi)]^N \quad (4.41)$$

Where N is the number of dimensions of an object. Values of N are stated in Table 4.2.

4.6 Testing the New Formulae for Regular Shapes

The chilling times for the thermal centre (t_c) and for the mass-average condition (t_m) predicted by the proposed empirical method were tested against their analytical or numerical counterparts. The calculated percentage errors in the times to reach certain thermal centre and mass-average temperatures are presented in Tables 4.3 and 4.4 for regular geometric shapes. The range of the percentage errors for the mass-average temperatures are larger than for the centre temperatures because the slopes of the plots such as Figure 4.1 are slightly different (this was ignored in the above analysis which used centre temperatures only to develop equations for E).

4.7 Comparison with Existing Chilling Time Prediction Methods

Methods similar in principle to the proposed method have been developed for chilling time prediction (Baehr 1953, Rutov 1958, Smith *et al.* 1967, Fikiin & Fikiina 1971 and Cleland & Earle 1982). Over 256 experimental tests Fikiin had found that his method was accurate within 9.1% compared to 10.3% for the Rutov method and 12.8% for the Baehr method. The accuracy of Cleland & Earle's method was assessed by the authors for a wide range of regular and irregular shapes, and for a variety of cooling conditions. The 95% confidence bounds compared to analytical solutions were ±12%. The proposed method is accurate within 7.6% of analytical solutions at the 95% level of confidence for the worst cases, which compares favourably with the other methods. Experiments were conducted by Smith and co-workers to test the validity of using the geometry index G in predicting internal temperature for the ellipsoidal model and irregular shapes. The results covered only a restricted range of conditions but suggested that the prediction method uncertainty was small compared to error in the experiments and in thermal property data, yet no concrete statistical figures were given.

TABLE 4.3 Percentage errors in predicted chilling times to selected thermal centre temperatures ($1 \leq \beta \leq 4$, $0.1 \leq Bi \leq 10$, $0.05 \leq Y_c \leq 0.55$).

Shape	mean	std deviation	95% Confidence Interval	
Infinite rectangular rods	0.3	1.7	-2.9	3.4
Bricks	-1.7	2.2	-7.6	1.7
Short cylinders	-1.3	2.1	-6.7	1.3
Squat cylinders	0.7	2.5	-4.3	5.6
Infinite ellipses	1.8	2.3	-1.7	6.2
Oblate spheroids	1.6	3.2	-5.4	7.6
Prolate spheroids	0.7	2.2	-4.6	4.1

TABLE 4.4 Percentage errors in predicted chilling times to selected mass-average temperatures. ($1 \leq \beta \leq 4$, $0.1 \leq Bi \leq 10$, Y_m corresponding to $0.05 \leq Y_c \leq 0.55$)

Shape	mean	std deviation	95% Confidence Interval	
Infinite rectangular rods	0.0	3.5	-5.7	7.1
Bricks	1.7	3.1	-2.6	7.5
Short cylinders	-3.6	2.4	-9.4	0.0
Squat cylinders	1.4	4.4	-5.5	9.2
Infinite ellipses	0.3	3.4	-9.4	6.1
Oblate spheroids	2.1	3.5	-3.5	8.7
Prolate spheroids	-1.7	2.5	-8.3	2.0

A full comparison between all the methods based on the same data base was not easily possible. Details of experimental data were not available at this stage so comparative tests could not be performed. However, sample comparisons were carried out for

1) a sphere comparing against the analytical solutions at various Bi values;
2) a brick comparing against the analytical solutions at various Bi values;
3) an ellipse comparing against the analytical solutions at $Bi = \infty$;
4) an oblate spheroid comparing against the numerical solution at various Bi values.

In making comparisons to other methods, only the predicted times for thermal centre positions were compared because some of the above methods are applicable only to thermal centres. The times calculated and percentage differences are shown in Table 4.5, in which the proposed method compares favourably to the other methods. The method of Smith *et al.* performs best when $Bi \rightarrow \infty$. The other previous methods do best when Bi $\rightarrow$ 0. The proposed new method performs well over full Bi range. Besides its accuracy, the advantages in using the new method include:

1. applicability to both thermal centre and mass-average temperatures, whereas the approaches of Baehr, Rutov, Fikiin & Fikiina and Cleland & Earle apply to only the thermal centre temperature/time history;
2. applicability to all geometric shapes, whereas the approach of Baehr applies to only geometries to which the analytical solutions (Carslaw & Jaeger 1959 and Newman 1936) apply. Rutov's and Fikiin & Fikiina's methods must incorporate particular shape factors to deal with irregular geometries;
3. absence of alignment charts, whereas the approaches of Baehr, Smith *et al.* and Cleland & Earle rely on graphic aids which introduce interpretation errors.

4.8 Summary of the Proposed Method

The complete procedure for application of the proposed method for regularly shaped geometries is as following:

1. Evaluation of the surface heat transfer coefficient (h);

2. Evaluation of the thermal properties of the object;

3. Evaluation of the object dimensions (D_1, D_2 and D_3) using the definitions in Section 4.3;

4. Calculation of characteristic dimension R and two dimensional ratios (β_1 and β_2) using eqns (4.5), (4.6) and (4.7) respectively;

5. Calculation of the Biot number (Bi) using eqn (2.21);

6. Calculation of the equivalent heat transfer dimensionality at $Bi = 0$ (E_0) using eqns (4.12), (4.13) or (4.14) according to the geometric shape of the object;

7. Calculation of the equivalent heat transfer dimensionality at $Bi = \infty$ (E_∞) using eqn (4.33);

8. Calculation of the equivalent heat transfer dimensionality (E) using eqn (4.37);

9. Calculation of the lag factor at $Bi = \infty$ (L_∞) using eqn (4.38);

10. Calculation of the alternative dimensional ratio (λ) using the expression given in Table 4.1;

11a. Calculation of the lag factor for thermal centre positions (L_c) using eqn (4.39);

11b. Calculation of the lag factor for mass-average situations (L_m) using eqn (4.40) (this step is required only for calculations related to mass-average conditions);

12. Calculation of the first root of the transcendental equation for a sphere (α) using eqn (2.29);

13. Calculation of the chilling time (t_c or t_m) or temperature reached (T_c or T_m):
For thermal centre:

$$T_c = L_c \exp\left(-\frac{k E t_c \alpha^2}{3 \rho c R^2}\right)(T_i - T_a) + T_a \tag{4.42}$$

or

$$t_c = \frac{3 \rho c R^2}{\alpha^2 k E} \ln\left(\frac{T_i - T_a}{T_c - T_a} L_c\right) \tag{4.43}$$

For mass-average:

$$T_m = L_m \exp\left(-\frac{k E t_c \alpha^2}{3 \rho c R^2}\right)(T_i - T_a) + T_a \tag{4.44}$$

or

$$t_m = \frac{3 \rho c R^2}{\alpha^2 k E} \ln\left(\frac{T_i - T_a}{T_m - T_a} L_m\right) \tag{4.45}$$

14. Checking of the range of fractional unaccomplished temperature change (Y) using eqns (2.19) and (2.20). If $Y_c > 0.7$ or $Y_m > 0.55$, results calculated using the prediction method are unreliable since the method is only valid for $0 < Y_c \leq 0.7$ and $0 < Y_m \leq 0.55$.

Although computer programmes and graphical aids are not essential for implementing the proposed method, they are desirable for the sake of ease. A computer programme called "CHILL" which runs under the "Micro-Soft Windows" environment on a IBM-compatible personal computer (286 or better) was developed. Also 21 alignment charts were plotted. Therefore, three ways to implement the new method are available:

i) using only mathematical formulae with the aid of an ordinary hand calculator;

ii) using alignment charts for finding the shape factor combined with a small number of mathematical formulae; and

iii) using a computer programme specifically designed for implementing the method.

A description of the proposed method and the computer programme "CHILL" including all the charts are given in Appendix A.

TABLE 4.5 Percentage Differences in redicted Times for Different Empirical Methods Against Analytical (#) or Numerical (*) Solutions (ρ = 1000 kg/m^3, c = 3740 J/kg K, k = 0.42 W/m K, T_i = 25°C, T_a = 2°C, T_c = 4°C and D_1 = 0.025 m, N/A = conditions for whichmethod does not apply or method application is difficult)

Shape	*Bi*	Chilling Time (s)	Baehr	Rutov	Smith *et al.*	Fikiin & Fikiina	Cleland & Earle	Proposed
Sphere	0.01	114642#	0.0	-7.6	-2.9	-0.9	-1.0	-0.4
	0.1	11682#	0.6	-5.6	-4.7	0.7	-1.6	-0.3
	1	1513#	-0.1	0.7	-3.4	4.5	0.8	1.7
	10	536#	0.2	11.6	-1.3	4.9	3.0	-0.2
	100	451#	-2.0	-1.6	-7.5	2.0	3.8	0.0
Brick $\beta_1 = \beta_2 = 2$	0.01	170767#	1.9	-4.2	N/A	-0.2	1.8	0.4
	0.1	18408#	0.3	-7.1	32.3	-4.1	7.3	-2.2
	1	3038#	8.8	-20.9	14.5	-22.0	5.5	1.2
	10	1385#	0.0	-33.6	-9.6	-39.1	-5.0	-0.5
	100	1207#	-2.5	-36.5	-15.8	-42.8	-11.8	-1.2
Ellipse $\beta_1 = 2$	∞	1127#	N/A	N/A	-4.3	-22.5	-18.9	4.3
Ellipsoid $\beta_1 = \beta_2 = 2$	0.01	164550*	N/A	-7.0	N/A	-1.4	2.6	-0.8
	0.1	17240*	N/A	-7.3	21.9	-2.5	12.3	-1.6
	1	2520*	N/A	-10.6	10.4	-10.4	22.1	5.6
	10	1066*	N/A	-18.8	1.1	-24.7	17.6	3.0
	100	925*	N/A	-24.1	0.8	-28.9	15.1	1.8

5. EXPERIMENTAL PROCEDURE AND DATA COLLECTION

In Chapter 4 the accuracy of the proposed method for regular shapes was illustrated. In Chapter 5 the methods used to collect data so that the method could be tested for two- and three-dimensional irregular shapes are described.

5.1 The Equipment

To test the newly proposed general empirical method for chilling time prediction at different Biot numbers, large variations of the surface heat transfer coefficient around a sample object were desirable. For this reason both an air environmental tunnel and a calcium chloride brine immersion tank were used. They are shown diagrammatically in Figure 5.1 and 5.2 respectively.

In the air tunnel, the fans circulate air around. The air passes over the refrigeration coil and then through the first mesh screen (aperture size 2 mm × 2 mm). The air then flows through the experimental section (2.0 m × 1.2 m × 1.1 m) and the second mesh screen (aperture size 3 mm × 3 mm). The mesh screens provide sufficient presure loss to equalise any unevenness in the air flow profile. The air velocity was set at a fixed value of approximately 2 m s^{-1} for all runs.

In the brine tank, the impeller circulates 29% calcium chloride brine around. The brine passes over the refrigeration coil and then through the experimental section (0.75 m × 0.45 m × 0.70 m). Liquid immersion gives much less variation of the surface heat transfer coefficient and ambient temperature around an object than an air cooling system.

To ensure that sample object orientation within the flow stream did not affect uniformity of surface conditions (thus minimising variation of the surface heat transfer coefficient over a sample object), it was found necessary to rotate or oscillate the object. The sample rotator, which is shown in Figure 5.3, was used for tests in the brine tank. The thermocouples were connected to the Squirrel data logger which was positioned above and rotated with the sample. One cycle length was 30 seconds approximately.

The sample oscillator, which is shown in Figure 5.4 and 5.5, was applied when the thermocouples were connected to the "FIX" Data Acquisition and Control System that is static. In this system, each sample was turned through an angle of 300° about every 30 seconds.

5.2 Experimental Error

A typical experiment involved measuring temperature/time history under carefully controlled chilling conditions. Some lack of agreement is inevitable whenever any chilling time prediction method is compared with experimental chilling data. This discrepancy may arise from one of several sources:

1) uncertainty in thermal property data for the food material undergoing the chilling process;
2) experimental error; that is ,imprecise knowledge and control of the chilling conditions (initial sample temperature, cooling medium temperature and surface heat transfer coefficient), and the sample geometric arrangement; and
3) imprecisions arising from assumptions made in the derivation of the prediction method.

Thermal property uncertainty depends on the material used for the experiments and is discussed later.

The first source of experimental error is that arising from imperfect control of experimental conditions. Ideally, variables are controlled to pre-set values, but control error exists within each run, so the same pre-set value is not achieved in all similar runs. The extent of the control error can be measured from the variability of replicate runs for the same nominal experimental conditions.

The second source of experimental error is that arising from imprecise knowledge of the experimental conditions. Uncertainty arises as a difference between the measured value of a parameter and the true value. The uncertainty can be reduced by using the mean of replicate determinations, but measurements are susceptible to systematic errors which replicate determinations will not discern. Systematic error cannot be easily

quantified and can only be minimised by ensuring that the measurement techniques used are valid and accurate. Sources of systematic error include: unwanted edge heat transfer, instrument calibration errors and heterogeneities in the sample material due to the presence of thermocouple wire and possibly air voids.

In order to assess as independently as possible the magnitude of the third source of inaccuracy (prediction method weakness), the aim of any experimental procedure or technique is to keep experimental errors randomly distributed and small in size.

5.3 Choice of Chilling Material

The material used for chilling experimentation should preferably:

1) be homogeneous;
2) have accurately known, relatively constant thermal properties throughout the entire chilling temperature domain;
3) give reproducible results;
4) be easy to use;
5) be able to be used repetitively; and
6) be cheap.

Food materials are rarely themselves homogeneous. Each sample life is relatively short due to microbial spoilage. Their thermal properties are difficult to measure or estimate precisely. For these reasons analogue materials have been commonly applied (Riedel 1960, Lentz 1961, Smith *et al.* 1967, Geuze *et al.* 1972, Badari Narayana & Krishna Murthy 1975, Albin *et al.* 1979). Developed by Riedel (1960), "Karlsruhe test substance" is probably the most successful and widely used. It is now commonly referred to by its trade name as "Tylose". It is a defined 23% (w/w) methylcellulose gel. Tylose has well characterised thermal properties similar to those of many high moisture foods (Cleland 1977). Because of its gel nature Tylose is easily formed to different desired shapes and is homogeneous once equilibration has occurred. It can be used repetitively for experiments without deterioration. For these reasons most of the experimental work was done with Tylose.

The gel was formed by mixing of the Tylose powder with water. In spite of best effort to avoid them, some air voids occurred in the final samples. Air bubbles within the gel were small (< 1 mm in diameter) and evenly distributed. The volume of air entrainment was very difficult to evaluate, but it was estimated as less than 0.5% of the total gel volume. The gel was not homogeneous initially but it was observed that the water content of the gel equilibrated within a period of several days leading to a close to homogeneous material. Errors in measuring components led to a moisture content of 76.9 ± 0.2% in the final gel. It was consider that the errors in making the gel, which would affect the thermal properties, due to heterogeneity and moisture content variation are small, and they would tend to be random between samples rather than systematic.

Uniform contact of the experimental material to the internal surface of the moulds used for various shapes is important because the surface conductance, and thus the surface heat transfer coefficient is affected by uniformity of the contact. Contact onto a surface can be assessed by breaking the contact and examining the surface. It is difficult to exclude air pockets totally to obtain perfect contact to the surface. Contact was found to be better than 95% for the cases examined and gaps were randomly distributed. Variations in quality of contact would tend to affect the total random error.

The density, specific heat capacity and thermal conductivity data were obtained from a recent unpublished research report of the Meat Industry Research Institute of New Zealand. These were of unknown accuracy, but they were best data available, and had been measured with good quality equipment.

TABLE 5.1 Thermal Properties of Chilling Test Materials

Material		ρ (kg m^{-3})	k (W $m^{-1}K^{-1}$)	c (J $kg^{-1}K^{-1}$)
Tylose	(0°C to 30°C)	1028	0.500	3784
Cheddar cheese	(-5°C to 20°C)	1055	0.306	3598

Because of its low rigidity, the Tylose gel can only be shaped into various geometries using moulds. Therefore it was not chosen for experimentation with the three-dimensional irregular shaped geometries with curved surfaces especially concave surfaces, for which the moulds would be difficult to design and costly to make. Cheddar cheese, a real food of high homogeneity and isotropy, was chosen as an alternative test material. It meets criteria 1 to 4 stated in Section 5.3. It can be reused several times before it become mildewed, but is more expensive than Tylose. One of the advantages of using Cheddar cheese is that it can be easily cut into any desirable shapes, and into small pieces.

Again, the specific heat capacity and thermal conductivity data were obtained from the unpublished research report of the Meat Industry Research Institute of New Zealand. The density data were obtained from Wood (1978). All thermal data used are given in Table 5.1. These are mean values across the temperature ranges used.

5.4 Temperature Measurement and Control

All temperature measurements were made with 24 gauge (SWG) copper/constantan thermocouples (0.5 mm wire diameter, 0.9 mm diameter including plastic insulation) connected to either a 1200 Series Squirrel meter/logger, or a "FIX" Data Acquisition and Control System on a 60 to 240 second record cycle, installed in the laboratory where measurements were made. Both of these devices were calibrated with the above thermocouple wire to within 0.3°C in the range of -50°C to 50°C. No detectable difference in temperatures measured by the two different devices was found.

Prior to chilling, the sample objects of Tylose or Cheddar cheese were kept in constant temperature rooms for long enough to attain a uniform temperature throughout. To reduce the variation in initial temperature during the time from removal of sample objects from the constant temperature rooms to the onset of chilling, the object were insulated. The objects were put in a insulated container or a cardboard box filled with polystyrene foam chips. The sample container was left in the same room as the sample object during the tempering process. Although the delays during sample transfer were

as long as 10 to 15 minutes, under these conditions the maximum measured difference in the initial temperature of the objects from the mean value was found to be ±1.0°C.

The ambient cooling medium was either air in the environmental tunnel or 29% calcium chloride brine held in the insulated tank. In the air case the temperature was measured by three thermocouples placed around the sample object, and in the brine case the temperature was measured by two thermocouples; one prior to and one after the experimental section. The difference between these two or three thermocouples was generally not greater than ±0.1°C.

The temperature of the air in the environmental tunnel was controlled by a Danfoss evaporator pressure regulating valve controller, and the temperature of the brine in the tank was controlled by a thermostat with a differential of ±0.1°C. In both cases the change in the cooling medium temperature was almost always less than 0.2°C on either side of the mean value throughout the entire chilling process.

The overall error in temperature measurement and control was estimated at less than ±0.5°C.

5.5 Chilling of Two-Dimensional Irregular Shapes

5.5.1 The Test Samples

The criteria set by Cleland (1985) for choosing experimental shapes from virtually infinite possibilities were to be able to:

1) accurately control and describe the shapes;
2) control and measure the surface heat transfer coefficient; and
3) prevent heat transfer in the third dimension.

Six polyvinyl chloride plastic (PVC) moulds constructed by Cleland *et al.* (1987a) were still available and were used. A further mould was constructed from 0.50 m length of corrugated galvanized steel sheet to see the affect of concavity on heat

transfer. The cross-sections of the four quasi-elliptical cylinders are given in Figure 5.6 to 5.9 (codes E_a, E_b, E_c and E_d), and those of the three highly irregular shapes in Figure 5.10 to 5.12 (codes I_a, I_b and I_c). To reduce end heat transfer effects in order to simulate an infinite geometry, polystyrene foam insulation caps of at least 0.08 m were put on the end of each shape in the manner shown in Figure 5.13.

The moulds were filled with Tylose from one end to a mid-point of their height. Thermocouples were then positioned at five or six points at this central level. This was done by drilling small holes in the mould wall just large enough for a thermocouple lead. By inserting the copper and constantan leads through separate holes and reconnecting, then tensioning them with the sample as shown in Figure 5.14, the thermocouple junction was accurately positioned. The thermocouple leads were held in place and the holes in the mould walls were sealed with small amount of Ados Contact Adhesive. Packing of the sample with Tylose was then completed and the polystyrene foam end caps were placed in position. The locations of the thermocouples for each shape are indicated on Figure 5.6 to 5.12. Each sample object could then be clamped in to the sample holder as shown in Figure 5.4, and chilled.

5.5.2 Dimension Measurement and Control

Because of the rigidity of PVC and steel moulds, no significant variation in shape or size was found during chilling processes. There was some variation in the cross-sectional shape of each mould along its length. Cross-sectional profiles from each end of the mould had been drawn and averaged by Cleland (1985) to estimate the final shape and size for six of the moulds (Figure 5.6 to 5.11) as accurately as possible. The same procedure was followed to decide the cross-sectional shape of the newly constructed steel mould (Figure 5.12). Variations from the mean shape along the sample length were less than ± 1.0 mm in dimensions and less than 1% in perimeter and cross-sectional area.

The characteristic dimension for the irregular shapes is defined as half the minimum thickness measured through the thermal centre. The position of the thermal

centre was found by analysis using the finite element method FEM (Cleland *et al.* 1986b) for typical chilling conditions. For all the shapes it was found that only one thermal centre existed, (because the surface heat transfer conditions were uniform and the geometries used were relatively uniform in shape).

5.5.3 Measurement and Control of Surface Heat Transfer Coefficients

For irregular shapes studied there were no satisfactory methods to estimate the surface heat transfer coefficient directly from experiments for each shape. The two-dimensional shapes E_a, E_b, E_c, E_d, I_a and I_b had been made by remoulding of PVC cylinders. Surface heat transfer coefficients were determined for cylinders of the PVC that were still cylindrical. As long as the heat transfer environmental conditions are equivalent at all parts of the surface and the PVC wall thickness is constant over the whole surface, then the surface heat transfer coefficient would be expected to be approximately the same as that for the equivalent PVC cylinder. A cylinder was constructed from a 0.50 m length of galvanized steel sheet to be used as the equivalent cylinder for shape I_c. Rotation or oscillation of the test samples ensured that the surface heat transfer condition was approximately uniform on all surfaces of all the sample objects. The wall thickness was the same for the irregular shapes as for the equivalent cylinders and did not vary significantly at different locations on the surface of the irregular shapes. Cleland (1985) found that variation in PVC wall thickness due to stretching during the moulding process had negligible effect on heat transfer. For the steel, because the wall thickness was only 20 to 25% of that of PVC and of higher thermal conductivity, variation in wall thickness due to changes in the degree of curvature of the steel had little effect on heat transfer resistance.

Separate chilling experiments with the equivalent PVC or steel sheet cylinder were used to estimate the surface heat transfer coefficient h for the two-dimensional irregular shapes. Four methods were available for measuring h:

1) a finite difference approximation method;
2) a heat balance method;

3) the Goodman plot (which is not applicable for cylindrical geometries);

4) the heat penetration method (Arce & Seat 1980).

The first three of these have been discussed in detail by Cleland & Earle (1976). Cleland (1977) concluded that the difference between the results from the three methods was not significant at the 99% level of confidence. The fourth method was used. For infinite cylinders, when $Y_c < 0.7$, the analytical solution for heat conduction without phase change, subject to the third kind of boundary condition, for constant thermal properties (Carslaw & Jaeger 1959) is closely approximated by taking only the first term in the series solution. The h value can be calculated from the slope of a plot of ln Y_c vs t (Charm 1963, Baker & Charm 1969, Kopelman *et al.* 1970). Cleland (1985) found that by using the centre temperature the effect of any variation in heat transfer conditions at the surface was effectively averaged and the h value was as truly representative of the true value as possible. A computer programme was written that used an iterative procedure to find the best-fit h value to give the right cooling rate. An advantage of this method is that it is independent of the exact location of the thermocouple within the cylinder. If the centre thermocouple is not precisely positioned on the central axis, this does not affect the estimation of h. Of the various thermocouples nominally at the centre position, the best estimate of the centre temperature was assumed to be the thermocouple that was slowest to change towards the ambient temperature.

To achieve wide ranges of h and thus greater variation of Bi, both air and brine immersion chilling were adopted, and a sheet of plastic foam of 4 mm thick was also glued to the outside of each cylinder for certain experimental runs. The plastic foam gave a uniform additional resistance to heat transfer over the whole cylinder. The plastic foam was cut accurately to avoid gaps at the joint. The contact adhesive used gave extremely good contact between plastic foam sheet and the mould wall, and between the both ends of the plastic foam sheet at the joint with no air spaces so that heat transfer through the plastic foam layer was uniform. Separate estimates of the surface heat transfer coefficient were made for each combination of cylinder material, wall thickness and presence of a foam plastic layer.

Chilling was carried out with the ambient medium (air or brine) temperature between 0.0°C and 2.0°C and the fluid velocity around the tunnel or the tank kept constant. Variation of the transport properties of air or brine during the experiments was small and therefore the film heat transfer coefficient would not be affected by errors from this source.

To determine h for the nine different combinations (the PVC cylinder of 5 mm wall thickness, the PVC cylinder of 4 mm wall thickness, the steel cylinder of 1 mm wall thickness, each chilled by both air and brine, and these three moulds plus a layer of 4 mm sheet plastic foam chilled by air), a total of 37 runs were made. The experimental conditions are reported in Table 5.2 which shows good repeatability of the replicates. The uncertainty in the mean values of h for the nine situations had 95% confidence bounds between 1.6% and 9.7%.

5.5.4 Analysis of Heat Transfer in Two-Dimensional Irregular Shapes

Cleland (1977) found that heat transfer effect of the voids in the Tylose was negligibly small for infinite cylinders. Cleland (1985) concluded that experiments for two-dimensional irregular shapes are subject to the same error to those for infinite cylinders and consequently the effect of the voids were similarly insignificant.

In the present work, the curved surfaces of both the irregular shapes and the cylinder gave effectively the same problem with voids and imperfect thermal contact at the surface. Tylose packing conditions and the occurrence and distribution of the surface voids were very similar in both cases. Therefore it was concluded that the effect of these factors were the same for the irregular shapes as for the cylinder shapes so that the estimated surface heat transfer coefficients were still representative.

It was discovered by Cleland (1985) that error in thermocouple placement was not a major source of uncertainty due to the way the leads were positioned and held in place. By dismantling of the sample objects, no detectable displacement of the thermocouple junctions from the recorded position was found over a number of runs.

The method used to insert the thermocouples did lead to errors due to heat conduction along the wires as they were not introduced along isothermal paths. Typically, four thermocouples were used to measure internal temperatures for each sample. Only one of these was located in close proximity to the thermal centre. Because all but one of the four thermocouples were positioned well away from the thermal centre and the sample volume and surface areas were large, the effect of heat conduction along the thermocouple was considered insignificant. Only 0.02% to 0.03% of the surface area within the central 100 mm length of the moulds was affected by the introduction of the thermocouple wire through the walls. This is very small.

The lengths of the sample objects were always greater than the second longest dimension by a factor of at least three, and insulating caps were used to minimise the effect of heat transfer along the length of the irregular shapes. The results of Cleland *et al.* (1994) suggested that the end-effect heat transfer would be negligibly small in these circumstances.

Ideally, the effect of the heat capacity of the plastic foam insulation and also of the mould wall materials should be zero. Cleland (1985), who used two layers of 2 mm rubber sheet as insulation, found that the heat given up by the rubber and the PVC wall material was less than 3.0% of the total heat transfer to each cylinder. Only one layer of plastic foam of 4 mm, which has lower volumetric heat capacity, was used in current research. Therefore, it was expected that less heat was given up by the insulating layer. By comparison of several types of packaging material, Cleland *et al.* (1994) concluded that low density materials such as insulting foam would be ideal provided that they were not crushed. The quality of plastic foam insulation was carefully maintained under laboratory conditions. Furthermore, the estimate of surface heat transfer coefficient to the Tylose surface was determined in such a way that only heat lost from the Tylose and transferred through the insulating layers was taken into account. Hence the main effect of heat release from the plastic foam and mould wall material would only be to distort to some extent the measured Tylose surface temperature early in the chilling process when the plastic foam and wall temperatures were changing most.

5.6 Chilling of Three-Dimensional Irregular Shapes

5.6.1 The Test Samples

Nine different three-dimensional objects were investigated (Figure 5.15). They were divided into three groups according to their geometric configurations. (1) Irregular shapes S_a, S_b, S_c and S_d were quasi-ellipsoids, each of which was close to uniform in shape; (2) Frustum of the square pyramid I_p is relatively uniform in shape; (3) Shapes I_q, I_r, I_s and I_t were highly irregular, and I_q and I_t had concave surfaces.

The pyramid-shaped mould I_p was constructed by Cleland (1987a) from polypropylene plastic sheet (5 mm thick) with all the joints screwed together (Figure 5.16❷). The presence of the screws altered the heat transfer resistance of less than 0.4% of the surface area. The effect of this was assumed to be insignificant and the corner assumed to approximate closely to the ideal type of joint shown in Figure 5.16❶. The box had a bolt attached to the lid to hold it onto the sample rotator or oscillator. The face furthest from the geometric centre was chosen to be the lid. This surface has the least effect on heat transfer in the shape and the bolt affected less than 0.1% the total surface area, so the effect of the bolt was assumed insignificant.

To provide information about heat transfer environmental conditions, three similar sized rectangular bricks, also constructed from polypropylene plastic sheet in exactly the same manner as that applied for the pyramid shape, were used. All these shapes had a bolt attached through a flange to allow connection to the sample rotator or oscillator. Each plastic mould was filled with Tylose. Thermocouples were introduced to various pre-determined points in a similar fashion to that used for two dimensional irregular shapes. Holes were drilled in the plastic for the individual copper or constantan wire leads. The wires were joined and tensioned in the appropriate position in the shapes and the holes sealed by Ados Contact Adhesive. Six thermocouples; two on the surface and four situated internally, were used for each shape. One thermocouple was always located as close as possible to the thermal centre. The geometric centre could be easily found for the pyramid and bricks.

Cheddar cheese was used as the test material (Section 5.3) for constructing the other eight irregular shapes. Cheese was cut into the different shapes using a knife. To avoid evaporation, the surfaces of each cheese sample were cover with a layer of "Glad Wrap" plastic film which adhered to the surface very well so as to ensure minimum air entrainment and thus minimum effect on heat transfer. To provide information about heat transfer environmental conditions, seven similar sized rectangular bricks, also constructed from Cheddar cheese in exactly the same manner as that applied for the irregular cheese samples, were used. They were also carefully covered with the "Glad Wrap" plastic film. Therefore similar air entrainment could be expected and the surface heat transfer conditions were realistically reproduced. Thermocouples were introduced to each of the cheese samples. Small diameter holes were drilled in the cheese for inserting the thermocouples into the appropriate position in the shapes. Five or six thermocouples, all situated internally, were used for each shape. Two or three thermocouples were placed approximately at the thermal centre, which for a homogeneous object is also the centre of gravity. The sample object was hung in turn in three different directions which were perpendicular to one another. Each of the perpendicular planes was marked as a contour line on the surface of the sample. The point of intersection of these three planes deep inside the sample was assumed to be the thermal centre. The weight of the fibreglass wire used to hang the sample was insignificant compared with that of the sample itself. Nevertheless this method for marking the contour lines and drilling thermocouple holes did introduce some error.

A steel net basket was used to hang the cheese samples from the rotator or the oscillator (Figure 5.5). The air tunnel was used except for the case of the pyramid shape which was tested in both the air tunnel and the brine tank.

5.6.2 Dimension Measurement and Control

The pyramid shape was flat sided and could be accurately measured. For each of the eight Cheddar cheese samples, the measurements of the three cross-sections, which went through the thermal centre, between each pair of points where the contour lines coincided were taken as the three geometric dimensions defined in Section 4.3

using a Vernier calliper. The characteristic dimension for each shape was calculated by halving the shortest dimension. The measurements were taken immediately prior to and after chilling processes and, in the case of the cheese samples, after dissection. No detectable differences were found between readings. The error in determining the geometric dimensions was considered to be less than ±2 mm for all the three-dimensional irregular shapes.

5.6.3 Measurement and Control of Surface Heat Transfer Coefficients

The polypropylene pyramid was identical in all respects to the polypropylene rectangular bricks used for finding the surface heat transfer coefficient except for the irregularities in shape. Both air and brine immersion chilling were applied, and for certain experimental runs, a sheet of plastic foam of 4 mm thick were glued to the outside of the pyramid in exactly the way as that used for the two-dimensional irregular shapes. For long chilling times the analytical solution (Carslaw & Jaeger 1959) is closely approximated by taking only the first term in the series solution. To determine h for the pyramid shape without a layer of sheet plastic foam chilled in the air environmental tunnel, six runs using three differently shaped bricks without the plastic foam layer were made in the air tunnel. The results are shown in Table 5.3. The uncertainty in the mean value of h at the 95% level of confidence was ±5.3%. Both the sample and the bricks were rotated or oscillated in a similar manner. The h values for the other two conditions (the pyramid with plastic foam insulation chilled in the air environmental tunnel and the pyramid without insulation foam chilled in the brine tank) were back-calculated from a summation of known individual heat transfer resistances from runs with two-dimensional shapes, rather than directly measured.

Only the air environmental tunnel was used for experimentation of the Cheddar cheese samples. Bi was altered by using sample objects of different characteristic dimensions. The surface heat transfer coefficient for these shapes cannot be measured directly without substantial difficulty. Hence the seven analogous rectangular bricks constructed from the same kind of cheese were used. Seven separate chilling runs, one for each brick, were undertaken. The results are shown in Table 5.4. The differences

between runs were considered to be largely due to experimental error. The error in the average value determined by the spread of h values was ±3.4% at the 95% level of confidence. It was assumed that the h value determined in this way accurately represented h for the three-dimensional irregular cheese samples covered by one layer of Glad Wrap film and put in the net basket.

5.6.4 Analysis of Heat Transfer in Three-Dimensional Irregular Shapes

Source of error for the three-dimensional irregular shapes were similar in some ways to those for the two-dimensional irregular shapes. Problems with voids in Tylose, inhomogeneity due to thermocouple wires and heat conduction along thermocouple wires were similar to those for the two-dimensional irregular shapes. Errors in placement of thermocouples for the pyramid shape were consider also considered similar in magnitude to those for the two-dimensional irregular shapes, but were considered larger for the Cheddar cheese samples, because (1) some objects were smaller in size; and (2) the actual thermocouple placement could not be seen (blind operation). All the cheese samples were dissected and the centre-thermocouple were found located generally within 3 mm from the pre-determined thermal centre (Section 5.5.1), which is about 10% of the radius in error for the worst cases (samples I_s and I_v).

The nature of a three-dimensional object means that end heat transfer effects were not a problem. However, the pyramid shape was affected by the presence of a bolt inserted through the wall. As was the case for the two dimensional irregular shapes, the presence of this bolt was assumed to be insignificant, and the volume of the plastic foam coating and box wall material for the pyramid was sufficiently small compared with the volume of the Tylose frustum of square pyramid itself to make the effect of the heat released by the plastic foam and wall material unimportant. Disruptions due to the presence of the basket may have affected heat transfer. The proportion of the surface area affected by the steel wires was very small and the thermal resistance the steel wires introduced was also very small compared with the film resistance. Any effect of the basket was probably taken into account in the value of h since it was also used for chilling the cheese bricks. Therefore its effect on heat transfer was considered minor.

Imperfect contact was a similar problem for the pyramid shape to that which occured for the two dimensional shapes. This problem was less significant for the cheese samples because the contact between the surfaces of cheese and the Glad Wrap film could be seen and regularly checked. Overlapping of the plastic film was carefully avoided. As before, it was considered that the effect of imperfect contact was equally frequent for all cheese sample objects and randomly distributed over the surface so that the effect on surface or overall heat transfer was not significant. It would contribute to the random error.

5.6.5 Summary

In total sixteen two- and three-dimensional irregularly shaped samples were used in experiments. Those samples were made of either Tylose gel or Cheddar cheese. Two pieces of equipment, an air tunnel and a brine immersion tank, were used. Both sample dimensions and pertinent temperatures were measured and controlled under carefully maintained laboratory conditions. Sources and magnitudes of experimental error have been discussed. The technique used for measurement and control surface heat transfer coefficients has been described in detail. Overall, it was considered that the methods used would lead to data of good quality.

Table 5.2 Experimental Conditions for Heat transfer Coefficient Measurements for Cylinders

Shape Code & Run Number	D_1 (m)	T_a (°C)	T_i (°C)	h (W $m^{-2}K^{-1}$)
average for samples with foam in the air tunnel, corresponding to E_a1, E_b1, E_b2, E_b3 and I_a1				5.6
C_a1	0.15	0.4	32.1	5.7
C_a2	0.15	0.1	32.3	5.6
C_a3	0.15	0.5	32.4	5.5
C_a4	0.15	0.7	30.7	5.7
average for samples without foam in the air tunnel, corresponding to E_a2, E_a3, E_a4, E_b4, I_a2, I_a3 and I_a4				14.5
C_a5	0.15	0.7	32.6	14.3
C_a6	0.15	0.4	32.4	13.6
C_a7	0.15	0.5	31.8	15.1
C_a8	0.15	0.5	32.6	15.0
average for samples in the brine tank, corresponding to E_a5, E_b5 and I_a5				35.4
C_a9	0.15	0.6	32.9	38.3
C_a10	0.15	0.7	31.8	35.4
C_a11	0.15	0.7	32.5	35.6
C_a12	0.15	0.5	32.6	32.2

...continued

Table 5.2 continued...

Shape Code & Run Number	D_1 (m)	T_a (°C)	T_i (°C)	h (W m^{-2}K^{-1})
mean for samples with foam in the air tunnel, corresponding to E_c1, E_d1, I_b0 and I_b1				6.3
C_b1	0.10	0.4	32.7	6.1
C_b2	0.10	0.5	32.0	6.5
C_b3	0.10	0.4	32.9	6.3
C_b4	0.10	0.2	32.1	6.3
mean for samples without foam in the air tunnel, corresponding to E_c2, E_d2 and I_b2				16.0
C_b5	0.10	0.4	30.9	16.2
C_b6	0.10	0.5	31.5	16.1
C_b7	0.10	0.5	31.9	15.3
C_b8	0.10	0.5	32.2	16.6
mean for samples in the brine tank, corresponding to E_c3, E_c4, E_c5, E_d3, E_d3, E_d5, E_d6, E_d7, I_b3, I_b4 and I_b5				36.2
C_b9	0.10	0.5	32.4	38.3
C_b10	0.10	0.3	31.7	35.6
C_b11	0.10	0.2	32.3	34.2
C_b12	0.10	0.8	31.6	36.7

...continued

Table 5.2 continued...

Shape Code & Run Number	D_1 (m)	T_a (°C)	T_i (°C)	h (W m^{-2}K^{-1})
mean for samples with foam in the air tunnel, corresponding to I_c2, I_c2 and I_c3				6.9
C_c0	0.15	0.3	32.2	7.0
C_c1	0.15	0.2	32.9	6.9
C_c2	0.15	0.3	33.2	6.9
C_c3	0.15	-0.1	32.6	6.9
C_c4	0.15	0.5	33.1	7.1
mean for samples without foam in the air tunnel, corresponding to I_c4				20.3
C_c5	0.15	0.5	32.5	21.4
C_c6	0.15	0.4	32.9	20.2
C_c7	0.15	0.4	34.0	20.0
C_c8	0.15	0.4	32.4	19.5
mean for samples in the brine tank, corresponding to I_c4				149.6
C_c9	0.15	0.4	29.3	148.0
C_c10	0.15	0.9	30.1	152.3
C_c11	0.15	0.6	29.3	147.9
C_c12	0.15	0.6	33.6	150.2

Table 5.3 Experimental Conditions for Heat Transfer Coefficient Measurements for Tylose Bricks

Shape Code & Run Number	$D_1 \times D_2 \times D_3$ (mm^3)	T_a (°C)	T_i (°C)	h ($W\ m^{-2}K^{-1}$)
B_a21	104×125×152	0.7	31.8	17.4
B_a22	104×125×152	0.2	31.2	16.9
B_a23	104×125×152	0.3	31.3	19.0
B_b21	81×151×151	1.3	31.8	17.3
B_c21	54×127×201	1.3	31.5	18.1
B_c22	54×127×201	0.3	30.9	16.6
mean				17.2

Table 5.4 Experimental Conditions for Heat Transfer Coefficient Measurements for Cheddar Cheese Bricks

Shape Code & Run Number	$D_1 \times D_2 \times D_3$ (mm^3)	T_a (°C)	T_i (°C)	h ($W\ m^{-2}K^{-1}$)
B_f	50×60×140	-5.4	18.2	24.0
B_g	50×70×121	-5.3	17.9	24.4
B_h	50×80×110	-5.4	18.2	26.9
B_i	112×122×155	-4.6	17.2	25.2
B_j	100×112×183	-4.5	18.6	24.3
B_k	100×141×181	-4.4	14.1	25.6
B_l	120×150×182	-5.3	13.5	24.7
mean				25.0

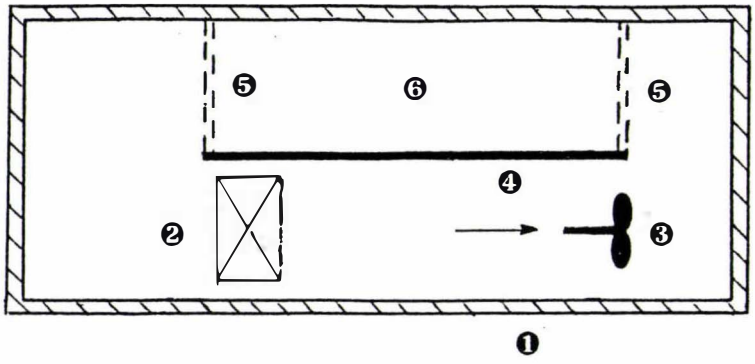

Figure 5.1 Schematic diagram of the air environmental tunnel
❶ - insulated wall, ❷ - cooling coils, ❸ - fan to circulate air,
❹ - baffle plate, ❺ - mesh screens, ❻ - experimental section

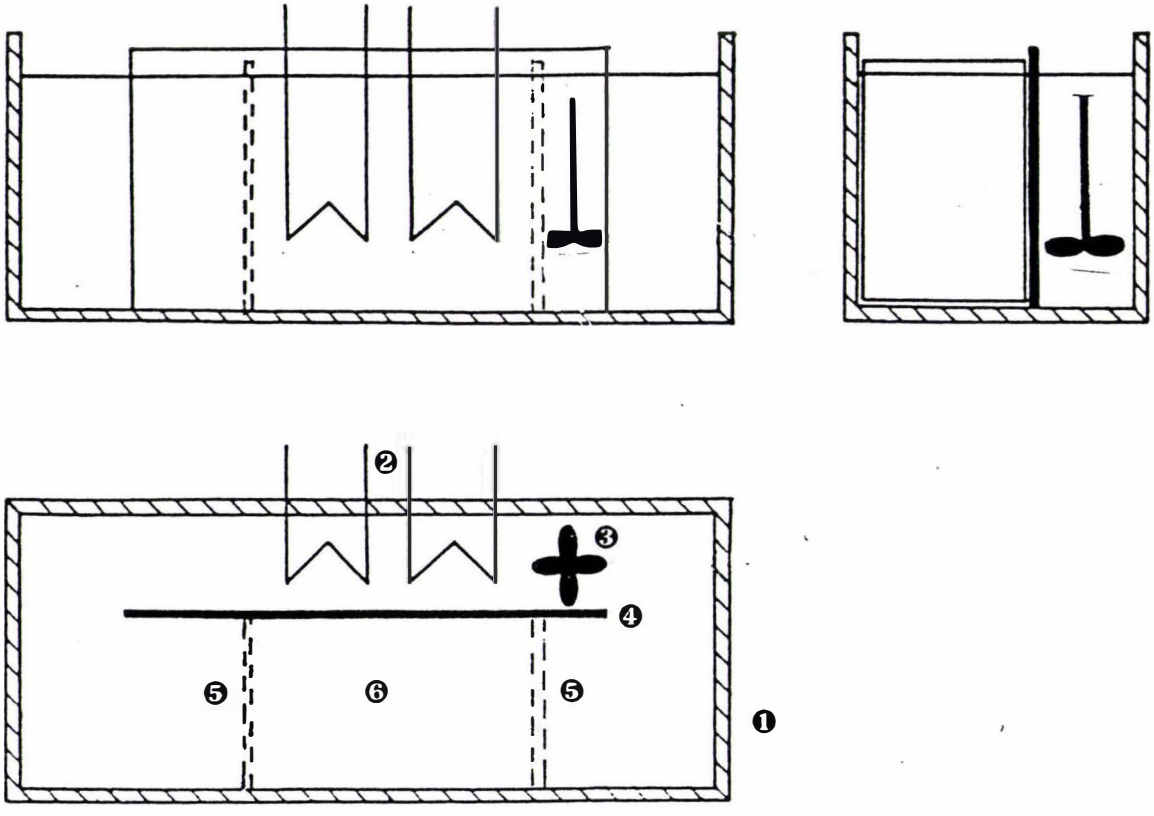

Figure 5.2 Schematic diagram of the brine immersion tank
❶ - insulated tank, ❷ - cooling coils, ❸ - Impeller to circulate brine,
❹ - baffle plate, ❺ - mesh screens, ❻ - experimental section

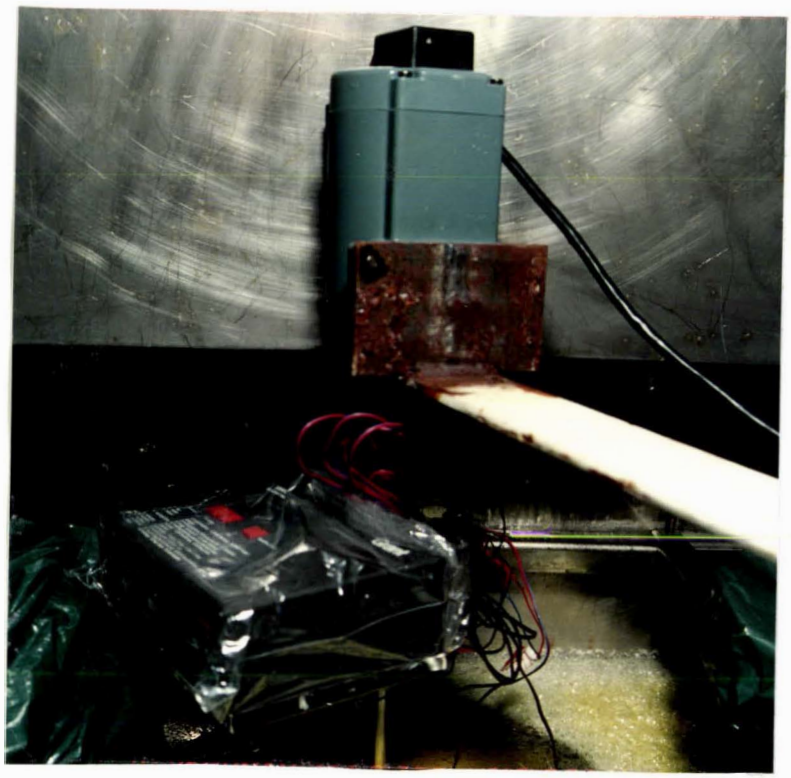

Figure 5.3 The sample rotator used in the brine immersion tank

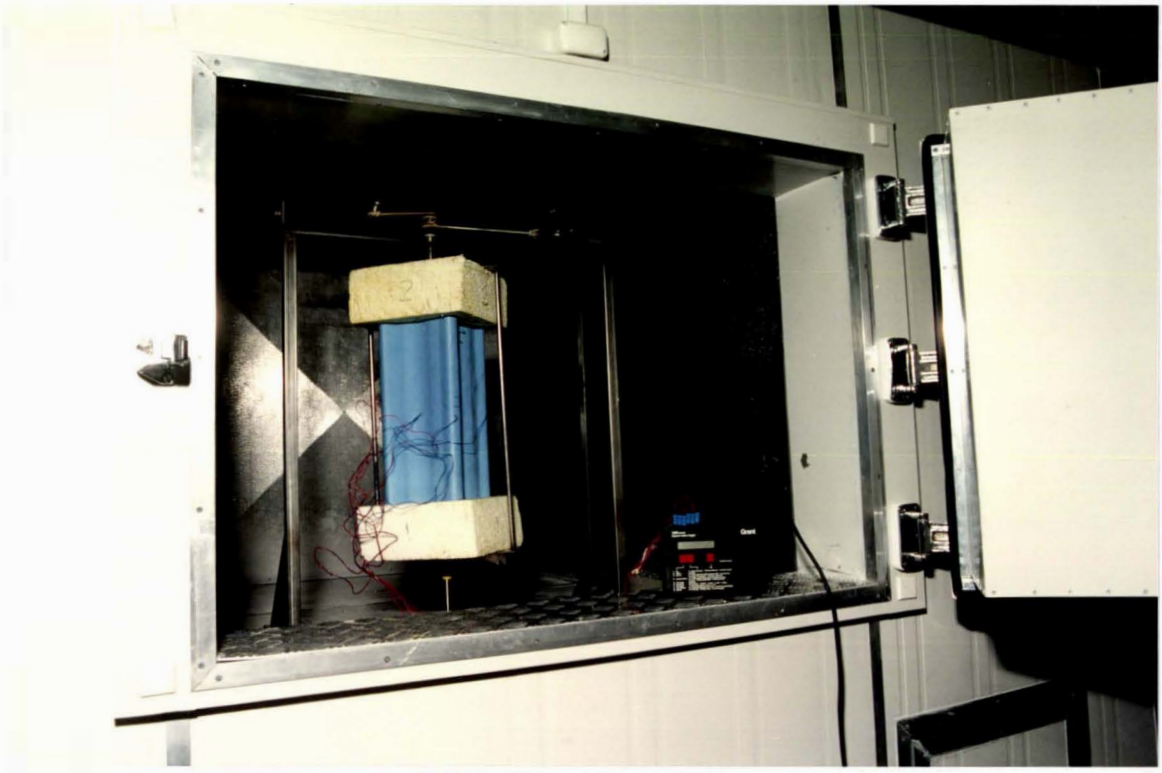

Figure 5.4 The sample oscillator and the two-dimensional irregularly shaped sample I_c used in the air environmental tunnel

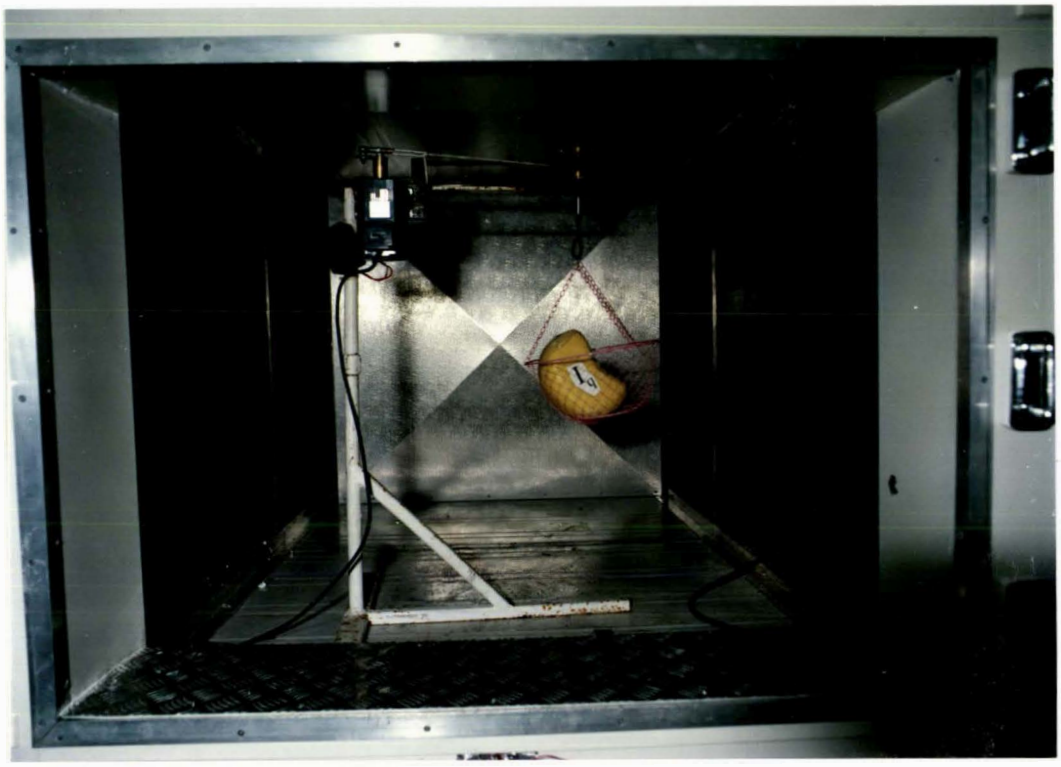

Figure 5.5 The sample oscillator and the three-dimensional irregularly shaped sample I_q used in the air tunnel

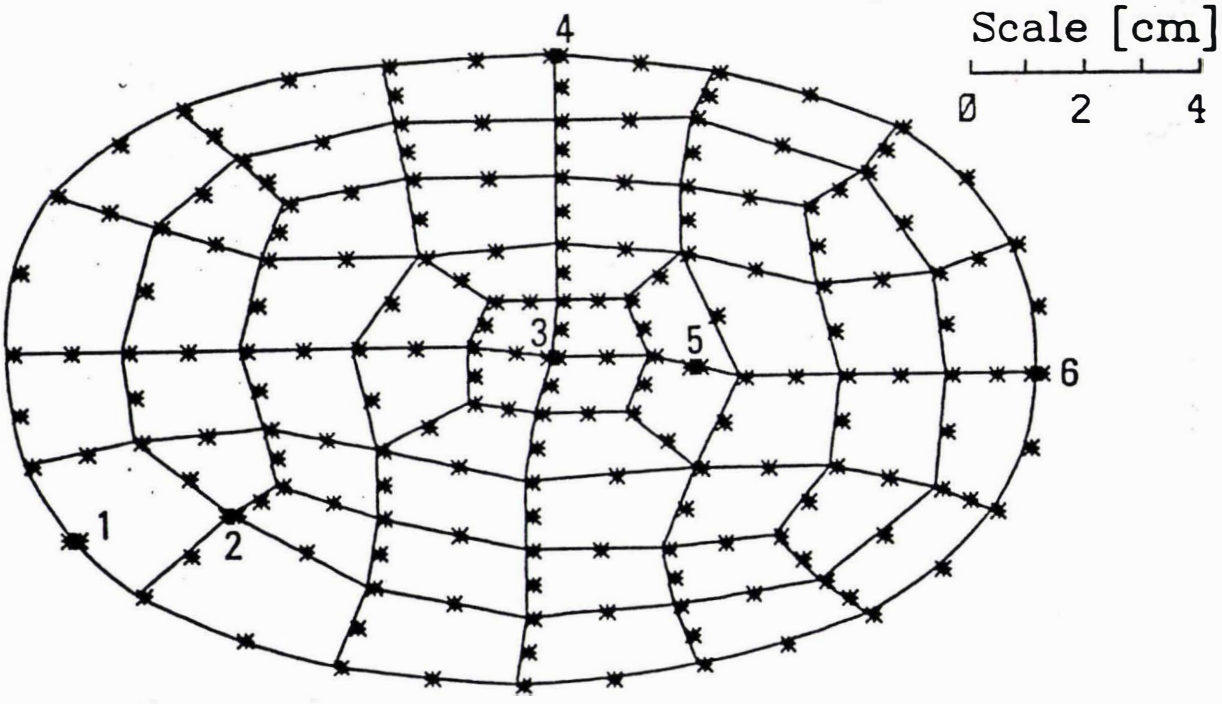

Figure 5.6 Cross-section and finite element method grid for the two-dimensional irregularly shaped sample E_a. * - nodes, ** - nodes corresponding to thermocouples positions, — - element boundaries

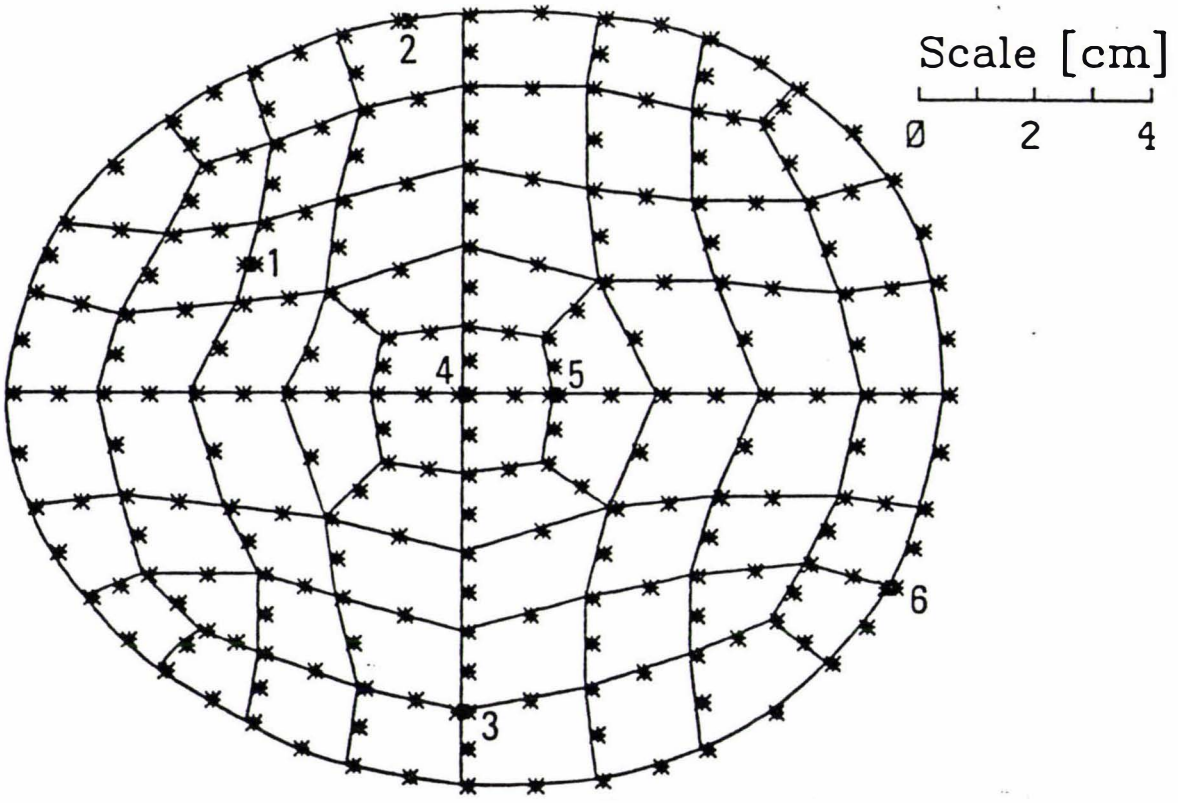

Figure 5.7 Cross-section and finite element method grid for the two-dimensional irregularly shaped sample E_b. * - nodes, ** - nodes corresponding to thermocouples positions, — - element boundaries

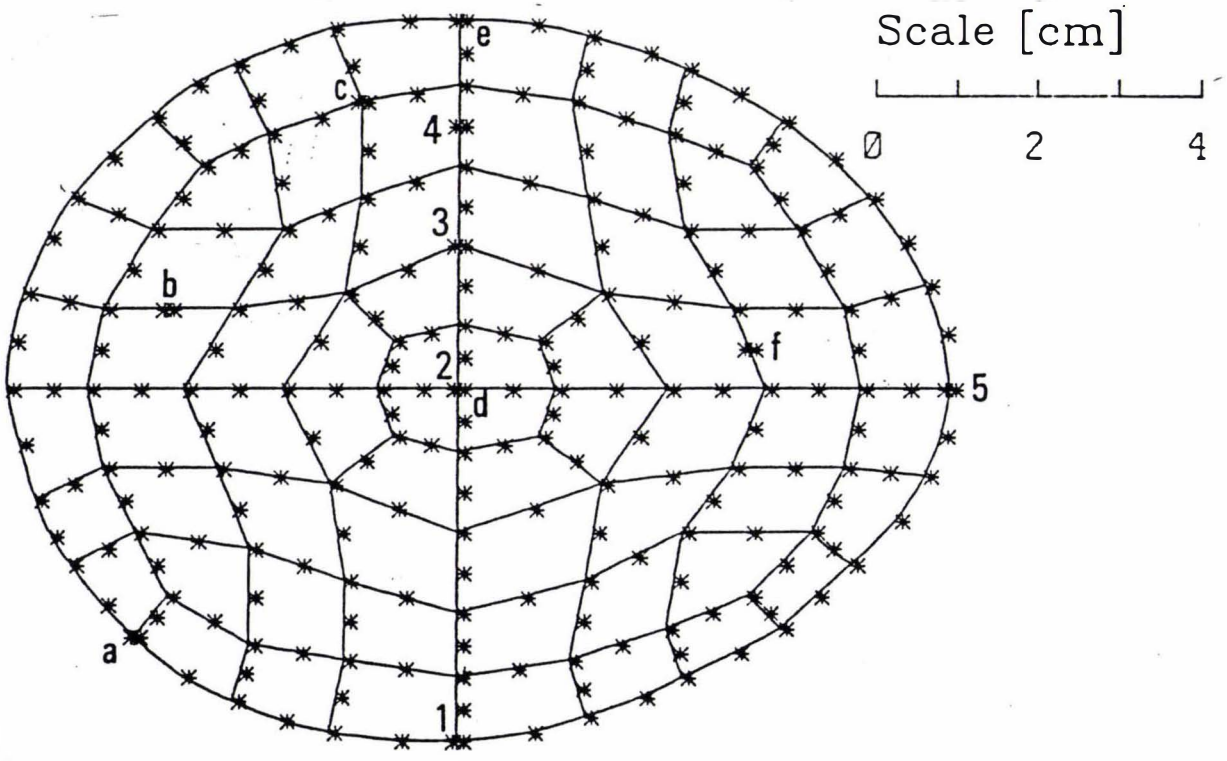

Figure 5.8 Cross-section and finite element method grid for the two-dimensional irregularly shaped sample E_c. * - nodes, ** - nodes corresponding to thermocouples positions, — - element boundaries

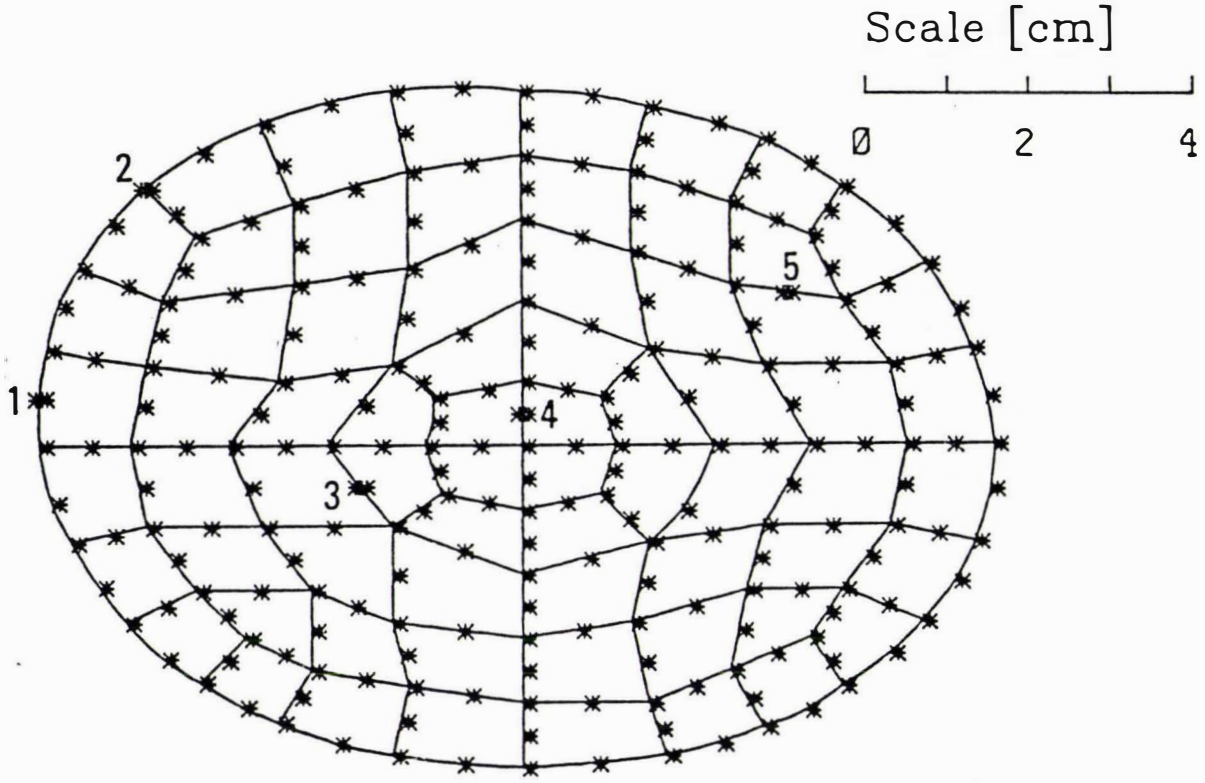

Figure 5.9 Cross-section and finite element method grid for the two-dimensional irregularly shaped sample E_d. * - nodes, ** - nodes corresponding to thermocouples positions, — - element boundaries

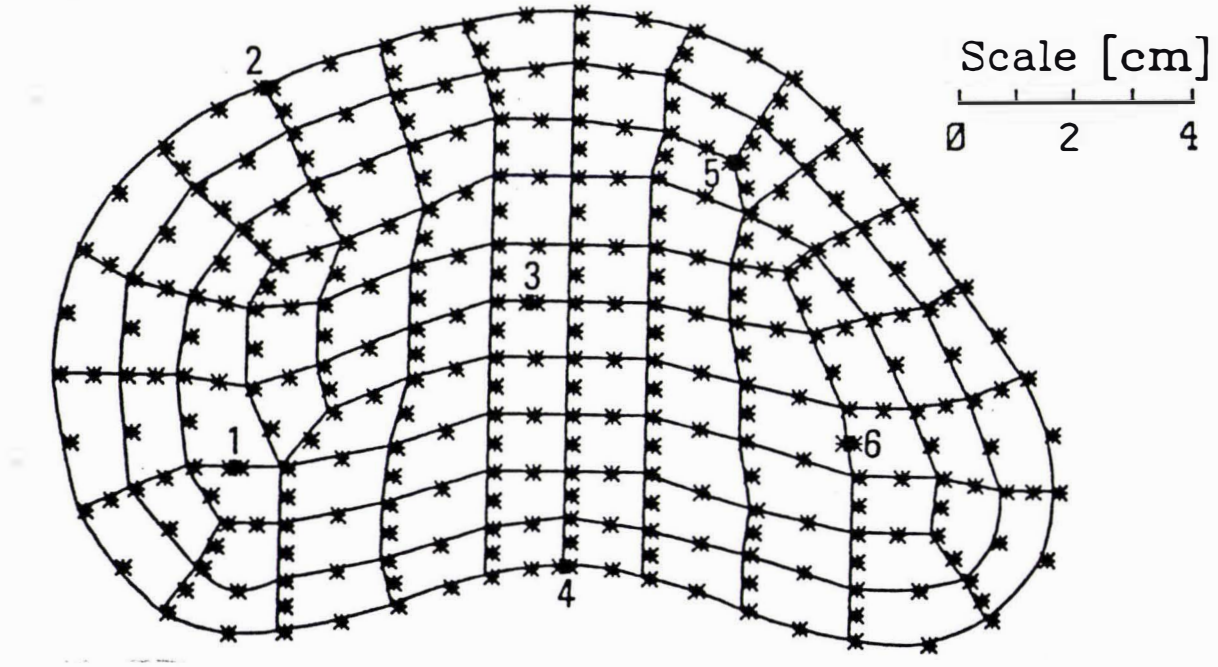

Figure 5.10 Cross-section and finite element method grid for the two-dimensional irregularly shaped sample I_a. * - nodes, ** - nodes corresponding to thermocouples positions, — - element boundaries

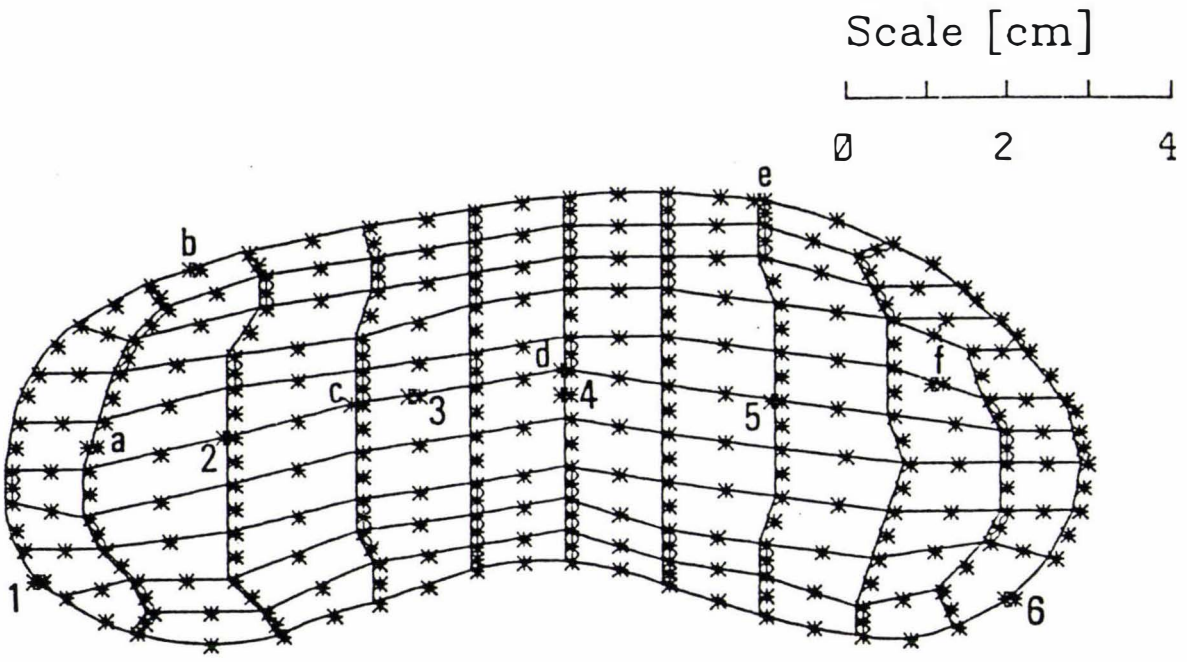

Figure 5.11 Cross-section and finite element method grid for the two-dimensional irregularly shaped sample I_b. * - nodes, ** - nodes corresponding to thermocouples positions, — - element boundaries

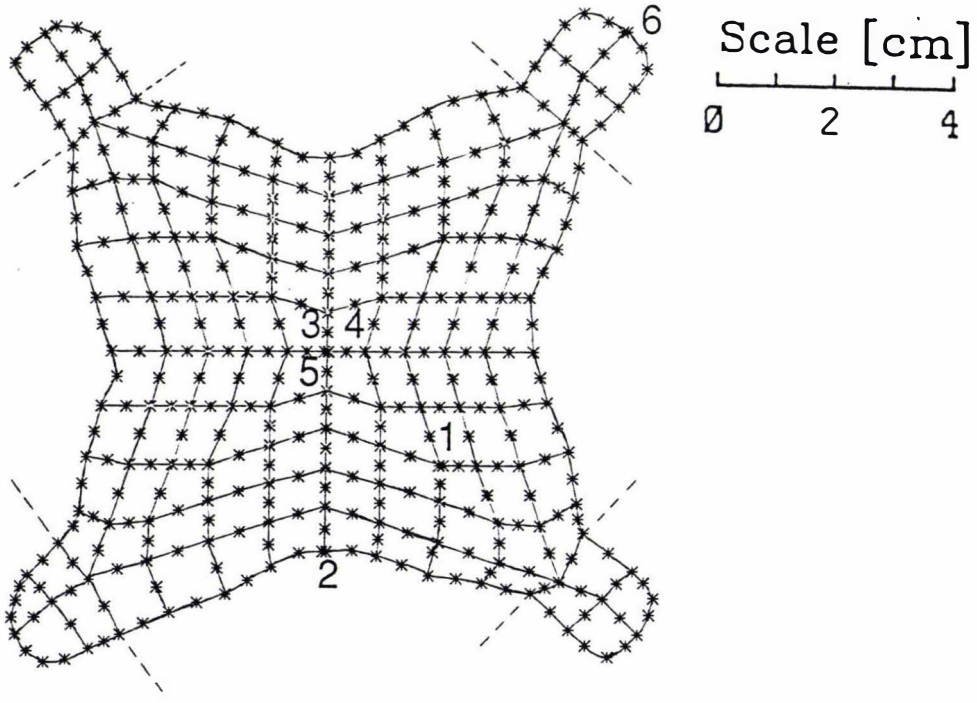

Figure 5.12 Cross-section and finite element method grid for the two-dimensional irregularly shaped sample I_c. * - nodes, ** - nodes corresponding to thermocouples positions, — - element boundaries, --- - protrusion excision

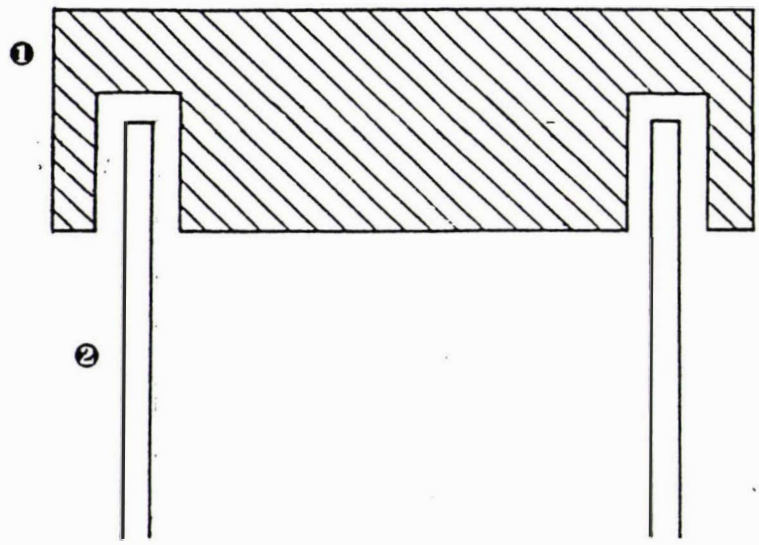

Figure 5.13 Schematic diagram showing the arrangement of the polystyrene foam caps for two-dimensional samples
❶ - polystyrene Foam Cap, ❷ - PVC mould wall

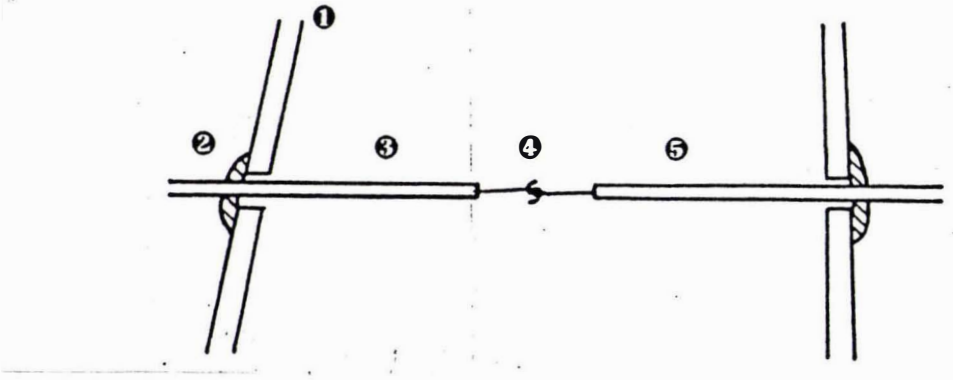

Figure 5.14 Schematic diagram showing the method of thermocouple insertion and position within the moulded multi-dimensional samples (not to scale)
❶ - mould wall, ❷ - Ados Contact Adhesive, ❸ - insulated constantan lead, ❹ - thermocouple junction, ❺ - insulated copper lead

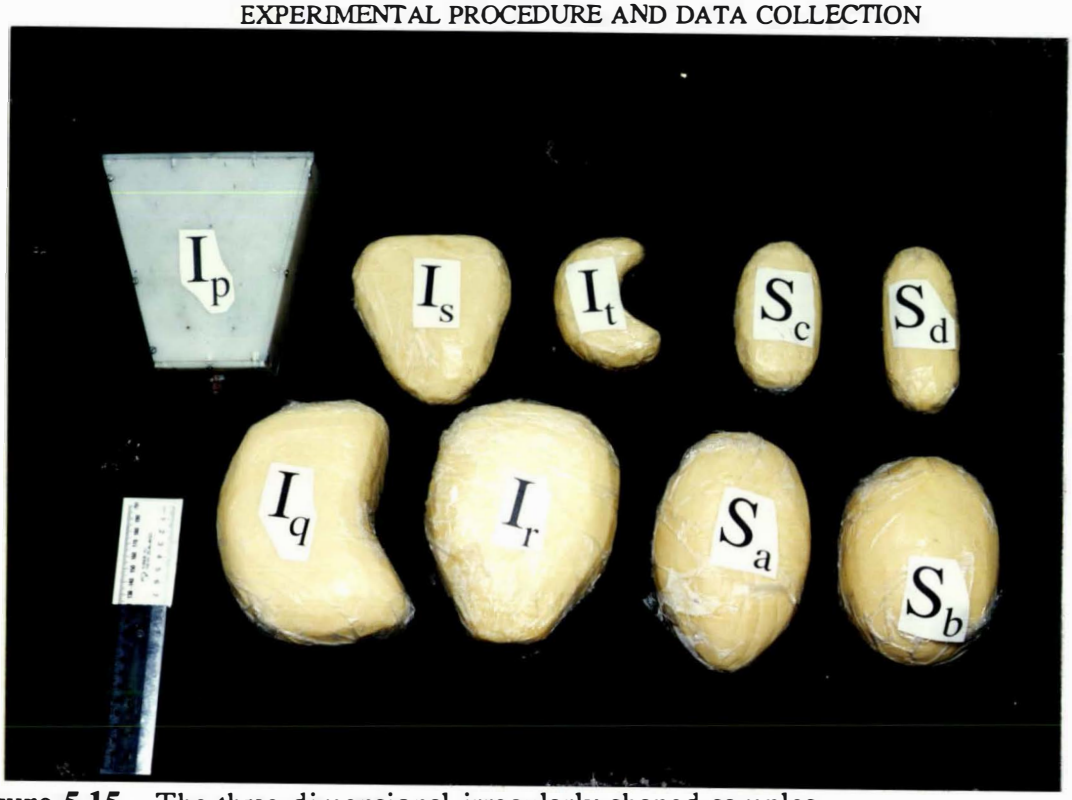

Figure 5.15 The three-dimensional irregularly shaped samples

Figure 5.16 Schematic diagram of box corner types
❶ - ideal corner, ❷ - polypropylene box corner

6. EXPERIMENTAL DESIGN AND RESULTS

In order to investigate the accuracy of the new generally applicable empirical method for predicting the chilling time of irregularly shaped foods, experiments must be conducted across a wide range of conditions covering those that occur in common chilling practice. The most important variables are the size and the geometry of the object to be chilled, its initial temperature, the surface heat transfer coefficient, and the ambient temperature. These are defined in five dimensionless numbers, the Biot number (*Bi*, defined in eqn 2.21), which takes account of the size of the object and the surface heat transfer coefficient; the Fourier number (*Fo*, defined in eqn 2.18), which includes the size of the object and the chilling time; the fractional unaccomplished temperature change (*Y*, defined in eqn 2.19), which takes account of the initial and final temperatures of the object and the ambient temperature; and the dimensional ratios $ß_1$ and $ß_2$ (defined in Section 4.3), which take account of the geometric arrangement of the object. The chilling time elapsed (t) is included in the Fourier number.

The use of fractional unaccomplished temperature change Y meant that a wide range of temperature need not be studied. The variables representing size (R), shape (the second and third dimensions D_2 and D_3), the initial temperature (T_i), the ambient medium temperature (T_a) and the surface heat transfer coefficient (h), were all investigated experimentally. It was decided to consider two- and three-dimensional shapes separately. Variables other than shape were altered independently for a variety of different shapes within each geometric category. An experimental design was sought in which the factors were varied over as wide a range as possible within the limitations of the experimental equipment.

Orthogonal experimental designs in terms of *Bi*, *Y*, $ß_1$ and $ß_2$ were not feasible because of physical limitations in controlling the variables, especially h, R, $ß_1$ and $ß_2$, to preselected values. Also, a statistically-based design was not essential as no mathematical model building was undertaken from the results. Values of the object size and geometric arrangement, and the surface heat transfer coefficients were, in most cases, determined more by considerations such as the availability of the appropriate

types of testing material, and moulds and their wall material, than by choice to give a specified *Bi* value. Biot number was varied as widely as reasonably possible by using different sample sizes and mould wall materials. Sufficient control and variability of h was achieved by using both the air tunnel and the brine immersion tank, and also by the addition of an insulating plastic foam layer for some shapes.

6.1 Treatment of the Effect of Geometry

In Chapter 4 it was shown that for regular multi-dimensional shapes use of the concepts of E and L led to accurate methods to take account of geometry in chilling time predictions. E and L are calculated as functions of the Biot number and the dimensional ratios (β_1 and β_2) that describe the regular geometries.

When considering irregular shapes it is not obvious how the geometry should be described. Smith *et al.* (1967, 1968), Clary *et al.* (1968), Smith & Nelson (1969), and Clary *et al.* (1971) defined a geometry index, for the case of chilling and $Bi \rightarrow \infty$. For irregular geometries they related the irregular shapes to an equivalent ellipsoidal model shape that has equal orthogonal cross-sectional areas and the same characteristic dimension as those of the irregular shape that it replaces. The orthogonal cross-sections taken were generally the smallest and largest cross-sections that pass through the thermal centre and lie in the same plane as the characteristic dimension. For freezing, Cleland (1985) used the ratio of the volume of the object compared with that of an infinite cylinder or a sphere of the same surface area for two- or three-dimensional irregular shapes respectively, to define an equivalent ellipsoid. Also for freezing, Hossain *et al.* (1992b, 1992c) related irregular shapes to an equivalent ellipsoid which has the same characteristic dimension R, the same cross-sectional area in the smallest cross-section, and the same volume. They also investigated replacing the same volume criterion with same surface area but found that this led to inferior results.

In the present work it was accepted that irregular shapes would have to be simulated by an "equivalency" concept. In developing this concept it was decided to investigate the following:

1. **Either** use of an equivalent ellipsoid (infinite ellipse for two-dimensional geometries)

   or use of an equivalent rectangular brick (infinite rectangular rod for two-dimensional geometries);

2. **Either** use of a dimensional measurement approach to define the dimensional ratios $ß_1$ and $ß_2$ for the equivalent shape (Section 4.3)

   or use of a "conservation" approach (*e.g.* of area or volume) in the irregular and equivalent shapes to define $ß_1$ and $ß_2$.

Of the two approaches for finding $ß_1$ and $ß_2$ the first has the advantage of real simplicity, involving a relatively simple single measurement in each direction. The latter requires more measurement: volume can be found from mass and density, but cross-sectional area must be measured and this is difficult. Using volume and cross-sectional area conservation as the criteria, it follows that:

For the equivalent ellipsoid,

$$\beta_1 = \frac{A_c}{\pi R^2} \tag{6.1}$$

where A_c = cross-sectional area (m).

$$\beta_2 = \frac{3V}{4\pi R^3 \beta_1} \tag{6.2}$$

For the equivalent rectangular brick,

$$\beta_1 = \frac{A_c}{4R^2} \tag{6.3}$$

$$\beta_2 = \frac{V}{8R^3 \beta_1} \tag{6.4}$$

The four possible combinations of equivalent shape and measurement approach were designated:

EA: the equivalent ellipsoid model plus the conservation of area-volume approach;
EM: the equivalent ellipsoid model plus the measured approach;
BA: the equivalent brick model plus the conservation of area-volume approach;
BM: the equivalent brick model plus the measured approach.

The dimensional ratios found using some of these different approaches are shown in Table 6.1 for the seven two-dimensional samples, and in Table 6.2 for the nine three-dimensional samples. It can be seen in Table 6.1 that approach BA led to two β_1 values below 1.0. This suggests the approach is unrealistic.

With four concave surfaces and four protrusions, the geometric configuration of two-dimensional irregular shape I_c (Figure 5.12) is relatively complex. Guidelines were sought to properly define the dimensions for the equivalent ellipses (EA and EM) for such geometries. It was decided to try two approaches:

1. equivalent ellipses derived from the original shape (I_c),
2. equivalent ellipses derived from a quasi-I_c shape with the four protrusions excised as shown in Figure 5.12.

The two approaches result in different dimensional ratios which are shown in Table 6.1. The second approach leads to a smaller β_1 value and thus a smaller elliptical model. Therefore, the four possible combinations of dimensional definition and measurement approach for the equivalent elliptical models were redesignated:

EAO: using the original shape I_c plus the conservation of area-volume approach for all objects;
EA: using the quasi-I_c shape with the four protrusions excised plus the area-volume approach for all objects;
EMO: using the original shape I_c plus the measured approach for all objects;

EM: using the quasi-I_c shape with the four protrusions excised plus the measured approach for all objects.

Therefore, there were totally six possible approaches including these four and the BA and BM approaches using bricks as the equivalent model.

6.2 Chilling of Two-Dimensional Irregular Shapes

As has been discussed, the range of Biot number that could be considered was physically limited by the first dimensions and mould wall material and thickness used. Seven different two-dimensional objects were used. The nine values of h for each combination of mould wall material and thickness, sheet plastic foam, and testing apparatus (the air environmental tunnel or the brine immersion tank) led to twenty-one different values of Biot number ranging from 0.3 to 15.0. Figures 5.6 to 5.12 show the cross-sectional geometries for these objects. For each shape at least three chilling runs were conducted. In each chilling experiment, the Y_c value typically changed from 1.0 till termination at $Y_c \approx 0.05$ (corresponding to values of T_i of about 30°C and T_c of about 1.5°C for T_a of about 0.1°C to 1°C). Beyond this, the potential inaccuracy in temperature difference measurement was too large for the data to be valuable. A wider range of temperatures was not used because variation of test sample thermal properties with temperature did occur, and it was considered that if there was significant inaccuracy arising from use of mean thermal property values this would hinder the testing of the proposed prediction method. The range 0 to 30°C was seen as the best compromise. Also, it coincided with the temperature range for which thermal properties were available (Table 5.1).

A total of 38 experiments, including replicates to estimate the experimental error, were conducted using Tylose as the test material. In presenting the experimental results, two derived parameters were calculated as follows:

1. Using the thermal properties of Table 5.1, sample dimensions in Table 6.1 plus the definitions of Y_c and Fo, the experimental data were converted to plots of ln Y_c vs Fo.

2. A best-fit line between Y_c = 0.70 and Y_c = 0.05 was found using linear regression:

$$\ln (Y_c) = \ln (L_{c\,exp}) - M_{exp}\, Fo \qquad (6.1)$$

where $L_{c\,exp}$ = experimentally determined lag factor for the thermal centre

M_{exp} = experimentally determined dimensionless cooling rate

The experimental results are given in Table 6.3, and Figures 6.1 to 6.7 show typical temperature/time profiles at the thermal centre for each shape.

Other than the use of the same measuring systems, the replicates were performed as independently from each other as possible to give a true indication of variability due to experimental techniques. The most important variable that could not be measured independently from the other experiments was the surface heat transfer coefficient. Total uncertainty introduced by errors in measurement, or due to any systematic error, could not be quantified from the spread of replicates because of the inability to achieve total independence of nominally replicate runs.

Numerical methods that solve the governing partial differential equation for heat transfer model the chilling process in a physically realistic manner. Provided time and spatial steps are small and grids accurately defined, they should gives predictions that are not affected by experimental errors. Comparison of predictions by the simple prediction method with the results for the numerical methods helps to identify how well the simple prediction method performs. It is convenient to use the correlation coefficient for comparing percentage differences in the manner of Cleland & Earle (1984). That is the correlation coefficient between (a) the percentage differences between the simple prediction method and experimental data and (b) the percentage differences between the numerical method and experimental data.

Finite element calculations (FEM) were carried out using the grids for the seven two-dimensional test samples shown in Figure 5.6 to 5.12. Using thermal data taken from Table 6.3, the FEM results were processed in similar manner to the experimental results (*i.e.* curve-fitted to eqn 6.1 for $0.05 \le Y_c \le 0.70$). The values of the slope and intercept were designated M_{FEM} and $L_{c\,FEM}$ respectively. These are tabulated in Table 6.3 and also plotted versus M_{exp} and $L_{c\,exp}$ in Figures 6.8 and 6.9.

Considering Figure 6.8, a line of slope 1.0 is shown. Perfect correlation of M_{exp} and M_{FEM} would occur if all points lay on this line. In practice, they are scattered around it in a random manner due to experimental error.

In contrast, Figure 6.9 shows an offset of $L_{c\ exp}$ from $L_{c\ FEM}$, the former being consistently lower. As was stated earlier, L values depend on position within an object, having their maximum at the thermal centre, and minimum at the surface. The FEM results were for the thermal centre. In the experimental work, every effort was made to place thermocouples at the thermal centre, but if inaccurately placed they must be closer to a surface, thus having a lower L value. The consistently lower $L_{c\ exp}$ values (relative to $L_{c\ FEM}$) probably arose almost entirely from this placement problem, but considerable scatter of the experimental data did occur.

The net result of the observations in Figures 6.8 and 6.9 is that the FEM results should overpredict the experimental data (due to the intercept effect). At high Y_c values the percentage error will be larger than at low Y_c values as Figure 6.10 shows. This is because on average $M_{exp} \approx M_{FEM}$ yet $L_{c\ exp} < L_{c\ FEM}$. Thus the error should be approximately constant in absolute chilling time terms, and so it should drop in percentage as chilling time elapses (as Y_c falls).

Tables 6.4 to 6.7 summarise performance results for the FEM method where calculations were carried out in three ways:

(a) FEM - as discussed above for the irregular shape,

(b) EA (FEM) - FEM calculation for an equivalent infinite ellipse of the dimensions given for EA in Table 6.1,

(c) EM (FEM) - FEM calculation for an equivalent infinite ellipse of the dimensions given for EM in Table 6.1.

The tables also summarise BA (analytical) calculations by the analytical method for an infinite rectangular rod of the dimensions given for BA in Table 6.1.

By comparing Tables 6.5, 6.6 and 6.7 it can be seen that predictions agree better with experimental data as Y_c decreases. This is probably due to the combined effect of the reason just discussed with reference to Figure 6.10 and the possibility of some non-linearity of the plot of ln Y_c vs Fo at high Y_c values.

Overall the errors of the FEM results (mean of +4.2%, standard deviation of 3.7%) give an indication of experimental error. The mean offset represents systematic errors particularly in thermocouple placement as discussed. The standard deviation indicates random experimental error.

By comparing predictions by EA, EM, BA and BM for the equivalent shapes to FEM predictions, an assessment of the adequacy of the geometric approximations can be made.

Firstly shape I_c with protrusions should be considered. Predictions were made using approaches FEM, EAO (FEM), EA (FEM), EMO (FEM) and EM (FEM) (Section 6.1). The results are summarised in the first part of Table 6.8. It should be noted that the FEM results modelled the protrusions. Both the mean prediction and standard deviation were improved significantly by using the EA (FEM) rather than the EAO (FEM) approach. Considerable improvement in the mean prediction was observed when using the EM (FEM) approach instead of EMO (FEM) approach. This difference is more marked than for the EAO (FEM) and EA (FEM) results. However, only a small improvement in standard deviation was gained.

The goal in defining an equivalent ellipse must be to match the FEM results. The EM approach produces results that best fit the FEM results, and the EA approach is the next best. The results in the first part of Table 6.8 suggests that the protrusions had little real effect on the heat transfer to the thermal centre for the real shape. Therefore, the method for defining the equivalent ellipsoid should not be overly influenced by the protrusions. A possible explanation for the lack of significance is that iso-thermal contour lines in the protrusions are relatively independent to those in the main body of the object surrounding the thermal centre.

By definition, the measured approach (EM) must be made to specifically exclude such protrusions if their effect is to be ignored. The difference between their inclusion and exclusion is dramatic. In contrast, the EA approach is less affected by their inclusion and exclusion because their contribution to the cross-sectional area is relatively small. Therefore, the EAO approach gives better predictions than the EMO approach. Also, the difference between EAO and EA is much less than between EMO and EM.

It was concluded that some method for excluding protrusions would be needed, but this could not be precisely defined to give a clearcut criterion for any situation as this analysis was based on only one shape with protrusions. It was decided to continue investigation of both EA and EM approaches.

Table 6.9 summarises the correlation coefficients and shows that both EA (FEM) and EM (FEM) predictions closely match the FEM results, which can be seen from the correlation coefficients of 0.677 and 0.692. Table 6.4 shows that the overall BA (analytical) results (mean of +7.9%, standard deviation of 6.6%) are inferior to both the EA approach (mean of +3.9%, standard deviation of 4.2%) and the EM approach (mean of +1.2%, standard deviation of 3.2%). The correlation coefficient for BA is much lower at 0.463. The BM (analytical) approach, calculated by the analytical method for an infinite rectangular rod of the dimensions given for BM, was not fully implemented because it was shown in Table 6.1 that the β_1 values for the BM approach are always greater than the β_1 values for the BA approach, thus indicating that the BM approach would have overpredicted even more than the BA approach.

Overall these results suggest that either the EA or EM approach may be suitable. The difference between the two approaches is that EM gives consistently lower predictions for the whole I group, but is particularly influenced by shape I_c.

6.3 Chilling of Three-Dimensional Irregular Shapes

Twenty-one experiments were conducted with the three-dimensional irregularly shaped samples chosen for study. The shapes are shown in Figure 5.15. The

experimental design used was similar to that used for the two-dimensional irregular shapes. The Biot number was effectively pre-set for each of the cheese samples by the material and size of construction for each object. The surface heat transfer coefficient could only have been altered by changing air velocity, and as only small changes were possible it was decided to leave air velocity constant to simplify surface heat transfer coefficient measurements.

The pyramid sample was chilled both using the air tunnel and the brine immersion tank. The sample was coated with a layer of sheet plastic foam for some air cooling runs, which led to three levels of Biot number in total. Table 6.10 gives the full set of the experimental results processed in a similar manner to those for two-dimensional irregular shapes (Section 6.2). Figures 6.11 to 6.19 show typical temperature/time profiles for each shape.

In each chilling experiment, for cheese samples the temperature of the samples was typically changed from about 17°C till termination at about -4°C, for a cooling medium temperature of about -5°C. Beyond this, the inaccuracy of temperature measurement was too significant for the data to be valuable. A wider range of temperatures was not used because variation of test sample thermal properties with temperature occurred, and it was considered that if there was significant inaccuracy arising from use of mean thermal property values this would hinder the testing of the proposed prediction method. The range -4 to 17°C was chosen to utilise the temperature interval between the freezing point of the water in the cheese and the melting point of some of the fats.

Due to the difficulty in grid preparation and limitation on computational time, finite element analysis was not carried out for the three-dimensional test samples. However, calculations by the analytical solution for an equivalent brick to the pyramid shape (test sample I_p, Figure 5.15) were carried out using dimensional ratios were found using the conservation of area-volume approach (BA). The results (Table 6.11) show over-prediction with large offsets for the means. These results are consistent with the BA results for two-dimensional irregular samples (Table 6.4). BM would have

performed even worse than BA. Thus only EA and EM approaches were further investigated even though they were not tested by FEM calculations.

6.4 Prediction of Chilling Times for Two-Dimensional Irregular Shapes by the Proposed Method

The calculation method summarised in Section 4.8 was used in conjunction with the geometric definitions EA and EM proposed in the Section 6.1, to predict chilling times for objects of any shape. Tables 6.11 and 6.12 summarise the predictions versus experimental results for two-dimensional irregular shapes. Figures 6.1 to 6.7 show some of these results graphically. The plotted results follow FEM predictions closely. However, they tend to overpredict the experimental data a little, particularly at high Y_c values. The contributing effects of thermocouple placement problem and non-linearity in the ln Y_c vs Fo plot at high Y_c values have already been discussed.

For shape I_c, predictions were made using approaches EAO, EA, EMO and EM (Section 6.1). The results are summarised in the second part of Table 6.8. As was the case when using the finite element method, the mean prediction was improved significantly by using the EA rather than the EAO approach. Larger change in the mean prediction was observed when using approach EM instead of EMO. However, only a small improvement in standard deviation occurred for both cases. Thus, as was the case with the numerical predictions for equivalent ellipses, it is necessary to excise the protrusions to achieve accurate predictions.

The main difference between the EA and EM approaches is for the I (highly irregular) group which is less elliptical in geometry than the E (quasi-elliptical) group. Approaches EA and EM yield virtually identical $ß_1$ values for quasi-elliptical objects modelled as ellipses. The difference between EA and EM for the proposed method is more exaggerated than for the EA (FEM) and EM (FEM) results. The EM mean prediction error for the I group is lower than that for the E group, but the standard deviation is higher, which is consistent with the FEM predictions. The correlation coefficients with FEM for the proposed method using both the EA and EM approaches

are high, and even higher than the FEM calculations for equivalent ellipses (Table 6.9). The mean prediction errors using the finite element method for the irregularly shaped samples (approach FEM, Table 6.4 to 6.7) were 4.2% offset from zero compared with 5.7% using the EM approach with the proposed simple method, and 9.5% using the EA approach. The 95% confidence interval of the percentage difference for the predictions (EM proposed) compared with the experimentally measured chilling times was from -3.1% to 14.4%.

Whilst there is no physical justification for it doing so, the EM approach tends to approximately compensate for the over-prediction arising from the non-linearity of the ln Y_c vs Fo plot. The EA approach apparently has no such compensatory factor. It was therefore concluded that the EM approach should be recommended for two-dimensional irregular shapes. It is simpler to use, and the results suggest that the unknown errors introduced by excising protrusions are unlikely to lead to significant under-prediction. In contrast, the EA approach appears to lead to overly conservative predictions, especially at high Y_c values, and the effect of excising the protrusions is unknown.

6.5 Prediction of Chilling Times for Three-Dimensional Irregular Shapes by the Proposed Method

The same calculation techniques as used for the two-dimensional irregular shapes were used to generate predicted data to compare to the three-dimensional experimental runs. The results are summarised in Table 6.13 and some are plotted in Figure 6.11 to 6.19. For the measured approach using the equivalent ellipsoidal model (EM), the mean prediction error was low at 2.6%, whereas for the conservation of area-volume approach (EA), the mean error was 9.9%. The 95% confidence interval of the percentage difference for the predictions (EM proposed) compared with the experimentally measured chilling times was from -6.4% to 11.6%.

In general, the standard deviations were similar to those in the experiments for the two-dimensional irregular shapes. The results support the same conclusions as were

reached for the two-dimensional work: that the EA approach is overly conservative, and that the EM approach seems to somehow compensate for the overprediction inherent in the method at high Y_c without major risk of under-prediction.

6.6 Discussion

Both the numerical and the experimental results suggest the use of ellipsoid rather than the rectangular brick as the equivalent model for irregular geometries.

To define the equivalent ellipsoid, the dimensional ratios $ß_1$ and $ß_2$ should be calculated using eqns (4.6) and (4.7) based on measured dimensions as for regular geometries. For complex geometries whose thermal centre is not obvious from visual examination of the object, the guidelines stated in Section 5.6.1 should be adopted in measurement. Special consideration may be needed for highly irregular geometries:

For shapes with protrusions the measurements of the three dimensions, denoted D_1, D_2 and D_3, should ignore the protrusions. Where there are sharp hollows these should be ignored. These rules are best explained by way of example. Figure 6.20(a) shows a carton shape. The three dimensions are easily measured. Figure 6.20(b) shows a shape with protrusions and how this is modelled, and Figure 6.20(c) shows how a hollow is modelled.

Using the ellipsoidal model, both the conservation of area-volume approach and the measured approach, (with excision of the protrusions), still tend to overpredict measured data, especially at high Y_c values due to the contributing effects of the thermocouple placement problem (which affects predictions at all Y_c values) and non-linearity in the ln Y_c vs Fo plot (which affects predictions at high Y_c values).

The EA approach appears overly conservative so the EM approach is recommended. The EM approach tends to approximately compensate the over-prediction arising from the non-linearity of the ln Y_c vs Fo plot in some manner that cannot be physically explained.

Using the above rules for the EM approach, the proposed chilling time prediction method performs well. Lack of fit is probably more due to experimental error than errors in the form of geometric approximation and the prediction method itself. The dimensional measurements for the regular geometries are defined in a "measured" manner. Thus the geometric definition (EM) is consistent for both regularly and irregularly shaped objects.

No experimental tests of Y_m predictions were possible due to difficulty in measuring T_m. There is no reason to expect that the prediction accuracy of the proposed method for Y_m would be vastly different to that for Y_c. For highly irregular shapes, especially those involving significant protrusions, prediction accuracy might deteriorate as protrusions will contribute to some extent to mass-average temperature. Experimental work would be difficult to carry out, but this is an area where there is potential for further study.

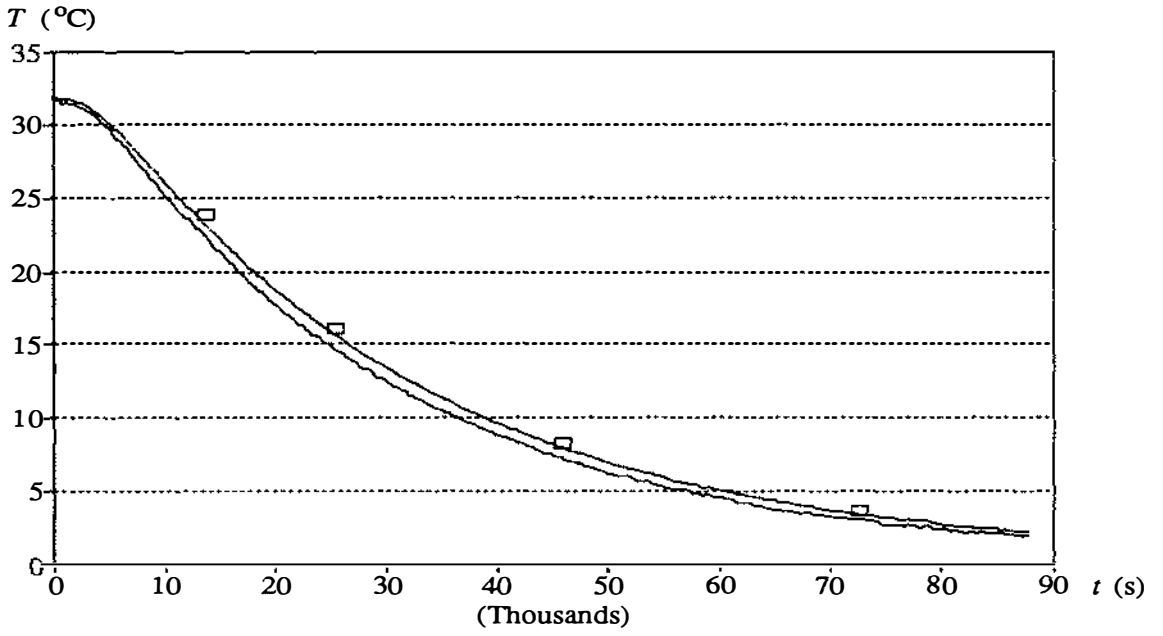

Figure 6.1 Temperature/time profile for chilling of the Tylose two-dimensional irregular shape E_a during Run E_a1. Thermocouple located as close to thermal centre as possible. —— experimental, ····· predicted by FEM, □ predicted by the proposed method using approach EM to define the equivalent ellipse

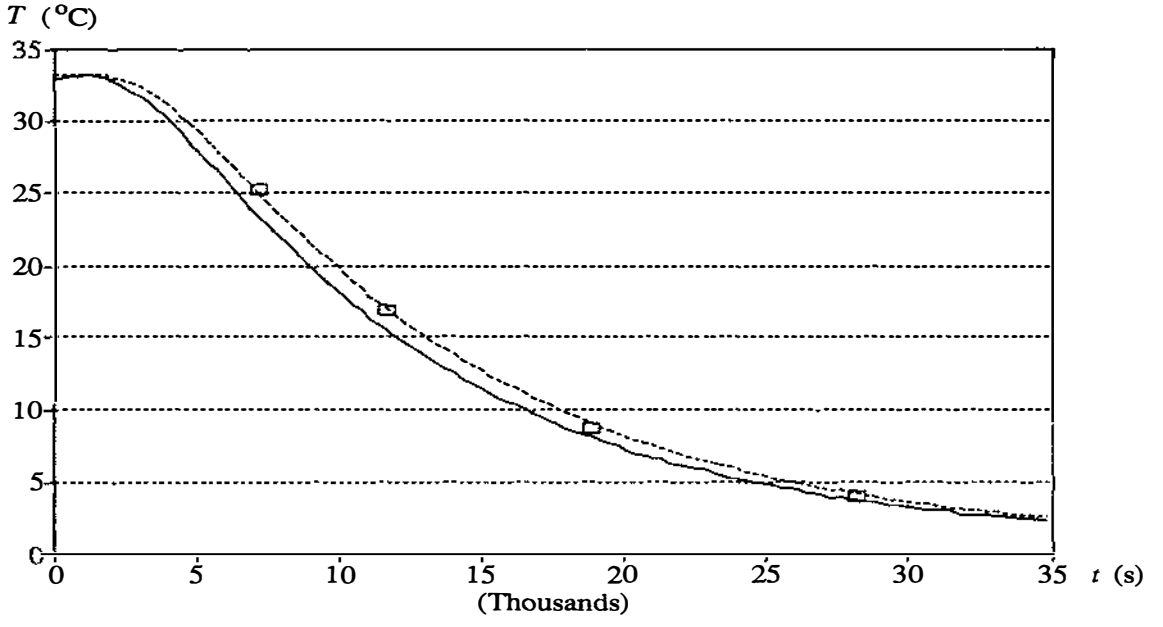

Figure 6.2 Temperature/time profile for chilling of the Tylose two-dimensional irregular shape E_b during Run E_b5. Thermocouple located as close to thermal centre as possible. Key as in Figure 6.1

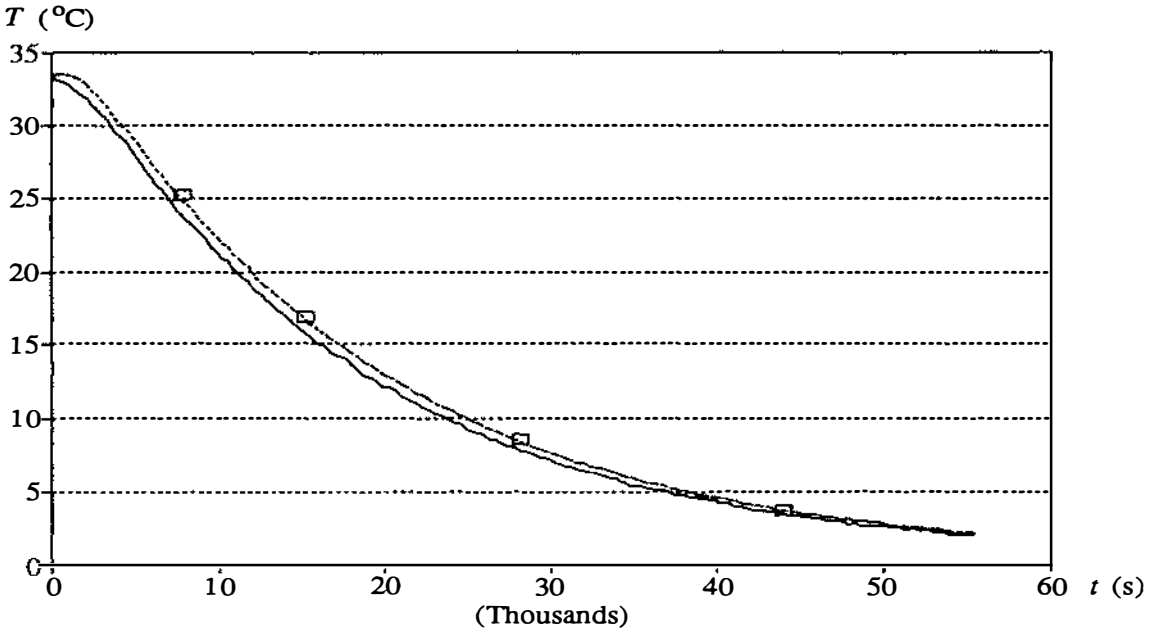

Figure 6.3 Temperature/time profile for chilling of the Tylose two-dimensional irregular shape E_c during Run E_c1. Thermocouple located as close to thermal centre as possible. Key as in Figure 6.1.

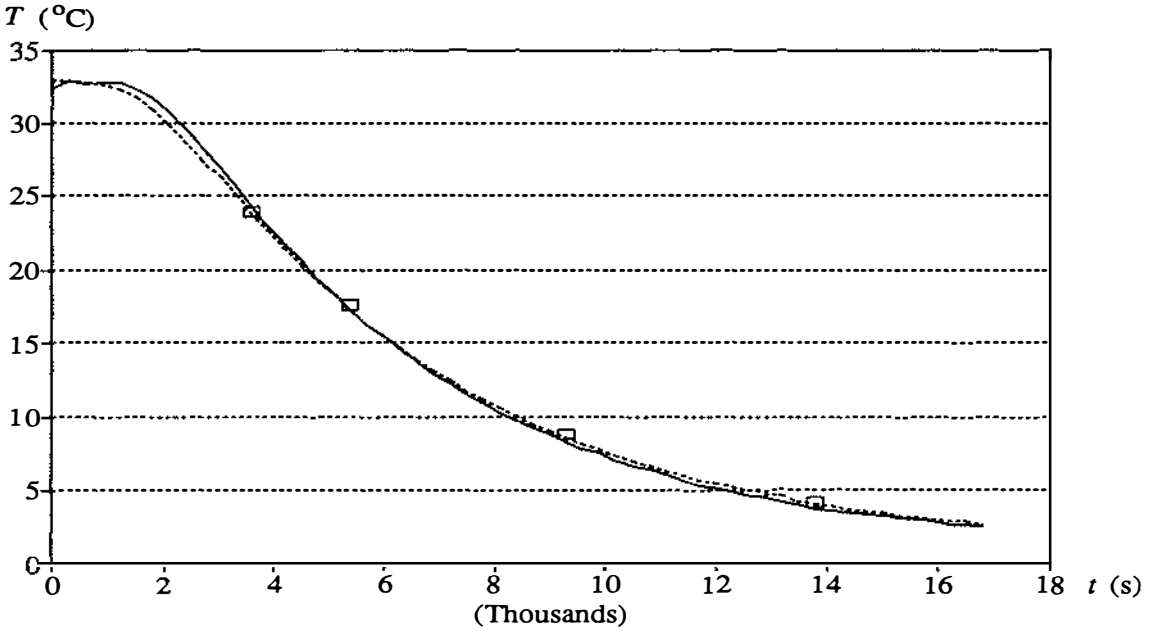

Figure 6.4 Temperature/time profile for chilling of the Tylose two-dimensional irregular shape E_d during Run E_d7. Thermocouple located as close to thermal centre as possible. Key as in Figure 6.1.

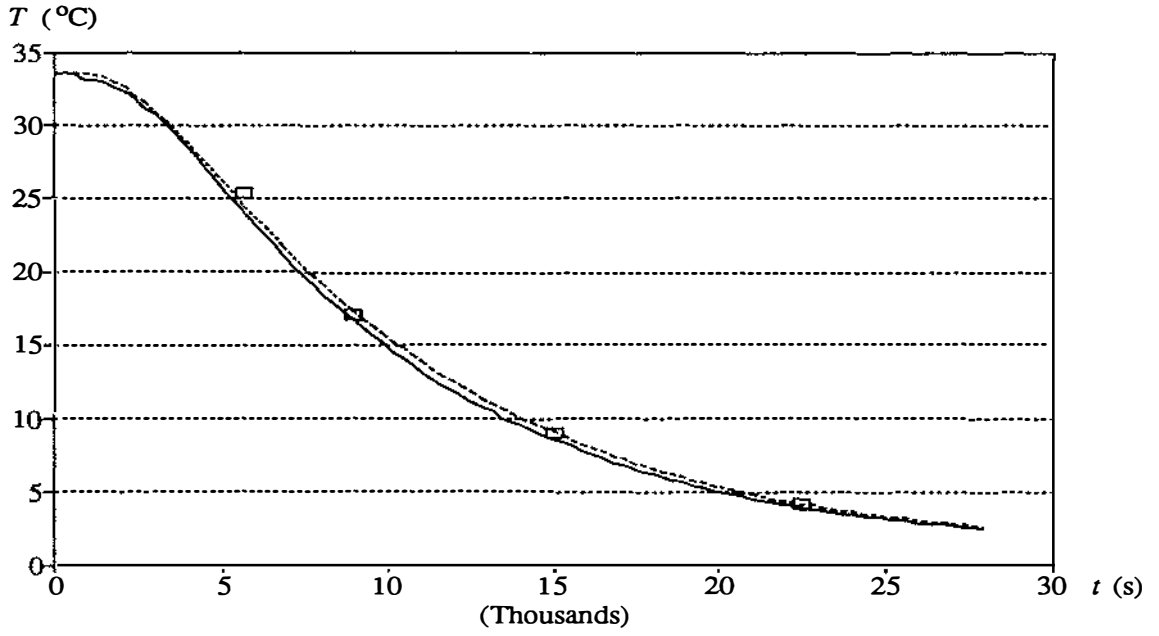

Figure 6.5 Temperature/time profile for chilling of the Tylose two-dimensional irregular shape I_a during Run I_a5. Thermocouple located as close to thermal centre as possible. Key as in Figure 6.1.

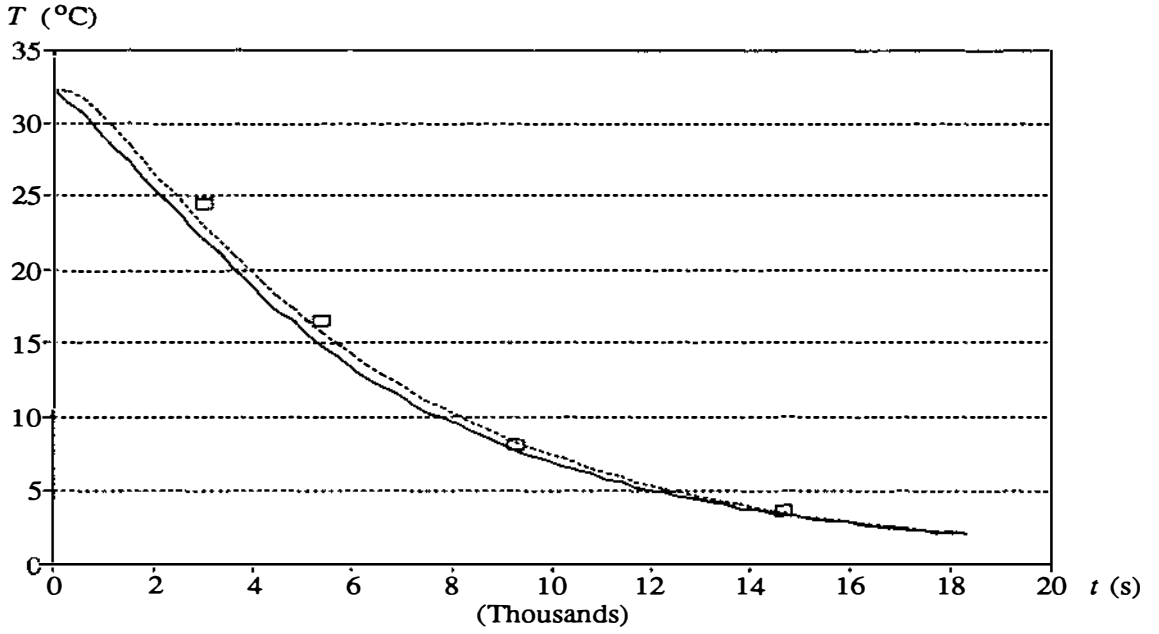

Figure 6.6 Temperature/time profile for chilling of the Tylose two-dimensional irregular shape I_b during Run I_b2. Thermocouple located as close to thermal centre as possible. Key as in Figure 6.1.

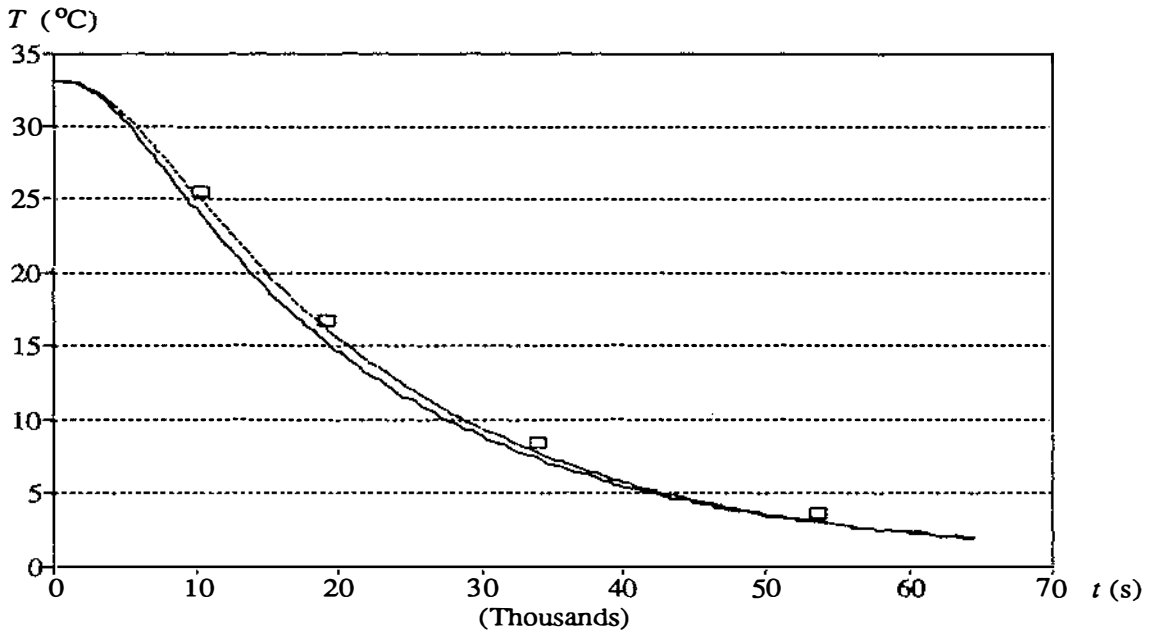

Figure 6.7 Temperature/time profile for chilling of the Tylose two-dimensional irregular shape I_c during Run I_c3. Thermocouple located as close to thermal centre as possible. Key as in Figure 6.1.

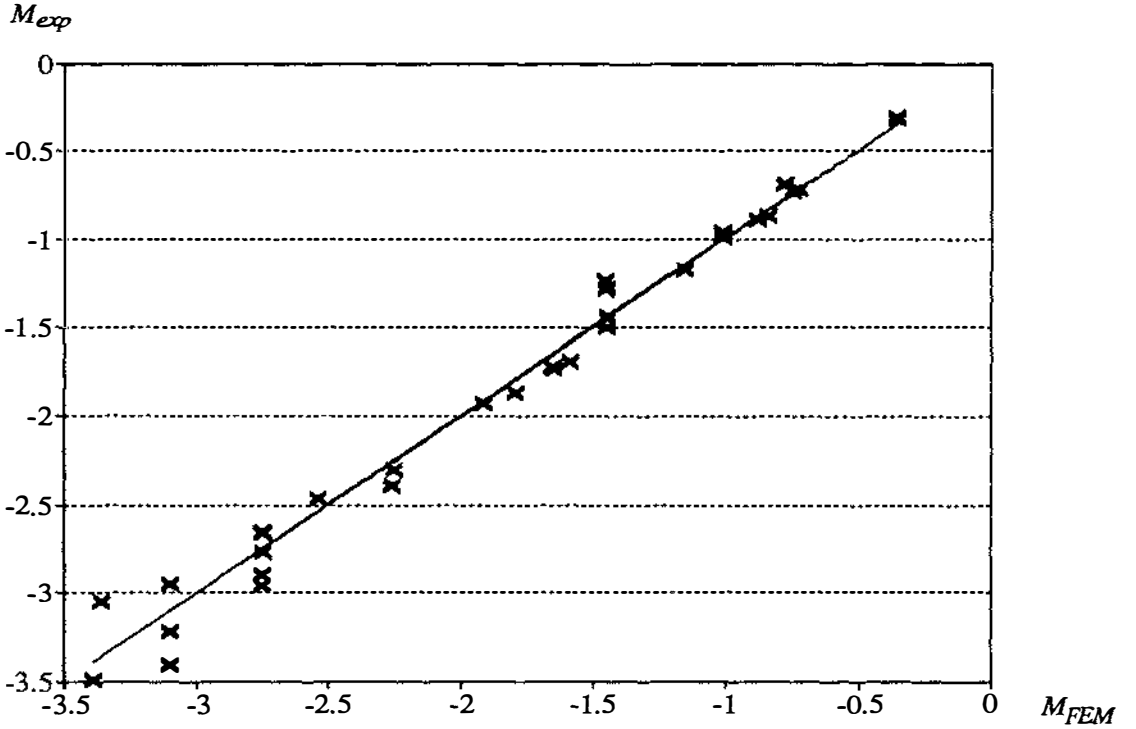

Figure 6.8 Plot of M_{exp} versus M_{FEM} for Tylose two-dimensional irregular shapes (the straight line represents $M_{exp} = M_{FEM}$)

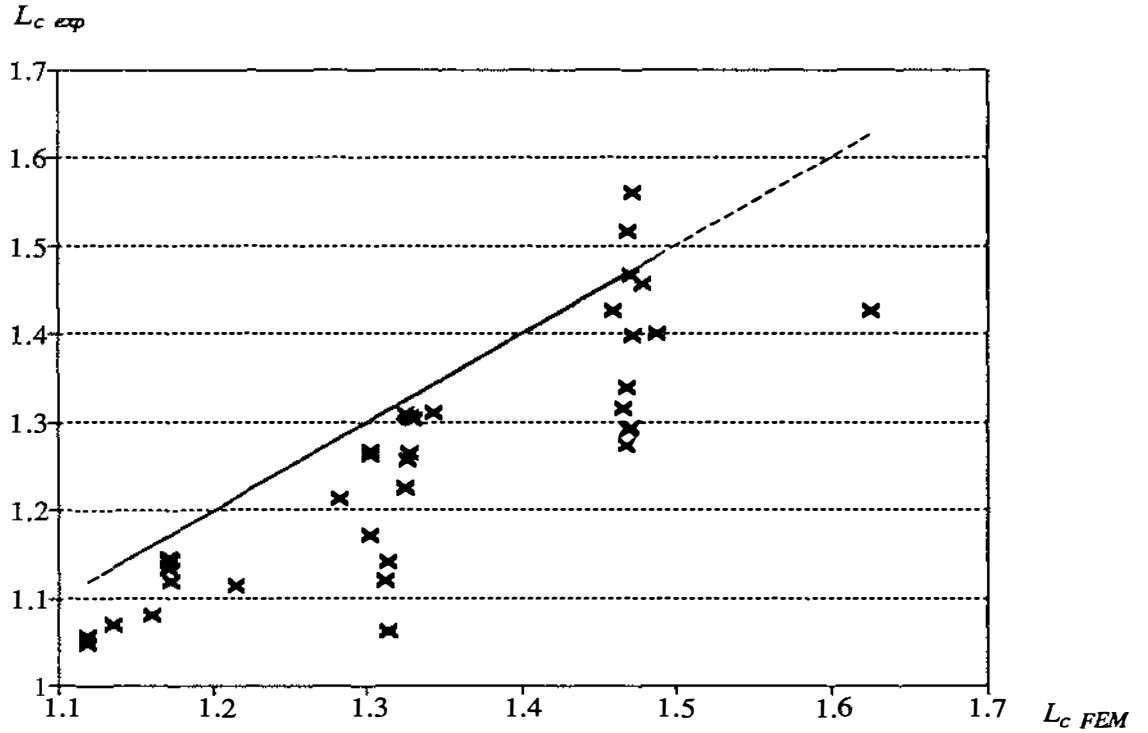

Figure 6.9 Plot of $L_{c\ exp}$ versus $L_{c\ FEM}$ for Tylose two-dimensional irregular shapes (the straight line represents that $L_{c\ exp} = L_{c\ FEM}$)

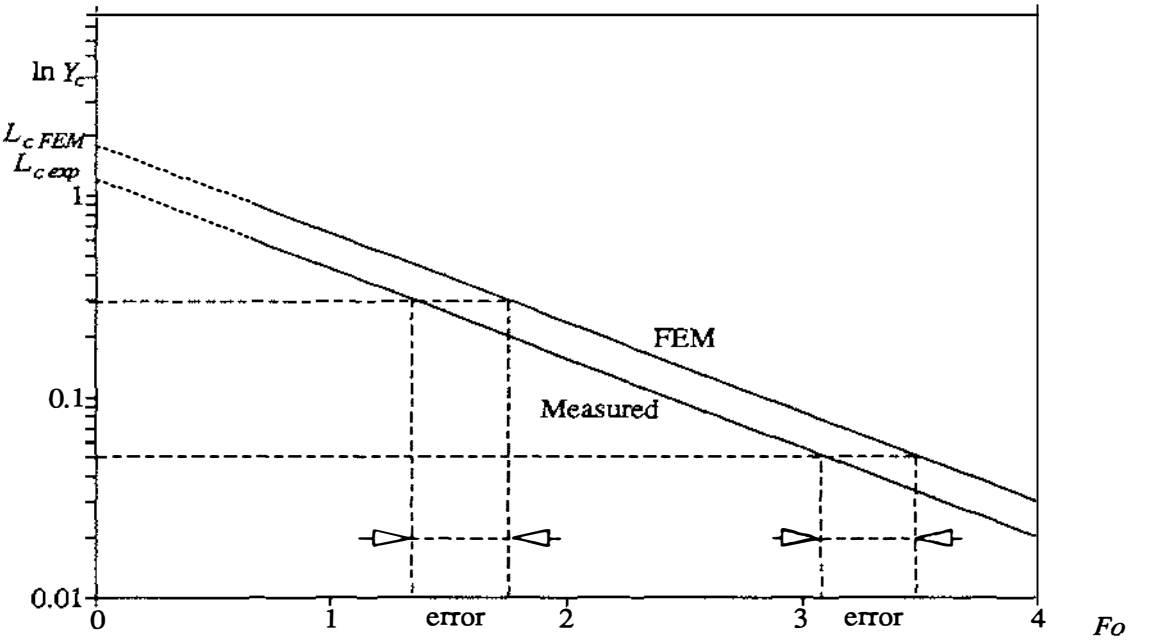

Figure 6.10 Errors arising from displacement of the thermocouple from the thermal centre

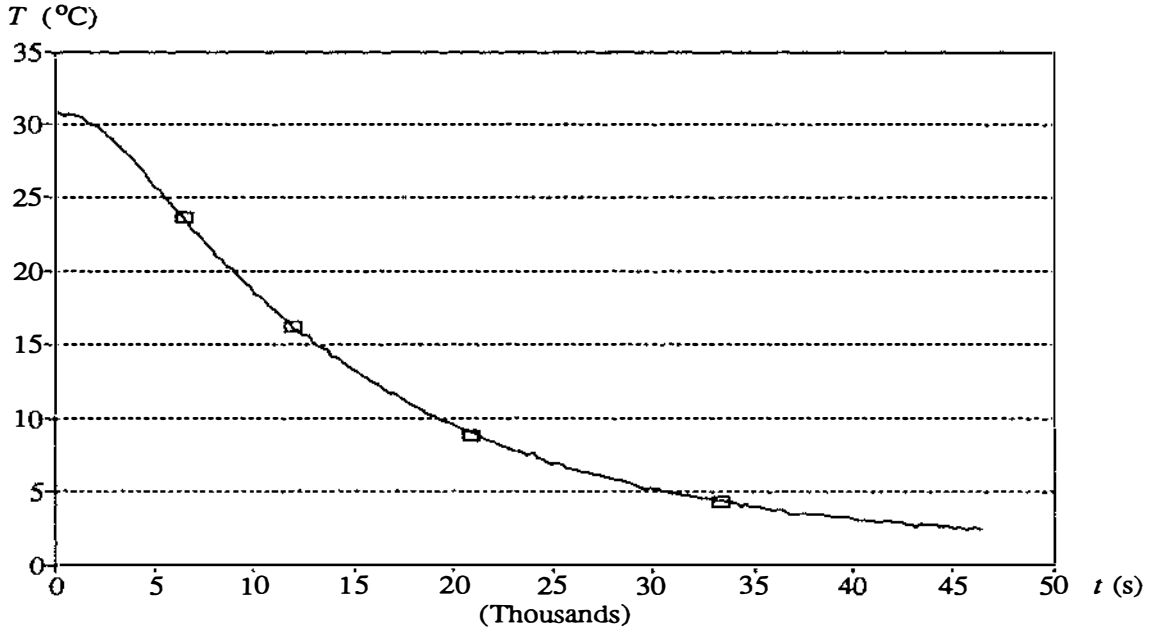

Figure 6.11 Temperature/time profile for chilling of the Tylose three-dimensional irregular shape I_p during Run I_p3. Thermocouple located as close to thermal centre as possible. —— experimental, □ predicted by the proposed method using approach EM to define the equivalent ellipsoid.

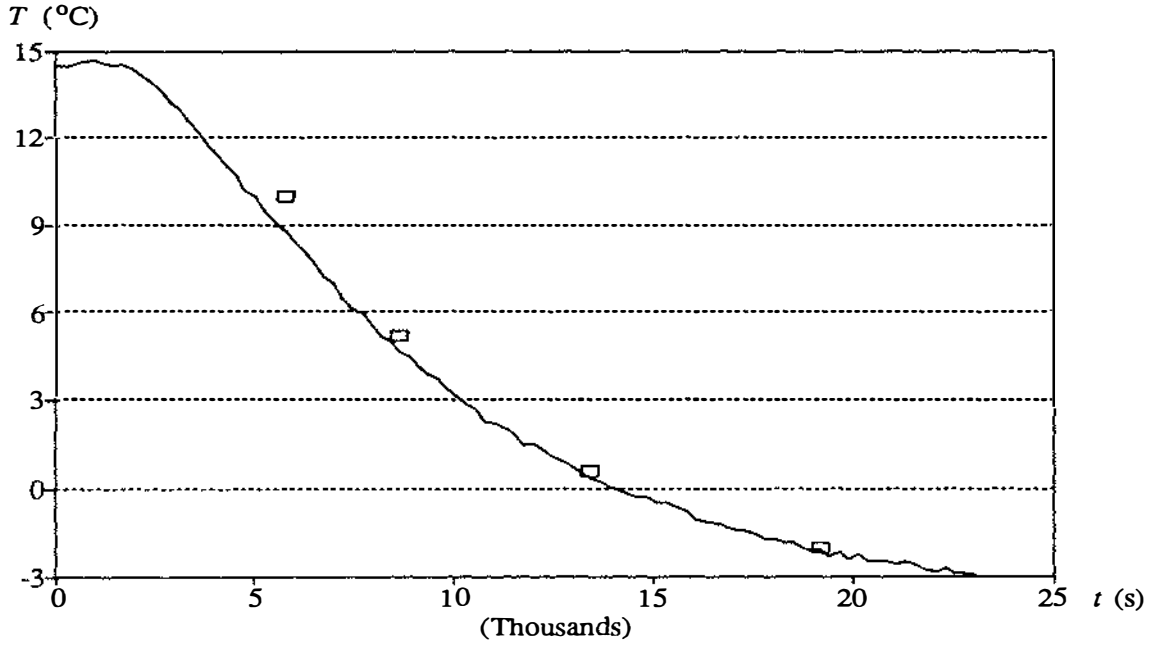

Figure 6.12 Temperature/time profile for chilling of the Tylose three-dimensional irregular shape I_q during Run I_q1. Thermocouple located as close to thermal centre as possible. Key as in Figure 6.11.

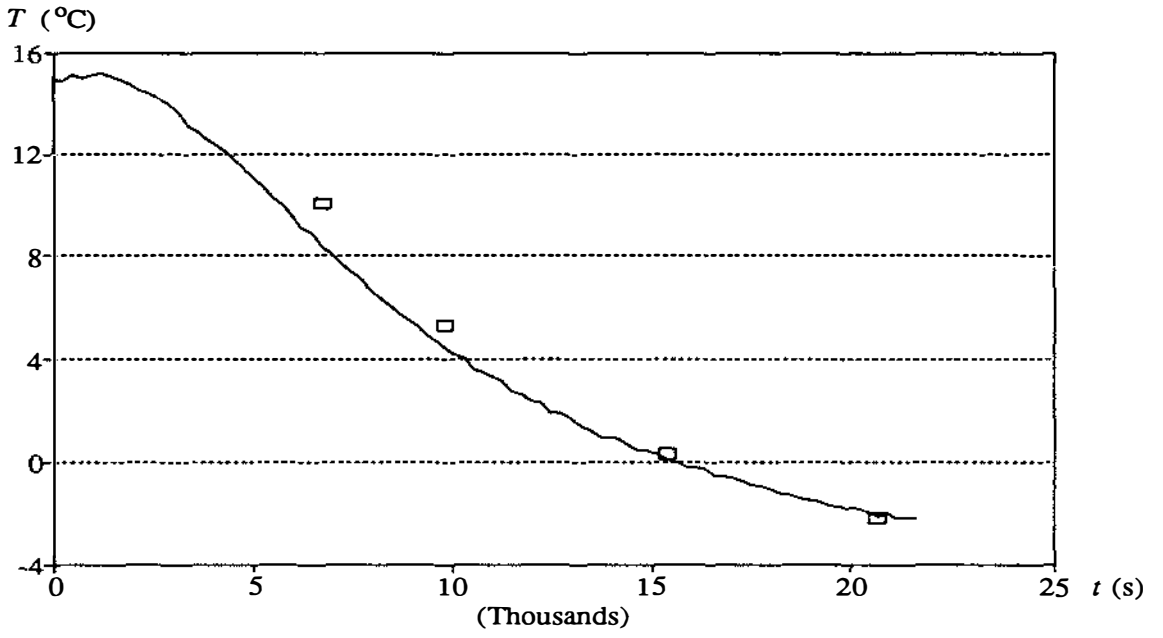

Figure 6.13 Temperature/time profile for chilling of the Tylose three-dimensional irregular shape I_r during Run I_r1. Thermocouple located as close to thermal centre as possible. Key as in Figure 6.11.

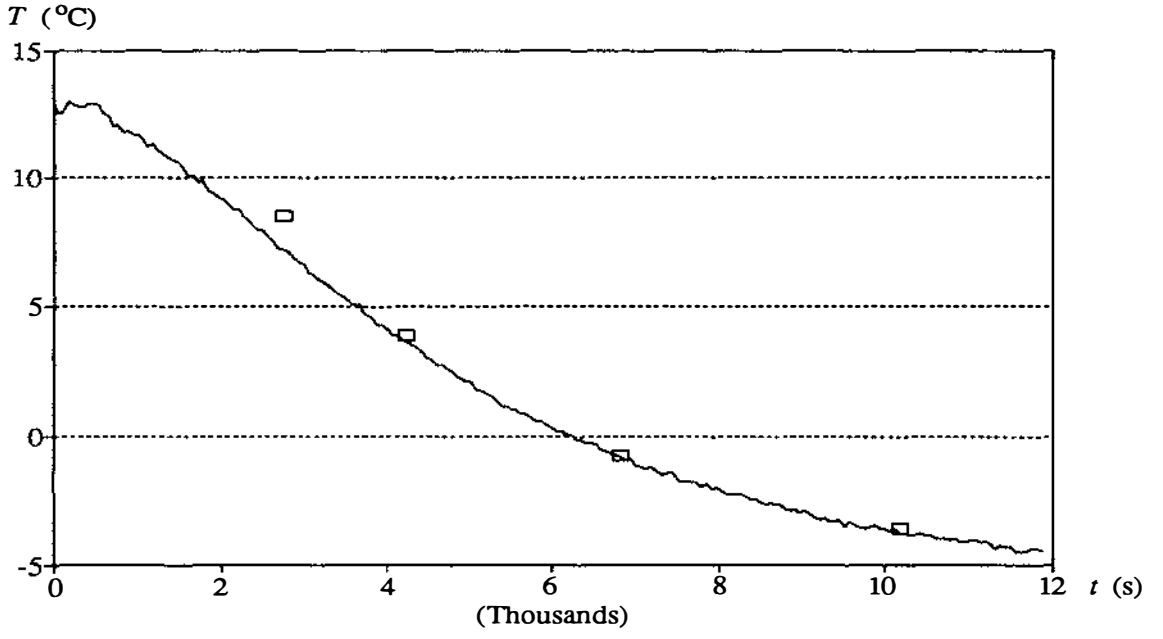

Figure 6.14 Temperature/time profile for chilling of the Tylose three-dimensional irregular shape I_s during Run I_s3. Thermocouple located as close to thermal centre as possible. Key as in Figure 6.11.

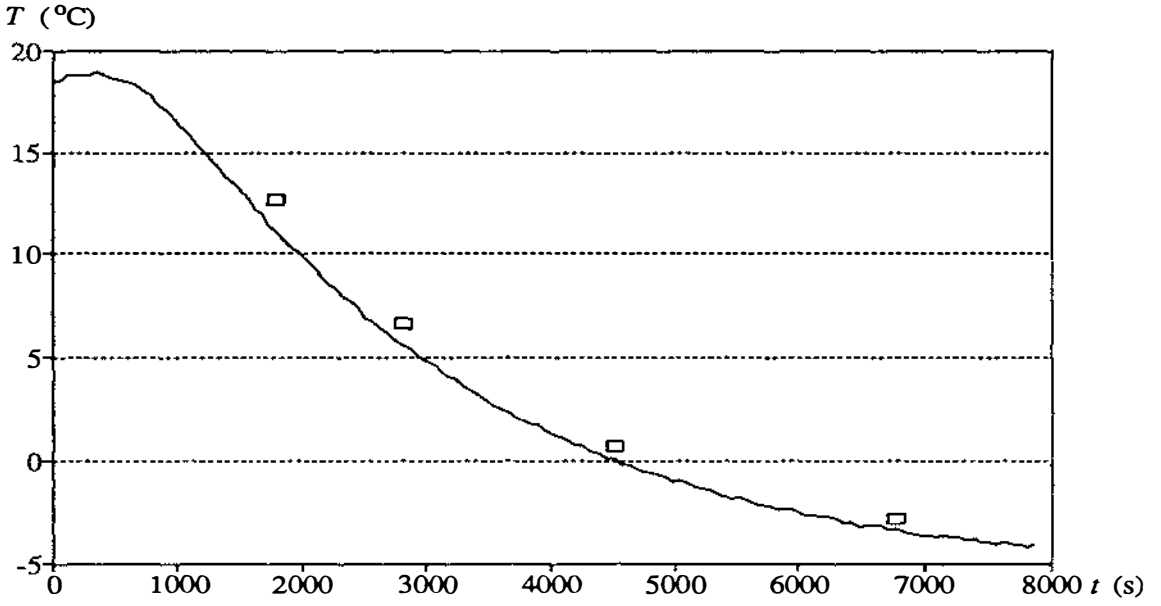

Figure 6.15 Temperature/time profile for chilling of the Tylose three-dimensional irregular shape I_t during Run I_t1. Thermocouple located as close to thermal centre as possible. Key as in Figure 6.11.

Figure 6.16 Temperature/time profile for chilling of the Tylose three-dimensional irregular shape S_a during Run S_a3. Thermocouple located as close to thermal centre as possible. Key as in Figure 6.11.

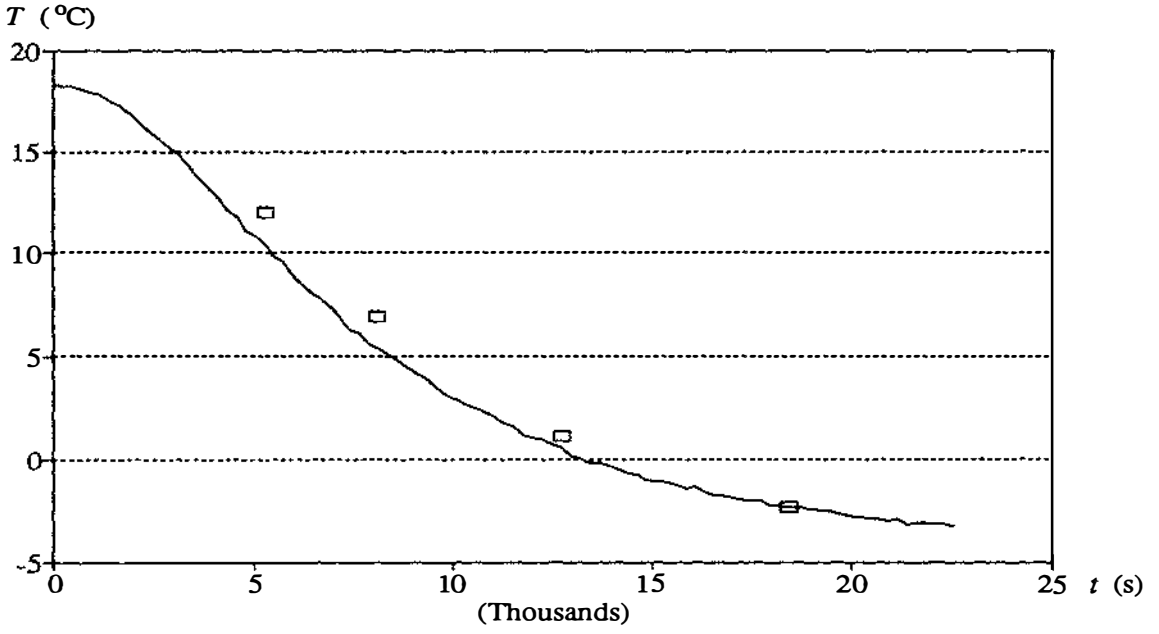

Figure 6.17 Temperature/time profile for chilling of the Tylose three-dimensional irregular shape S_b during Run S_b1. Thermocouple located as close to thermal centre as possible. Key as in Figure 6.11.

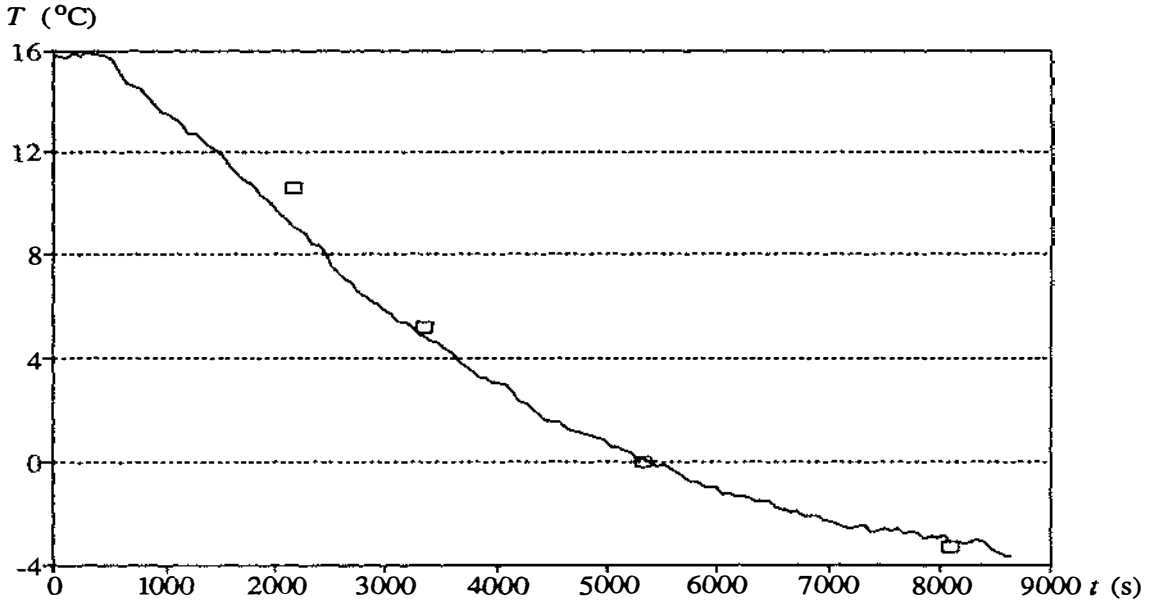

Figure 6.18 Temperature/time profile for chilling of the Tylose three-dimensional irregular shape S_c during Run S_c1. Thermocouple located as close to thermal centre as possible. Key as in Figure 6.11.

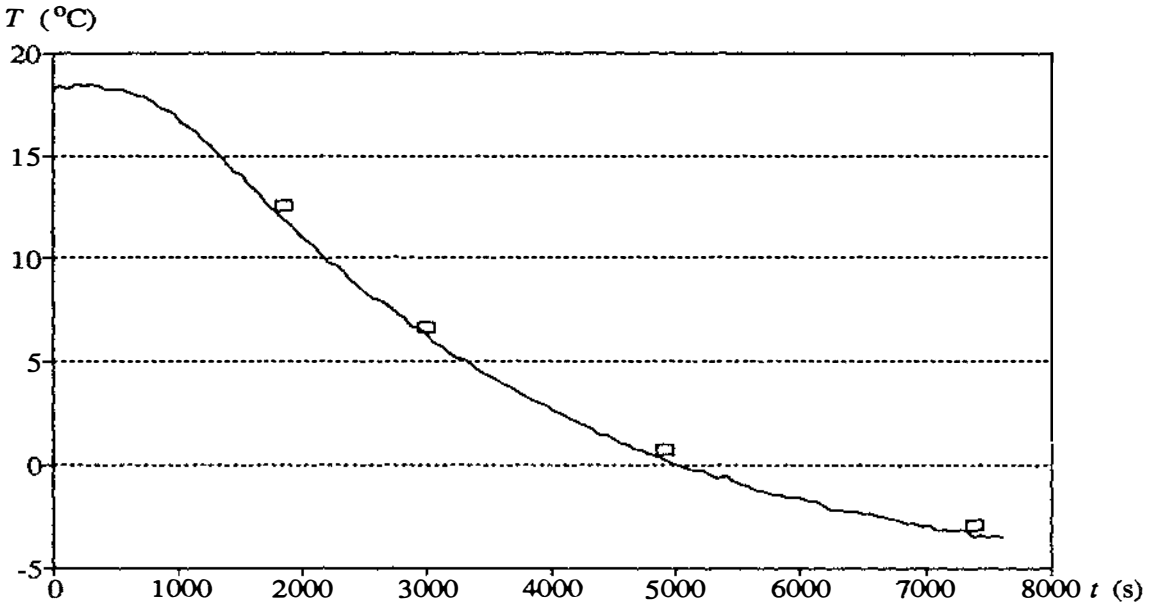

Figure 6.19 Temperature/time profile for chilling of the Tylose three-dimensional irregular shape S_d during Run S_d1. Thermocouple located as close to thermal centre as possible. Key as in Figure 6.11.

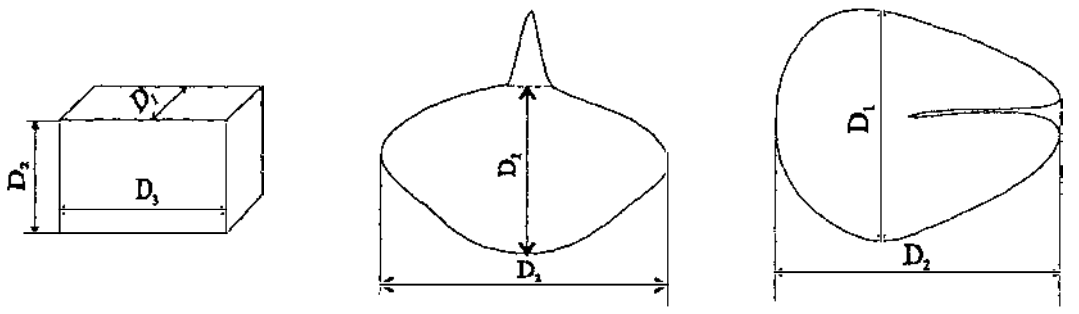

Figure 6.20 Examples of measurement of object geometry. (a) regular shape, (b) shape with protrusion, (c) shape with hollow

Table 6.1 Geometric Parameters of Two-Dimensional Samples

	A_c (m^2)	R (m)	$ß_1$ (EM, BM)	$ß_1$ (EA)	$ß_1$ (BA)
E_a	0.01640	0.0558	1.63	1.68	1.32
E_b	0.01770	0.0685	1.18	1.20	0.94
E_c	0.00811	0.0455	1.26	1.25	0.98
E_d	0.00796	0.0425	1.44	1.40	1.10
I_a	0.01520	0.0495	1.74	1.98	1.55
I_b	0.00586	0.0238	2.74	3.31	2.60
I_c	0.01626	0.5000	2.07	2.15	1.63
I_c^*	0.01412	0.5000	1.60	1.80	1.41

* Protrusions excised.

Table 6.2 Geometric Parameters of Three-Dimensional Samples

	A_c (m^2)	V (m^3)	R (m)	$ß_1$ (EM)	$ß_2$ (EM)	$ß_1$ (EA)	$ß_2$ (EA)
I_p	0.010148	0.001297	0.0413	1.49	1.86	1.90	2.32
I_q	0.009587	0.001626	0.0500	1.22	1.83	1.22	2.55
I_r	0.012715	0.001699	0.0500	1.40	1.82	1.62	2.01
I_s	0.005961	0.000592	0.0250	2.50	2.68	3.04	2.98
I_t	0.002322	0.000273	0.0250	1.10	2.20	1.18	3.53
S_a	0.011296	0.001323	0.0560	1.09	1.39	1.15	1.57
S_b	0.008931	0.001147	0.0500	1.03	1.81	1.14	1.93
S_c	0.003002	0.000291	0.0250	1.40	2.42	1.53	2.91
S_d	0.002625	0.000301	0.0250	1.20	2.80	1.34	3.44

Table 6.3 Experimental Data and Finite Element Predictions for Chilling of Two-Dimensional Irregular Shapes. Replicates Marked *

Shape Code & Run Number	R (m)	h (W m^{-2} K^{-1})	T_a (°C)	T_i (°C)	$M_{exp.}$	$L_{c\ exp.}$	M_{FEM}	$L_{c\ FEM}$
E_a1	0.056	5.6	0.5	31.7	0.874	1.144	0.833	1.172
E_a2 *	0.056	14.5	0.5	32.0	1.737	1.306	1.649	1.327
E_a3 *	0.056	14.5	0.5	33.0	1.723	1.304	1.651	1.330
E_a4 *	0.056	14.5	0.5	31.8	1.723	1.309	1.649	1.325
E_a5	0.056	35.4	0.6	33.0	2.456	1.316	2.536	1.466
E_b1 *	0.069	5.6	0.3	31.0	1.178	1.134	1.154	1.171
E_b2 *	0.069	5.6	0.4	32.5	1.172	1.142	1.153	1.171
E_b3 *	0.069	5.6	0.1	33.0	1.176	1.147	1.154	1.171
E_b4	0.069	14.5	0.5	32.5	2.394	1.311	2.255	1.343
E_b5	0.069	35.4	0.7	33.2	3.498	1.400	3.390	1.488
E_c1	0.046	6.3	0.4	33.5	0.891	1.082	0.879	1.160
E_c2	0.046	16.0	0.3	30.4	1.868	1.265	1.795	1.327
E_c3 *	0.046	36.2	0.5	32.8	2.944	1.293	3.098	1.472
E_c4 *	0.046	36.2	1.0	32.0	3.223	1.398	3.099	1.473
E_c5 *	0.046	36.2	1.0	30.8	3.420	1.516	3.095	1.470
E_d1	0.043	6.3	0.4	32.2	0.695	1.071	0.776	1.136
E_d2	0.043	16.0	0.4	32.1	1.692	1.213	1.588	1.283
E_d3 *	0.043	36.2	1.0	33.3	2.758	1.340	2.744	1.468

...continued

Table 6.3 continued...

Shape Code & Run Number	R (m)	h (W m^{-2} K^{-1})	T_a (°C)	T_i (°C)	$M_{exp.}$	$L_{c\ exp.}$	M_{FEM}	$L_{c\ FEM}$
E_d4 *	0.043	36.2	0.9	32.0	2.651	1.292	2.746	1.470
E_d5 *	0.043	36.2	0.8	32.6	2.659	1.274	2.745	1.469
E_d6 *	0.043	36.2	1.0	33.1	2.960	1.468	2.747	1.471
E_d7 *	0.043	36.2	1.0	32.8	2.898	1.560	2.749	1.473
I_a1	0.050	5.6	0.4	31.4	0.727	1.121	0.720	1.173
I_a2 *	0.050	14.5	0.6	30.3	1.497	1.310	1.438	1.324
I_a3 *	0.050	14.5	0.5	32.6	1.444	1.257	1.439	1.326
I_a4 *	0.050	14.5	0.4	32.5	1.455	1.225	1.438	1.324
I_a5	0.050	35.4	0.9	33.6	2.298	1.428	2.250	1.460
I_b0 *	0.024	6.3	0.4	32.2	0.314	1.049	0.350	1.118
I_b1 *	0.024	6.3	0.3	32.1	0.316	1.056	0.350	1.118
I_b2	0.024	16.0	0.4	32.2	0.735	1.112	0.750	1.215
I_b3 *	0.024	36.2	0.8	32.5	1.281	1.119	1.440	1.312
I_b4 *	0.024	36.2	0.6	30.5	1.237	1.062	1.446	1.315
I_b5 *	0.024	36.2	0.5	31.9	1.290	1.142	1.446	1.315
I_c1 *	0.050	6.9	0.4	30.8	0.995	1.262	1.004	1.303
I_c2 *	0.050	6.9	0.2	32.8	0.995	1.267	1.004	1.303
I_c3 *	0.050	6.9	0.4	33.1	0.970	1.173	1.004	1.303
I_c4	0.050	20.3	0.6	30.8	1.929	1.457	1.910	1.479
I_c5	0.050	149.6	0.6	29.8	3.054	1.428	3.359	1.626

Table 6.4 Percentage Differences Between Experimental and Calculated Chilling Times for Two-Dimensional Irregular Shapes (Cumulative Results for Y_c = 0.50, 0.25, 0.10, std = standard deviation, * protrusions excised)

approach	FEM		EA (FEM)		EM (FEM)		BA (analytical)	
shape	mean	std	mean	std	mean	std	mean	std
E_a	5.5	1.8	5.0	1.8	3.6	1.9	6.8	2.7
E_b	4.8	2.1	3.8	4.8	1.0	1.9	-0.7	3.5
E_c	5.7	2.4	5.1	3.1	3.5	2.2	5.7	6.4
E_d	4.4	5.3	1.6	5.1	2.4	4.2	6.8	8.6
E-group	5.1	2.9	3.9	3.7	2.6	2.5	4.7	5.3
I_a	4.2	1.7	3.9	2.0	-0.5	1.8	12.0	6.9
I_b	4.2	8.4	2.7	7.0	-1.4	5.3	6.9	12.2
I_c	0.3	4.2	5.2*	5.4*	-0.4*	5.2*	17.8	6.2
I-group	2.9	4.8	3.9	4.8	-0.8	4.1	12.2	8.4
Overall	4.2	3.7	3.9	4.2	1.2	3.2	7.9	6.6

Table 6.5 Percentage Differences Between Experimental and Calculated Chilling Times for Two-Dimensional Irregular Shapes When Y_c = 0.50 (std = standard deviation, * protrusions excised)

approach	FEM		EA (FEM)		EM (FEM)		BA (analytical)	
shape	mean	std	mean	std	mean	std	mean	std
E_a	6.8	0.6	6.3	1.0	4.7	1.4	1.3	9.2
E_b	5.9	2.0	6.7	2.1	2.3	1.6	1.6	3.2
E_c	6.7	2.7	6.5	2.9	4.8	1.0	6.9	6.0
E_d	5.6	5.2	2.7	5.0	3.7	4.1	8.3	8.0
E-group	6.3	2.7	5.6	2.7	3.8	2.0	4.6	6.6
I_a	5.3	1.2	5.5	1.9	0.9	1.9	15.2	7.3
I_b	6.6	9.6	8.1	7.4	1.8	5.6	12.0	13.8
I_c	2.1	4.7	4.3*	5.6*	-1.0*	4.7*	17.8	7.0
I-group	4.7	5.2	6.0	5.0	0.6	4.1	15.0	9.4
Overall	5.6	3.7	5.7	3.7	2.5	2.9	9.0	7.8

Table 6.6 Percentage Differences Between Experimental and Calculated Chilling Times for Two-Dimensional Irregular Shapes When Y_c = 0.25 (std = standard deviation, * protrusions excised)

approach	FEM		EA (FEM)		EM (FEM)		BA (analytical)	
shape	mean	std	mean	std	mean	std	mean	std
E_a	5.7	1.1	5.4	0.9	3.9	1.3	6.9	1.9
E_b	5.3	1.9	3.0	6.1	1.3	1.5	-0.6	2.9
E_c	5.7	1.5	5.1	2.5	3.5	1.7	5.8	5.9
E_d	3.0	4.9	0.3	4.6	0.8	4.0	6.8	8.7
E-group	4.9	2.4	3.5	3.6	2.4	2.1	4.7	4.9
I_a	4.6	1.4	4.0	1.0	-0.5	1.2	11.5	6.3
I_b	4.8	7.5	2.2	4.5	-1.3	3.8	6.1	10.4
I_c	0.7	3.4	6.0*	5.1*	0.4*	5.3*	18.6	6.0
I-group	3.4	4.1	4.1	3.6	-0.5	3.4	12.1	7.5
Overall	4.3	3.1	3.7	3.6	1.2	2.7	7.9	6.1

Table 6.7 Percentage Differences Between Experimental and Calculated Chilling Times for Two-Dimensional Irregular Shapes When Y_c = 0.10 (std = standard deviation, * protrusions excised)

approach	FEM		EA (FEM)		EM (FEM)		BA (analytical)	
shape	mean	std	mean	std	mean	std	mean	std
E_a	3.9	2.0	3.4	1.7	2.0	1.7	4.4	2.3
E_b	3.3	1.3	1.8	3.8	-0.6	1.1	-3.0	2.6
E_c	4.9	2.5	3.7	3.2	2.3	2.8	4.4	6.8
E_d	3.0	4.9	0.3	4.6	0.8	4.0	5.4	8.7
E-group	3.8	2.7	2.3	3.3	1.1	2.4	2.8	5.1
I_a	2.6	1.0	2.2	1.4	-1.8	0.8	9.3	5.5
I_b	1.3	7.1	-2.1	4.3	-4.8	4.1	2.5	10.2
I_c	-2.1	3.3	5.1*	5.2*	-0.5*	5.5*	16.9	5.5
I-group	0.6	3.8	1.7	3.6	-2.4	3.4	9.6	7.1
Overall	2.4	3.1	2.1	3.4	-0.0	2.8	5.7	10.4

Table 6.8 Comparison of Percentage Errors in Predicted Times by Different Methods for Shape I_c With and Without Excision of Protrusions (std = standard deviation, proposed = method of Section 4.8)

	Y_c = 0.50		Y_c = 0.25		Y_c = 0.10		Cumulative Results	
Approach	mean	std	mean	std	mean	std	mean	std
FEM	2.1	4.7	0.7	3.4	-2.1	3.3	0.3	4.2
EAO (FEM)	10.6	10.2	12.0	9.1	10.5	8.5	11.0	9.3
EA (FEM)*	4.3	5.6	6.1	5.2	5.1	5.2	5.2	5.4
EMO (FEM)	14.0	7.9	14.9	5.0	13.3	4.9	14.0	6.1
EM (FEM)*	-1.0	4.7	0.4	5.3	-0.5	5.5	-0.4	5.2
EAO (proposed)	17.1	6.9	14.9	5.9	15.7	5.3	15.9	6.1
EA (proposed)*	10.4	6.5	11.1	5.7	9.5	5.5	10.3	5.9
EMO (proposed)	20.1	6.8	20.4	5.9	18.6	5.8	19.7	6.3
EM (proposed)*	4.1	6.3	5.0	5.8	3.6	5.8	4.2	6.0

* protrusions excised.

Table 6.9 Correlations in Percentage Errors Between Finite Element Calculations and Other Approaches for Two-Dimensional Irregular Shapes

Approach	EA (FEM)	EM (FEM)	BA (analytical)	EA (proposed)	EM (proposed)
Correlation	0.677	0.692	0.463	0.774	0.722

Table 6.10 Experimental Data for Chilling of Three-Dimensional Irregular Shapes

Shape Code & Run Number	R (m)	h (W m^{-2} K^{-1})	T_a (°C)	T_i (°C)	$M_{exp.}$	$L_{c\ exp.}$
I_p1	0.042	6.5	1.2	30.2	1.010	1.269
I_p2	0.042	6.5	0.0	29.6	1.027	1.278
I_p3	0.042	6.5	1.4	30.9	0.998	1.244
I_p4	0.042	17.5	0.7	32.0	1.972	1.415
I_p5	0.042	17.5	1.4	31.6	2.031	1.421
I_p6	0.042	17.5	0.9	31.8	2.137	1.539
I_p7	0.042	44.9	1.4	31.6	3.558	1.773
I_p8	0.042	44.9	- 0.1	31.4	3.428	1.903
I_p9	0.042	44.9	- 0.5	24.6	3.519	1.925
I_q1	0.050	25.0	- 4.1	14.7	4.189	1.607
I_r1	0.050	25.0	- 4.8	15.2	3.318	1.403
I_s1	0.025	25.0	- 5.3	18.4	1.747	1.320
I_s2	0.025	25.0	- 5.5	13.4	1.703	1.350
I_s3	0.025	25.0	- 5.4	13.2	1.826	1.374
I_t1	0.025	25.0	- 5.3	18.9	3.140	1.494
S_a1	0.056	25.0	- 4.6	15.5	5.015	1.621
S_a2	0.056	25.0	- 4.5	15.6	5.097	1.485
S_a3	0.056	25.0	- 4.4	15.0	4.711	1.520
S_b1	0.050	25.0	- 4.7	18.3	4.296	1.440
S_c1	0.025	25.0	- 5.5	16.0	2.244	1.330
S_d1	0.025	25.0	- 5.3	18.9	2.798	1.526

Table 6.11 Mean Percentage Differences in Analytically Predicted Chilling Time for the Equivalent Brick Model for Shape I_p Using the Conservation of Area-Volume Approach ($ß_1$ =1.49, $ß_2$ = 1.55)

	Y_c = 0.50	Y_c = 0.25	Y_c = 0.10	Cumulative Results
mean	8.8	7.6	8.7	8.3
std	5.7	5.1	4.8	5.3

Table 6.12 Summary of Percentage Differences Between Experimental and Proposed Method Predicted Chilling Times for Two-Dimensional Irregular Shapes (m = mean, std = standard deviation, * protrusion excised)

	Y_c = 0.50				Y_c = 0.25				Y_c = 0.10				Cumulative Results			
Approach	EA (Proposed)		EM (Proposed)		EA (Proposed)		EM (Proposed)		EA (Proposed)		EM (Proposed)		EA (Proposed)		EM (Proposed)	
Shape	m	std	m	std	m	std	m	std	m	std	m	std	m	std	m	std
E_a	13.9	1.2	12.6	1.2	10.5	1.8	10.3	1.8	9.0	2.5	7.8	2.4	11.5	2.8	10.2	2.7
E_b	11.2	2.6	7.0	2.3	8.8	2.2	4.8	1.9	5.9	2.2	2.3	1.7	8.6	3.2	4.7	2.8
E_c	9.7	1.0	8.8	0.9	8.0	2.3	7.1	2.3	6.7	2.9	6.2	3.0	8.1	2.5	7.4	2.5
E_d	8.4	6.0	9.0	5.2	4.6	5.6	5.1	5.6	4.6	5.6	5.1	5.6	6.4	6.1	6.8	6.0
E-group	10.8	2.7	9.4	2.4	8.2	3.0	6.9	2.9	6.5	3.3	5.4	3.2	8.6	3.6	7.3	3.5
I_a	14.3	2.8	8.4	2.6	10.8	2.0	5.4	1.7	8.7	1.8	3.5	1.3	11.3	3.2	5.8	2.8
I_b	16.2	14.5	6.9	9.1	9.2	10.4	-0.3	4.9	5.1	9.8	-3.9	5.1	10.2	12.6	0.9	8.0
I_c^*	10.4	6.5	4.1	6.3	11.1	5.7	5.0	5.8	9.5	5.5	3.6	5.8	10.3	5.9	4.2	6.0
I-group	13.6	7.9	6.5	6.0	10.4	6.0	3.4	4.1	7.8	5.7	1.1	4.1	10.6	7.2	3.6	5.6
Overall	12.0	4.9	8.1	3.9	9.1	4.3	5.4	3.4	7.1	4.3	3.5	3.5	9.5	5.2	5.7	4.4

Table 6.13 Percentage Differences Between Experimental Results and Chilling Times Predicted by the Proposed Method for Three-Dimensional Shapes (m = mean, std = standard deviation)

	$Y_c = 0.50$				$Y_c = 0.25$				$Y_c = 0.10$				Cumulative Results			
Approach	EA		EM		EA		EM		EA		EM		EA		EM	
Shape	m	std	m	std	m	std	m	std	m	std	m	std	m	std	m	std
S_a	15.5	-	9.3	-	9.9	-	3.5	-	3.5	-	-3.4	-	9.6	-	3.1	-
S_b	17.2	-	12.1	-	10.9	-	6.6	-	4.0	-	-2.0	-	10.7	-	5.6	-
S_c	9.3	-	3.8	-	3.3	-	-2.7	-	2.6	-	-4.0	-	5.1	-	-1.0	-
S_d	8.0	-	2.2	-	9.8	-	3.3	-	12.9	-	5.3	-	10.2	-	3.6	-
S-Group	12.5	5.3	6.9	4.7	8.5	3.4	2.7	3.4	5.8	3.6	-1.0	3.2	8.9	5.4	2.8	5.4
I_p	15.1	3.9	0.5	3.0	13.9	2.9	-0.2	2.1	15.0	2.6	1.2	2.7	14.7	3.2	0.5	2.7
I_q	15.7	-	5.8	-	11.8	-	1.7	-	11.5	-	0.5	-	13.0	-	2.7	-
I_r	16.7	-	8.1	-	9.3	-	1.7	-	3.4	-	-4.3	-	9.8	-	1.8	-
I_s	3.6	-	2.4	-	-0.2	-	-2.6	-	-0.9	-	-4.0	-	0.8	-	-1.4	-
I_t	14.3	-	9.2	-	14.6	-	7.8	-	17.1	-	8.0	-	15.3	-	8.3	-
I-Group	13.1	5.7	5.2	3.8	9.9	6.2	1.7	3.3	9.2	7.4	0.3	4.3	10.7	6.6	2.4	4.0
Overall	12.8	5.6	5.9	4.7	9.2	5.6	2.1	3.6	7.7	7.1	-0.3	4.1	9.9	6.3	2.6	4.5

7. CHILLING OF OBJECTS WITH UNIFORMLY DISTRIBUTED VOIDS

7.1 Introduction

In Chapters 4 and 6 it has been shown that the proposed simple method is accurate for regularly shaped objects and that it can be applied with reasonable accuracy to irregularly shaped objects via the use of an equivalent ellipse or equivalent ellipsoid. However, the method is still restricted to relatively "idealistic" heat transfer conditions as stated in Chapter 3, including: homogeneity, constant thermal properties and ambient temperature, and uniform initial temperature and heat transfer coefficient.

As stated in Chapter 3, in the second stage of the study, it was decided to try to remove one of the restrictions, specifically considering the significance of uniformly distributed air or gas voids within the product, which can be either internal to product items, *e.g.* in bakery products, or between product items in a container.

7.2 Variables Considered Important

One interest was to establish whether the mode(s) of heat transfer in voids is virtually pure conduction through thin air gaps, or whether it involves natural convection as well. The significance of the effect of natural convection (if it exists) on heat transfer through the voids might depend on:

- the size of voids,
- the frequency of occurrence and interlinking of voids, and
- the thermal gradient across the voids, which is considered to be a function of heat transfer conditions.

7.3 Approach Undertaken

A series of experiments were conducted in which variables related to voidage were varied. Means to extend the proposed simple prediction method to fit these data could then be investigated.

Due to the physical nature of air or gas voids, the variables stated in Section 7.1 could not be directly controlled. Therefore, alternative parameters that would have effects on these variables were studied. These alternative variables were:

(1) solid particle size, denoted S (the experimental samples were constructed from a number of particles in a container),
(2) fraction of volume as voids, denoted ε,
(3) Biot number (Bi, defined in eqn 2.21), which takes account of the size of the object (R) and the surface heat transfer coefficient (h), and
(4) ratio of particle size to test object size (S/R).

Although the geometric shape of an object would affect the thermal gradient within the object, due to difficulties in construction of test samples, the effect of shape was not studied.

Cheddar cheese was used as the test material, and the temperature of the samples was typically changed from about 17°C till termination at about -4°C with a cooling medium temperature of about to -5°C for the reasons stated in Section 6.3. Further, the use of fractional unaccomplished temperature change Y to normalise data meant that a wider range of temperatures need not be studied.

7.4 Experimental Methods

In Chapter 5 the methods used to collect experimental data for two- and three-dimensional irregular shapes were described. Similar techniques were applied to the voidage experiments. The same air environmental tunnel was used.

7.4.1 The Test Samples

Five different rectangular boxes, constructed from polypropylene plastic sheet in the same manner as that used for the pyramid shape in Section 5.5.1, were used. Table 7.1 gives the three dimensions for each of these bricks. For each shape, at least nine

chilling runs were conducted. All of the rectangular boxes had a 4 mm diameter hole cut into the lid to allow a bolt to be inserted to hold them onto the rotator or oscillator in the same way as used for the pyramid. The face of each box furthest from the geometric centre was chosen to be the lid. Up to 0.1% of the surface of each box was affected in this way, an insignificant amount. Each plastic box was filled with pre-determined amounts of grated Cheddar cheese or Cheddar cheese cubes of 5, 8, 10, 20 and 40 mm side length, which enabled control of the size of voids. To vary the voidage fraction compression of the cheese samples was needed. This was applied by hand several times during filling. Uniform voidage was not guaranteed by this procedure and this was a major cause of experimental error. Thermocouples were introduced in a different way from that stated in both Sections 5.5.1 and 5.6.1. After the container were filled holes were made and the thermocouples were inserted as close as possible to the geometric centre of each brick and at four to five places between the centre and the surface. The leads were all introduced through a small hole at one of the edges of the lid. The reasons for using this technique were: (1) pre-set thermocouple wires would have hindered pressing while filling causing more unevenness in voids distribution, and (2) the pre-set thermocouple wires would have been moved away from the pre-set positions when compression was applied.

7.4.2 Dimension Measurement and Control

The dimensions of each rectangular brick were measured prior to and after the chilling process. No observable variations were found. Taking this into consideration with construction and measurement imprecision, the box dimensions were accurate to ± 1.0 mm for all five samples.

7.4.3 Measurement and Control of Surface Heat Transfer Coefficients

The polypropylene rectangular bricks were identical in all respects to those used previously for measuring the surface heat transfer coefficient for the pyramid shape (Section 5.5.1). To alter the surface heat transfer coefficient, one layer of plastic foam sheet was glued to each face of the rectangular boxes in a similar manner to that used

for the two-dimensional shapes and the pyramid shape. The same h values were assumed to hold for the rectangular boxes in these experiments as in the previous ones so no further experiments relating to h were conducted. The error in the mean h value for these rectangular boxes should be of the same order as that for the pyramid (5.3% at 95% C.I.). The sample rectangular bricks were rotated or oscillated in a similar way to that of the rectangular bricks used in Section 5.5.1.

7.4.4 Analysis of Heat Transfer in Rectangular Bricks with Uniformly Distributed Voids

In each chilling experiment, as stated in Section 7.1, the temperature of the samples was typically changing from about 17°C till termination at about -4°C, for a cooling medium temperature of about -5°C. Beyond this, the inaccuracy of temperature measurement was too significant for the data to be valuable. As stated above the sample containers were covered with a layer of sheet plastic foam for some experimental runs. The two values of h and various containers led to twenty-one different values of Biot number ranging from 0.57 to 5.66.

In contrast to the experiments with homogeneous irregular shapes, the effect on external heat transfer caused by the presence of voids at the sample surface was not considered to be a problem. The fact that a large fraction of the surface area was deliberately occupied by voids made it unnecessary to distinguish between regions of perfect and imperfect contact. Evenness of contact was an issue.

Suitable isothermal regions for thermocouple lead location do not occur in brick shaped objects. Placement of thermocouples was not critically important because as will be shown later in the data analysis, the slope of the ln Y vs t plot was of more interest than the intercept.

As was the case for the two-dimensional shapes and the pyramid, the effect of the heat released by the plastic coating and box wall material was considered insignificant compared with the heat released by the cheese inside the box.

7.5 Experimental Design

In order to investigate the effect of air or gas voidage on the chilling rate of foods, experiments must be conducted across a wide range of conditions covering those that occur in common chilling practice. As previously stated in Section 7.1, the most important variables were:

- the Biot number (*Bi*, defined in eqn 2.21), which takes account of the size of the object and the surface heat transfer coefficient (*h*); the box size (*R*), and the fraction of volume as voids (ε) indirectly through its effect on product thermal conductivity,
- the particle size (*S*), and
- the ratio of particle size versus box size (*S*/*R*).

An experimental design was sought so that the factors were varied over as wide a range as possible within the limitations of the experimental equipment.

An orthogonal experimental design in terms of the above variables would be desirable but ranges of conditions available were restricted by physical limitations in controlling the variables, especially *h* and *R*, to preselected values. The range of Biot number that could be considered was physically limited by the first dimensions, as well as the mould wall material and thickness used. Values of the object size and the surface heat transfer coefficients were, in most cases, determined more by considerations such as the availability of the appropriate types of moulds and their wall material, than by choice to give a specified *Bi* value. It was decided to vary the Biot number as widely as possible by using different sample sizes. Using the addition of an insulating plastic foam layer for some shapes gave increased control and variability of *h*. The levels of each variables used are as follows:

Bi = 0.57 to 5.66;

h = 6.5 and 17.2 W $m^{-2}K^{-1}$;

R = 0.027 to 0.101 m;

S = 0.001 to 0.040 m; and

S/*R* = 0.010 to 0.526.

The correlation coefficients between these variables in the experimental design used are

shown in Table 7.2. Details of the level of these variables for each run are given in Table 7.3. Since it is a function of both h and R, Bi was naturally correlated to both. Due to the small number (5) of different sample containers, the ratio of particle size to object size was highly correlated to the object size. All the other coefficients representing the correlation between these variables were relatively low and not considered to be significant.

A total of 58 experiments, including replicates to estimate the experimental error, were conducted. In presenting the experimental results, two parameters, $L_{c\,exp}$ and m, were derived as follows:

1. Using the sample dimensions in Table 7.1 plus the definitions of Y_c, the experimental data were converted to plots of ln Y_c vs t. Values of the thermal properties, especially the thermal conductivity were unknown. Hence values of the Fourier number (defined in eqn 2.18) could not be calculated. Consequently, lines of ln (Y_c) vs t (which is dimensional), instead of ln (Y_c) vs Fo were plotted. The dimensional cooling rate m rather than the dimensionless cooling rate M had to be employed.

2. A best-fit line between Y_c = 0.70 and Y_c = 0.05 was found using linear regression:

$$\ln (Y_c) = \ln (L_{c\,exp}) - m\,t \qquad (7.1)$$

where $L_{c\,exp}$ = experimentally determined lag factor for the thermal centre

m = dimensional cooling rate (s^{-1})

For each run, $L_{c\,exp}$ and m were found and the experimental results are given in Table 7.3.

Other than the use of the same measuring systems, the replicates were performed as independently from each other as possible (including refilling of the cheese in the containers) to give a true indication of variability due to experimental techniques. The most important variable that could not be measured independently from the other experiments was the surface heat transfer coefficient. Total uncertainty introduced by

errors in measurement, or due to any systematic error, could not be quantified from the spread of replicates because of the inability to achieve total independence of nominally replicate runs. The difficulties in achieving homogeneous void distribution were significant. In Table 7.3 replicates are marked and considerable variations can be seen. The worst group is Runs B_e4 and B_e5, in which m varied from 1.70×10^{-4} to 1.88×10^{-4} s^{-1}. Two experiments gave $L_{c\ exp}$ values smaller than 1, which indicated that the centre thermocouples for theses runs were in fact located well away from the thermal centre. The impact of this displacement will be further analyzed in Chapter 8.

Table 7.1 Geometric Measurements of the Rectangular Bricks Used in Voidage Experiments

Code	B_a	B_b	B_c	B_d	B_e
D_1 (mm)	104	81	54	201	72
D_2 (mm)	125	151	127	201	72
D_3 (mm)	152	151	201	201	300
ß$_1$	1.20	1.86	2.35	1.00	1.00
ß$_2$	1.46	1.86	3.72	1.00	4.17

Table 7.2 Correlation Coefficients Between Variables Used in Voidage Experiments

Variable	R	h	Bi	ε	S
h	-0.023				
Bi	0.643	0.694			
ε	0.094	0.049	0.079		
S	0.297	-0.295	0.036	0.165	
S/R	-0.123	-0.424	-0.302	0.016	0.850

Table 7.3 Experimental Data for the Cheddar Cheese Bricks with Uniformly Distributed Voids (Data in last three columns are determined and discussed in Chapter 8)

Shape Code & Run Number	Replicates	R (m)	h (W m^{-2}K^{-1})	ε	S (m)	S/R	$m \times 10^4$ (s^{-1})	$L_{c\ exp}$	$L_{c\ model}$	Bi	k_e (W m^{-1}K^{-1})
B_a1	Group 1	0.052	17.2	0.138	0.001	0.019	0.993	1.114	1.709	2.93	0.239
B_a2		0.052	17.2	0.138	0.001	0.019	1.132	1.329	1.689	2.93	0.269
B_a3		0.052	17.2	0.138	0.001	0.019	1.010	1.390	1.791	2.93	0.245
B_b1		0.041	17.2	0.095	0.001	0.024	1.156	1.436	1.596	2.28	0.277
B_c1		0.027	17.2	0.134	0.010	0.370	1.848	1.148	1.382	1.52	0.256
B_d1		0.101	17.2	0.100	0.001	0.010	0.398	1.117	1.867	5.66	0.224
B_e1		0.038	17.2	0.100	0.001	0.026	1.465	0.757	1.443	2.14	0.224
B_a4		0.052	17.2	0.289	0.001	0.019	0.904	1.459	1.765	2.93	0.158
B_b2	Group 2	0.041	17.2	0.333	0.001	0.024	1.142	1.370	1.642	2.28	0.171
B_b3		0.041	17.2	0.333	0.001	0.024	1.134	1.398	1.643	2.28	0.169
B_b4		0.041	17.2	0.333	0.001	0.024	1.127	1.457	1.644	2.28	0.168
B_d2		0.101	17.2	0.250	0.001	0.010	0.395	1.563	1.888	5.66	0.177
B_a5		0.052	17.2	0.400	0.001	0.019	1.101	1.290	1.761	2.93	0.164

...continued

Table 7.3 continued...

Shape Code & Run Number	Replicates	R (m)	h (W $m^{-2}K^{-1}$)	ε	S (m)	S/R	$m \times 10^4$ (s^{-1})	$L_{c\ exp}$	$L_{c\ model}$	Bi	k_e (W $m^{-1}K^{-1}$)
B_b5		0.041	17.2	0.400	0.001	0.024	1.292	1.573	1.764	2.28	0.126
B_c3		0.027	17.2	0.512	0.001	0.037	1.997	1.399	1.425	1.52	0.139
B_c4		0.027	17.2	0.318	0.001	0.037	1.627	1.071	1.414	1.52	0.171
B_d3		0.101	17.2	0.400	0.001	0.010	0.441	1.476	1.898	5.66	0.155
B_d4		0.101	17.2	0.250	0.020	0.198	0.383	1.355	1.891	5.66	0.170
B_d5		0.101	17.2	0.408	0.020	0.198	0.577	1.326	1.873	5.66	0.210
B_e2		0.038	17.2	0.400	0.001	0.026	1.860	1.438	1.487	2.14	0.168
B_e3		0.038	17.2	0.250	0.020	0.526	1.589	1.200	1.474	2.14	0.187
B_e4	Group 3	0.038	17.2	0.400	0.010	0.263	1.881	1.390	1.486	2.14	0.171
B_e5		0.038	17.2	0.400	0.010	0.263	1.702	1.462	1.506	2.14	0.146
B_e6		0.038	17.2	0.100	0.020	0.526	1.518	1.387	1.439	2.14	0.240
B_a6		0.052	17.2	0.309	0.008	0.154	0.974	1.385	1.757	2.93	0.169
B_b6		0.041	17.2	0.299	0.008	0.195	1.182	1.402	1.632	2.28	0.193
B_c5		0.027	17.2	0.321	0.005	0.185	1.800	1.405	1.403	1.52	0.201

...continued

Table 7.3 continued...

Shape Code & Run Number	Replicates	R (m)	h (W $m^{-2}K^{-1}$)	ε	S (m)	S/R	$m \times 10^4$ (s^{-1})	$L_{c\ exp}$	$L_{c\ model}$	Bi	k_e (W $m^{-1}K^{-1}$)
B_a7		0.052	17.2	0.435	0.008	0.154	0.951	1.417	1.786	2.93	0.126
B_b7		0.041	17.2	0.436	0.008	0.195	0.960	1.434	1.673	2.28	0.108
B_c6		0.027	17.2	0.438	0.005	0.185	1.800	1.125	1.422	1.52	0.147
B_d6		0.101	17.2	0.291	0.040	0.396	0.513	1.191	1.891	5.66	0.229
B_d7	Group 4	0.101	17.2	0.397	0.040	0.396	0.629	1.080	1.859	5.66	0.240
B_d8		0.101	17.2	0.397	0.040	0.396	0.579	1.216	1.870	5.66	0.216
B_c7		0.027	6.5	0.100	0.010	0.370	0.758	1.184	1.314	0.57	0.174
B_c8		0.027	6.5	0.250	0.010	0.370	0.815	1.153	1.348	0.57	0.133
B_a8		0.052	6.5	0.100	0.020	0.385	0.549	1.166	1.629	1.10	0.193
B_b8		0.041	6.5	0.100	0.020	0.488	0.585	1.345	1.491	0.86	0.185
B_e8		0.038	6.5	0.250	0.001	0.026	0.873	1.217	1.344	0.81	0.155
B_c9		0.027	6.5	0.400	0.010	0.370	1.031	1.138	1.415	0.57	0.137
B_d9		0.101	6.5	0.400	0.001	0.010	0.249	1.554	1.851	2.13	0.097
B_e9		0.038	6.5	0.400	0.001	0.026	0.888	1.207	1.428	0.81	0.097

...continued

Table 7.3 continued...

Shape Code & Run Number	Replicates	R (m)	h (W $m^{-2}K^{-1}$)	ε	S (m)	S/R	$m \times 10^4$ (s^{-1})	$L_{c\ exp}$	$L_{c\ model}$	Bi	k_e (W $m^{-1}K^{-1}$)
B_d10		0.101	6.5	0.250	0.020	0.198	0.221	1.445	1.834	2.13	0.111
B_a9		0.052	6.5	0.250	0.020	0.385	0.453	0.893	1.697	1.10	0.097
B_b9		0.041	6.5	0.250	0.020	0.488	0.634	1.235	1.533	0.86	0.149
B_d11		0.101	6.5	0.127	0.001	0.010	0.214	1.395	1.828	2.13	0.131
B_e11		0.038	6.5	0.250	0.010	0.263	0.889	1.125	1.334	0.81	0.163
B_d12		0.101	6.5	0.250	0.001	0.010	0.168	1.392	1.876	2.13	0.077
B_e12	Group 5	0.038	6.5	0.250	0.020	0.526	0.773	1.172	1.399	0.81	0.115
B_e13		0.038	6.5	0.250	0.020	0.526	0.725	1.133	1.421	0.81	0.101
B_a10		0.052	6.5	0.400	0.020	0.385	0.720	1.277	1.612	1.10	0.147
B_b10		0.041	6.5	0.400	0.020	0.488	0.752	1.147	1.551	0.86	0.134
B_d13		0.101	6.5	0.291	0.040	0.396	0.379	1.289	1.680	2.13	0.240
B_d14		0.101	6.5	0.271	0.040	0.396	0.290	1.221	1.793	2.13	0.159
B_b11		0.041	6.5	0.200	0.001	0.024	0.682	1.454	1.477	0.86	0.198
B_b12		0.041	6.5	0.333	0.001	0.024	0.749	1.021	1.515	0.86	0.164
B_b13		0.041	6.5	0.400	0.001	0.024	0.791	1.439	1.534	0.86	0.148

8. PREDICTION METHODS TO ACCOUNT FOR UNIFORMLY DISTRIBUTED VOIDS

8.1 Introduction

The most obvious approach to account for uniformly distributed voids is to adjust the thermal properties. Usually density and specific heat are calculated by summing up the component properties in mass or volume proportion. The density and specific capacity of the air or gas in voids are negligibly small compared with that of the solid phase for most foods concerned, therefore:

$$\rho_e \approx (1 - \varepsilon)\, \rho_s \tag{8.1}$$

where ρ_s = density of the solid phase (kg m^{-3}), and

$$c_e \approx c_s \tag{8.2}$$

where c_s = specific heat capacity of the solid phase (J $kg^{-1}K^{-1}$).

Thermal conductivity of composite materials such as foods depends not only on the properties of its components but also on the food structure. For example, common food materials such as meat have different thermal conductivities, parallel to and perpendicular to the fibres. It was decided to investigate the concept of "equivalent thermal conductivity", designated k_e, to extend the newly proposed method to applications involving uniformly distributed voids.

8.2 Determination of the Equivalent Thermal Conductivity from the Experimental Data

Considering the analytical solution for the rectangular brick (which is the product of the analytical solutions for three infinite slabs of characteristic dimensions R, $\beta_1 R$ and $\beta_2 R$ respectively), if only the first term in the analytical solution for each of the three dimensions is significant, the analytical solution (eqn 2.22 or 2.23, 2.34 and 2.33) can be approximated as:

$$Y_c = L_{c\,model} \exp(-M\, Fo) \tag{8.3}$$

where

$$Fo = f(k_e, \rho, c, R, t) \tag{8.4}$$

$$L_{c\ model} = f(Bi, \text{position within the brick}) = f(k_e, h, R, x/R) \tag{8.5}$$

$$M \text{ (dimensionless cooling rate)} = f(k_e, h, R, \beta_1, \beta_2) \tag{8.6}$$

The problem is that for the bricks, it is not clear how the three terms (dimensions) come into calculation and whether it is valid to assumed only one term in each of the analytical solutions is significant. Therefore, it was decided to find values of k_e from the experimental data in such a way that the slope of a best fit line of ln Y_c versus time for $0.05 \leq Y_c \leq 0.70$ had a slope given by:

$$m = -\omega^2 \frac{k_e}{\rho c R^2} \tag{8.7}$$

A computer programme was written that used an iterative procedure to find the best-fit k_e value to match the particular measured cooling rate m. The values of ρ and

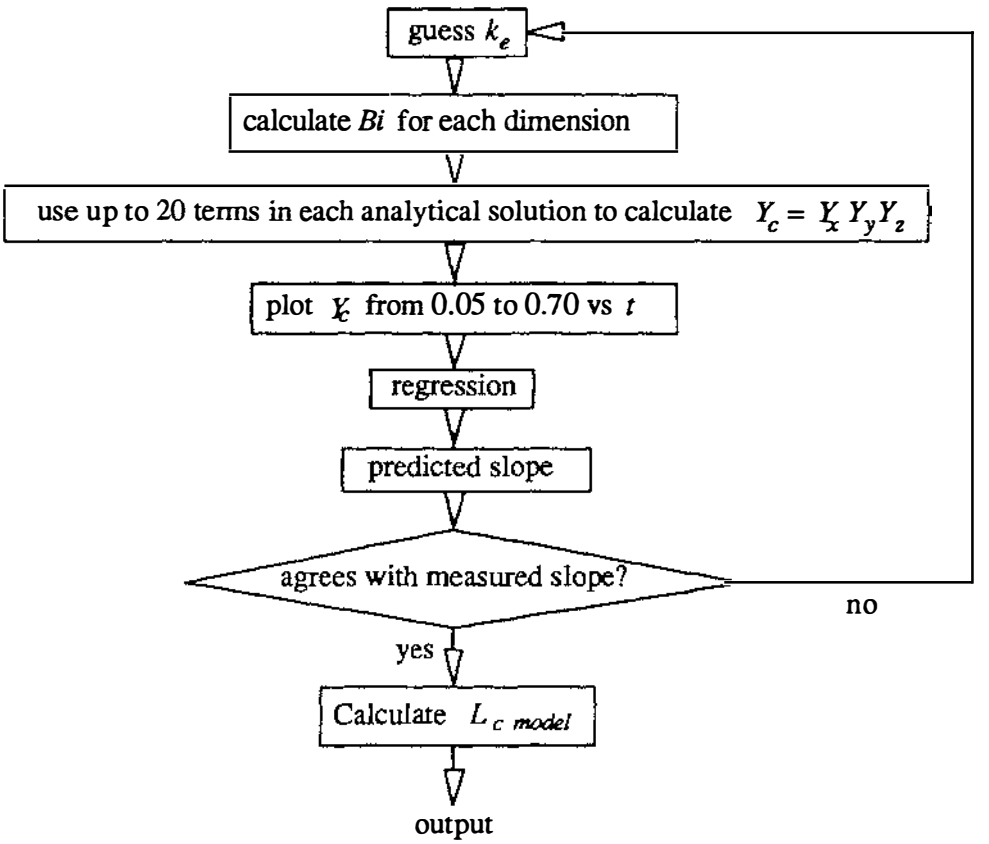

Figure 8.1 Data analysis procedure used to find k_e and $L_{c\ model}$

c were found using eqns 8.1 and 8.2. The procedure is illustrated in Figure 8.1. Themain difficulty with using the Fourier series solutions is that they are slow to converge for short lengths of time. Therefore 20 terms in the series were retained in each case. This ensured errors from failure of the series to converge in calculations were negligibly small.

An advantage of the method is that it is relatively insensitive to the exact location of the thermocouple within the brick. If the centre thermocouple is not precisely positioned at the thermal centre (remembering that this was more likely for voidage runs than runs without voidage since the thermocouples were not firmly fixed in position), this should not significantly affect the estimation of k_e. This process finds k_e and also allowed the theoretical intercept, $L_{c\ model}$ to be found using the analytical method. The values of both k_e and $L_{c\ model}$ are tabulated in Table 7.2.

The next question was whether a model for the equivalent thermal conductivity that predicted the data with reasonable accuracy could be found.

8.3 Existing Equivalent Thermal Conductivity Models

A large number of models have been proposed.

The Maxwell-Eucken model was first reported by Eucken (1940). One component forms a continuous phase, with the other components being widely dispersed as bubbles:

$$k_e = k_s\left(\frac{1 - 2C_1\varepsilon}{1 + C_1\varepsilon}\right) \tag{8.8}$$

where k_s = thermal conductivity of the solid phase,

k_g = thermal conductivity of the gas phase, and

$$C_1 = \frac{k_s - k_g}{2k_s + k_g} \tag{8.9}$$

The Maxwell-Eucken equation gives different numerical results for the thermal conductivity of two component mixtures or solutions depending on which phase is assumed to be continuous and which is dispersed within the continuous phase. To overcome this, Levy (1981) introduced an additional parameter which was a function of the ratio of the thermal conductivities of the components. The parameter F was proposed to replace ε in the Maxwell-Eucken equation (8.8).

$$2F = \frac{2}{C_2} - 1 + 2\varepsilon - \left[\left(\frac{2}{C_2} - 1 + 2\varepsilon\right)^2 - \frac{8\varepsilon}{C_2}\right]^{\frac{1}{2}} \tag{8.10}$$

where

$$C_2 = \frac{(k_g - k_s)^2}{(k_s - k_g)^2 + \frac{k_s k_g}{2}} \tag{8.11}$$

Hill *et al.* (1967) proposed that thermal conductivity values of meat could be predicted by the formula:

$$k_e = (2C_3 - C_3^2)k_g + (1 - 4C_3 + 3C_3^2)k_s + \frac{8(C_3 - C_3^2)k_s k_g}{C_3 k_s + (4 - C_3)k_g} \tag{8.12}$$

where

$$C_3 = 2 - \sqrt{4 - 2\varepsilon} \tag{8.13}$$

Hill *et al.* reported thermal conductivity measurements for various meats. The data show the dependence of conductivity on temperature, moisture content, and direction of heat flow (perpendicular or parallel to the grain of the meat). The conductivity values of beef samples measured parallel to the grain were compared with values that were predicted by the proposed model.

Mattea *et al.* (1986) reported that the Effective Medium Theory (EMT), known in the field of physics to model conductive properties in heterogeneous chaotic media, had been applied to predict the thermal conductivity of sugar-based fruits and of potatoes as a function of the water content. With the thermal conductivity of the constituents, the composition and porosity as data, the equation derived from EMT for continuous media was applied to apples, pears and potatoes. For a system of two components, the equivalent thermal conductivity k_e is given by

$$(1 - \varepsilon)\frac{k_e - k_s}{k_s + 2k_e} + \varepsilon\frac{k_e - k_g}{k_g + 2k_e} = 0 \tag{8.14}$$

The results were compared with experimental values and data from the literature. Good agreement was obtained, with differences not larger than 8%, although the model appeared to over predict, particularly for higher water contents.

Thermal conductivity of fresh lamb meat offal and fat was measured by Pham & Willix (1989). With independently obtained values of physical parameters, several of the theoretical models were tested to see if thermal conductivity could be calculated from composition. Those tested including:

(a) the parallel model, wherein each component forms a parallel heat-conducting path:

$$k_e = (1 - \varepsilon)k_s + \varepsilon k_g \tag{8.15}$$

(b) the series model, in which heat flows successively through each component so that their resistances are added:

$$\frac{1}{k_e} = \frac{1 - \varepsilon}{k_s} + \frac{\varepsilon}{k_g} \tag{8.16}$$

Also tested were the models of Maxwell-Eucken, Levy's and Hill *et al.* Over a wide range of compositions, best predictions were obtained with Levy's modification to the Maxwell-Eucken equation. Its accuracy was not unduly sensitive to the uncertainties in the values of the physical parameters.

Murakami & Okos (1989) reported a comprehensive study of thermal conductivity modelling for foods with voidage. Published models on thermal conductivity prediction were grouped according to their appropriate food system. It was proposed in this paper that the thermal conductivity model of foods be made up of its components and a structural model that accounts for the components arrangement in the system. Nine models were evaluated, including some of those above plus:

(a) Keey (1972) which couples series and parallel thermal conductivities using a distribution factor f. Murakami and Okos (1989) modelled f as a function of the voidage fraction and moisture content of the food:

$$\frac{1}{k_e} = \frac{1 - f}{(1 - \varepsilon) k_s + \varepsilon k_g} + f \left(\frac{1 - \varepsilon}{k_s} + \frac{\varepsilon}{k_g} \right) \tag{8.17}$$

where f = distribution factor determined by the material structure.

(b) Kopelman (1966):

$$k_e = \frac{k_s (1 - C_4)}{1 - C_4 (1 - \varepsilon^{1/3})} \tag{8.18}$$

where

$$C_4 = \frac{\varepsilon^{2/3}}{1 - k_g / k_s} \tag{8.19}$$

(c) solid-continuous model (a restatement of Maxuell-Eucken model):

$$\frac{k_e}{k_s} = \frac{3 C_5 + 2 (1 - \varepsilon) (1 - C_5)}{3 - (1 - \varepsilon) (1 - C_5)} \tag{8.20}$$

where

$$C_5 = \frac{k_g}{k_s} \tag{8.21}$$

(d) random distribution model:

$$4 k_e = C_6 k_s + C_7 k_g + [(C_6 k_s + C_7 k_g)^2 + 8 k_s k_g]^{1/2} \tag{8.22}$$

where

$$C_6 = 2 - 3\varepsilon \qquad \text{and} \qquad C_7 = 3\varepsilon - 1 \tag{8.23}$$

The Keey model was found to give the best performance for porous foods in Murakami & Okos' work.

Singh & Mannapperuma (1990) suggested that thermal conductivity of composite materials such as foods depends not only on the properties of its components but also on its structure. A common food material such as meat has different thermal conductivities parallel to its fibres than perpendicular to the fibres. The effect of voidage on thermal conductivity is also not as simple compared to its effect on density, or even specific heat capacity which is a thermodynamic property that can be derived by summing up the component properties in mass proportion.

8.4 Results from Application

All the methods above were tested.

The thermal conductivity of Cheddar cheese is stated in Table 5.1 and the mean k value used for air was 0.025 W/m K for the temperature range of -5 to 20°C. Using these data, values of the equivalent thermal conductivity were calculated using the various methods and compared against the experimentally determined k_e values. The results are tabulated in Table 8.1.

The parallel approach tended to over predict the experimental results with a mean offset of 40%, a particularly high standard deviation and large 95% confidence interval.

In contrast, the series approach tended to under predict with a mean offset of -50%, and also a large 95% confidence interval.

The Maxwell-Eucken and Solid-continuous formulae are the same and were similar in accuracy to the parallel approach, but with slightly less over prediction.

Levy's approach was much less overpredictive with the mean prediction at 6%. There was some improvement in the standard deviation and 95% confidence interval.

Kopelman's and Hill *et al.*'s approaches lie between the parallel and Maxwell-Eucken's approaches.

Both the effective medium theory and the random distribution theory had slightly lower mean predictions than the Maxwell-Eucken approach, but were otherwise similar to the Maxwell-Eucken's approach.

The key issue for Keey's method is to find a simple and reasonably accurate algebraic formula for the distribution factor f. Initially a constant $f = 0.824$ was found by curve-fitting, which was designated Keey (1). This led to results better than any other method. The results are shown in the third last column of Table 8.1. It thus justified further investigation.

Murakami and Okos (1989) had suggested that f was dependent on ε and moisture content of the product. The latter was not varied in the present work. However, if natural convection in the voids was important, this might correlated with Bi. Figure 8.2 shows the values of f back-calculated from measured k_e plotted versus Bi, indicating a possible negative reciprocal relationship. However, this is not the only possible explanation. Another possibility was that the 12 data points for which $f < 0.6$ on Figure 8.2 are in fact those with the greatest experimental error, and in fact f is relatively constant (ignoring these points) at about 0.85. The 12 experimental runs were individually examined, and are marked in Table 8.1. They are some of the data worst predicted by all models, but not the only badly predicted data. Thus there was real doubt as to how authentic the apparent Bi dependency is. It was decided to include a Bi term in initial curve-fitting of f, but to re-evaluate that decision later. Hence f was considered a function of both ε and Bi. The function

$$f = a + b\varepsilon - \frac{c}{Bi} \tag{8.24}$$

was considered. All possible combinations within the right-hand side of eqn (8.24) were used to best fit the data (*e.g.* a, b, c $\neq$ 0, a = 0, b = 0, c = 0, *etc.*). Besides Keey (1), two possibilities (Table 8.2) of different complexity were found to perform significantly better than the others combinations. The two formulae were designated Keey (2) and (3). The results are shown in the last two columns of Table 8.1. Formulae for f involving quadratic and cubic terms, as suggested by Murakami and Okos (1989), were also considered in a similar manner, but no further improvement in accuracy was obtained.

Further analysis was then performed with Keey's method to ascertain whether the lack of fit was purely due to experimental error, or whether prediction method error was significant, and whether *Bi* dependence should be included.

In Figure 8.3 to 8.5, the absolute differences found by comparing the experimental k_e values and their counterparts predicted by the approaches of Keey (1), (2) and (3) respectively were ranked and plotted on normal-probability paper in the manner discussed by Draper & Smith (1981). The results show that the lack of fit follows a normal distribution. This suggests that experimental error alone is largely responsible for most of the lack of fit and no runs had particularly abnormal experimental error from a statistical viewpoint. Nevertheless further checking was carried out.

The mean absolute differences between the experimental data and the predictions of Keey (1), (2) and (3) are plotted versus the ratio of ($L_{c\ exp}$ / $L_{c\ model}$) in Figure 8.6 to 8.8 respectively. If thermocouples were at the centre then $L_{c\ exp}$ / $L_{c\ model}$ = 1 by definition. In all cases the spread of data increases as the ratio decreases. However, the correlation coefficients are low (*e.g.* 0.073 for Keey (1)), which shows that the thermocouple placement problem is mainly a random contributor to the experimental errors. It is probable that when a thermocouple has moved away from the centre this has been associated with uneven compression of the cheese particles, and hence heterogeneity leading to amplification of experimental error.

The prediction errors using the Keey (1), (2) and (3) approaches were plotted respectively against *Bi* and ε (Figure 8.9 to 8.14), while the prediction errors using the Keey (2) approach were plotted respectively against *R, S* and *S/R* (Figures 8.15 to 8.17).

It is observed in Figure 8.9 and in Figure 8.10 that, as the *Bi* increases, the difference between the predicted and experimental values tends from positive to negative. The trend largely disappears as the *f* function incorporates *Bi* as a variable (Figure 8.11).

A similar phenomenon is observed in Figure 8.12 as ε increases. In Figures 8.13 and 8.14, there is no such trend because a term in ε has been fitted.

No particular trends can be found from the plots of prediction errors in k_e versus *R, S* and *S/R* (Figure 8.15 to 8.17) for Keey (2) indicating that influence of voids size, object size and relative void size is probably insignificant compared to the size of random error. Similar graphs arise for Keey (1) and (3).

Table 8.1 shows that the value of making *f Bi*-dependent is small (standard deviation for Keey (2) is 27.9%, that for Keey (3) 26.7%). Possible explanations for *Bi*-dependence include:

1. At high *Bi*, the convective heat transfer in the gas phase within the objects may not be negligible due to a high thermal gradient across the voids and a high proportion of gas phase increasing *Bi* by reducing k_e. Any effect would be to increase the chilling rate and hence the measured equivalent thermal conductivity so *f* needs to be *Bi* dependent; or

2. Uncertainties in thermal property (especially thermal conductivity) data of the test material (Cheddar cheese) which would be more significant at high *Bi* due to the greater influence of internal resistance to heat transfer have led to an apparent relationship of *f* with *Bi*.

Because the increase in accuracy moving from Keey (2) to Keey (3) was modest, it was decided to adopt the conservative approach of Keey (2) in case the *Bi* dependency arose solely from systematic error in thermal properties. The recommended equation is therefore:

$$\frac{1}{k_e} = \frac{0.435 - 0.718\,\varepsilon}{(1-\varepsilon)k_s + \varepsilon k_g} + (0.565 + 0.718\,\varepsilon)\left(\frac{1-\varepsilon}{k_s} + \frac{\varepsilon}{k_g}\right) \qquad (8.25)$$

Testing has been limited to $0 \leq \varepsilon \leq 0.5$, $0.5 \leq Bi \leq 5.6$ and to one product, Cheddar cheese. The breadth of applicability of eqn (8.25) can only be ascertained by more testing. However because k_s and k_g are very different in numerical value and k_g is effectively fixed, the errors arising from using eqn (8.25) for k_s values likely to arise in typical chilled foods (k = 0.3 - 0.6 W/m K) may in fact be quite small.

8.5 Discussion

The experimental data for uniformly distributed voids have high variability due to experimental error. Keey's method is the most accurate if the distribution factor (f) is curve-fitted to voidage fraction, and possibly *Bi*;

It is not clear whether natural convection or thermal property uncertainty is responsible for the apparent reliance of f on *Bi*. The conservative approach, omitting *Bi* from the curve-fit equation is recommended. Because testing was in a three-dimensional heat transfer situation (rectangular brick), it has not been established whether the equation would apply for different heat transfer conditions, *e.g.* one-dimensional heat transfer in a slab.

Table 8.1 Percentage Error in Predicted Thermal Conductivities for Objects with Uniformly Distributed Voids Using Various Approaches (* indicates a run for which the experimentally determined value of f in Keey's formula < 0.6)

approach		Parallel	Series	Maxwell-Eucken	Levy	Kopelman	Hill *et al.*	Effective Medium Theory	Solid-Continuous	Random Distribution	Keey (1)	Keey (2)	Keey (3)
mean		40.8	-50.5	27.2	6.0	32.8	27.3	19.7	27.2	15.3	5.3	0.1	0.2
std.		41.5	17.7	38.2	34.0	39.9	39.9	37.8	38.2	33.7	32	27.9	26.7
95% C.I.	min	-42.6	-86.1	-49.6	-62.3	-47.4	-52.9	-56.3	-49.6	-52.4	-58.2	-56.0	-53.5
	max	124.2	-14.9	104.0	74.3	113.0	107.5	95.7	104.0	83.0	69.6	56.2	53.9
B_a1		12.0	-49.3	6.2	-3.4	9.8	9.5	5.0	6.2	-10.6	-7.7	-20.4	-15.1
B_a2		-0.6	-55.0	-5.8	-14.3	-2.6	-2.8	-6.8	-5.8	-20.7	-18.1	-29.3	-24.7
B_a3		9.0	-50.6	3.4	-5.9	6.9	6.7	2.3	3.4	-13.0	-10.1	-22.5	-17.4
B_b1		0.8	-46.4	-2.9	-9.1	-0.4	-0.3	-3.4	-2.9	-20.0	-12.7	-23.8	-20.9
B_c1		4.7	-52.0	-0.6	-9.3	2.7	2.5	-1.6	-0.6	-16.5	-13.4	-25.3	-24.6
B_d1		23.7	-35.4	19.0	11.1	22.3	22.3	18.3	19.0	-1.7	6.5	-7.2	0.2
B_e1		24.0	-35.3	19.2	11.3	22.5	22.5	18.6	19.2	-1.5	6.7	-7.0	-3.7

...continued

Table 8.1 continued...

approach	Parallel	Series	Maxwell-Eucken	Levy	Kopelman	Hill *et al.*	Effective Medium Theory	Solid-Continuous	Random Distribution	Keey (1)	Keey (2)	Keey (3)
B_a4	41.7	-54.2	27.5	5.1	33.6	29.2	20.8	27.5	15.8	3.5	-4.0	5.2
B_b2	24.1	-62.0	10.1	-11.6	15.6	9.8	2.3	10.1	2.3	-11.3	-14.0	-8.2
B_b3	25.5	-61.6	11.3	-10.6	16.8	11.0	3.4	11.3	3.4	-10.3	-13.0	-7.2
B_b4	26.6	-61.2	12.3	-9.8	17.8	12.0	4.3	12.3	4.3	-9.5	-12.3	-6.4
B_d2	33.0	-54.3	21.2	2.5	26.9	24.1	16.6	21.2	8.0	-0.5	-10.6	2.1
B_a5	17.6	-65.9	2.3	-20.9	7.3	-1.5	-8.6	2.3	-1.6	-17.8	-13.6	-4.2
B_b5	53.2	-55.5	33.2	3.0	39.8	28.3	19.1	33.2	28.1	7.1	12.5	20.1
B_c3	16.9	-67.0	-1.3	-27.8	3.1	-13.5	-19.2	-1.3	1.0	-19.3	-0.1	-3.3
B_c4	26.9	-60.4	13.1	-8.3	18.7	13.5	5.9	13.1	4.3	-8.6	-12.9	-13.2
B_d3	25.2	-63.6	8.9	-15.8	14.3	4.9	-2.6	8.9	4.8	-12.5	-8.0	8.9
B_d4	38.3	-52.5	26.1	6.6	31.9	29.0	21.3	26.1	12.3	3.5	-7.0	6.1
B_d5	-9.0	-73.7	-21.1	-39.2	-17.2	-24.3	-29.8	-21.1	-23.8	-36.5	-32.6	-20.1

...continued

Table 8.1 continued...

approach	Parallel	Series	Maxwell-Eucken	Levy	Kopelman	Hill *et al.*	Effective Medium Theory	Solid-Continuous	Random Distribution	Keey (1)	Keey (2)	Keey (3)
B_e2	15.4	-66.5	0.4	-22.4	5.3	-3.3	-10.3	0.4	-3.4	-19.3	-15.2	-10.4
B_e3	25.9	-56.7	14.7	-3.0	20.1	17.4	10.4	14.7	2.2	-5.8	-15.4	-10.9
B_e4	13.3	-67.1	-1.5	-23.8	3.4	-5.1	-11.9	-1.5	-5.2	-20.8	-16.8	-12.1
B_e5	32.8	-61.4	15.5	-10.7	21.2	11.3	3.3	15.5	11.1	-7.2	-2.4	3.0
B_e6	15.9	-39.5	11.5	4.0	14.5	14.6	10.9	11.5	-7.9	-0.2	-13.0	-10.0
B_a6	29.7	-59.1	16.0	-5.5	21.7	16.8	9.0	16.0	6.4	-6.2	-11.3	-2.6
B_b6	14.9	-63.4	3.0	-15.5	8.0	4.1	-2.8	3.0	-5.9	-16.5	-21.9	-16.8
B_c5	7.2	-66.7	-4.6	-22.8	0.1	-4.3	-10.8	-4.6	-11.9	-2.3	-26.3	-26.6
B_a7	46.3	-58.3	26.0	-4.4	32.0	18.4	9.9	26.0	23.5	1.5	12.0	24.3
B_b7	69.3	-51.7	45.8	10.6	52.8	37.0	27.1	45.8	42.9	17.5	29.7	38.5
B_c6	24.4	-64.5	7.0	-18.9	12.2	0.4	-6.8	7.0	5.0	-13.7	-4.5	-6.3
B_d6	-2.3	-68.5	-12.1	-27.6	-7.9	-11.0	-16.7	-12.1	-20.1	-28.7	-33.8	-23.5

...continued

Table 8.1 continued...

approach	Parallel	Series	Maxwell-Eucken	Levy	Kopelman	Hill *et al.*	Effective Medium Theory	Solid-Continuous	Random Distribution	Keey (1)	Keey (2)	Keey (3)
B_d7	-19.1	-76.5	-29.5	-45.4	-26.1	-32.0	-36.9	-29.5	-32.3	-43.4	-40.8	-29.9
B_d8	-9.9	-73.8	-21.6	-39.3	-17.7	-24.3	-29.8	-21.6	-24.7	-37	-34.1	-22.0
B_c7 *	60.0	-16.5	53.8	43.6	58.0	58.1	53.0	53.8	27.1	37.7	20.0	5.4
B_c8 *	76.7	-39.3	61.1	36.2	68.5	64.9	55.0	61.1	43.5	32.3	18.8	-6.6
B_a8 *	43.8	-25.0	38.2	29.0	42.0	42.1	37.5	38.2	14.2	23.8	7.9	5.2
B_b8 *	50.3	-21.6	44.5	34.9	48.5	48.5	43.7	44.5	19.4	29.4	12.8	6.4
B_e8	52.1	-47.7	38.7	17.2	45.1	41.9	33.4	38.7	23.5	13.8	2.3	-10.6
B_c9	41.3	-59.0	22.9	-5.0	28.9	18.4	9.8	22.9	18.2	-1.2	3.8	-25.7
B_d9 *	100.1	-41.9	74.0	34.5	82.6	67.6	55.6	74.0	67.4	39.8	47.0	55.1
B_e9 *	100.1	-41.9	74.1	34.6	82.6	67.7	55.6	74.1	67.4	39.9	47.0	20.6
B_d10 *	112.2	-27.1	93.4	63.5	102.3	97.9	86.1	93.4	72.2	58.8	42.6	50.2
B_a9 *	142.2	-16.8	120.7	86.6	131.0	125.9	112.4	120.7	96.6	81.2	62.8	53.6

...continued

Table 8.1 continue...

approach	Parallel	Series	Maxwell-Eucken	Levy	Kopelman	Hill *et al.*	Effective Medium Theory	Solid-Continuous	Random Distribution	Keey (1)	Keey (2)	Keey (3)
B_b9	58.6	-45.5	44.6	22.2	51.3	48.0	39.1	44.6	28.7	18.7	6.6	-5.2
B_d11 *	105.7	-3.3	95.8	79.5	102.2	101.9	94.1	95.8	64.0	71.6	48.2	54.2
B_e11	44.9	-50.2	32.0	11.6	38.2	35.1	27.0	32.0	17.6	8.4	-2.6	-14.9
B_d12 *	204.2	4.5	177.2	134.4	190.1	183.8	166.7	177.2	146.9	127.6	104.4	115.3
B_e12 *	104.7	-29.7	86.5	57.7	95.2	90.9	79.5	86.5	66.1	53.1	37.6	20.3
B_e13 *	133.5	-19.7	112.8	80.0	122.7	117.9	104.8	112.8	89.6	74.7	57.0	37.2
B_a10	31.6	-61.8	14.5	-11.5	20.1	10.3	2.3	14.5	10.1	-8.0	-3.3	-12.2
B_b10	44.1	-58.2	25.3	-3.1	31.5	20.7	12.0	25.3	20.5	0.7	5.8	-33.1
B_d13	-6.5	-69.8	-15.9	-30.7	-11.9	-14.8	-20.3	-15.9	-23.6	-31.8	-36.6	2.5
B_d14	44.2	-52.1	30.6	9.0	36.8	33.0	24.7	30.6	17.5	6.5	-2.8	-22.6
B_b11	26.0	-52.1	16.9	2.0	21.8	20.5	14.1	16.9	1.5	-2.1	-14.5	-22.9
B_b12	29.2	-60.4	14.6	-7.9	20.3	14.3	6.5	14.6	6.5	-7.6	-10.5	-19.6
B_b13	30.5	-62.1	13.5	-12.2	19.1	9.4	1.5	13.5	9.2	-8.7	-4.1	-11.2

Table 8.2 Curve-fit Coefficients Used in Eqn (8.24) for the Different Versions of Keey's Method

	a	b	c
Keey (1)	0.824	0	0
Keey (2)	0.565	0.718	0
Keey (3)	0.713	0.651	0.196

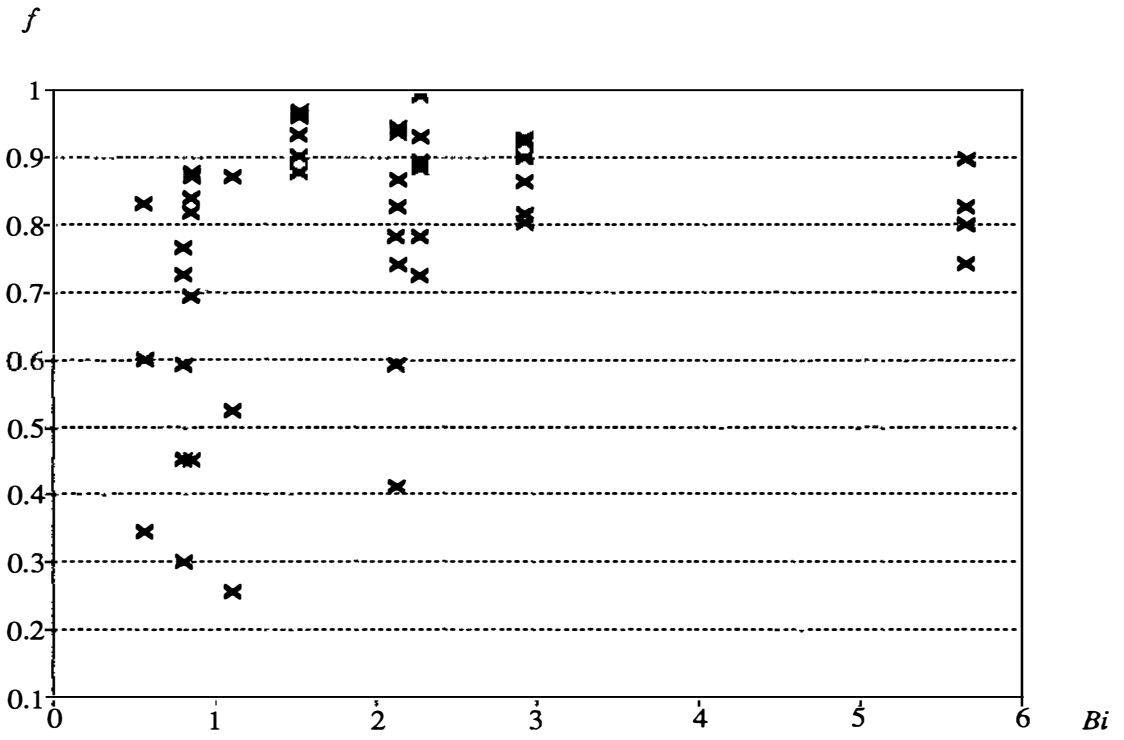

Figure 8.2 Plot of f, the distribution factor in Keey's method determined from experimental k_e data vs Bi

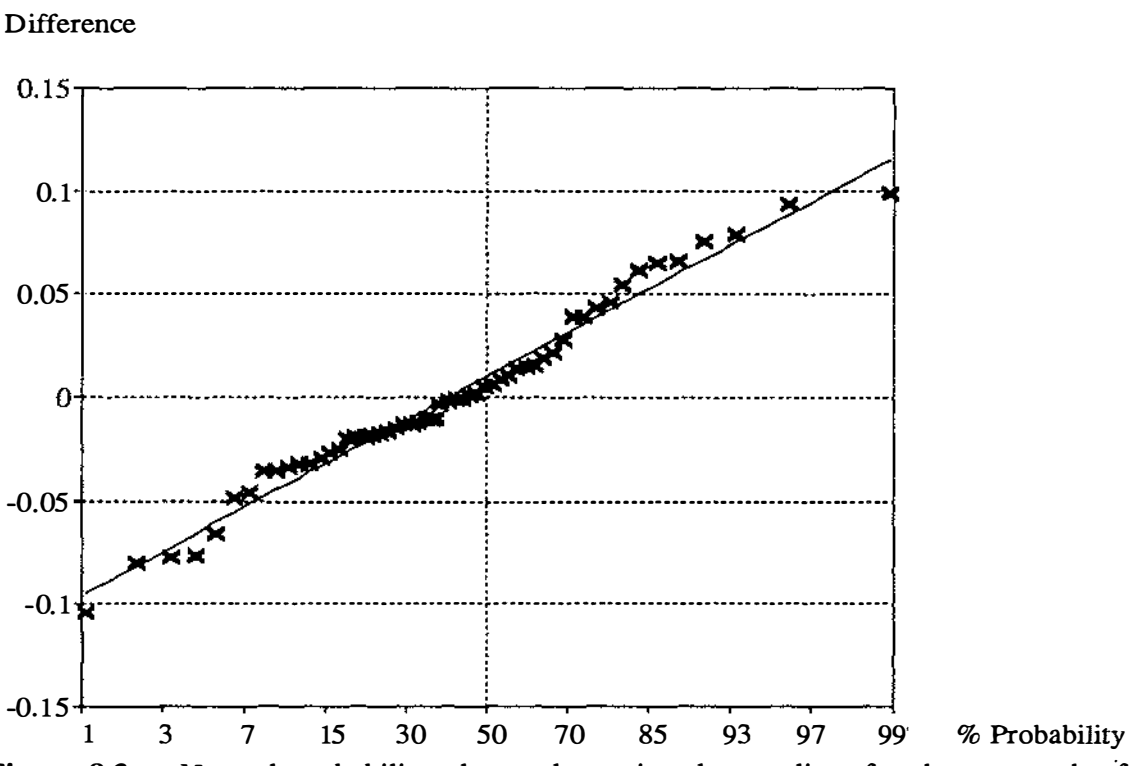

Figure 8.3 Normal probability plot to determine data outliers for the approach of Keey (1). (Predicted - measured) k_e is plotted on y axis

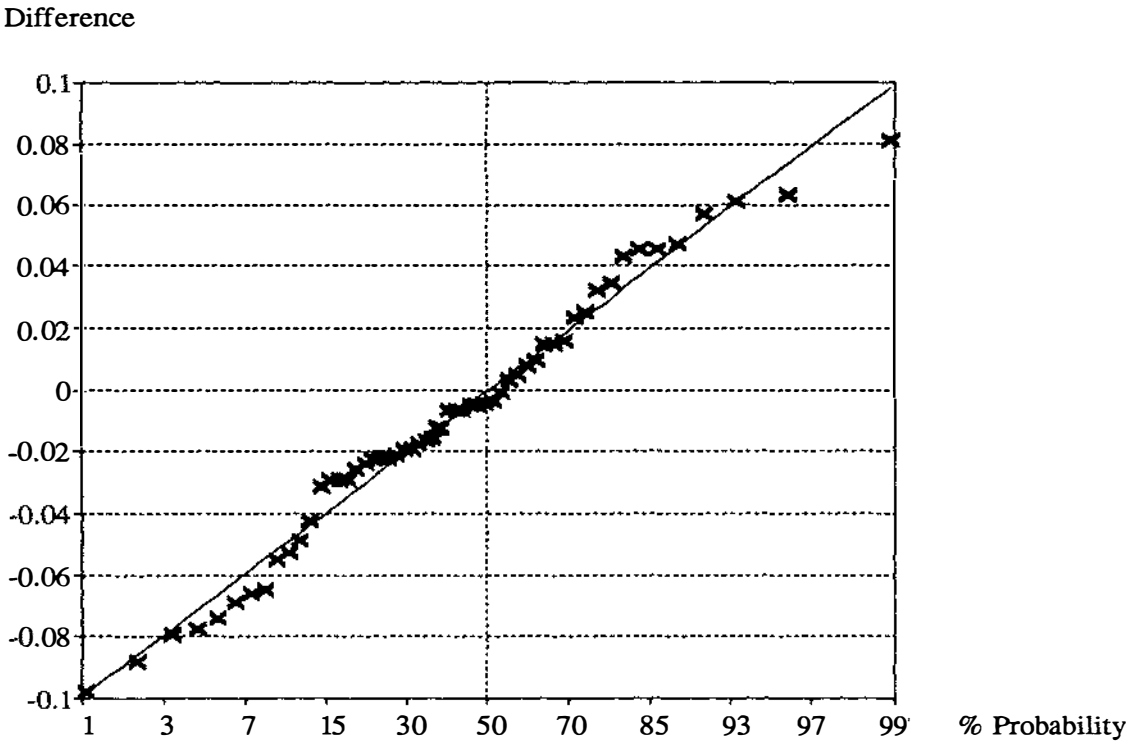

Figure 8.4 Normal probability plot to determine data outliers for the approach of Keey (2). (Predicted - measured) k_e is plotted on y axis

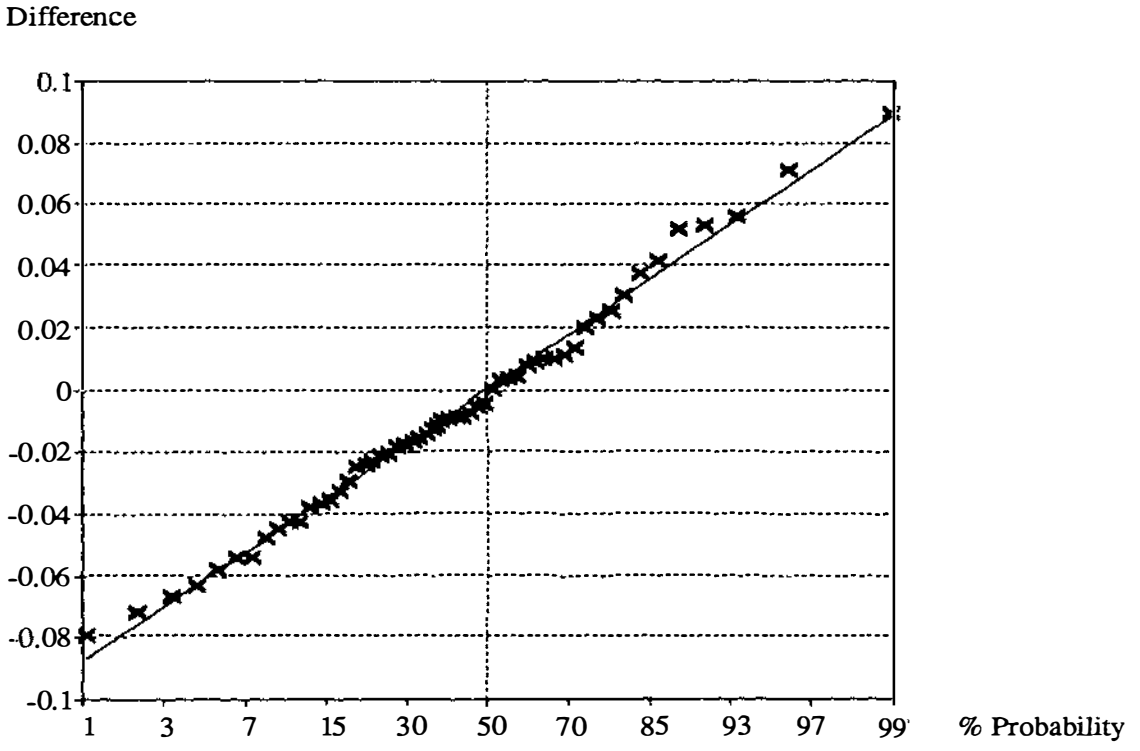

Figure 8.5 Normal probability plot to determine data outliers for the approach of Keey (3). (Predicted - measured) k_e is plotted on y axis

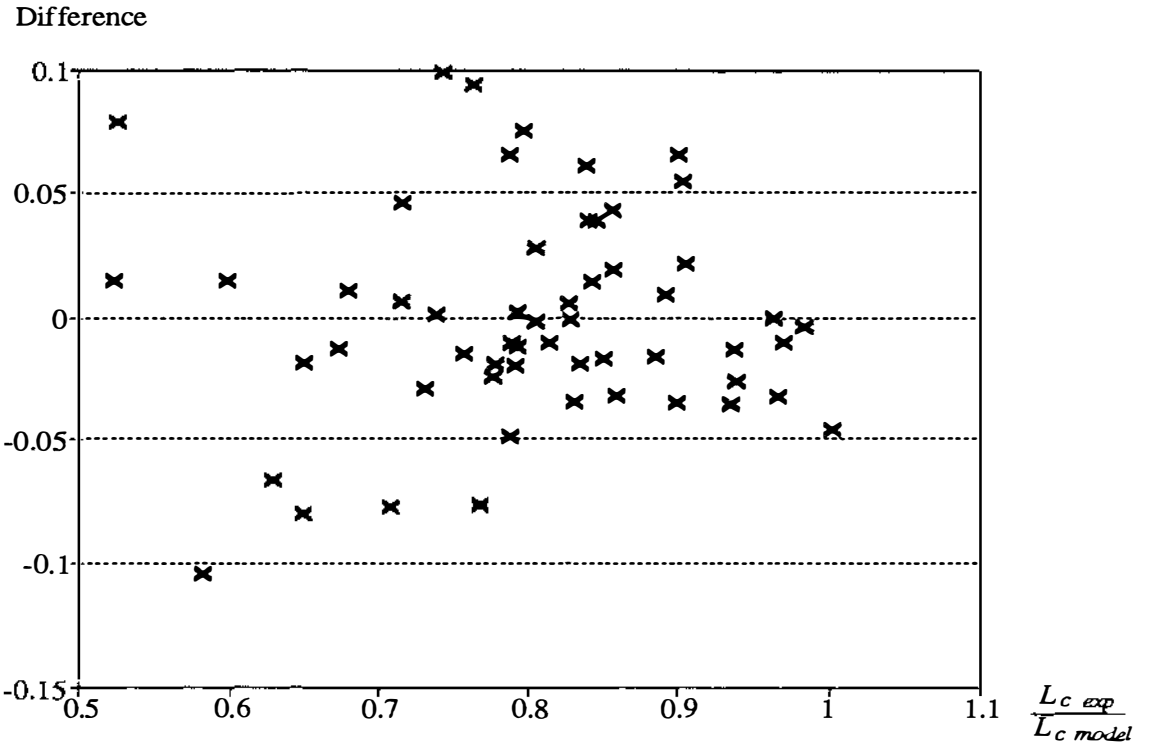

Figure 8.6 Plot of mean differences between the predictions of Keey (1) and the experimental data for k_e versus ratio of ($L_{c\ exp}$ / $L_{c\ model}$)

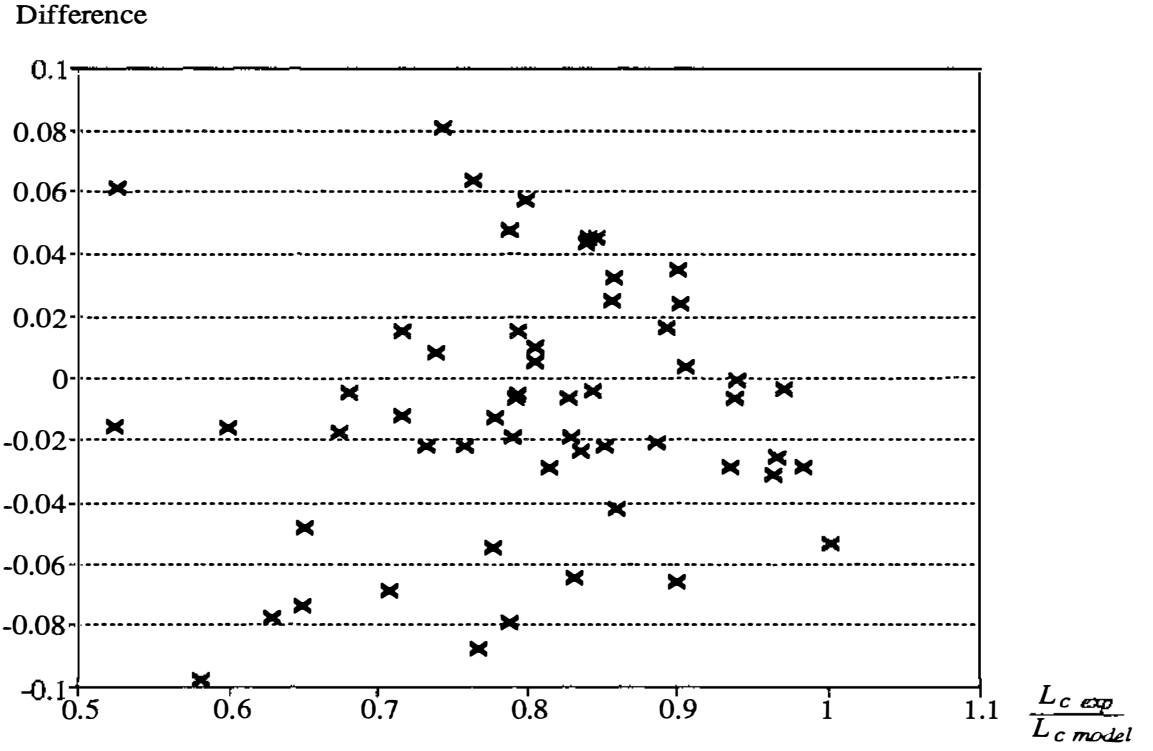

Figure 8.7 Plot of mean differences between the predictions of Keey (2) and the experimental data for k_e versus ratio of ($L_{c\ exp}$ / $L_{c\ model}$)

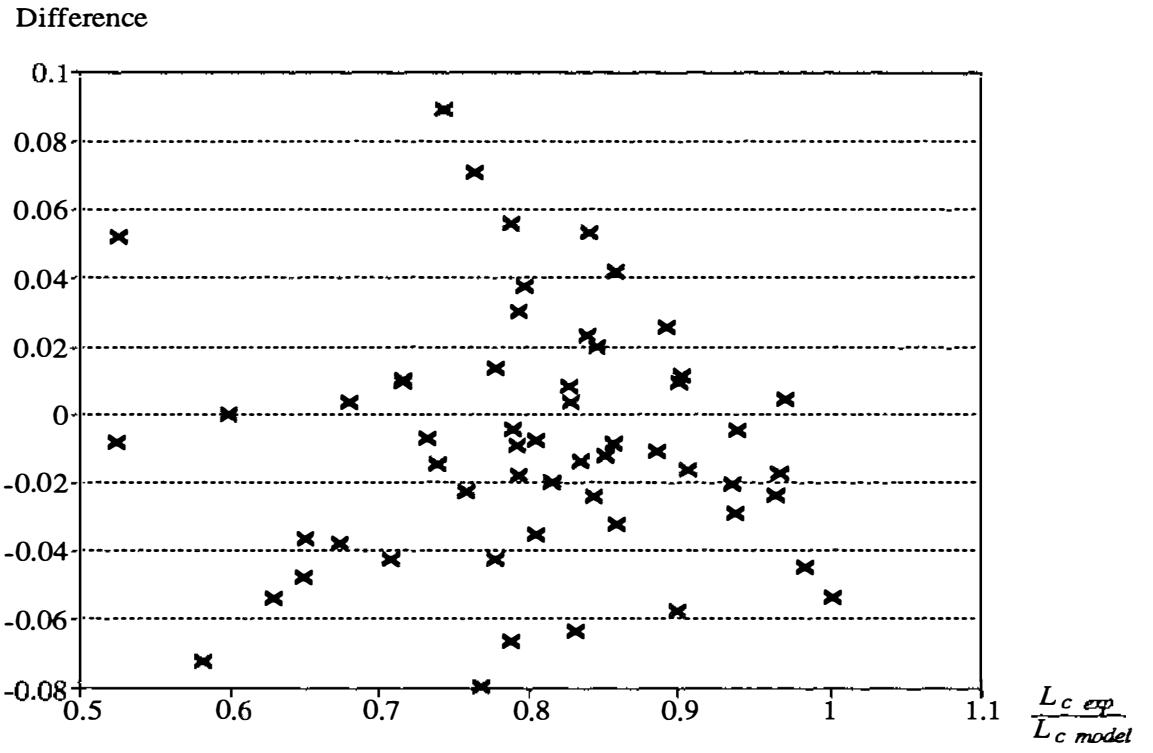

Figure 8.8 Plot of mean differences between the predictions of Keey (3) and the experimental data for k_e versus ratio of ($L_{c\ exp}$ / $L_{c\ model}$)

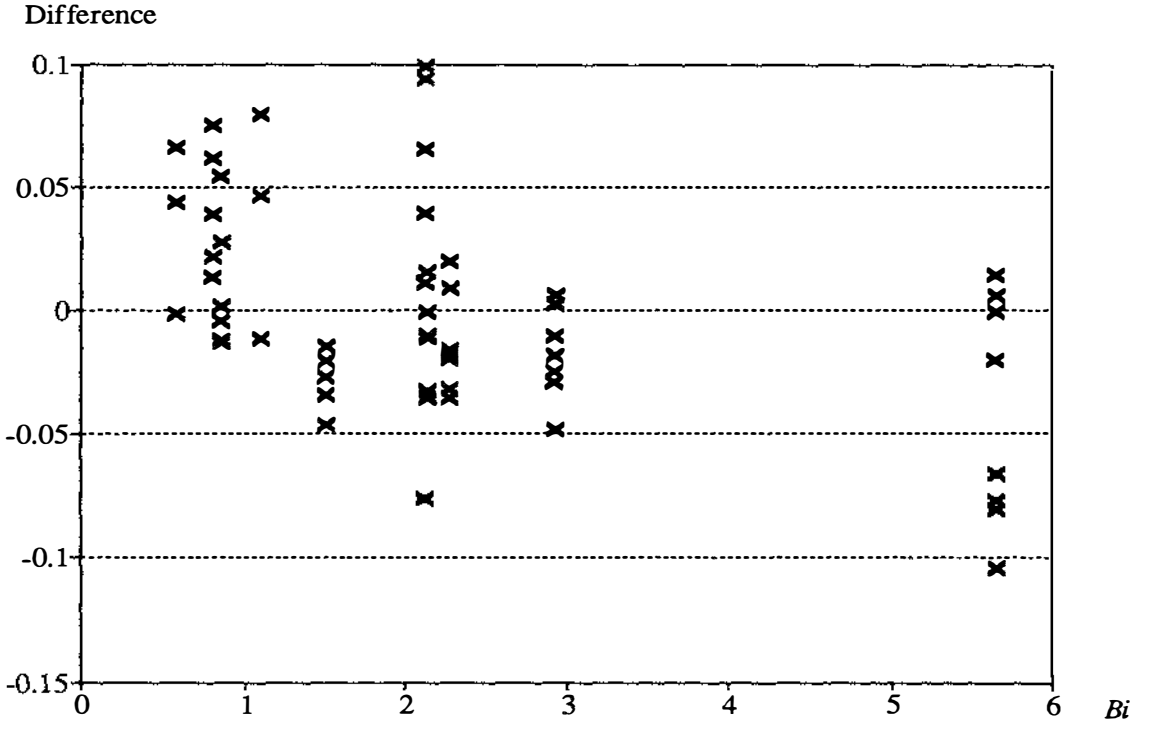

Figure 8.9 Plot of differences between the predictions of k_e by the Keey (1) approach and experimental k_e values versus Biot number

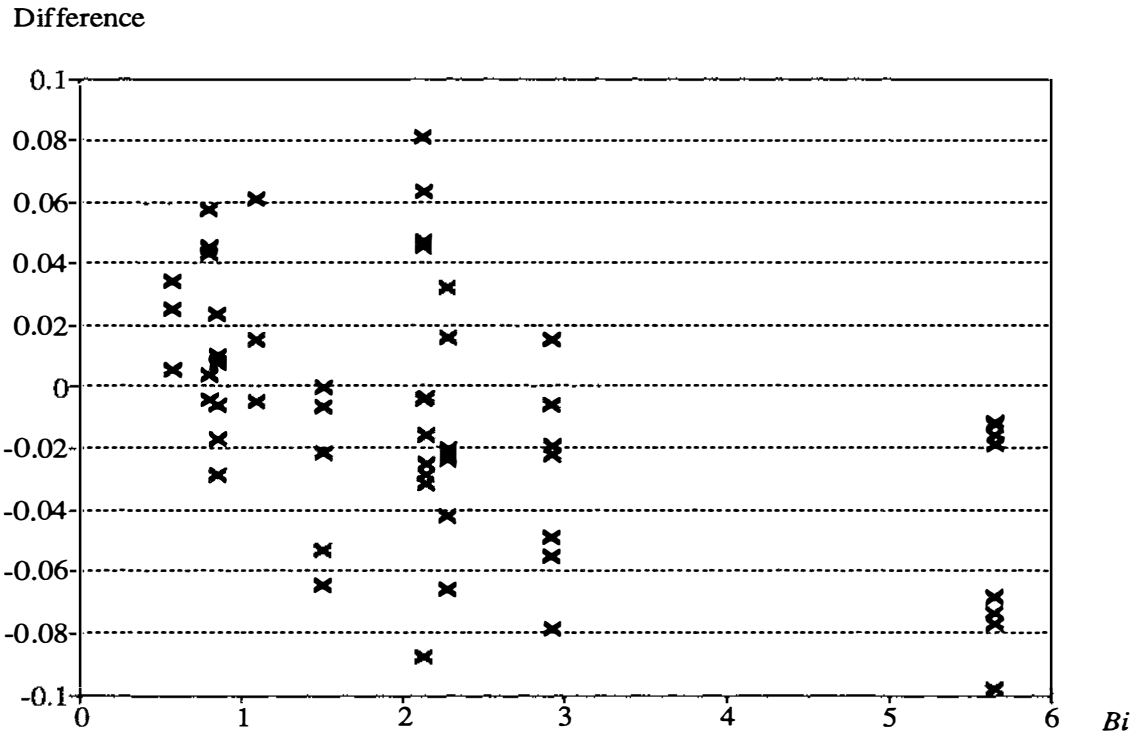

Figure 8.10 Plot of differences between the predictions of k_e by the Keey (2) approach and experimental k_e values versus Biot number

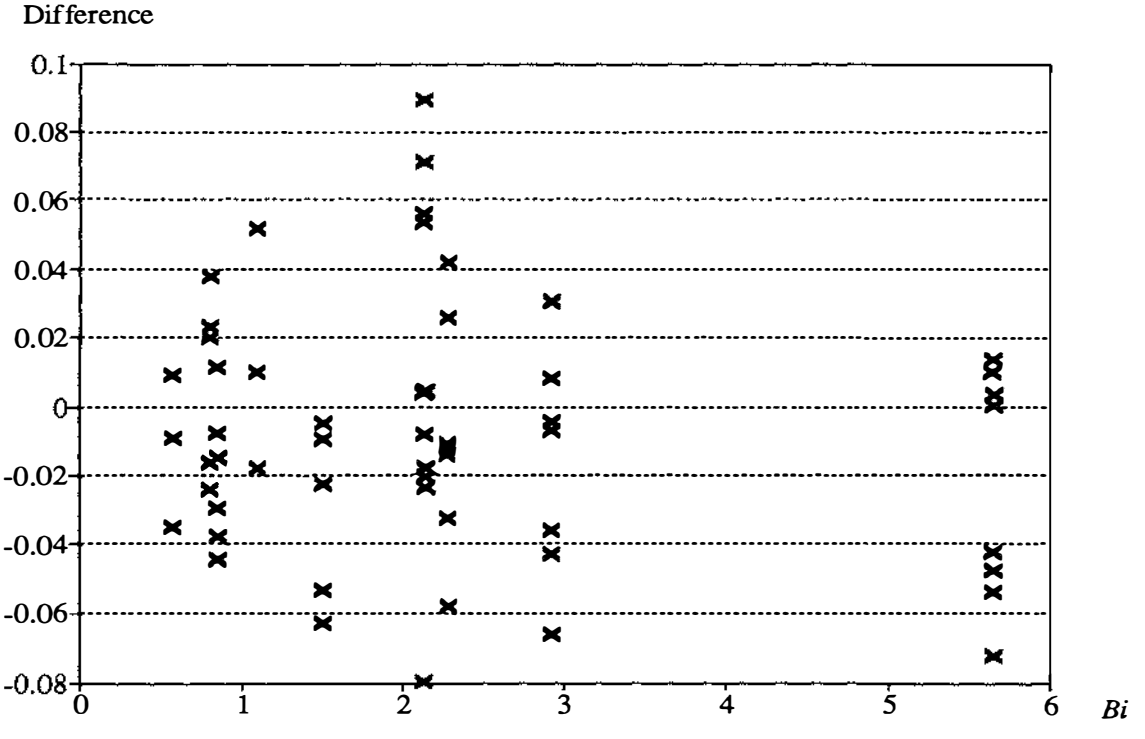

Figure 8.11 Plot of differences between the predictions of k_e by the Keey (3) approach and experimental k_e values versus Biot number

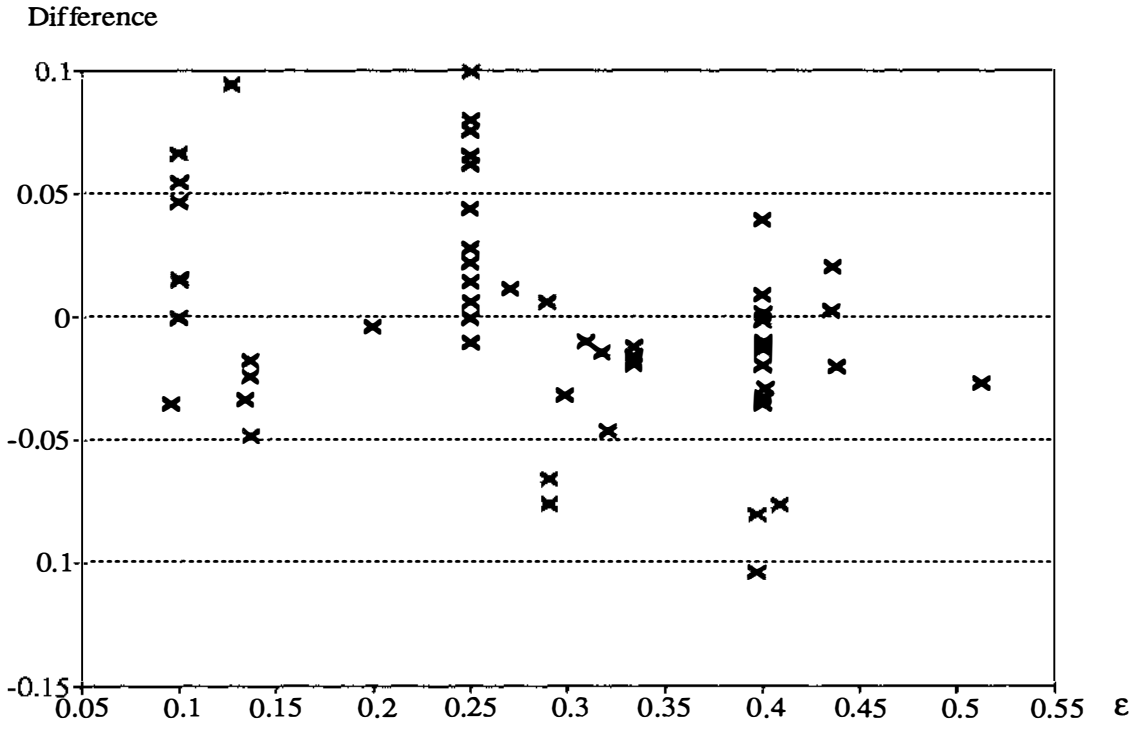

Figure 8.12 Plot of differences between the predictions of k_e by the Keey (1) approach and experimental k_e values versus voidage fraction

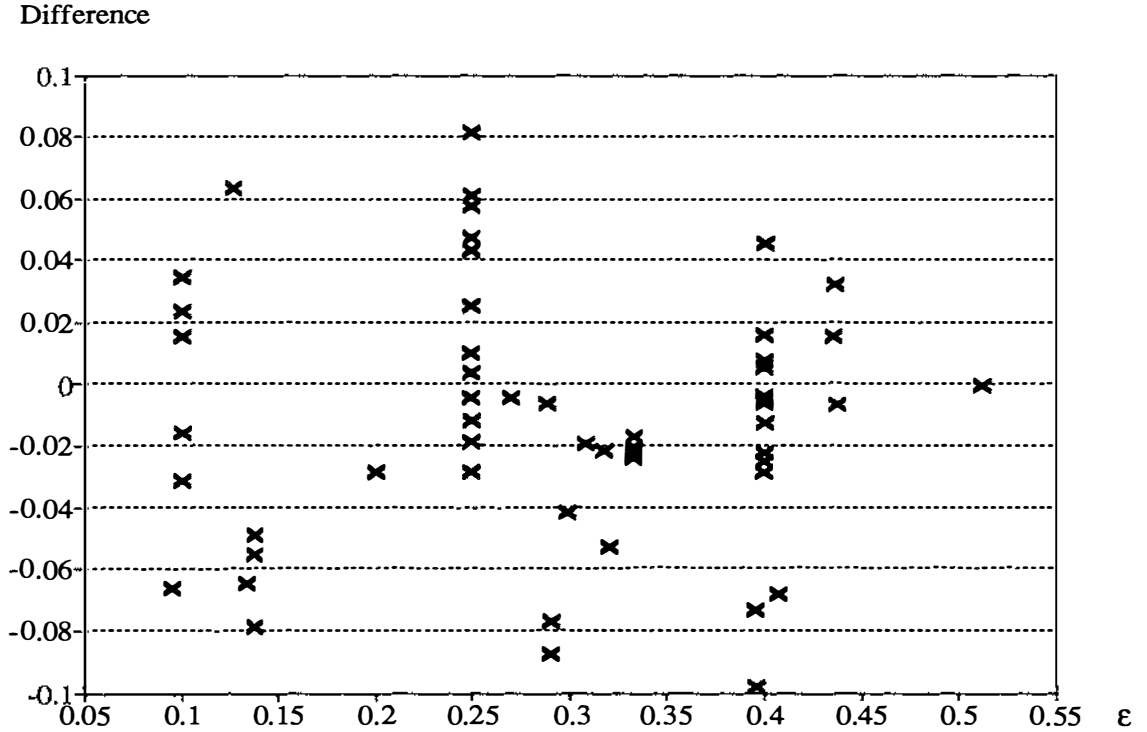

Figure 8.13 Plot of differences between the predictions of k_e by the Keey (2) approach and experimental k_e values versus voidage fraction

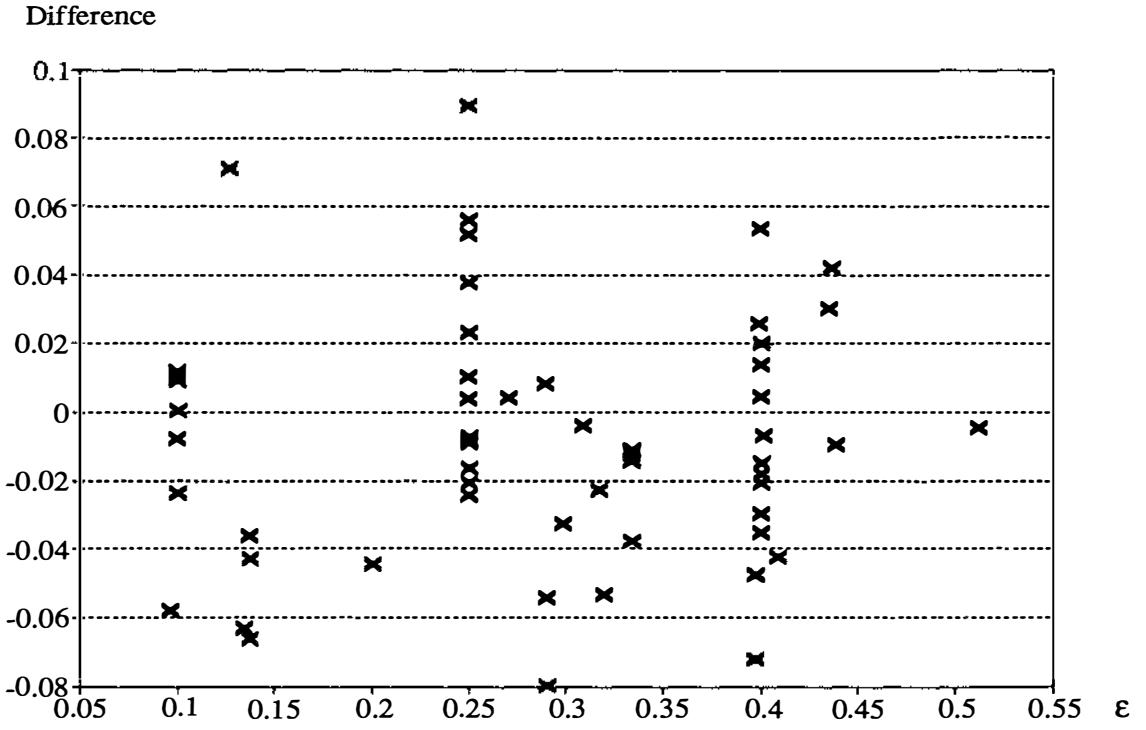

Figure 8.14 Plot of differences between the predictions of k_e by the Keey (3) approach and experimental k_e values versus voidage fraction

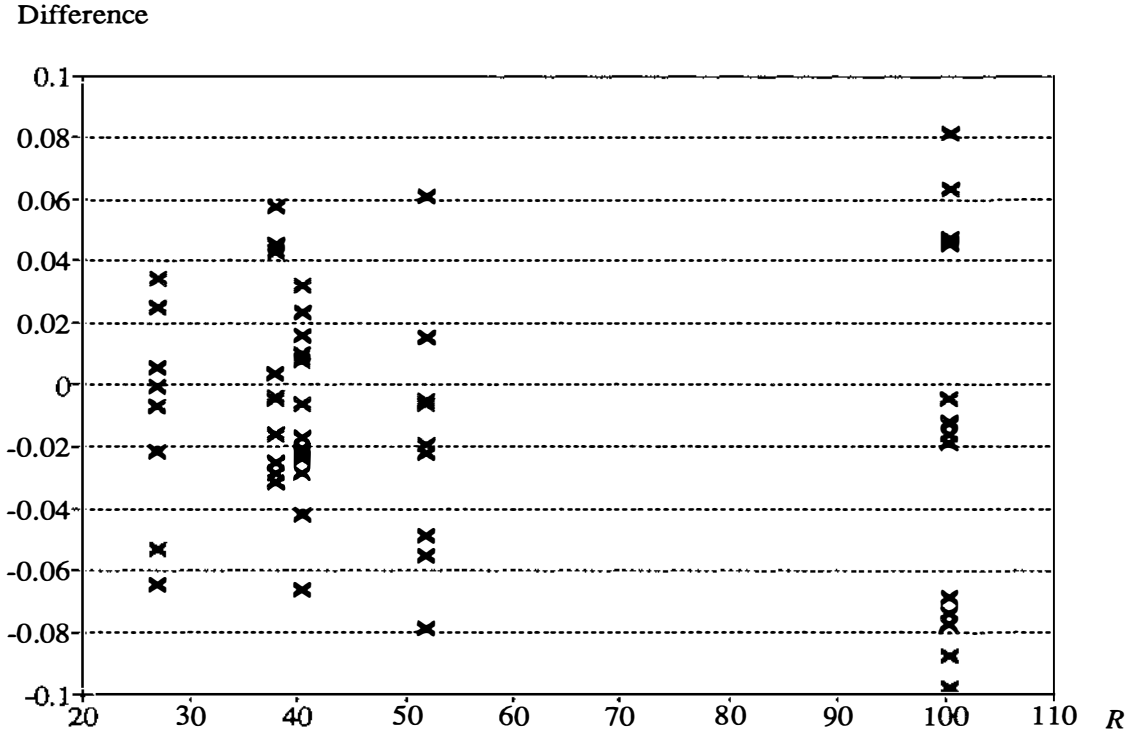

Figure 8.15 Plot of differences between the predictions of k_e by the Keey (2) approach and experimental k_e values versus box size

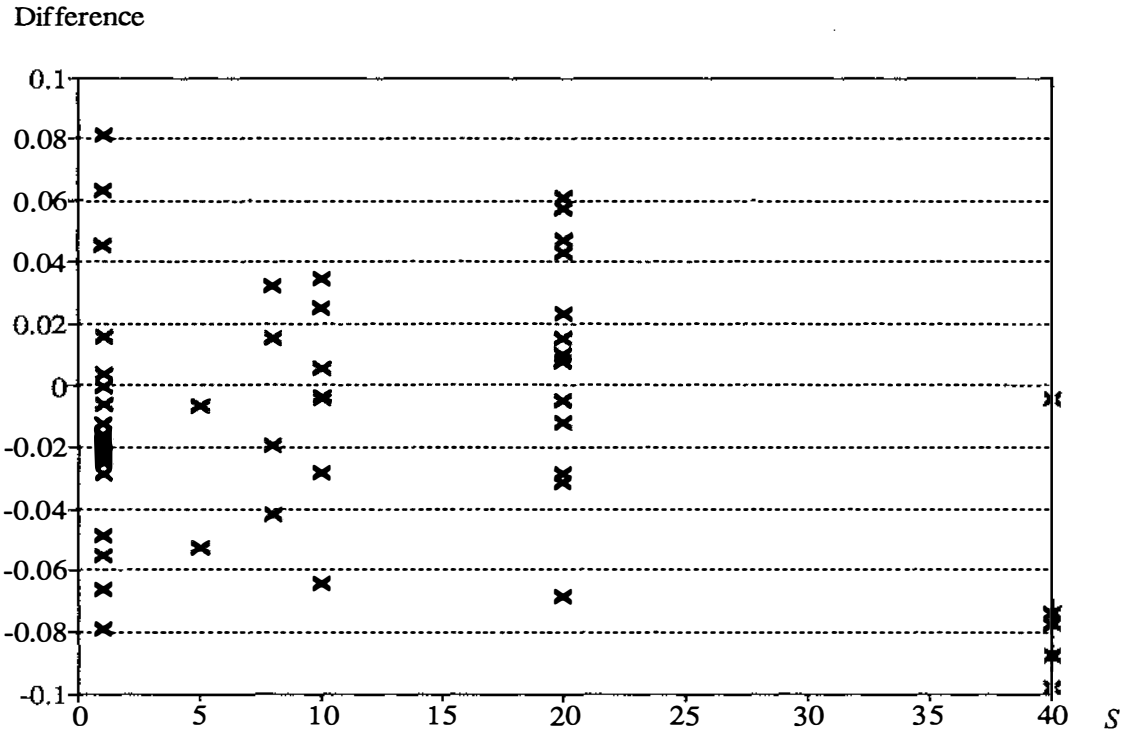

Figure 8.16 Plot of differences between the predictions of k_e by the Keey (2) approach and experimental k_e values versus particle size

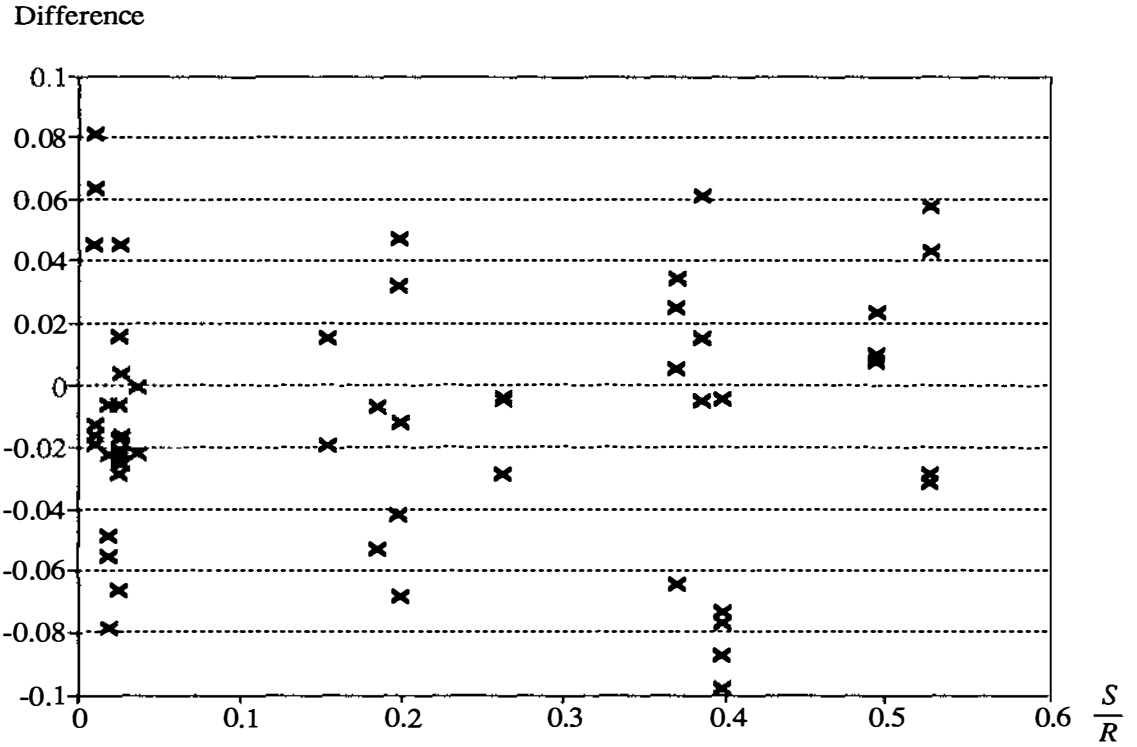

Figure 8.17 Plot of differences between the predictions of k_e by the Keey (2) approach and experimental k_e values versus particle size/box size

9. CONCLUSIONS

No simple method for predicting chilling times for a wide range of geometric shapes that has no major disadvantages was found in the literature. Investigation via a set of test problems showed that prediction inaccuracy was significant for each method under some sets of conditions. This justified development and testing of a new method.

To develop a generally applicable simple prediction method, mathematical expressions were derived to extend the existing concept of equivalent heat transfer dimensionality (E) to take account of the effect of product geometry on the rate of unsteady state heat conduction processes. These expressions cover a wide range of heat transfer environmental conditions, and multi-dimensional regular and irregular geometries. Formulae for the lag factor (L) as a function of geometric shape were also found for thermal centre and mass-average temperatures. The final prediction method uses curve-fit equations for E and L in conjunction with one term in the series analytical solution for the sphere.

For regular geometries (short cylinder, squat cylinder, infinite rectangular rod, rectangular brick, oblate and prolate spheroids), and across a wide range of conditions and product shape ratios the methodology predicted chilling times to within -7.6 to 5.6% of the theoretical solutions for the thermal centre position and ±9.4% for the mass-average condition. For many commonly encountered conditions the lack of fit was considered acceptably low when likely data uncertainties are taken into account.

Guidelines were established to define object geometry for irregular shapes. The recommended dimensional measurement approach uses actual measurements of the three

dimensions of an irregularly shaped object to define the dimensional ratios for an equivalent ellipsoid. The neglect of sharp protrusions and of hollows in taking measurements is recommended.

For thermal centre temperatures of two-dimensional irregular geometries, the 95% confidence interval of the percentage differences of predicted versus experimental chilling times was -3.1 to 14.4%. For three-dimensional irregular geometries, the interval was -6.4 to 11.6%. Lack of fit was probably more due to experimental error than errors in the form of geometric approximation or the prediction method itself. Although not tested against experimental data, accuracy of chilling time predictions for mass-average situations is expected to be similar to that for thermal centres for shapes that are not highly irregular.

In situations where the product contains significant uniformly distributed voids, the use of an "equivalent thermal conductivity" allows either the proposed simple method or any applicable analytical solution to be applied. An equivalent thermal conductivity calculated by Keey's method, with a distribution factor dependent on voidage fraction, is recommended but ranges of applicability require further investigation. It could not be established whether natural convection in the voids was significant.

The proposed simple chilling time prediction method and geometric analysis methodology are recommended for routine use in industrial situations where convective cooling occurs. Accuracy in such applications would probably be more limited by uncertainties in the data to be used in the predictions, than by limitations in the methods themselves.

NOMENCLATURE

a	awater ctivity of the product surface
A	surface area (m^2)
Bi	Biot number = $h\ R\ /\ k$
c	specific heat capacity ($J\ kg^{-1}K^{-1}$)
D	dimension (m)
E	equivalent heat transfer dimensionality
f	distribution factor
F_{12}	radiation view factor
Fo	Fourier number = $k\ t\ /\ (C\ R^2)$
G	geometry index
h	heat transfer coefficient ($W\ m^{-2}K^{-1}$)
j	time for a 90% reduction in Y (s)
k	thermal conductivity ($W\ m^{-1}K^{-1}$)
l	latent heat of evaporation ($J\ kg^{-1}$)
L	lag factor or intercept
m	dimensional cooling rate (s^{-1})
M	dimensionless cooling rate
N	number of heat transfer dimensions of an object or geometry
p	partial pressure of water vapour (Pa)
P	parameter
Q	internal heat generation (W)
r	displacement along the radius from the object centre (m)
R	object radius or half-thickness (m)
S	solid particle size (m)
t	chilling time (s)
T	temperature (K or °C)
u	mass transfer coefficient ($s\ m^{-1}$)
V	volume (m^3)
x	displacement in x coordinate (m)
Y	fractional unaccomplished temperature change = $(T - T_a)\ /\ (T_i - T_a)$
y	displacement in y coordinate (m)
z	displacement in z coordinate (m)
α	first root of the transcendental equation for a sphere
β	dimensional ratio
γ	alternative dimensional ratio
ε	fraction of volume as voids
ζ	first root of the transcendental equation for an infinite slab
λ	alternative dimensional ratio
μ	ratio of lag factors for mass-average and centre temperatures
ξ	first root of the transcendental equation for an infinite cylinder
ρ	density ($kg\ m^{-3}$)
ϕ	sum of heat flows to a surface (W)
σ	Stefan-Boltzmann constant ($W\ m^{-2}K^{-4}$)
ω	root of transcendental equation

Subscripts

0	for $Bi = 0$
1	ratio of second shortest dimension to the shortest; or parameter 1
2	ratio of the longest dimension to the shortest; or parameter 2
3	parameter 3
∞	for $Bi = \infty$
a	cooling medium
c	centre; or cross-sectional
conv	convective
e	equivalent
exp	experimental
evap	evaporative
FEM	finite element calculation
g	gas phase
i	initial
m	mass-average
r	relative; or radial
rad	radiative
s	surface or solid phase
w	water
x	x direction
y	y direction
z	z direction

REFERENCES

Abdul Majeed, P.M. (1982). Prediction of cooling characteristics during air cooling of cylindrical food products with a flowing film of cold water at the surface (air-film cooling). *Trans. ASAE*, **25**, 508-514.

Abdul Majeed, P.M., Srinivasa Murthy, S. & Krishna Murthy, M.V. (1980). Prediction of air cooling characteristics of moist food products. *Trans. ASAE*, **23**, 788-792.

Albin, F.V., Srinivasa Murthy, S. & Krishna Murthy, M.V. (1979). Prediction of the Freezing Characteristics of Spherical-Shaped Food Products. Int. J. Refrig., **2**, 129.

Arsari, F.A., Charan, V. & Varma, H.K. (1984). Heat and mass analysis in air cooling of spherical products. *Int. J. Refrig.*, **7**, 194-197.

Ansari, F.A., Afaq, A. (1986). New method for estimating thermal diffusivity of spherical products. *Int. J. Refrig.*, **9**, 158-160.

Arce, J.A. & Sweat, V.E. (1980). Survey of published heat transfer coefficients encountered in food refrigeration processes. *ASHRAE Trans.*, **86**(2), 235.

ASHRAE (1993). *ASHRAE Handbook - Fundamentals.* American Society of Heating, Refrigeration and Air Conditioning Engineers Inc., Atlanta.

Badari Narayana, K & Krishna Murthy, M.V. (1975). Thermal properties of a model food gel. *Ind. J. Technol.*, **13**, 415.

Badari Narayana, K & Krishna Murthy, M.V. (1981). Heat and mass transfer characteristics and the evaluation of thermal properties of moist food materials. *Trans. ASAE*, **24**, 789-793.

Baehr, H.D. (1953). Die berechnung der kuhldauer bei ein- und mehrdimensionalen warmefluss. *Kaltechnik*, **5**, 255-259.

Baker, D.W. & Charm, S.E. (1969). Freezing rates of sea foods as influenced by heat transfer coefficients of liquid refrigerants. In *Freezing and Irradiation of Fish*, ed. R. Kreuzer. Fishing News (Books) Ltd., London, pp.94-98.

Califano, A.N. & Zaritzky, N.E. (1993). A numerical method for simulating heat transfer in heterogeneous and irregularly shaped foodstuffs. *J. Food Process Engng.*, **16**, 159-171.

Carslaw, H.S. & Jaeger, J.C. (1959). *Conduction of Heat in Solids (2nd edn).* Clarerdon Press, Oxford.

Charm, S.E. (1963). A method for experimentally evaluating heat transfer coefficients in freezers and thermal conductivity of frozen foods. *Food Technol.*, **17**, 1305-1308.

Chau, K,V., Gaffney, J.J. & Baird, C.D. (1985). Transient heat and mass transfer for oranges in closed containers. *Refrig. Sci. Technol.*, 1985-5, 283-290.

Chuntranuluck, S., Serrallach, G.F. & Cleland, A.C. (1989). Shape factors for prediction of chilling times of irregular shapes. *Refrig. Sci. Technol.*, Proceedings of meeting, 9-12 July, Davis, California, 215-222.

Clary, B.L., Nelson, G.L., & Smith, R.E. (1968). Heat transfer from hams during freezing by low temperature air. *Trans. ASAE*, **11**, 496-499.

Clary, B.L., Nelson, G.L., & Smith, R.E. (1971). Applications of geometry analysis technique in determining the heat transfer rates from biological materials. *Trans. ASAE*, **14**, 586-589.

Cleland, A.C. (1977). *Heat Transfer during Freezing of Foods and Prediction of Freezing Times.* Ph.D. Thesis, Massey University, New Zealand.

Cleland, A.C. (1990). *Food Refrigeration Processes — Analysis, Design and Simulation.* Elsevier Applied Science, London and New York.

Cleland, A.C. & Earle, R.L. (1976). A new method for prediction of surface heat transfer coefficients in freezing. *Refrig. Sci. Technol.*, 1976-1, 361-368.

Cleland, A.C. & Earle, R.L. (1982). A simple method for prediction of heating an d cooling rates in solids of various shapes. *Int. J. Refrig.*, **5**, 98-106.

Cleland, A.C. & Earle, R.L. (1984). Assessment of freezing time prediction methods. *J. Food Sci.*, **49**, 1034-1042.

Cleland, D.J., Cleland, A.C. & Jones, R.S. (1994). Collection of accurate experimental data for food freezing time prediction. *J. Food Process Engng.*, **17**, No. 1, 93-119.

Cleland, D.J., Cleland, A.C., Earle,R.L. & Byrne, S.J. (1984). Prediction of rates of freezing, thawing and cooling in solids of arbitrary shape using the finite element method. *Int. J. Refrig.*, **7**, 6-13.

Clelend, D.J. (1985). *Prediction of Freezing and Thawing Times For Foods. Ph.D. Thesis*, Massey University, New Zealand.

Cleland, D.J., Cleland, A.C., Earle,R.L. & Byrne, S.J. (1987a). Experimental data for freezing and thawing of multi-dimensional objects. *Int. J. Refrig.*, **10**, 22-31.

Cleland, D.J., Cleland, A.C., Earle,R.L. & Byrne, S.J. (1987b). Prediction of freezing and thawing times for multi-dimensional shapes by numerical methods. *Int. J. Refrig.*, **10**, 32-39.

Cuesta, J.F., Lamúa, M. & Moreno, J. (1990). Graphical calculation of half-cooling times. *Int. J. Refrig.*, **13**, 317-324.

de Baerdemaeker, J.,Singh, R.P. & Segerlind, L.J. (1977). Modelling heat transfer in foods using the finite element method. *J. Food Proc. Engng.*, **1**, 37-50.

Dincer, I. (1994). Precooling of cylindrical shaped grapes: experimental and theoretical heat transfer rates. *J. Food Proc. Engng.*, **17**(1), 57-71.

Dincer, I., Yildiz, M., Loker, M. & Gun, H. (1992). Process parameters for hydrocooling apricots, plums, and peaches. *Int. J. Food Sci. Technol.*, **27**, 347-352.

Dixon, W.J. (chief editor), Brown, M.B., Engelman, L., Frane, J.W., Hill, M.A., Jennrich, R.I. & Toporek, J.D. (1984). *Biomedical Statistical Software (BMDP).* University of California Press, Los Angeles.

Draper, N.R. & Smith, H. (1981). *Applied Regression Analysis (2nd edn).* John Wiley & Sons, New York.

Earle, R.L. & Fleming, A.K. (1967). Cooling and freezing of lamb and mutton carcasses - 1. Cooling and freeezing rate in legs. *Food Technol.*, **21**(1), 79-84.

Eucken, A. (1940). Allgemeine gesetzmassig keiten fur das warmeleitvermogen versciediner stoffarten und aggregatzustande. *Forsch. Gebiete Ingenieur (Ausgabe A)* **11**, 6.

Fikiin, A.G. (1983). Application des méthodes analytiques pour déterminer la durée du refroidissement des produits alimentaires et d'autre corps solides. Proc. 16th Int. Congr. Refrig., **4**, 109-116.

Fikiin, K.A. (1992). Solution numérique généralisée du problème de la conduction thermique dans les solides de diverse configuration lors d'un refroidissement convectif. *Int. J. Refrig.*, **15**, 221-226.

Fikiin, A.G. & Fikiina, I.K. (1971). Calculation de la durée de réfrigération des produits alimentaires et des corps solides. *Proc. 13th Int. Congr. Refrig.*, **2**, 411-414.

Fikiin, K.A. & Fikiin, A.G. (1989). Modèle numérique du refroidissementde matières alimentaires et d'autre corps solides de forme géométrique variée. *Int. J. Refrig.*, **12**, 224-231.

Fleming, A.K. (1967). Immersion freezing of small meat-products. *Proc. 12th Int. Congr. Refrig.*, **2**, 684-695.

Fleming, A.K. (1970). Physical aspect of meat cooling. *Refrig. Sci. Technol.* 1970-1, 151-160.

Fleming, A.K. (1971a). The numerical calculation of freezing processes. *Proc. 13th Int. Congr. Refrig.*, **2**, 303-311.

Fleming, A.K. (1971b). Applications of a computer programme to freezing processes. *Proc. 13th Int. Congr. Refrig.*, **2**, 403-410.

Gaffney,J.J., Baird,C.G. & Chau, K.V. (1985). Methods for calculating heat and mass transfer in fruit and vegetables, individually and in bulk. *ASHRAE Trans.*, **91**(2B), 333-352.

Geuze, C.A., Betten, A. & Touber, S. (1972). Non-steady heat transfer in freezing a model substance. *Refrig. Sci. Technol.*, 1972-1, 211.

Gröber, H., Erk, S. & Grigull, Ulrich (1961). *Fundamentals of Heat Transfer.* McGraw-Hill.

Güemes, D.R., Pirovani, M.E. & Di Pentima, J.H. (1989). Heat transfer characteristics during air precooling of strawberries. *Int. J. Refrig.*, **12**, 169-173.

Haas, E. & Felsenstein, G. (1985). Factors affecting the cooling rates of avocados packed in corrugated cartons. *Refrig. Sci. Technol.*, 1985-5, 291-300.

Hallstrom, B.,Skjoldebrand, C. & Tragardh, C. (1988). *Heat Transfer and Food Products.* Elsevier Applied Science, London.

Hayakawa, K. (1970). Experimental formulas for accurate estimation of transient temperature of food and their application to thermal process evaluation. *Food Technol.*, **24**, 1407-1418.

Hayakawa, K. (1971). Estimating food temperatures during various processing or jangling treatments. *J. Food Sci.*, **36**, 378-385.

Hayakawa, K. (1978). Computerised simulation for heat transfer and moisture loss from an idealised fresh product. *Trans. ASAE*, **21**, 1015-1024.

Hayakawa, K. & Succar, J. (1982). Heat transfer and moisture loss of spherical fresh product. *J. Food Sci.*, **47**, 596-605.

Hayakawa, K. & Villalobos, G. (1989). Formulas for estimating Smith *et al.* parameters to determine the mass average temperature of irregularly shaped bodies. In *ASHRAE Handbook - Fundamentals.* American Society of Heating, Refrigeration and Air Conditioning Engineers Inc., Atlanta, pp.29.8-29.16.

Heldman, D.R. & Lund, D.B. (ed.) (1992). *Handbook of Food Engineering.* Marcel Dekker, New York.

Hill, J.E., Leitman J.D. & Sunderland, J.E. (1967). Thermal conductivity of various meats. *Food Technol.*, **21**, 1143-1148.

Hossain, Md.M., Cleland, D.J. & Cleland, A.C. (1992a). Prediction of freezing and thawing times for foods of regular multi-dimensional shape by using an analytically derived geometric factor. *Int. J. Refrig.*, **15**, 227-234.

Hossain, Md.M., Cleland, D.J. & Cleland, A.C. (1992b). Prediction of freezing and thawing times for foods of two-dimensional irregular shape by using a semi-analytical geometric factor. *Int. J. Refrig.*, **15**, 235-240.

Hossain, Md.M., Cleland, D.J. & Cleland, A.C. (1992c). Prediction of freezing and thawing times for foods of three-dimensional irregular shape by using a semi-analytical geometric factor. *Int. J. Refrig.*, **15**, 241-246.

James, S.J. & Swain, M.J. (1983). The effect of surface fat layer on the chilling time of meat. *Proc. 16th Int. Congr. Refrig.*, **2**, 473-478.

James, S.J. & Bailey, C. (1986). Temperature chanes, weight loss and product loads during beef chilling. *Refrig. Sci. Technol.*, 1986-3, 105-114.

James, S.J., Fulton, G.S., Swain, M.V.L. & Burfoot, D. (1988). Modelling the effect of temperature and relative humidity fluctuations on weight loss in retail display. *Refrig. Sci. Technol.*, 1988-3, 111-120.

Jiang, H., Thompson, D.R. & Morey, R.V. (1987). Finite element model of temperature distribution in broccoli stalks during forced-air processing. *Trans. ASAE*, **30**, 1473-1477.

Jowitt, R. (edn.) (1983). *Physical Properties of food.* Applied Science Publishers, London.

Keey, R.B. (1972). *Drying Principles and Practice.* Pergamon Press, New York.

Kirkpatrick, E.T. & Stokey, W.F. (1959). Transient heat conduction in elliptical plates and cylinders. *J. Heat Transfer*, **80**, 54-58.

Kopelman, I.J. (1966). *Transient Heat Transfer and thermal Properties in Food Systems.* Ph.D. Thesis, Food Sci. Dept., Michigan State Univ., East Lansing.

Kopelman, I.J., Borrero, C. & Pflug, I.J. (1967). Evaluation of surface film heat conduction problems. In *Numerical Methods in Thermal Problems*, ed. R.W. Lewis & K. Morgan. Pineridge Press, Swansea, pp.31-37.

Langston, L.S. (1982). Heat transfer from multidimensional objects using one-dimensional solutions for heat loss. *Int. J. Heat Mass Transfer*, **25**, 149-150.

Lentz, C.P. (1961). Thermal conductivity of meats, fats, gelatin gels and ice. *Food Technol.*, **15**, 243-247.

Levy, F.L. (1978). A new diagram for evaluating the relationship between convective and evaporative heat transfer during cooling of carcasses. *Int. J. Refrig.*, **1**, 229-232.

Levy, F.L. (1981). A modified maxwell-eucken equation for calculating the thermal conductivity of two-component solutions or mixtures. *Int. J. Refrig.*, **4**, 223-225.

Lovatt, S.J., Pham, Q.T., Cleland, A.C. & Loeffen, M.P.E. (1992a). A new method of predicting the time- variability of product heat load during food cooling — part 1: theoretical considerations. *J. Food Engng.*, **18**, 13-36.

Lovatt, S.J., Pham, Q.T., Cleland, A.C. & Loeffen, M.P.E. (1992b). A new method of predicting the time- variability of product heat load during food cooling — part 2: experimental testing. *J. Food Engng.*, **18**, 37-62.

Lovett, D.A. (1988). Performance of a simple mathematical model for predicting thermal changes in meat. *Proc. 34th Int. Congr. Meat Sci. Technol.*, 655-659.

McAdams, W.H. (1954). *Heat Transmission (3rd edn.)*. McGraw Hill, Tokyo.

McLachlan, N.W. (1945). Heat conduction in elliptical cylinder, and an analogues electromagnetic problem. *Philosophical Magazine*, **36**, 600-609.

McNabb, A., Wake, G.C., Hossain, Md.M. (1990). Transition times between steady states for heat conduction with or without phase change for various shapes and biot number. Part I — general theory and some exact results. *Occas. Pubs. Maths. Stat.*, No. 20, Massey Univ., New Zealand.

Mattea, M., Urbicain, M.J. & Rotstein, E. (1986). Prediction of thermal conductivity of vegetable foods by the effective medium theory. *J. Food Sci.*, **51**, 113-115, 134.

Murakami, E.G. & Okos, M.R. (1989). Measurement and prediction of thermal properties of foods. In *Food Properties and Computer-Aided Engineering of Food Processing Systems*. Kluewer Academic Publishers, Amsterdam.

Nesvadba, P. (1982). Methods for the measurement of thermal conductivity and diffusivity of foodstuffs. *J. Food Engng.*, **1**, 93-113.

Newman, A.B. (1936). Heating and cooling rectangular and cylindrical solids. *Ind. Engng Chem.*, **28**(5), 545-548.

Nolan, E.J. (1987). Calculation of an approximate cooling curve for cooked roast beef. *J. Food Process Engng.*, **9**, 247-263.

Pan, J.C. & Bhowmik, S.R. (1991). The finite element analysis of transient heat transfer in fresh tomatoes during cooling. *Trans. ASAE*, **34**, 972-976.

Patanker, S.V. (1980). *Numerical Heat Transfer and Fluid Flow.* Hemisphere Publishing Co., Washington.

Pflug, I.J., Blaisdell, J.L. & Kopelman, J. (1965). Temperature-time curves that can be approximated by a sphere, infinite plate, or infinite cylinder. *ASHRAE Trans.*, **71**(1), 238-248.

Pham, Q.T. (1984). An extension to Plank's equation for predicting freezing times for foodstuffs of simple shapes. *Int. J. Refrig.*, **7**, 377-383.

Pham, Q.T. (1985). An approximate analytical method for predicting freezing times for rectangular blocks of foodstuffs. *Int. J. Refrig.*, **8**, 43-47.

Pham, Q.T. (1986). Simplified equation for predicting the freezing time of foodstuffs. *J. Food Technol.*, **21**, 209-219.

Pham, Q.T. (1987). Moisture changes due to temperature changes or fluctuations. *J. Food Engng.*, **6**, 33-50.

Pham, Q.T. (1991). Shape factor for the freezing time of ellipses and ellipsoids. *J. Food Engng.*, **13**, 159-170.

Pham, Q.T. & Willix, J. (1989). Thermal conductivity of fresh lamb meat, offals and fat in the range -40 to +30°c: measurements and correlations. *J. Food Sci.*, **54**, 508-515.

Radford, R.D., Herbert, L.S. & Lovett, D.A. (1976). Chilling of meat — a mathematical model for heat and mass transfer. *Refrig. Sci. Technol.*, 1976-1, 323-330.

Riedel, L. (1960). Eine prufsubstanz fur gefrierversuche. *Kaltetechnik*, **12**, 222-226.

Rutov, D.G. (1958). Calculation of the time of cooling of food products. *Refrig. Sci. Technol.*, 1958-1, 415-421.

Ryan, B.F., Joiner, B.l. & Ryan, T.A. (1985). *MINITAB Handbook (2nd edn.)*. PWS-Kent Publishing Company, Boston.

Sainsbury, G.F. (1985). Practical application of cooling performance data for perishable commodities. *Refrig. Sci. Technol.*,1985-5, 275-282.

Sanz, P.D., Mascheroni, R.H., Domniguez, M. & Garcia de Vinuesa, S. (1986). Time-temperature prediction curves of food stuffs by means of the z-transfer function method. *Int. J. of Refrig.*, **9**, 89-92.

Schneider, K.C., Sweat, V.E., Arce, J.A., Dutson, T.R. & Dahm, P.F. (1982). Factor affecting beef carcass chilling rate. *Trans. ASAE*, **25**, 498-507.

Seem, J.E., Klein, S.A., Beckman, W.A. & Mitchell, J.W. (1989). Transfer functions for efficient calculation of multidimensional transient heat transfer. *J. Heat Transfer*, **111**, 5-12.

Singh, R.P. & Mannapperuma, J.D. (1990). Development in food freezing. In *Biotechnology and Food Process Engineering*. Marcel Dekker Inc, New York.

Smith, R.E., Nelson, G.L. & Henrichson, R.L. (1967). Analyses on transient heat transfer from anomalous shapes. *Trans. ASAE*, **10**, 236-245.

Smith, R.E., Nelson, G.L. & Henrichson, R.L. (1968). Applications of geometry analysis of anomalous shapes to problems in transient heat transfer. *Trans. ASAE*, **11**, 296-302.

Smith, R.E. & Nelson, G.L. (1969). Transient heat transfer in solids: theory versus experimental. *Trans. ASAE*, **12**, 833-836, 844.

Smith, R.E., Bennett, A.H. & Vacinek, A.A. (1971). Convection film coefficients related to geometry for anormalous shapes. *Trans. ASAE*, **10**, 236-245.

Srinivasa Murthy, S., Krishna Murthy, M.V. & Ramachandran, A. (1974). Heat transfer during air cooling and storing of moist food products. *Trans. ASAE*, **17**, 769-773.

Srinivasa Murthy, S., Krishna Murthy, M.V. & Ramachandran, A. (1976). Heat transfer during air cooling and storing of moist food products, ii. spherical and cylindrical shapes. *Trans. ASAE*, **19**, 577-583.

Stemer, R.A., Camp, T.H. & Brasington, C.F. (1984). A liquid chill system for rapid cooling of meats. *J. Food Protect.*, **47**, 871-875.

Stemer, R.A., Brasington, C.F., Camp, T.H. & Vanderzant, C. (1986). Hydro-chilling — a rapid method for cooling meats. *Trans. ASAE*, **29**, 306-311.

Sweat, V.E. (1985). Thermal conductivity of food; present state of the data. *ASHRAE Trans.*, **91**(2B), 299-311.

Tang, L. & Johnson, A.T. (1992). Mixed convection about fruits. *J. Agric. Engng. Res.*, **51**, 15-27.

Tucker, G.S. & Holdsworth, S.D. (1991). Mathematical modelling of sterilisation and cooking process for heat preserved foods — application of a new heat transfer model. *Trans. Inst. Chem. Engr.*, **69**(C), 5-12.

van Gerwen, R.J.M., van der Sluis, S.M. & van Oort, H. (1991). Computer modelling of carcass chilling processes. *Proc. 18th Int. Congr. Refrig.*, Montreal, **4**, 1893-1897.

Wade, N.L. (1984). Estimation of the refrigeration capacity required to cool horticultural produce. *Int. J. of Refrig.*, **7**, 358-366.

Wadsworth J.I. & Spadaro, J.J. (1969). Transient temperature distribution in whole sweet roots during immersion heating. I. Thermal diffusivity of sweet potatoes. *Food Technol.*, **23**(2), 219-223.

Wadsworth J.I. & Spadaro, J.J. (1970) Transient temperature distribution in whole sweet roots during immersion heating. II. Computer simulation. *Food Technol.*, **24**(8), 913-920.

Wood, P.W. (1978). Physical Properties of Dairy Products. *Ministry of Agriculture and Fishery Report T3/78*, New Zealand.

Wrobel, L.C. & Brebbia, C.A. (1979). The Boundary element method for steady state and transient heat conduction. In *Numerical Methods in Thermal Problems*, ed. R.W. Lewis & K. Morgan. Pineridge Press, Swansea, pp.58-73.

Wrobel, L.C. & Brebbia, C.A. (1981). A formulation of the boundary element method for axisymmetric transient heat conduction. *Int. J. Heat Mass Transfer*, **24**, 834-850.

A GENERALLY APPLICABLE METHOD FOR CHILLING TIME PREDICTION

MANUAL

Z. Lin, A.C. Cleland, G.F. Serrallach and D.J. Cleland
Department of Process and Environmental Technology
Massey University
Private Bag 11-222
Palmerston North

Contents

1. Introduction A-5
2. Method Accuracy A-6
3. Case A - Use of Computer Programme A-9
3.1. Shape A-9
3.2. Environment A-9
3.3. Calculation Type A-12
3.4. Thermal Properties A-14
3.5. Packaging Type A-16
3.6. Help, Reset and Run A-16
4. Case B - Alignment Charts and Some Equations A-16
4.1. Brick and Ellipsoidal or 3-dimensional Irregular Shapes A-17
4.1.1. Find object dimensions A-17
4.1.2. Dimensional ratios β_1 and β_2 . . . . . A-17
4.1.3. Surface heat transfer coefficient (h) A-17
4.1.4. Biot number (Bi) A-17
4.1.5. Equivalent heat transfer dimensionality E at $Bi = 0$ (E_0) A-17
4.1.6. Equivalent heat transfer dimensionality E at $Bi = \infty$ (E_∞) A-18
4.1.7. Equivalent heat transfer dimensionality (E) A-18
4.1.8. Lag L factor at $Bi = \infty$ (L_∞) A-18
4.1.9. Alternative dimensional ratio (λ) A-19
4.1.10a. Lag factor for thermal centre calculations (L_c) A-19
4.1.10b. Lag factor for mass-average calculations (L_m) A-19
4.1.11. First root of the transcendental equation for a sphere (α) A-19
4.1.12. Chilling time or temperature reached A-19
4.1.13. Ranges of fractional unaccomplished temperature change (Y_c and Y_m) . . A-19
4.2. Short Cylinder, Squat Cylinder, Infinite Ellipse, Infinite Rectangular Rod and 2-dimensional Irregular Shapes A-21
4.2.1. Object dimensions A-21
4.2.2. Dimensional ratios β_1 and β_2 . . . . . A-21
4.2.3. Surface heat transfer coefficient (h) A-21
4.2.4. Biot number (Bi) A-21
4.2.5. Equivalent heat transfer dimensionality (E) A-21
4.2.6a. Lag factor for thermal centre calculations (L_c) A-21
4.2.6b. Lag factor for mass-average calculations (L_m) A-22
4.2.7. First root of the transcendental equation for a sphere (α) A-22
4.2.8. Chilling time or temperature reached A-22

4.2.9. Ranges of fractional unaccomplished temperature change (Y_c and Y_m) . . . A-22
5. Case C - Full Mathematical Implementation A-22
5.1 Find object dimensions A-22
5.2. Calculate two dimensional ratios β_1 and β_2 . . . . . A-23
5.3. Calculate the surface heat transfer coefficient (h) A-23
5.4. Calculate the Biot number (Bi) A-23
5.5. Find the equivalent heat transfer dimensionality E at $Bi = 0$ (E_0) A-23
5.6. Find the equivalent heat transfer dimensionality E at $Bi = \infty$ (E_∞) A-23
5.7. Find the equivalent heat transfer dimensionality (E) A-23
5.8. Find the lag L factor at $Bi = \infty$ (L_∞) A-24
5.9. Find the alternative dimensional ratio (λ) A-24
5.10a. Find the lag factor for thermal centre calculations (L_c) A-24
5.10b. Find the ratio of lag factors for mass-average and centre temperatures (μ), hence the lag factor for mass-average calculations (L_m) A-24
5.11. Find the first root of the transcendental equation for a sphere (α) A-24
5.12. Calculate the chilling time or temperature reached A-24
5.13. Check the range of fractional unaccomplished temperature change (Y_c and Y_m) A-24
6.1. Sample Calculation 1 (Case B Calculation) A-25
6.2. Sample Calculation 2 (Case B Calculation) A-27
6.3. Sample Calculation 3 (Case B Calculation) A-29
7. Disclamation A-31
8. Acknowledgement A-31
9. Terminology A-31
10. Nomenclature A-34
Figure 4 Values of E_0, the equivalent heat transfer dimensionality at $Bi = 0$, for bricks as a function of β_1 and β_2 . . . . . A-35
Figure 5 Values of E_∞, the equivalent heat transfer dimensionality at $Bi = \infty$, for bricks as a function of β_1 and β_2 . . . . . A-36
Figure 6 Values of E / E_0 as a function of Bi and E_0 / E_∞, for all 3-dimensional shapes A-37
Figure 7 Values of L_∞, the lag factor at $Bi = \infty$, for bricks as a function of β_1 and β_2 . . . . . A-38
Figure 8 Values of L_c, the lag factor for the thermal centre, for bricks as a function of ($Bi\ \lambda$) and L_∞ A-39
Figure 9 Values of μ, the ratio of lag factors for mass-average and thermal centre temperatures, for all shapes as a function of Bi A-40

Figure 10 Values of E_0, the equivalent heat transfer dimensionality at Bi = 0,for ellipsoid and 3-dimensional irregular shapes as a function of β_1 and β_2 . . . . . A-41

Figure 11 Values of E_∞, the equivalent heat transfer dimensionality at $Bi = \infty$, for ellipsoid and 3-dimensional irregular shapes as a function of β_1 and β_2 . . . . . A-42

Figure 12 Values of L_∞, the lag factor at $Bi = \infty$, for ellipsoid and 3-dimensional irregular shapes as a function of β_1 and β_2 . . . . . A-43

Figure 13 Values of L_c, the lag factor for the thermal centre, for ellipsoid and 3-dimensional irregular shapes as a function of ($Bi\ \lambda$) and L_∞ A-44

Figure 14 Values of E, the equivalent heat transfer dimensionality for infinite ellipses and 2-dimensional irregular shapes as a function of Bi and β_1 . . . . . A-45

Figure 15 Values of L_c, the lag factor for thermal centre temperatures for infinite ellipses and 2-dimensional shapes as a function of Bi and β_1 . . . A-46

Figure 16 Values of L_m, the lag factor for mass-average temp. for infinite ellipses and 2-dimensional irregular shapes as a function of Bi and β_1 . . . A-47

Figure 17 Values of E, the equivalent heat transfer dimensionality for infinite rectangular rods as a function of Bi and β_1 . . . . . A-48

Figure 18 Values of L_c, the lag factor for thermal centre temperature for infinite rectangular rods as a function of Bi and β_1 . . . . . A-49

Figure 19 Values of L_m, the lag factor for mass-average temperature for infinite rectangular rods as a function of Bi and β_1 . . . . . A-50

Figure 20 Values of E, the equivalent heat transfer dimensionality for short cylinders (height > diameter) as a function of Bi and β_2 . . . . . A-51

Figure 21 Values of L_c, the lag factor for thermal centre temperature for short cylinders (height > diameter) as a function of Bi and β_2 . . . . . A-52

Figure 22 Values of L_m, the lag factor for mass-average temperature for short cylinders (height > diameter) as a function of Bi and β_2 . . . . . A-53

Figure 23 Values of E, the equivalent heat transfer dimensionality for squat cylinders (height ≤ diameter) as a function of Bi and β_1 . . . . . A-54

Figure 24 Values of L_c, the lag factor for thermal centre temperatures for squat cylinders (height ≤ diameter) as a function of Bi and β_1 . . . . . A-55

Figure 25 Values of L_m, the lag factor for mass-average temperatures for squat cylinders (height ≤ diameter) as a function of Bi and β_1 . . . . . A-56

1. INTRODUCTION

There is a continuing need for simple chilling time prediction methods that can be applied by engineers in the refrigeration industry. IRHACE and RACCA recognised this need by contributing to the costs of a research project at Massey University, which aimed to develop a simple but accurate prediction method. This manual illustrates how refrigeration engineers might be able to use the method developed.

The most common industrial chilling situations involve exposing a product at some warm starting temperature (we will call this T_i) to a cooling medium, often air, at some lower temperature (T_a). The rate at which the temperature in the product will change with time depends on factors such as:

- the density, thermal conductivity and specific heat capacity of the food itself (these are given the symbols ρ, k and c respectively),
- the size of the object (determined by the distance from the slowest cooling point to the nearest surface - denoted R),
- the degree of exposure of the object to the cooling medium (this depends on the air velocity, type of packaging used etc. - it can be described by a surface heat transfer coefficient h),
- the shape of the object (so-called "regular shapes" are the infinite slab, infinite cylinder, sphere, infinite rectangular rod, brick, finite cylinder, infinite ellipse and ellipsoid; irregular shapes can be approximated to one of these).

The chilling time prediction method must take account of all these factors, yet be accurate and simple. The data required for the prediction must also be available. Good data is often difficult to find, especially for the surface heat transfer coefficient. Therefore the application of the new method is therefore introduced as follows:

1. Equations relating the various parameters above to chilling time are presented. Hence calculations can be carried out by hand.
2. Because some of the equations are difficult to use, alignment charts are given to replace the complex equations so that hand calculations can carried out more easily.
3. The easiest way of calculation is using the computer programme.
4. Help with finding data (especially food thermal properties and surface heat transfer coefficients) is available in this manual, and is also included in the computer program.

Users of the method therefore have three choices:

A. A computer program with help on thermal properties and heat transfer coefficient,
B. Alignment charts, a few equations and tabular data to help find thermal properties and heat transfer coefficients, and
C. Equations only, plus tabular data for properties and heat transfer coefficients.

Those requiring a ready made computer package should choose option A; Those who wish to write their own computer programmes should choose option C; And those with only hand calculators should choose B or C.

2. METHOD ACCURACY

After development, the method which is described in following sections was extensively tested. For the regular shapes, the test criterion was the range of percentage differences between known accurate computer simulations and the results predicted by the method, within which 95% of the tests lie. Tables 1 and 2 present results for prediction of centre and mass-average temperatures respectively. Generally the predictions are within ±8% of the computer simulations.

For irregular shapes, infinite ellipses and ellipsoids the testing was differently based. A total of about 100 chilling experiments using 16 different shapes (some of which are shown in Figure 1) were carried out under very carefully controlled laboratory conditions. Temperature/time histories were recorded during each experiment, and heat transfer conditions measured as accurately as possible. Table 3 compares predictions with measured data. In these cases the agreement is not as good as for the regular shapes due to experimental error. However if the contribution of experimental error was removed it is expected that accuracy of the prediction method alone is about ±8%.

The testing work was very time-consuming, taking two years of full-time work. Although the method still has some inaccuracy, it is much less than previous methods.

The remainder of this manual concentrates on the use of the method.

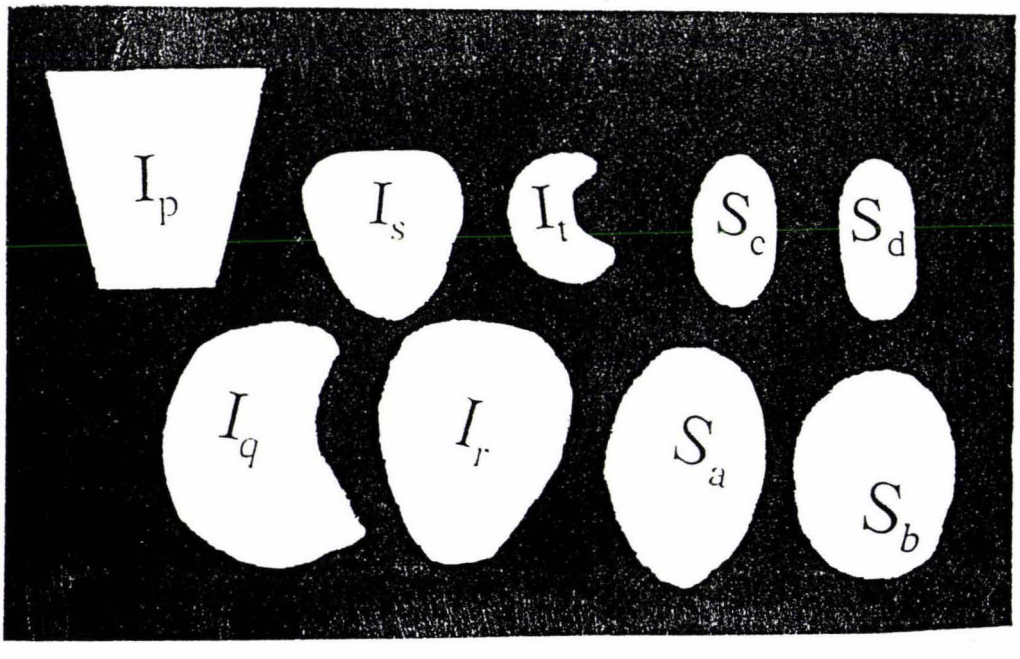

FIGURE 1 Some experimental samples used for prediction method testing

TABLE 1

Percentage errors in predicted chilling times to reach selected thermal centre temperatures ($1 \leq \beta \leq 4$, $0.1 \leq Bi \leq 10$, $0.05 \leq Y_c \leq 0.55$)

Shape	mean	std deviation	95% Confidence Interval	
Infinite rectangular rods	0.3	1.7	-2.9	3.4
Bricks	-1.7	2.2	-7.6	1.7
Short cylinders	-1.3	2.1	-6.7	1.3
Squat cylinders	0.7	2.5	-4.3	5.6

TABLE 2

Percentage errors in predicted chilling times to reach selected mass-average temperatures ($1 \leq \beta \leq 4$, $0.1 \leq Bi \leq 10$, Y_m corresponding to $0.05 \leq Y_c \leq 0.55$)

Shape	mean	std deviation	95% Confidence Interval	
Infinite rectang. rods	0.0	3.5	-5.7	7.1
Bricks	1.7	3.1	-2.6	7.5
Short cylinders	-3.6	2.4	-9.4	0.0
Squat cylinders	1.4	4.4	-5.5	9.2

TABLE 3

Percentage differences between predicted chilling times and times measured experimentally for elliptical, ellipsoidal and irregular shapes

Shape	mean	std deviation	95% Confidence Interval	
Infinite ellipses	7.3	3.5	Not evaluated due to small number of data points	
2-dim. irregular shapes	3.6	6.0		
Ellipsoids	3.2	5.5		
3-dim. irregular shapes	1.2	3.9	-7.4	8.1

Shape, Ambient Environment	Calculation Type	Thermal Properties	Packaging Type	Help, Run, Initialise
Shape Selection	Thermal centre *or* Mass-average	Product type *or* Composition *or* Thermal properties of the product	Layer 1: Type and thickness *or* Thermal conductivity and thickness	
Dimension 1 Dimension 2 Dimension 3				
Chilling process situation, medium velocity and temp. *or* Surface heat transfer coefficient and medium temp.	Time *or* Temperature		Layer 2: Type and thickness *or* Thermal conductivity and thickness	

FIGURE 2: Definition of menus used in "CHILL" computer program

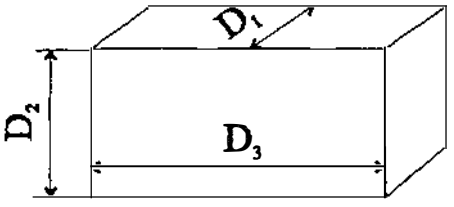

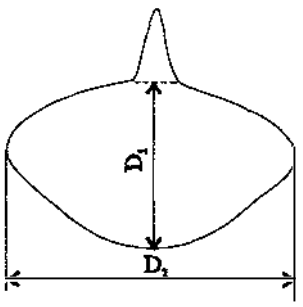

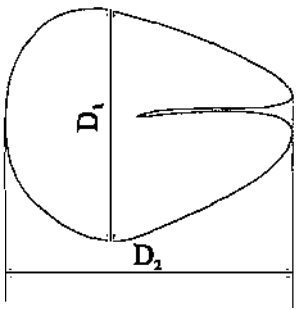

FIGURE 3: Examples of measurement of object geometry. (a) regular shape, (b) shape with protrusions, (c) shape with hollows.

3. CASE A - USE OF COMPUTER PROGRAM

The computer programme called "CHILL" runs under the "Microsoft Windows" environment on an IBM-compatible personal computer (286 or better). The programme is menu-driven, so no commands need to be remembered. The main menu is illustrated in Figure 2. The key inputs to the programme, and their location in the menus are discussed in this section.

3.1. SHAPE

The user must first decide the shape of the object from the following list:

Infinite slab	Infinite cylinder
Sphere	Infinite rectangular rod
Infinite ellipse	2-dimensional irregular shape
Rectangular brick	Finite (short) cylinder
Ellipsoid	3-dimensional irregular shape

Each of these is further described in Chapter 10.

It is then necessary to determine the object's dimensions. For shapes such as cartons ("bricks") this is straightforward, but note that the carton inside dimensions should be used. For irregular shapes it is more difficult. The rules are as follows:

For regular shapes and "smooth" irregular shapes without major "protrusions" or "hollows",

D_1 = shortest dimension through the geometric centre of the object (first dimension);
D_2 = shortest dimension through geometric centre of the object taken at right angles to the first dimension (second dimension);
D_3 = dimension through geometric centre of the object at right angles to both the first and second dimensions (third dimension).

For shapes with protrusions the measurements should ignore the protrusions. Where there are sharp hollows these should be ignored. These rules are best explained by way of an example. Figure 3(a) shows a carton shape. The three dimensions are easily measured. Figure 3(b) and 3(c) show how shapes with protrusions and hollows are modelled, respectively.

3.2. ENVIRONMENT

In this menu the nature of the cooling medium (air or water) and the heat transfer coefficient are defined. The default is to ask for a heat transfer coefficient and a medium temperature, but alternatively, the user can choose from a list of 10 types of environment, medium temperature and the relevant fluid flow condition. The program

then calculates a heat transfer coefficient using a correlation available from the literature. Surface heat transfer coefficients are very much depend on chilling situation - they may vary with position, which makes their prediction difficult. None of the correlations can be regarded as very accurate, but they represent the "state of the art" available in the literature. The best accuracy possible is likely to be ±10%, and if the programme is used wisely accuracy to about ±15% should normally be achieved.

i) For flow of air over large flat surfaces (e.g. for chilling of large cartons, or of smaller cartons pushed together; surface can be vertical or horizontal; correlation most accurate for 1-5 m/s)

$$h = 7.3\ v^{0.8}$$

where h = surface heat transfer coefficient (W/m^2K),
v = air flow velocity (m/s).

ii) For small objects ($D_1 < 0.1$ m) that are spherical or close to spherical, exposed to air flow but not touching other objects. Examples include chilling of quasi-spherical product such as peas, oranges, etc., but not in packed or fluidised beds. Avoid velocities below about 1 m/s.

$$h = 3.6\ v^{0.5} D_1^{0.5}$$

where h = surface heat transfer coefficient (W/m^2K),
v = air flow velocity (m/s),
D_1 = 1st dimension (m).

iii) For objects of small diameter ($D_1 < 0.1$ m) that have one long dimension so that they can be treated as two-dimensional and which are undergoing air cooling. Air flow is parallel to the longest dimension, and objects do not touch each other. Examples include infinite cylinders, infinite ellipses and infinite rectangular rods. Avoid velocities of less than 1 m/s.

$$h = 4.2\ v^{0.52} D_1^{-0.48}$$

where h = surface heat transfer coefficient (W/m^2K),
v = air flow velocity (m/s),
D_1 = 1st dimension (m).

iv) For small objects ($D_1 < 0.1$ m) that have one long dimension so that they can be treated as two-dimensional and which are undergoing water cooling. Water flow is parallel to the longest dimension and objects do not touch each other. Examples include infinite cylinders, infinite ellipses and infinite rectangular rods. Avoid velocities of less than 0.2 m/s.

$$h = 764\ v^{0.52} D_1^{-0.48}$$

where h = surface heat transfer coefficient (W/m^2K),
v = water flow velocity (m/s),
D_1 = 1st dimension (m).

v) For objects of small diameter ($D_1 < 0.1$ m) that have one long dimension so that they can be treated as two-dimensional and which are undergoing air cooling. Air flow is perpendicular to the longest dimension. Objects do not touch each other. Examples include infinite cylinders, infinite ellipses and infinite rectangular rods. Avoid velocities of less than 1 m/s.

$$h = 4.77\ v^{0.6} D_1^{-0.4}$$

where h = surface heat transfer coefficient (W/m^2K),
v = air flow velocity (m/s),
D_1 = 1st dimension (m).

vi) For small objects ($D_1 < 0.1$ m) that have one long dimension so that they can be treated as two-dimensional, and which are undergoing water cooling. Water flow is perpendicular to the longest dimension and objects do not touch each other. Examples include infinite cylinders, infinite ellipses and infinite rectangular rods. Avoid velocities of less than 0.2 m/s.

$$h = 1060\ v^{0.6} D_1^{-0.4}$$

where h = surface heat transfer coefficient (W/m^2K),
v = water flow velocity (m/s),
D_1 = 1st dimension (m).

vii) For large objects ($D_1 > 0.1$m) which have primarily "curved surfaces" and are exposed to air flow in which single product items are independently placed relative to others. Avoid air velocities below 0.5 m/s. Examples include large irregularly shaped items such as animal carcasses and large vegetables or fruit.

$$h = 12.5\ v^{0.6}$$

where h = surface heat transfer coefficient (W/m^2K),
v = air flow velocity (m/s),

viii) For small objects ($D_1 < 0.025$ m) in packed beds where these objects are close to spherical in shape.

$$h = 18\ v^{0.585} D_1^{-0.415}$$

where h = surface heat transfer coefficient (W/m^2K),
v = air flow velocity (m/s),
D_1 = 1st dimension (m).

ix) For small objects ($D_1 < 0.025$ m) in fluidised beds where these objects are close

to spherical in shape. Velocity must exceed that required for fluidisation of the product

$$h = 300\ v^{1.5} D_1^{0.5}$$

where h = surface heat transfer coefficient (W/m^{2}K),
v = air flow velocity (m/s),
D_1 = 1st dimension (m).

x) For a range of small object shapes ($D_1 < 0.1$ m) undergoing water immersion cooling.

$$h = 1060\ v^{0.564} D_1^{-0.436}$$

where h = surface heat transfer coefficient (W/m^{2}K),
v = water flow velocity (m/s),
D_1 = 1st dimension (m).

The program then calculates a heat transfer coefficient.

In the programme "help" available so that you can be sure that you have selected the most appropriate option.

3.3. CALCULATION MODE

The user decides whether to find the chilling time (the time taken for the product to reach a specified temperature); or the final temperature reached after a specified chilling time. The user has the choice of whether to base the predictions on the thermal centre temperature or the mass-average temperature, which is the mean temperature over the object, which is the mean temperature over the object, it is the same as the final equilibrium temperature if the object is put in an insulated box and left for some time.

TABLE 4

Thermal properties of some common food products

Product	k (W/mK)	ρ (kg/m^3)	c (J/kgK)
beef, muscle	0.48	1060	3600
beef, whole carcass	0.46	1030	3400
lamb, muscle	0.46	1060	3500
lamb, whole carcass	0.45	1020	3200
pork, muscle	0.50	1050	3600

Product	k (W/mK)	ρ (kg/m^3)	c (J/kgK)
pork, whole carcass	0.44	1000	3100
chicken	0.44	1070	3550
lean fish	0.53	1030	3650
fatty fish	0.46	1020	3250
egg	0.48	980	3550
cheese, cheddar	0.32	1055	3400
cheese, mozzarella	0.38	1055	2700
butter, salted	0.28	925	4000
butter, unsalted (0 to 20 °C)	0.28	925	4000
butter, unsalted (- 10 to 20 °C)	0.30	925	4850
ham	0.48	1030	3450
sausage	0.38	875	3550
salami	0.31	960	3000
cake	0.11	350	2600
bread	0.24	520	2800
french friend	0.36	1100	2550
carrot	0.55	1000	3900
corn	0.52	1050	3500
corn on cob	0.46	986	3400
cucumber	0.58	1000	4100
onion	0.56	1000	3950
potato	0.50	1055	3650
tomato	0.57	1000	4000
apple, red delicious	0.42	840	3800
apple, braeburn	0.42	870	3800
kiwifruit	0.43	1040	3650
orange	0.42	880	3800
strawberry	0.35	590	4000
grapefruit	0.54	1060	3800

TABLE 5

Thermal properties of some common food components

Product	k (W/mK)	ρ (kg/m^3)	c (J/kg)
water	0.59	1000	4180
fat	0.18	850	1900
air	0.0253	1.23	1006
solids	0.245	1300	1400

3.4. THERMAL PROPERTIES

The thermal properties of the food material are defined in this menu. The default is to ask for density, specific heat capacity and thermal conductivity, but alternatively, the 34 products declared in Table 4 are available for the user to choose. The programme then finds thermal properties itself. A third alternative is for the user to input the composition (percentage of fat and water on a mass basis, voidage fraction) of the product and the programme estimates the thermal properties using a weighted average of the data in Table 5. Equations used are:

$$I = \frac{F}{850} + \frac{S}{1300} + \frac{W}{1000} \tag{1}$$

where I = intermediate value

F, S, W = mass fractions of fat, solid and water respectively.

$$k = \frac{1}{I}\left(\frac{0.18\,F}{850} + \frac{0.245\,S}{1300} + \frac{0.059\,W}{1000}\right) \tag{2}$$

where k = thermal conductivity (W/mK)

For product with voidage:

$$\frac{1}{k_e} = \frac{0.435 - 0.718\,\varepsilon}{(1-\varepsilon)\,k_s + \varepsilon\,k_g} + (0.565 + 0.718\,\varepsilon)\left(\frac{1-\varepsilon}{k_s} + \frac{\varepsilon}{k_g}\right) \tag{3}$$

where k_e = equivalent thermal conductivity (W/mK)

ε = voidage fraction (fraction of the product volume in voids)

$$\rho = \frac{1 - \varepsilon}{I} \quad (4)$$

where ρ = density (kg/m^3)

$$c = 1900F + 1400S + 4180W \quad (5)$$

where c = specific heat capacity (J/kg K)

Inaccuracy in thermal property data can affect the accuracy of predictions. Many different prediction formulae for density, specific heat and thermal conductivity can be found in literature for various food products. Normally density and specific heat are calculated by summing up the component properties in mass or volume proportion. In the case of density, knowledge of material porosity is also required. Thermal conductivity of composite materials such as foods depends not only on the properties of its components but also on the food structure. Common food materials such as meat have different thermal conductivities, parallel to and perpendicular to the fibres. The effect of porosity on thermal conductivity is not as simple as its effect on density. The programme uses methods considered to be reliable but there is no guarantee that they will be accurate for all products.

TABLE 6

Thermal conductivity (W/m K) of some common packaging materials

Material	Thermal conductivity (W/mK)
Aluminium	235
Stainless steel (302)	16
Steel	40
Tin	60
Corrugated cardboard	0.048
Solid wall cardboard	0.065
Borosilicate glass	1.13
Nylon (type 6/6)	0.24
Polyethylene (high density)	0.49
Polyethylene (low density)	0.33
Polypropylene	0.12
Polystyrene	0.13
Teflon	0.26

3.5. PACKAGING TYPE

If the user declares packaging is present, the default is to ask for thermal conductivities and thicknesses of up to two packaging materials; Alternatively, the use can select one of the 12 materials pre-declared in Table 6, and then input only the thickness (e.g. 0.005 m). The total thickness of air gaps beneath the packaging is declared if there is any such gap. The thickness of packaging layer includes the corrugation depth for corrugated materials. If there are overlaps, the mean total thickness is found by multiplying layer the thickness by mean number of layers. Air gap thickness is the average thickness of the total air gaps (between the food product and packaging, and between packaging layers).

3.6. HELP, INITIALISE AND RUN

"Help" contains a series of help topics and indices which are written text displayed to the screen. For example, if the user wishes to know what "Calculation Mode" is, click "Help", then "Topic", find the phrase "Calculation Mode" and click. The definition will appear on the screen. If the user would like to know what "Mass-average temperature" is, just simply click the underlined phrase "Mass-average temperature" and the programme tell what it is. This is one of the so-called "help indices". Furthermore online help is also available. By pressing the "Alt" key and moving cursor to the concerned menu item or sub-item then pressing the key "Enter", a help text box shows on the screen. For example, press "Alt", go to "Calculation Mode" and press "Enter", the user can also get the help on the item.

When "Run" is chosen, the calculation is carried out, taking only a few seconds. All the input data and results available to be output are shown in the background of the window. They are also available in a results file for printing, which may be named by the user.

"Initialise" resets all the values to zero.

4. CASE B - ALIGNMENT CHARTS AND SOME EQUATIONS

This method of implementation involves a series of calculations using alignment charts. In total there are 21 charts included in this manual. This method of implementation also requires the user to calculate surface heat transfer coefficients. Methods used by the computer program for doing this are described in the manual discussed in Section 3.2. They could be used by hand. The calculation proceeds as follows:

4.1. BRICK, ELLIPSOID AND 3-DIMENSIONAL IRREGULAR SHAPES

4.1.1. Object dimensions

After the user has decided the shape of the object is one of the following: rectangular brick, ellipsoid and 3-dimensional irregular shape; it is necessary to determine the object's dimensions. For shapes such as cartons ("bricks") this is straightforward, but note that carton inside dimensions should be used. For irregular shapes it is difficult. The rules are as follows:

For regular and "smooth" irregular shapes without major "protrusions" or "hollows",

D_1 = shortest dimension through the geometric centre of the object (first dimension);
D_2 = shortest dimension through geometric centre of the object taken at right angles to the first dimension (second dimension);
D_3 = dimension through geometric centre of the object at right angles to both the first and second dimensions (third dimension).

For shapes with protrusions the measurements should ignore the protrusions. Where there are sharp hollows these should be ignored. These rules are best explained by way of example. Figure 3(a) shows a carton shape. The three dimensions are easily measured. Figure 3(b) and 3(c) show how shapes with protrusions and hollows are modelled, respectively.

Define R, as half of D_1, i.e. R is the so-called characteristic dimension that is the shortest distance from the thermal centre to the surface:

$$R = 0.5\,D_1 \tag{6}$$

4.1.2. Dimensional ratios (β_1) and (β_2)

$$\beta_1 = D_2/D_1 \qquad \textit{and} \qquad \beta_2 = D_3/D_1 \tag{7}$$

4.1.3. Surface heat transfer coefficient (h)

Section 3.2 describes the methodology to be applied.

4.1.4. Biot number (Bi)

$$Bi = hR/k \tag{8}$$

4.1.5. Equivalent heat transfer dimensionality at $Bi = 0$ (E_0)

E_0 is determined using Figure 4 or 10 with the β_1 and β_2 values found in Section 4.1.2.

4.1.6. Equivalent heat transfer dimensionality at $Bi = \infty$ (E_∞)

E_∞ is to be found using Figure 5 or 11 for the values β_1 and β_2 found in Section 4.1.2.

4.1.7. Equivalent heat transfer dimensionality (E)

The ratio E_0 / E_∞ is calculated using the results of Section 4.1.5 and 4.1.6. Then Bi and E_0 / E_∞ are used on Figure 6 so that the ratio E / E_0 can be decided. E then can be calculated from known E / E_0 and E_0.

4.1.8. Lag factor at ($Bi = \infty$), denoted L_∞

L_∞ is read from Figure 7 or 12 for the values of β_1 and β_2 found in Section 4.1.2.

TABLE 7

Values of geometric parameters for various shapes.

SHAPE	N	P_1	P_2	P_3	γ_1	γ_2	λ
Infinite slab ($\beta_1 = \beta_2 = \infty$)	1	0	0	0	∞	∞	1
Infinite rectangular rod ($\beta_1 \geq 1$, $\beta_2 = \infty$)	2	0.75	0	-1	$4\beta_1/\pi$	∞	γ_1
Infinite ellipse ($\beta_1 > 1$, $\beta_2 = \infty$)	2	1.01	0	1	β_1	∞	γ_1
2-dim. irregular shapes ($\beta_1 > 1$, $\beta_2 = \infty$)	2	1.01	0	1	β_1	∞	γ_1
Ellipsoid ($\beta_1 \geq 1$, $\beta_2 \geq \beta_1$)	3	1.01	1.24	1	β_1	β_2	γ_1
3-dim. irregular shapes ($\beta_1 \geq 1$, $\beta_2 \geq \beta_1$)	3	1.01	1.24	1	β_1	β_2	γ_1
Brick ($\beta_1 \geq 1$, $\beta_2 \geq \beta_1$)	3	0.75	0.75	-1	$4\beta_1/\pi$	$1.5\beta_2$	γ_1
Infinite cylinder ($\beta_1 = 1$, $\beta_2 = \infty$)	2	1.01	0	0	1	∞	1
Squat cylinder ($\beta_1 = \beta_2$, $\beta_1 \geq 1$)	3	1.01	0.75	-1	$1.225\beta_1$	$1.225\beta_2$	γ_1
Short cylinder ($\beta_1 = 1$, $\beta_2 \geq 1$)	3	1.01	0.75	-1	β_1	$1.5\beta_2$	γ_1
Sphere ($\beta_1 = \beta_2 = 1$)	3	1.01	1.24	0	1	1	1

4.1.9. Alternative dimensional ratio (λ)

λ is found using Table 7.

4.1.10a. Lag factor for thermal centre calculations (L_c)

For known *Bi*, L_m and λ, L_c can be found using Figure 8 or 13. This step is required for calculations of temperature or chilling time related to the thermal centre.

4.1.10b. Lag factor for mass-average calculations (L_m)

For known *Bi*, the value of μ, the ratio of lag factors for mass-average and thermal centre temperatures, is found using Figure 9. Then the value of L_m is given by:

$$L_m = \mu L_c \tag{9}$$

4.1.11. First root of the transcendental equation for sphere (α)

α is read from Table 8 for the value of *Bi* from Section 4.1.4.

4.1.12. Chilling time or temperature reached

For thermal centre:

$$T_c = L_c \exp\left(-\frac{kEt_c\alpha^2}{3\rho cR^2}\right)(T_i - T_a) + T_a \quad or \quad t_c = \frac{3\rho cR^2}{\alpha^2 kE}\ln\left(\frac{T_i - T_a}{T_c - T_a}L_c\right) \tag{10}$$

For mass-average:

$$T_m = L_m \exp\left(-\frac{kEt_m\alpha^2}{3\rho cR^2}\right)(T_i - T_a) + T_a \quad or \quad t_m = \frac{3\rho cR^2}{\alpha^2 kE}\ln\left(\frac{T_i - T_a}{T_m - T_a}L_m\right) \tag{11}$$

4.1.13. Ranges of fractional unaccomplished temperature change (Y_c and Y_m)

$$Y_c = \frac{(T_c - T_a)}{(T_i - T_a)} \quad and \quad Y_m = \frac{(T_m - T_a)}{(T_i - T_a)} \tag{12}$$

If $Y_c > 0.7$ or $Y_m > 0.55$, results calculated using the prediction method are unreliable because the method is only valid for $0 < Y_c \leq 0.7$ and $0 < Y_m \leq 0.55$.

TABLE 8

Values of the first root of the transcendental equation for a sphere (α)

Bi	α	*Bi*	α	*Bi*	α	*Bi*	α
0.01	0.173	0.60	1.264	1.80	1.959	8.50	2.786
0.02	0.244	0.65	1.310	2.00	2.029	9.00	2.804
0.03	0.299	0.70	1.353	2.20	2.092	9.50	2.821
0.04	0.345	0.75	1.393	2.40	2.148	10.00	2.836
0.05	0.385	0.80	1.432	2.60	2.200	11.00	2.863
0.06	0.422	0.85	1.469	2.80	2.246	12.00	2.885
0.08	0.486	0.90	1.504	3.00	2.289	13.00	2.904
0.10	0.542	0.95	1.538	3.20	2.328	14.00	2.921
0.12	0.593	1.00	1.571	3.40	2.364	15.00	2.935
50.14	0.639	1.05	1.602	3.60	2.397	16.00	2.948
0.16	0.682	1.10	1.632	3.80	2.427	18.00	2.969
0.18	0.722	1.15	1.661	4.00	2.456	20.00	2.986
0.20	0.759	1.20	1.689	4.50	2.518	25.00	3.017
0.25	0.845	1.25	1.716	5.00	2.570	30.00	3.037
0.30	0.921	1.30	1.741	5.50	2.615	35.00	3.052
0.35	0.990	1.35	1.766	6.00	2.654	40.00	3.063
0.40	1.053	1.40	1.791	6.50	2.687	50.00	3.079
0.45	1.111	1.45	1.814	7.00	2.717	60.00	3.089
0.50	1.16	1.50	1.837	7.50	2.742	80.00	3.102
0.55	1.27	1.60	1.880	8.00	2.765	100.00	3.110

4.2. SHORT CYLINDER, SQUAT CYLINDER, INFINITE ELLIPSE, INFINITE RECTANGULAR ROD AND 2-DIMENSIONAL IRREGULAR SHAPES

4.2.1. Object dimensions

This is discussed in Section 4.1.1 but note that D_3 need not be found except for finite cylinders.

4.2.2. Dimensional ratios (β_1) and (β_2)

Except for finite cylinders, β_1 is determined using eqn.(7) from Section 4.1.2, and $\beta_2 = \infty$; for short cylinders (height > diameter) $\beta_1 = 1$ and β_2 = height/diameter; for squat cylinders (height ≤ diameter), $\beta_1 = \beta_2$ = diameter/height.

4.2.3. Surface heat transfer coefficient (h)

Section 3.2 describes the methodology to be applied.

4.2.4. Biot number (Bi)

Bi is determined using eqn.(8) from Section 4.1.4.

4.2.5. Equivalent heat transfer dimensionality (E)

For infinite ellipses or infinite 2-dimensional shapes, E is to be found using Figure 14, for the values of Bi found in Section 4.2.4 and β_1 found in Section 4.2.2; for infinite rectangular rods Bi (from Section 4.2.4) and β_1 (from 4.2.2) are used on Figure 17; for short cylinders Bi and β_2 are used on Figure 20; and for squat cylinders Bi and β_1 are used on Figure 23.

4.2.6a. Lag factor for thermal centre calculations (L_c)

For infinite ellipses or infinite 2-dimensional shapes, L_c is to be found using Figure 15, for the values of Bi found in Section 4.2.4 and β_1 found in Section 4.2.2; for infinite rectangular rods Bi (from Section 4.2.4) and β_1 (from 4.2.2) are used on Figure 18; for short cylinders Bi and β_2 are used on Figure 21; and for squat cylinders Bi and β_1 are used on Figure 24. This step is required for calculations of temperature or chilling time related to the thermal centre.

4.2.6b. Lag factor for mass-average calculations (L_m)

For infinite ellipses or infinite 2-dimensional shapes, L_m is to be found using Figure 16, for the values of *Bi* found in Section 4.2.4 and β_1 found in Section 4.2.2; for infinite rectangular rods *Bi* (from Section 4.2.4) and β_1 (from 4.2.2) are used on Figure 19; for short cylinders *Bi* and β_2 are used on Figure 22; and for squat cylinders *Bi* and β_1 are used on Figure 25. This step is required for calculations of temperature or chilling time related to the mass-average conditions.

4.2.7. First root of the transcendental equation for sphere (α)

α is determined using Table 8 introduced in Section 4.1.11.

4.2.8. Chilling time or temperature reached

Section 4.1.12 describes the calculation formulae to be applied.

4.2.9. Ranges of fractional unaccomplished temperature change (Y_c and Y_m)

Section 4.1.13 describes the methodology to be applied.

4.3. INFINITE SLAB, INFINITE CYLINDER AND SPHERE

Due to the simple nature of these three geometries, calculation aids in the form of alignment charts are unnecessary. Problems involving these three basic geometries can be solved without much complexity via either the Case A approach discussed in Chapter 3 or the Case C approach which will be introduced in the next Chapter.

For infinite slabs $\beta_1 = \beta_2 = \infty$; for infinite cylinders $\beta_1 = 1$ and $\beta_2 = \infty$; for spheres $\beta_1 = \beta_2 = 1$ and $E = 3$.

5. CASE C - FULL MATHEMATICAL IMPLEMENTATION

In case C, the alignment charts are substituted by mathematical formulae for finding the heat transfer dimensionalities E_0, E_∞ and E, and the lag factors L_∞, L_c and L_m.

5.1. OBJECT DIMENSIONS

This is discussed in Section 4.2.1.

5.2. DIMENSIONAL RATIOS (β_1) AND (β_2)

β_1 and β_2 are determined using eqn.(7) from Section 4.1.2.

5.3. SURFACE HEAT TRANSFER COEFFICIENT (*h*)

Section 3.2 describes the methodology to be applied.

5.4. BIOT NUMBER (*Bi*)

Bi is determined using eqn.(8) from Section 4.1.4.

5.5. HEAT TRANSFER DIMENSIONALITY AT $Bi = 0$ (E_0)

For a regular shape (infinite slab, infinite cylinder, sphere, infinite rectangular rod, rectangular brick, short cylinder, squat cylinder):

$$E_0 = 1 + 1/\beta_1 + 1/\beta_2 \tag{13}$$

For an ellipse:

$$E_O = (1 + 1/\beta_1)(1 + ((\beta_1 - 1)/(\beta_1 + 1))^2/4) \tag{14}$$

For an ellipsoid or an irregular shape ($1<\beta_1<10$, $1<\beta_2<10$):

$$E_0 = \frac{3(\beta_1 + \beta_2 + \beta_1^2(1 + \beta_2) + \beta_2^2(1 + \beta_1))}{2(\beta_1\beta_2(1 + \beta_1 + \beta_2))} - \frac{1}{19}[(\beta_1 - \beta_2)^2]^{0.4} \tag{15}$$

5.6. HEAT TRANSFER DIMENSIONALITY AT $Bi = \infty$ (E_∞)

$$E_\infty = 0.75 + P_1 f(\beta_1) + P_2 f(\beta_2) \tag{16}$$

$$f(\beta) = 1/\beta^2 + 0.01 P_3 \exp(\beta - 0.166\beta^2) \tag{17}$$

Values of P_1, P_2 and P_3 are stated in Table 7.

5.7. HEAT TRANSFER DIMENSIONALITY (*E*)

$$E = (Bi^{4/3} + 1.85) / (Bi^{4/3} / E_\infty + 1.85 / E_0) \tag{18}$$

5.8. LAG FACTOR AT $Bi = \infty$ (L_∞)

$$L_\infty = 1.271 + 0.305\exp(0.172\gamma_1 - 0.115\gamma_1^2) + 0.425\exp(0.09\gamma_2 - 0.128\gamma_2^2) \quad (19)$$

Values of γ_1 and γ_2 are found using Table 7.

5.9. ALTERNATIVE DIMENSIONAL RATIO (λ)

γ is determined using Table 7 from Section 4.1.9.

5.10a. LAG FACTOR FOR THERMAL CENTRE CONDITION (L_c)

$$L_c = (Bi^{1.35} + 1/\lambda) / (Bi^{1.35}/L_\infty + 1/\lambda) \quad (20)$$

This step is required for calculations of temperature or chilling time of the thermal centre.

5.10b. RATIO OF LAG FACTORS FOR MASS-AVERAGE AND CENTRE TEMPERATURES μ, AND HENCE THE LAG FACTOR FOR MASS-AVERAGE TEMPERATURE L_c

$$\mu = [(1.5 + 0.69\ Bi) / (1.5 + Bi)]^N \quad (21)$$

Where N is read from Table 7.

$$L_m = \mu\ L_c \quad (22)$$

This step is required for calculations related to mass-average conditions.

5.11. FIRST ROOT OF THE TRANSCENDENTAL EQUATION FOR SPHERE (α)

Use Table 8 or solve:

$$\alpha \cot\alpha + (Bi - 1) = 0 \quad (23)$$

5.12. CHILLING TIME OR TEMPERATURE REACHED

Section 4.1.12 describes the calculational formulae to be applied.

5.13. RANGES OF FRACTIONAL UNACCOMPLISHED TEMPERATURE CHANGE (Y_c AND Y_m)

Section 4.1.13 describes the methodology to be applied.

6. WORKED EXAMPLES (CASE B CALCULATION)

6.1. Sample Calculation 1 (Case B Calculation)

Calculate the thermal centre and mass-average temperatures for a carton (brick shape) of dimensions 200 × 300 × 400 mm initially at 30°C after 65600 seconds chilling if the ambient temperature is 0°C, the surface heat transfer coefficient (h) is 20 W/m^{2}K, and thermal properties of the material are: c = 3900 J/kgK, ρ = 1000 kg/m^3 and k = 0.5 W/mK.

Solution:

1. Find object dimensions (Section 4.1.1)

   D_1 = 0.2 m, D_2 = 0.3 m, D_3 = 0.4 m, $R = D_1 / 2$ = 0.1 m;

2. Calculate β_1 and β_2 (Section 4.1.2)

   $\beta_1 = 0.3 / 0.2 = 1.5$ and $\beta_2 = 0.4 / 0.2 = 2.0$;

3. Calculate h (Section 4.1.3)

   h = 20 W/mK;

4. Calculate Bi (Section 4.1.4)

   $Bi = h R / k = 20 \times 0.1 / 0.5 = 4.0$;

5. Find E_0 (Section 4.1.5)

   For $\beta_1 = 1.5$ and $\beta_2 = 2.0$, E_0 = 2.17 (Figure 4);

6. Find E_∞ (Section 4.1.6)

   For $\beta_1 = 1.5$ and $\beta_2 = 2.0$, E_∞ = 1.22 (Figure 5);

7. Find E (Section 4.1.7)

   For $E_0 / E_\infty = 2.17 / 1.22 = 1.78$ and $Bi = 4$, E / E_0 = 0.64 (Figure 6),

   $E = 0.64\ E_0 = 0.64 \times 2.17 = 1.39$;

8. Find L_∞ (Section 4.1.8)

   For $\beta_1 = 1.5$ and $\beta_2 = 2.0$, L_∞ = 1.73 (Figure 7);

9. Find λ (Section 4.1.9)

   From Table 4, for a rectangular brick $\lambda = \gamma_1 = (4 / \pi)\ \beta_1 = (4 / \pi) \times 1.5 = 1.91$;

10a. Find L_c (Section 4.1.10a)

For $(Bi\ \lambda) = 4.0 \times 1.91 = 7.64$ and $L_\infty = 1.73$, $L_c = 1.60$ (Figure 8);

10b. Find L_m (Section 4.1.10b)

For Bi = 4.0, $\mu = 0.46$ (Figure 9), $L_m = \mu \times L_c = 0.46 \times 1.60 = 0.736$;

11. Find α (Section 4.1.11)

For $Bi = 4.0$, $\alpha = 2.456$ (Table 8);

12. Find T_c and T_m (Section 4.1.12)

$$T_c = L_c \exp\left(-\frac{kEt_c\alpha^2}{3\rho cR^2}\right)(T_i - T_a) + T_a$$

$$= 1.64\exp\left(-\frac{0.5 \times 1.39 \times 65600 \times 2.456^2}{3 \times 1000 \times 3900 \times 0.1^2}\right)(30 - 0) + 0 = 4.6\ ^\circ C$$

$$T_m = L_m \exp\left(-\frac{kEt_m\alpha^2}{3\rho cR^2}\right)(T_i - T_a) + T_a$$

$$= 0.76\exp\left(-\frac{0.5 \times 1.39 \times 65600 \times 2.456^2}{3 \times 1000 \times 3900 \times 0.1^2}\right)(30 - 0) + 0 = 2.1\ ^\circ C$$

The analytical solution predicts 5.0°C and 1.95°C for the thermal centre and mass-average temperatures respectively.

13. Check Y ranges (Section 4.1.13)

$$Y_c = (T_c - T_a)/(T_i - T_a) = (4.6 - 0)/(30 - 0) = 0.153$$

$$Y_m = (T_m - T_a)/(T_i - T_a) = (2.1 - 0)/(30 - 0) = 0.07$$

Thus result calculated is valid because $0 < Y_c < 0.7$ and $0 < Y_m < 0.55$.

6.2. Sample Calculation 2 (Case B Calculation)

Calculate the chilling time needed for the cheddar cheese experimental sample of irregular shape (I_1) shown in Figure 1 initially at 18.9°C to reach a centre temperature of -2.9°C (above the freezing point of cheese) when the dimensions are 50 mm by 55 mm by 110 mm, the ambient temperature is -5.3°C, the surface heat transfer coefficient is 25 W/m^{2}K, and the thermal properties of the cheese are c = 3410 J/kg°K, ρ = 1055 kg/m^3 and k = 0.31 W/mK. Also calculate mass-average temperature of the sample.

Solution:

1. Find object dimensions (Section 4.1.1)

   D_1 = 0.05 m, D_2 = 0.055 m, D_3 = 0.11 m, $R = D_1 / 2$ = 0.025 m;

2. Calculate β_1 and β_2 (Section 4.1.2)

   $\beta_1 = 0.055 / 0.05 = 1.1$ and $\beta_2 = 0.11 / 0.05 = 2.2$;

3. Calculate h (Section 4.1.3)

   h = 25 W/mK;

4. Calculate Bi (Section 4.1.4)

   $Bi = h R / k = 25 \times 0.025 / 0.31 = 2.02$;

5. Find E_0 (Section 4.1.5)

   For $\beta_1 = 1.1$ and $\beta_2 = 2.2$, E_0 = 2.44 (Figure 10);

6. Find E_∞ (Section 4.1.6)

   For $\beta_1 = 1.1$ and $\beta_2 = 2.2$, E_∞ = 1.90 (Figure 11);

7. Find E (Section 4.1.7)

   For $E_0 / E_\infty = 2.4 / 1.9 = 1.28$ and Bi = 2.02, E / E_0 = 0.87 (Figure 6),

   $E = 0.87\ E_0 = 0.87 \times 2.4 = 2.12$;

8. Find L_∞ (Section 4.1.8)

   For $\beta_1 = 1.1$ and $\beta_2 = 2.2$, L_∞ = 1.89 (Figure 12);

9. Find λ (Section 4.1.9)

   From Table 4, for a 3-dimensional irregular shape $\lambda = \gamma_1 = \beta_1 = 1.1$;

10a. Find L_c (Section 4.1.10a)

For $(Bi\ \lambda) = 2.02 \times 1.1 = 2.22$ and $L_\infty = 1.87$, $L_c = 1.48$ (Figure 13);

10b. Find L_m (Section 4.1.10b)

For Bi = 2.02, $\mu = 0.57$ (Figure 9), $L_m = \mu \times L_c = 0.57 \times 1.48 = 0.84$;

11. Find α (Section 4.1.11)

For $Bi = 2.02$, $\alpha = 2.034$ (Table 8);

12. Find t_c and T_m (Section 4.1.12)

$$t_c = \frac{3\rho c R^2}{\alpha^2 k E} \ln\left(\frac{T_i - T_a}{T_c - T_a} L_c\right)$$

$$= \frac{3 \times 1055 \times 3410 \times 0.025^2}{2.034^2 \times 0.31 \times 2.12} \ln\left(\frac{18.9 - (-5.3)}{-2.9 - (-5.3)} \times 1.48\right) = 6710 \text{ seconds}$$

The experimental result is 6300 seconds which is 6.5% different.

$$T_m = L_m \exp\left(-\frac{k E t_m \alpha^2}{3\rho c R^2}\right)(T_i - T_a) + T_a$$

$$= 0.84 \exp\left(-\frac{0.31 \times 2.11 \times 6300 \times 2.034^2}{3 \times 1055 \times 3410 \times 0.025^2}\right)[18.9 - (-5.3)] + (-5.3) = -3.6\ ^\circ C$$

13. Check Y ranges (Section 4.1.13)

$$Y_c = (T_c - T_a)/(T_i - T_a) = (-2.9 - (-5.3))/(18.9 - (-5.3)) = 0.099$$

$$Y_m = (T_m - T_a)/(T_i - T_a) = (-3.6 - (-5.3))/(18.9 - (-5.3)) = 0.07$$

Thus result calculated is valid because $0 < Y_c \leq 0.7$ and $0 < Y_m \leq 0.55$.

6.3. Sample Calculation 3 (Case B Calculation)

Calculate the chilling time needed for the Cheddar cheese with uniformly distributed voids experimental sample of rectangular brick shape (B_e) initially at 15.0°C to reach a centre temperature of 0.3°C (above the freezing point of the water in the cheese) when the dimensions are 72 mm by 72 mm by 300 mm, the ambient temperature is -3.9°C, the surface heat transfer coefficient is 17.2 W/m^{2}K, and the thermal properties of Cheddar cheese are k_s = 0.306 W/m K, c_s = 3410 J/kg°C and ρ_s = 1055 kg/m^3. The voidage fraction ε = 0.40. Also calculate mass-average temperature of the sample.

Solution:

1. Find object dimensions (Section 4.1.1)

D_1 = 0.072 m, D_2 = 0.72 m, D_3 = 0.300 m, $R = D_1 / 2$ = 0.036 m;

2. Calculate β_1 and β_2 (Section 4.1.2)

$\beta_1 = 0.072 / 0.072 = 1.00$ and $\beta_2 = 0.300 / 0.072 = 4.17$;

3. Calculate h (4.1.3)

h = 17.2 W/mK;

4. Find k_e, ρ and c (Section 3.4)

$$\frac{1}{k_e} = \frac{0.435 - 0.718\,\varepsilon}{(1-\varepsilon)\,k_s + \varepsilon\,k_g} + (0.565 + 0.718\,\varepsilon)\left(\frac{1-\varepsilon}{k_s} + \frac{\varepsilon}{k_g}\right)$$

$$= \frac{0.435 - 0.718 \times 0.40}{(1 - 0.40) \times 0.306 + 0.40 \times 0.025} +$$

$$(0.565 + 0.718 \times 0.40)\left(\frac{1 - 0.40}{0.306} + \frac{0.40}{0.025}\right)$$

k_e = 0.142 W/mK,

$\rho = (1 - \varepsilon)\,\rho_s = (1 - 0.40) \times 1055 = 633$ W/m^3, and

$c = c_s$ = 3410 kg/m^3;

5. Calculate Bi (Section 4.1.4)

$Bi = h\,R / k_e = 17.2 \times 0.036 / 0.142 = 4.36$;

6. Find E_0 (Section 4.1.5)

For β_1 = 1 and β_2 = 4.17, E_0 = 2.24 (Figure 4);

7. Find E_∞ (Section 4.1.6)

For $\beta_1 = 1$ and $\beta_2 = 4.17$, $E_\infty = 1.50$ (Figure 5);

8. Find E (Section 4.1.7)

For $E_0 / E_\infty = 2.24 / 1.50 = 1.49$ and $Bi = 4.36$, $E / E_0 = 0.72$ (Figure 6),

$E = 0.72\ E_0 = 0.72 \times 2.24 = 1.61$;

9. Find L_∞ (Section 4.1.8)

For $\beta_1 = 1$ and $\beta_2 = 4.17$, $L_\infty = 1.59$ (Figure 7);

10. Find λ (4.1.9)

From Table 4, for a 3-dimensional irregular shape $\lambda = \gamma_1 = 4\beta_1/\pi = 1.27$;

11a. Find L_c (Section 4.1.10a)

For $(Bi\ \lambda) = 4.36 \times 1.27 = 5.55$ and $L_\infty = 1.59$, $L_c = 1.50$ (Figure 8);

11b. Find L_m (Section 4.1.10b)

For Bi = 4.36, $\mu = 0.46$ (Figure 9), $L_m = \mu \times L_c = 0.46 \times 1.5 = 0.69$;

12. Find α (Section 4.1.11)

For $Bi = 4.36$, $\alpha = 2.5$ (Table 8);

13. Find t_c and T_m (Section 4.1.12)

$$t_c = \frac{3\rho c R^2}{\alpha^2 k_e E} \ln\left(\frac{T_i - T_a}{T_c - T_a} L_c\right)$$

$$= \frac{3 \times 633 \times 3410 \times 0.036^2}{2.5^2 \times 0.142 \times 1.67} \ln\left(\frac{15 - (-3.9)}{0.3 - (-3.9)} \times 1.5\right) = 10810 \text{ seconds}$$

The experimental result is 10810 seconds which is 4.1% different.

$$T_m = L_m \exp\left(-\frac{k_e E t_m \alpha^2}{3\rho c R^2}\right)(T_i - T_a) + T_a$$

$$= 0.69 \exp\left(-\frac{0.142 \times 1.67 \times 10810 \times 2.5^2}{3 \times 633 \times 3410 \times 0.036^2}\right)[15. - (-3.9)] + (-3.9) = -2.0\ ^\circ C$$

14. Check Y ranges (Section 4.1.13)

$$Y_c = (T_c - T_a)/(T_i - T_a) = (-0.3 - (-3.9))/(15. - (-3.9)) = 0.222$$

$$Y_m = (T_m - T_a)/(T_i - T_a) = (-2 - (-3.9))/(15 - (-3.9)) = 0.101$$

Thus result calculated is valid because $0 < Y_c \leq 0.7$ and $0 < Y_m \leq 0.55$.

7. DISCLAIMER

The quality of thermal property and environmental data can, sometimes largely, affect the accuracy of prediction. Due to the complicated nature of the problem and large variety of food product, it cannot be guaranteed that all the data and formulae applied in the programme are always unconditionally valid, although care had been taken to make them as accurate as possible. The method must not be used if freezing occurs or major fat phase change takes place during the cooling process.

8. ACKNOWLEDGEMENT

The authors gratefully acknowledge the financial support of the Institute of Refrigeration, Heating and Air Conditioning Engineers of New Zealand for this work.

9. TERMINOLOGY

1st dimension: the shortest dimension through the geometric centre of the object;

2nd dimension: the shortest dimension through geometric centre of the object taken at right angle to the 1st dimension;

2-dimensional Irregular Shape: an object is infinitely long (practically its length is 10 times greater than its width) and all sections perpendicular to the long axis are of the same shape yet not a rectangular, circular or elliptical shape.

3rd dimension: the dimension through geometric centre of the object at right angles to both the 1st and 2nd dimensions.

3-dimensional Irregular Shape: an object is finite in magnitude and not a sphere, a rectangular brick or an ellipsoid.

Air Gap Thickness: average thickness of the total air gaps (between the food product and packaging and between packaging layers).

Brick: a six-surface object, each surface is flat and rectangular.

Calculation Mode: decide whether to find chilling time (a time to reach a certain temperature) or temperature (a temperature reached after a certain chilling time). The choice of whether to base the predictions on mass-average or thermal centre temperature can also be made.

Composition: nature of ingredients of the food product (mass fractions).

Cooling Medium Temperature: temperature of the cooling medium (air or water), which must be approximately constant.

Ellipse: a regular oval, traced by a point moving in a plane so that the sum of its distances from two other points is constant (a "squatted circle).

Ellipsoid: an object of which all the plane sections perpendicular to one axis are circles and all the other plane sections are ellipses.

Finite Cylinder: a uniform object with finite straight sides and a circle section.

Height: length of the axis of a finite cylinder;

Imperfect Contact: air gap(s) exist between food product and packaging or between packaging layers.

Infinite Slab: an object is infinitely long and wide (practically the length and width are 10 times greater the thickness) and its thickness is identical throughout the whole object.

Infinite Cylinder: a uniform object with infinite straight sides and a circle section right angle to the 1st dimension;

Infinite Rectangular Rod: an object is infinite long and its cross sections are all rectangles of the same size.

Initial Temperature: initial temperature of the object undergoing chilling process.

Layer 1: 1st layer of the packaging.

Layer 2: 2nd layer of the packaging.

Mass-average Temperature: mean temperature of particles all over the object, it is the final equilibrium temperature if an object is put in an insulating box.

Material: type or name of the packaging material used.

Packing Type: whether or not and how many packaging layer are used.

Perfect Contact: packaging layer(s) touch each other and the food product directly, with no air gap.

Product: food product undergoing chilling process.

Radius: a straight line from the axis to the nearest surface point.

Shape: decide the geometric category to which the object belongs, i.e. what kind of shape it is. It must fall in one of the following categories:

Infinite slab	Infinite cylinder
Sphere	Infinite rectangular rod
Infinite ellipse	2-dimensional irregular shapes
Rectangular brick	Short cylinder
Squat Cylinder	Ellipsoid
3-dimensional irregular shapes	

Short Cylinder: a uniform object with finite straight sides and a circle section, the length of the sides is longer than the diameter of the circle section.

Sphere: an object with every point on its surface equidistant from its centre.

Squat Cylinder: a uniform object with finite straight sides and a circle section, the length of the sides is shorter than the diameter of the circle section.

Thermal Data: thermophysical properties such as density, specific heat capacity and thermal conductivity are decided directly or indirectly.

Thickness: thickness of the layers of packaging. It equals the corrugation depth for corrugated materials and it equals the average thickness if there are overlaps.

Time for Mass-average Temperature: a time for mass-average temperature to reach certain value.

Time for Thermal Centre Temperature: a time for thermal centre temperature to reach certain value.

10. NOMENCLATURE

Bi	Biot number = $h\,R\,/\,k$
c	specific heat capacity (J/kg K)
D_1	first dimension (m)
D_2	second dimension (m)
D_3	third dimension (m)
E	equivalent heat transfer dimensionality
E_0	equivalent heat transfer dimensionality at $Bi = 0$
E_∞	equivalent heat transfer dimensionality at $Bi = \infty$
F	fat fraction
h	surface heat transfer coefficient (W/m^2K)
I	intermediate value
k	thermal conductivity (W/mK)
k_e	equivalent thermal conductivity (W/mK) of product with voidage
L_∞	lag factor for thermal centre at $Bi = \infty$
L_c	lag factor for thermal centre
N	number of heat transfer dimensions of an object or shape
P_1, P_2, P_3	parameter defined in Table 4
R	the characteristic half thickness (m)
S	solid fraction
t_c	chilling time (s) for thermal centre
t_m	chilling time (s) for mass-average
T_c	temperature of thermal centre (°C)
T_m	mass-average temperature (°C)
T_i	initial temperature (°C)
T_a	cooling medium temperature (°C)
v	cooling medium velocity (m/s)
W	solid fraction
Y_c	fractional unaccomplished temp. change for thermal centre $= (T_c - T_a) / (T_i - T_a)$
Y_m	fractional unaccomplished temp. change for mass-average $= (T_m - T_a) / (T_i - T_a)$
α	first root of the transcendental equation for a sphere (eqn. 32)
β_1	ratio of dimension 2 to dimension 1
β_2	ratio of dimension 3 to dimension 1
γ_1	alternative dimensional ratio 1
γ_2	alternative dimensional ratio 2
ε	voidage fraction
λ	alternative dimensional ratio
μ	ratio of lag factors for mass-average and thermal centre temperatures
ρ	density (kg/m^3)

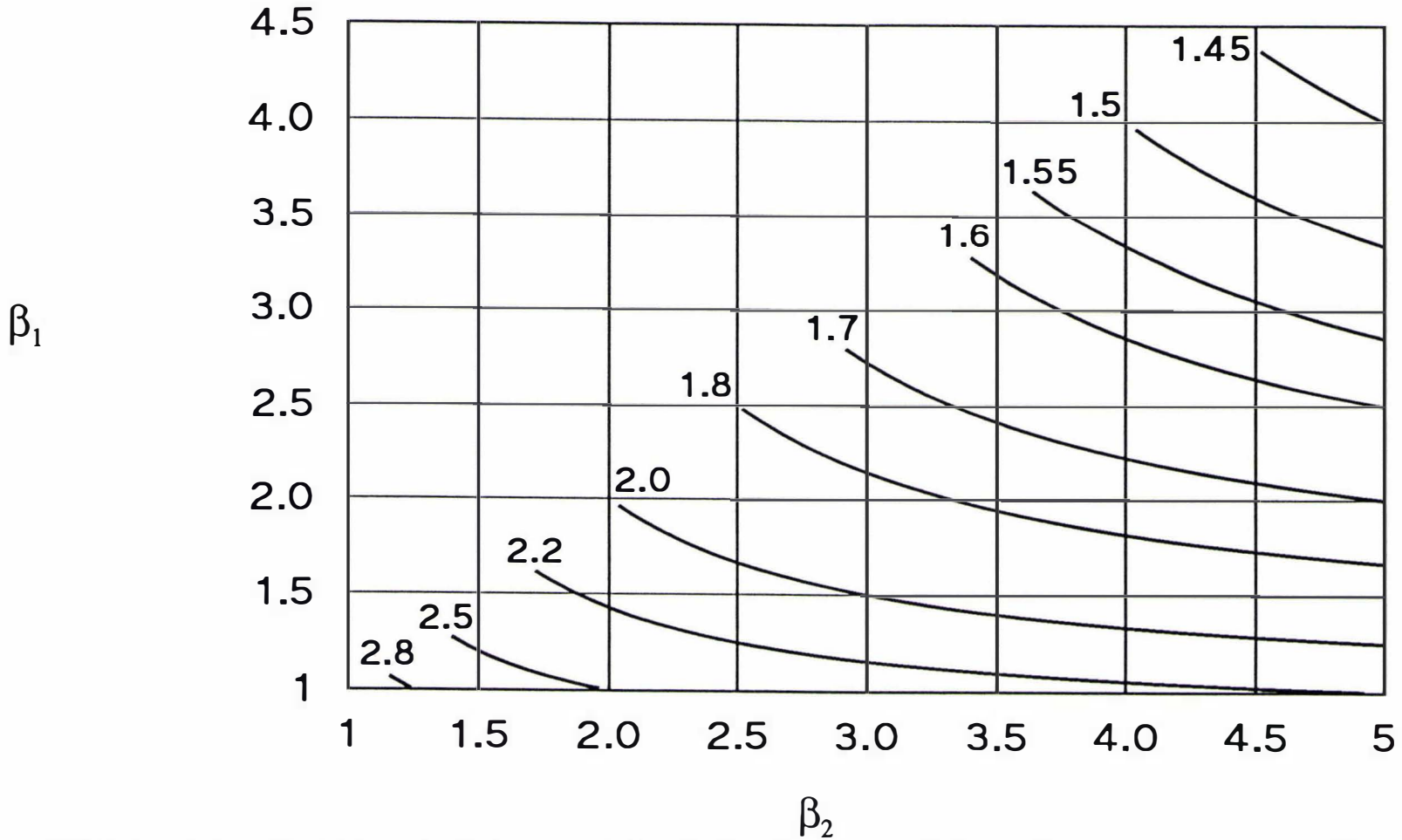

FIGURE 4 Values of E_0, the equivalent heat transfer dimensionality at $Bi = 0$, for bricks as a function of β_1 and β_2

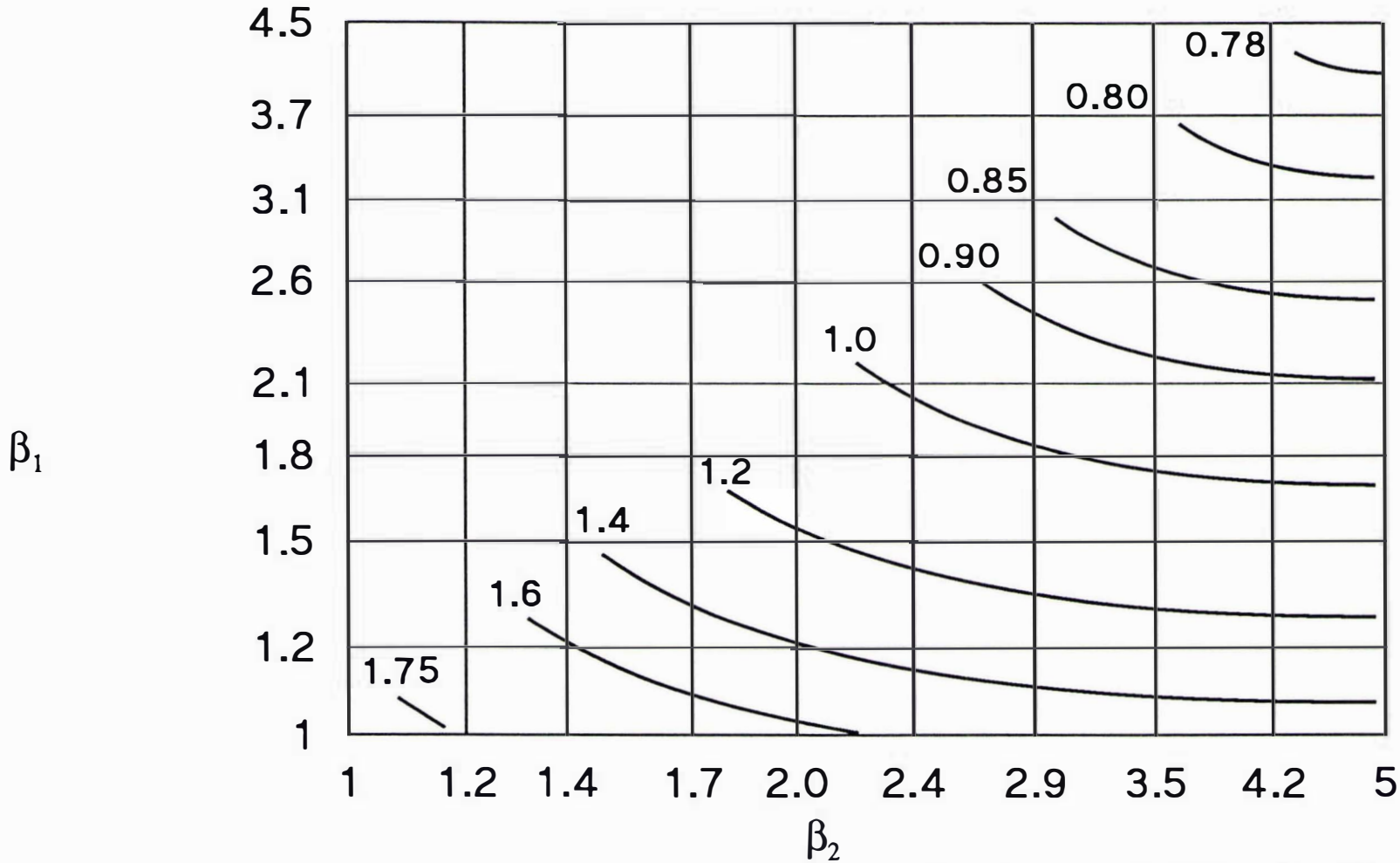

FIGURE 5 Values of E_∞, the equivalent heat transfer dimensionality at $Bi = \infty$, for bricks as a function of β_1 and β_2

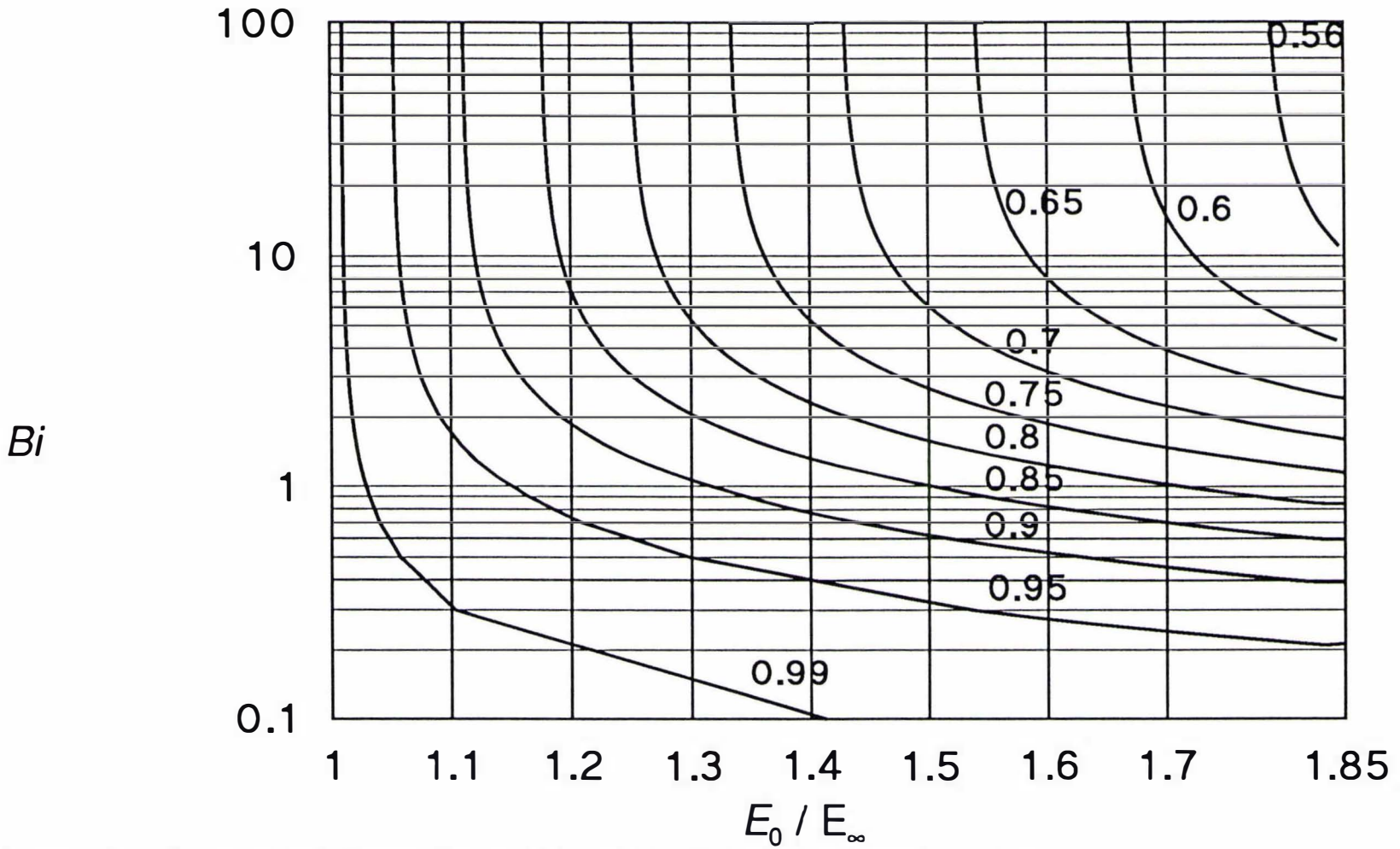

FIGURE 6 Values of E / E_0 as a function of Bi and E_0 / E_∞, for all 3-dimensional shapes

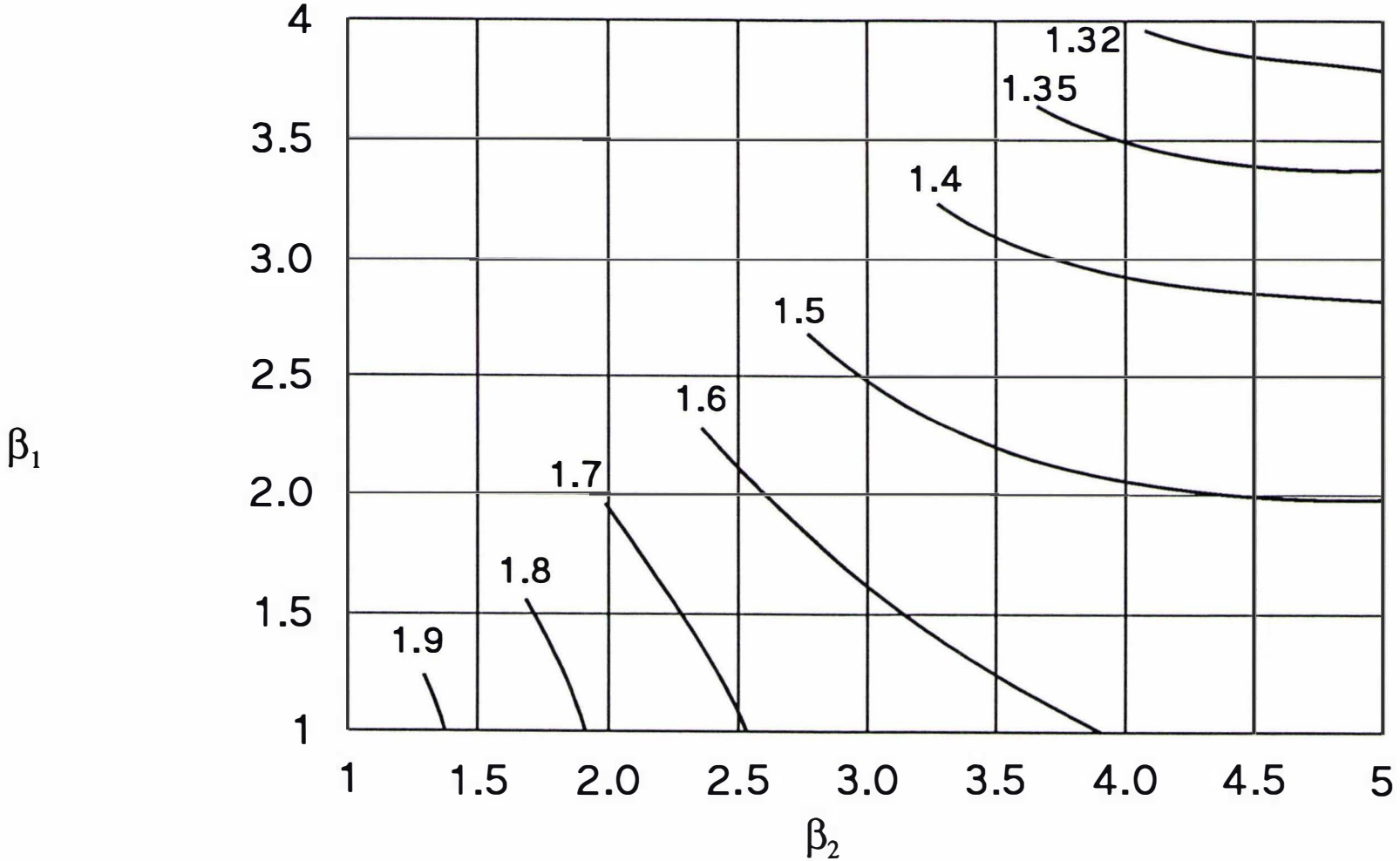

FIGURE 7 Values of L_∞, the lag factor at $Bi = \infty$, for bricks as a function of β_1 and β_2

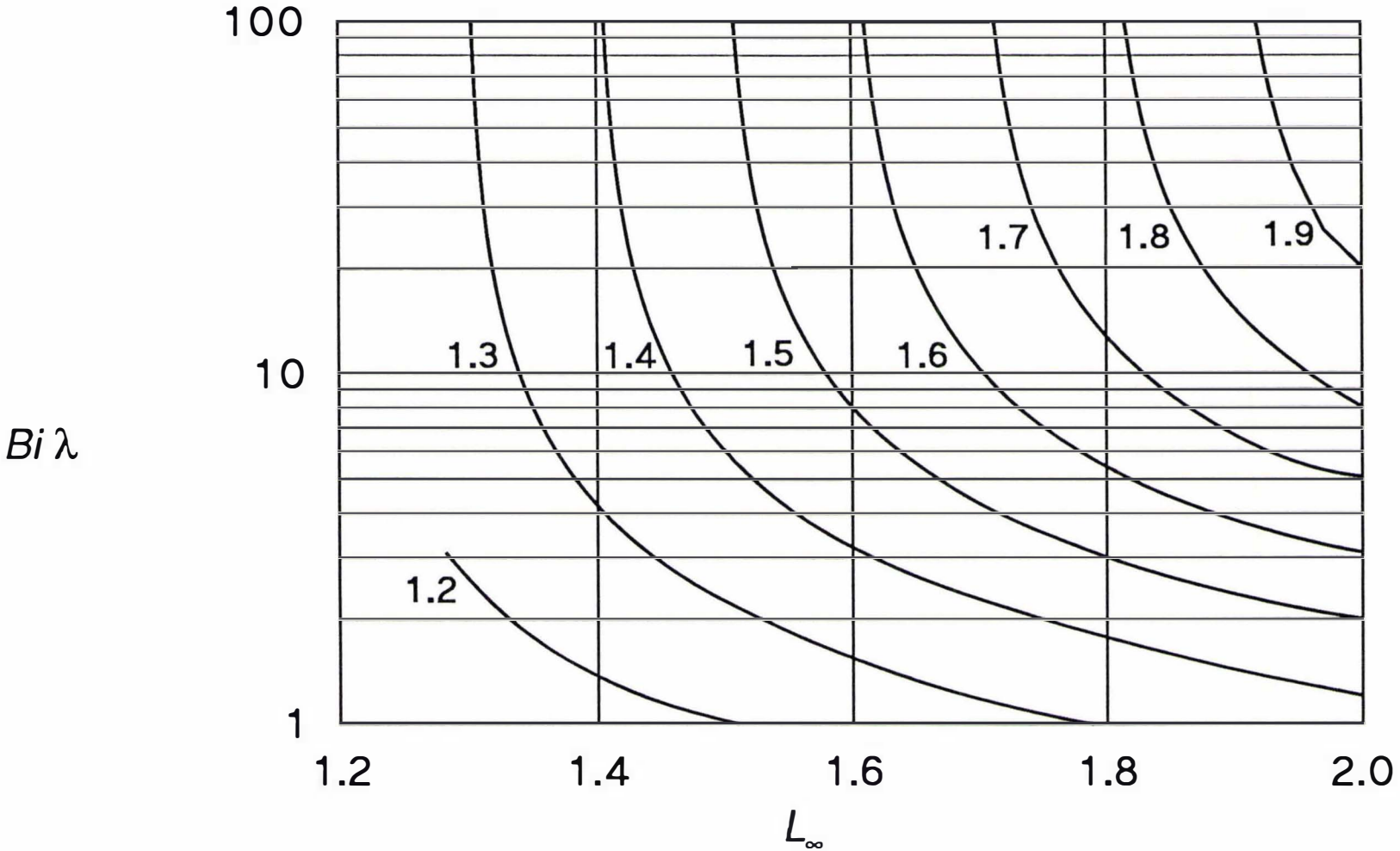

FIGURE 8 Values of L_c, the lag factor for the thermal centre, for bricks as a function of ($Bi\ \lambda$) and L_∞

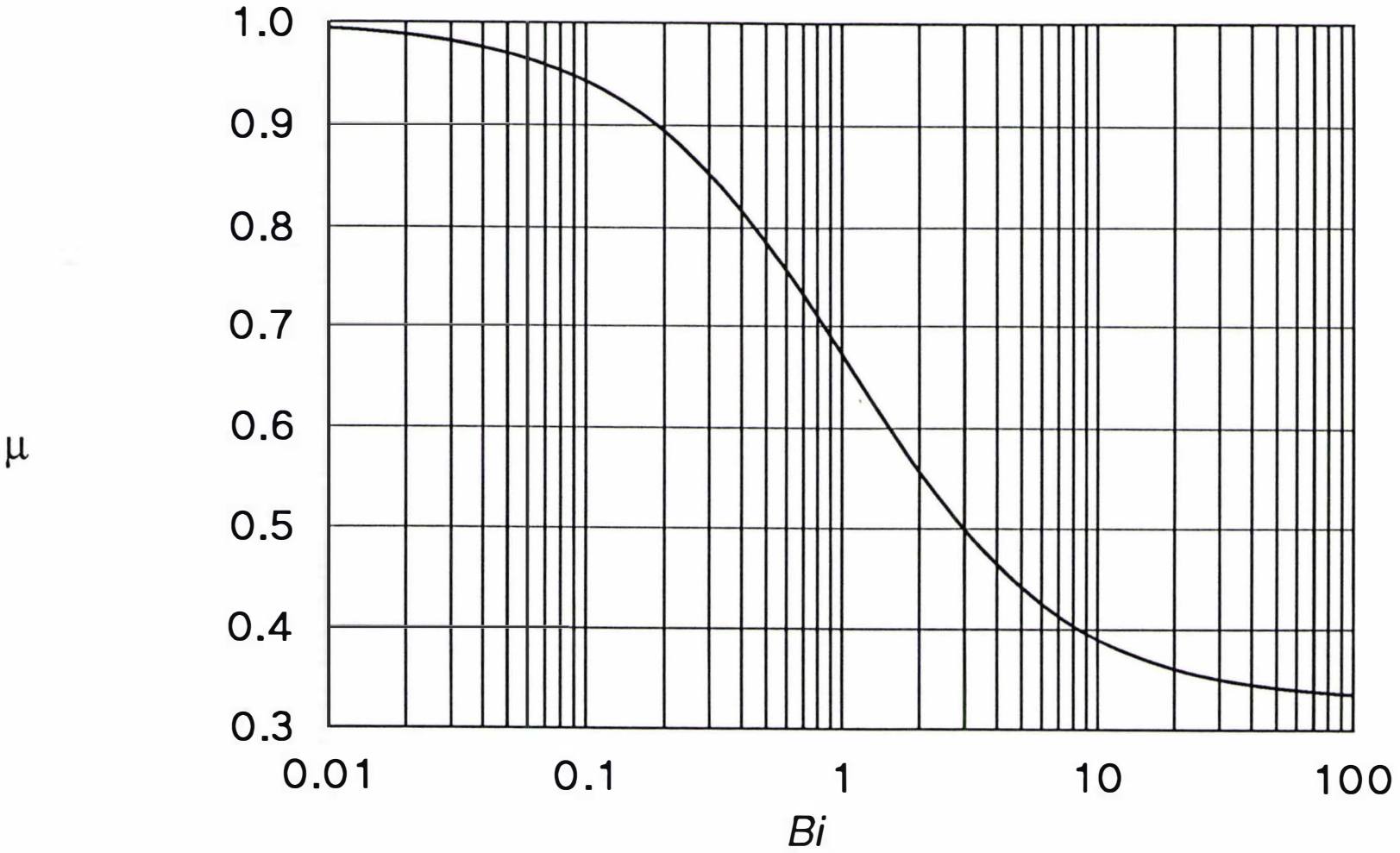

FIGURE 9 Values of μ, the ratio of lag factors for mass-average and thermal centre temperatures, for all shapes as a function of *Bi*

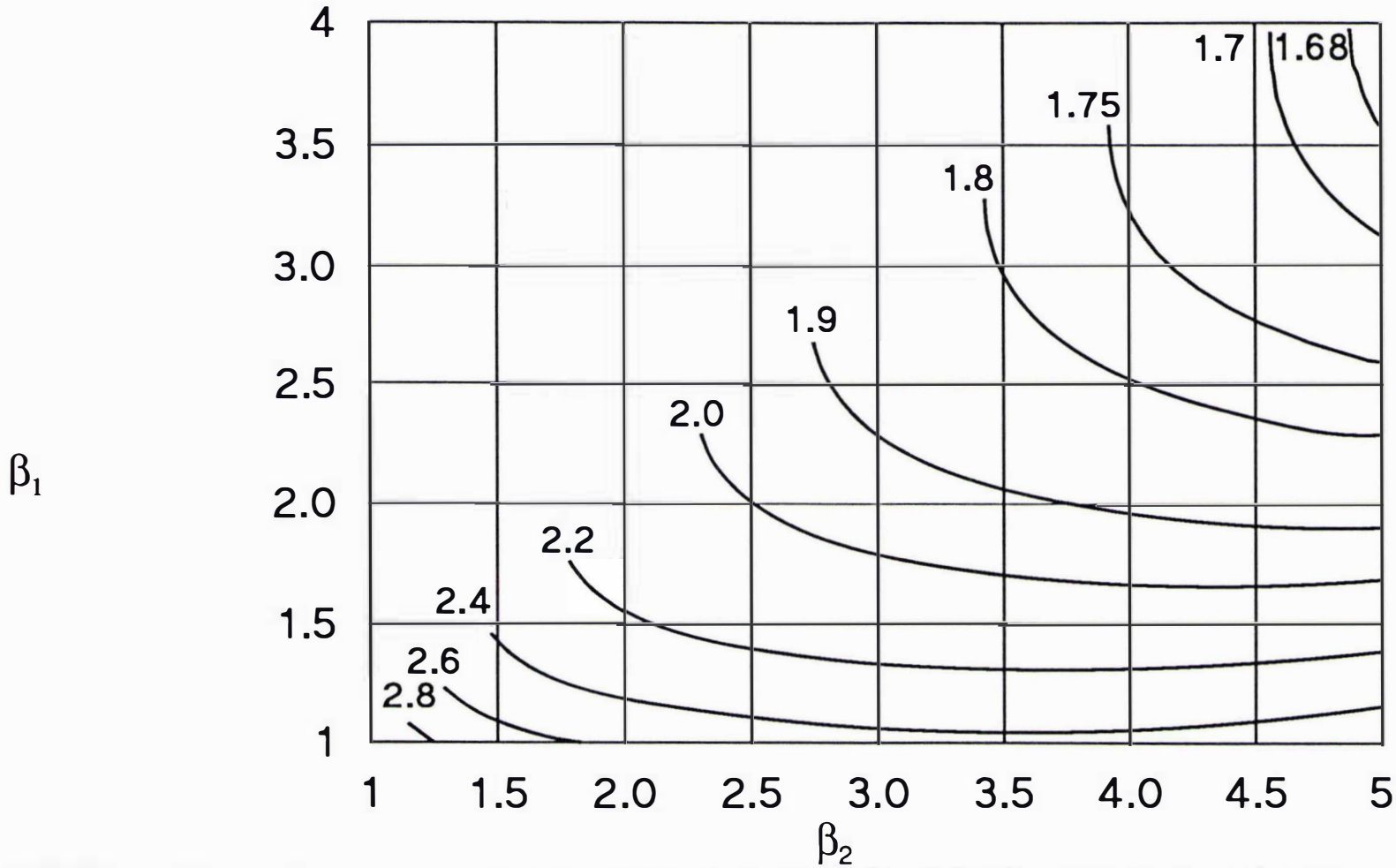

FIGURE 10 Values of E_0, the equivalent heat transfer dimensionality at $Bi = 0$, for ellipsoid and 3-dimemsional irregular shapes as a function of β_1 and β_2

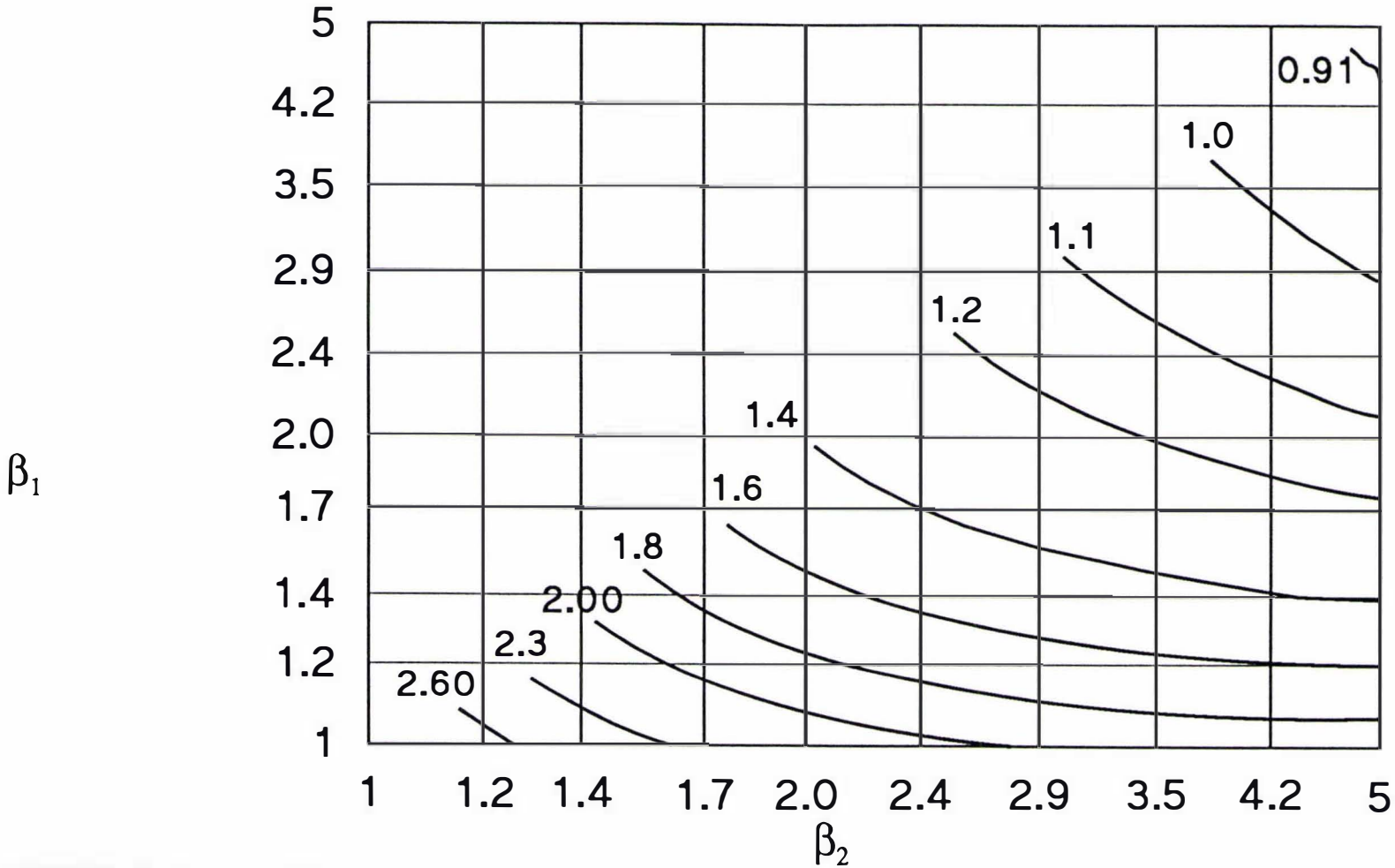

FIGURE 11 Values of E_∞, the equivalent heat transfer dimensionality at $Bi = \infty$, for ellipsoid and 3-dimensional irregular shapes as a function of β_1 and β_2

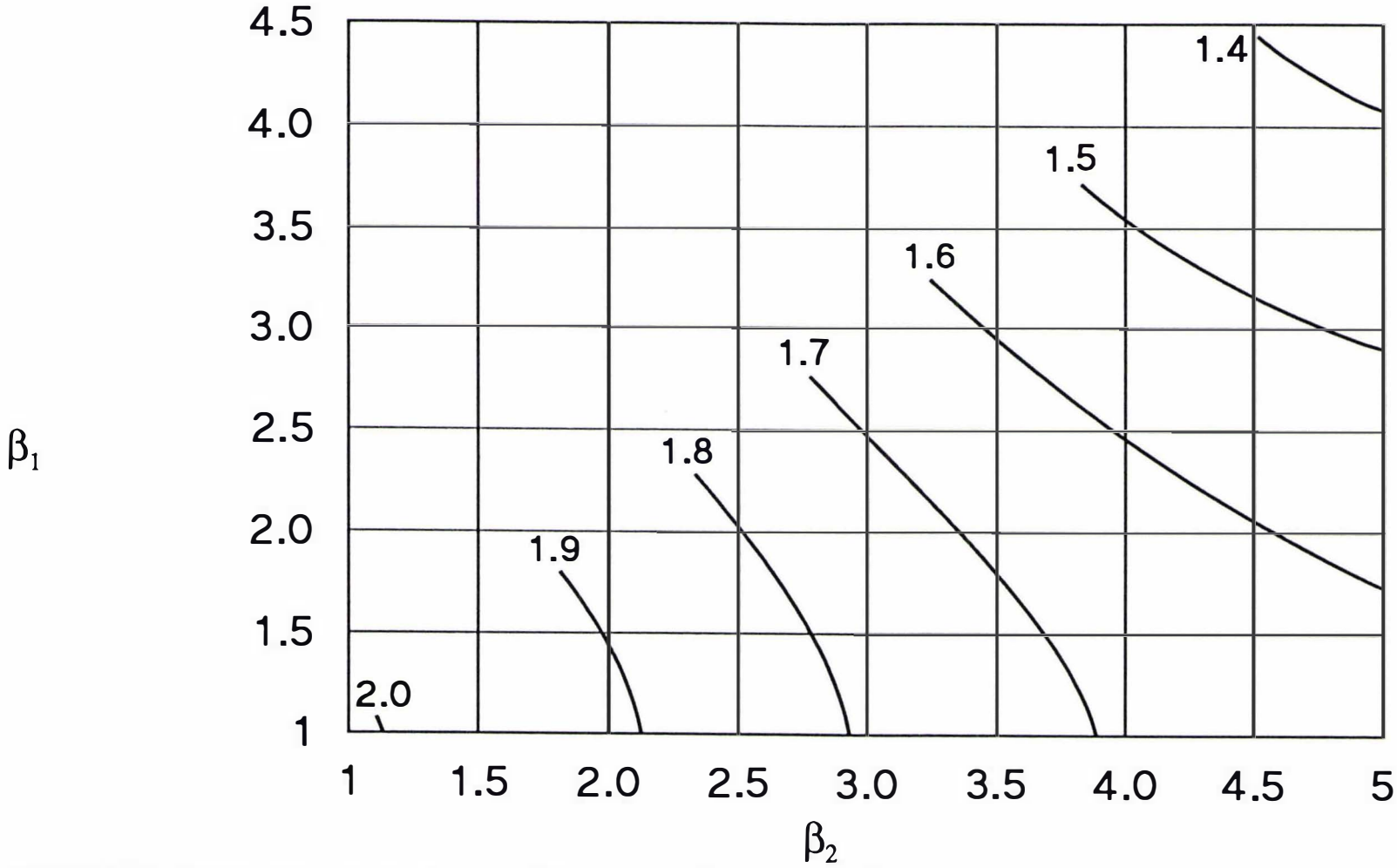

FIGURE 12 Values of L_∞, the lag factor at $Bi = \infty$, for ellipsoid and 3-dimensional irregular shapes as a function of β_1 and β_2

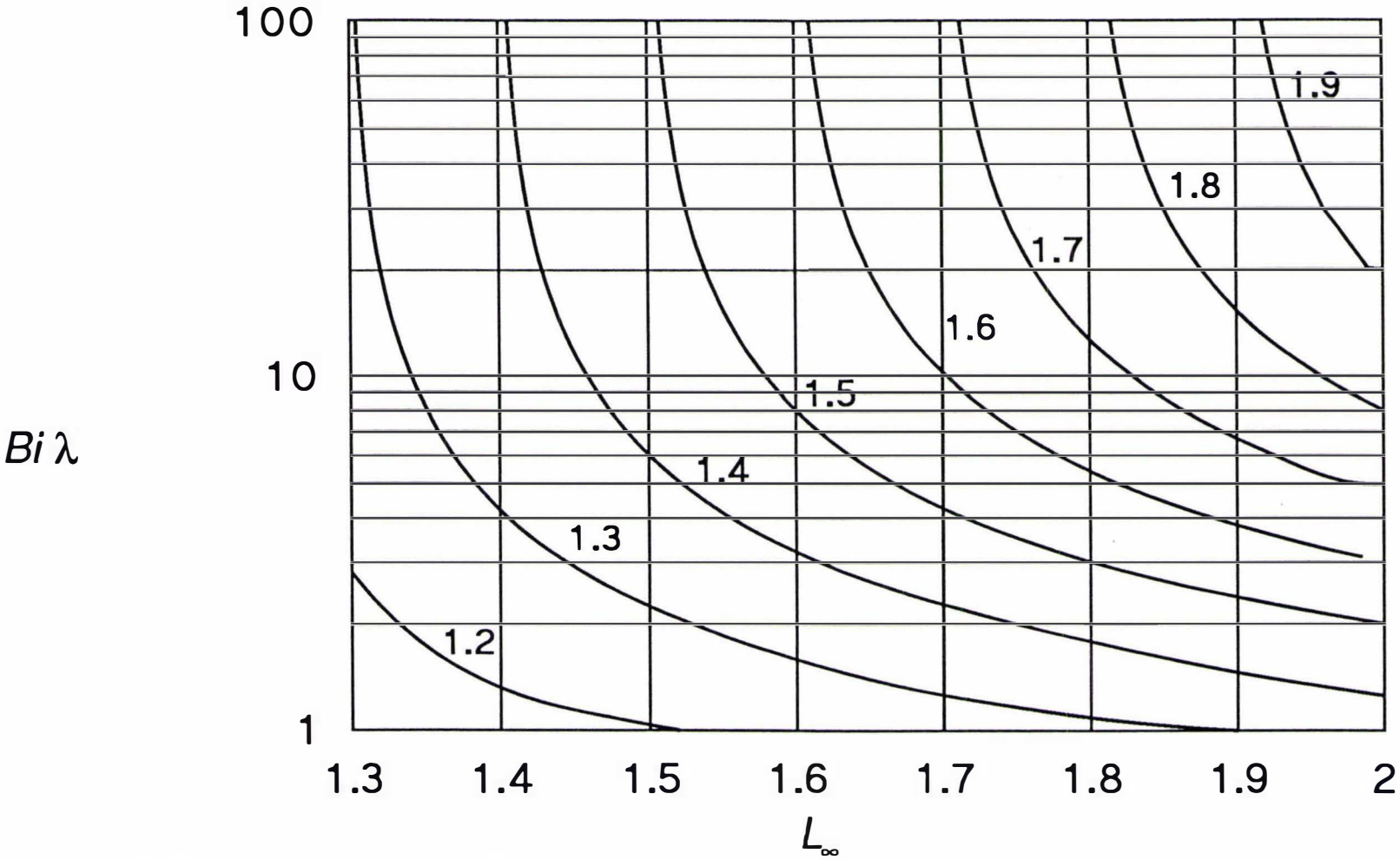

FIGURE 13 Values of L_c, lag factor for the thermal centre, for ellipsoid and 3-dimensional irregular shapes as a function of ($Bi\ \lambda$) and L_∞

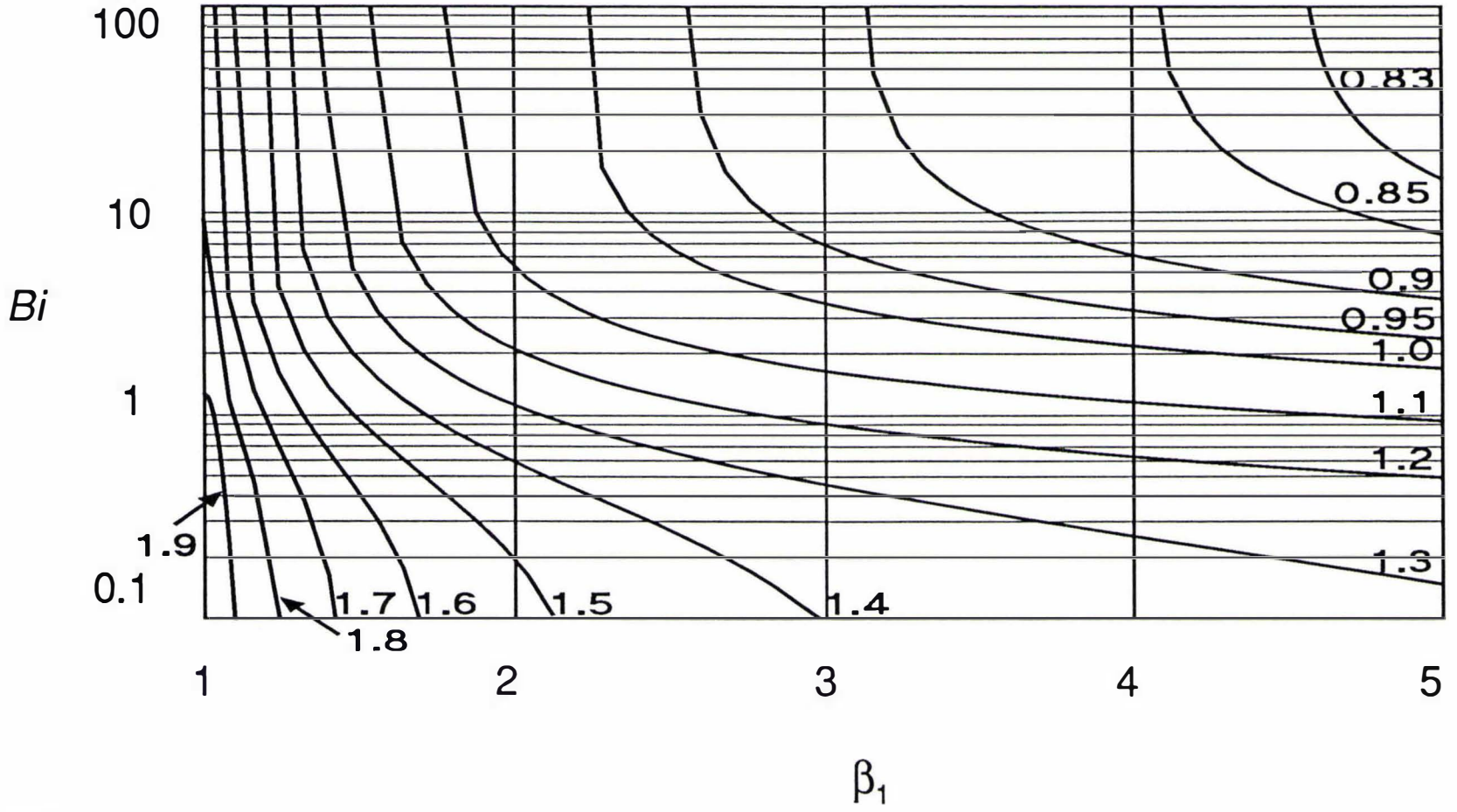

FIGURE 14 Values of E, the equivalent heat transfer dimensionality for infinite ellipses and 2-dimensional irregular shapes as a function of Bi and β_1

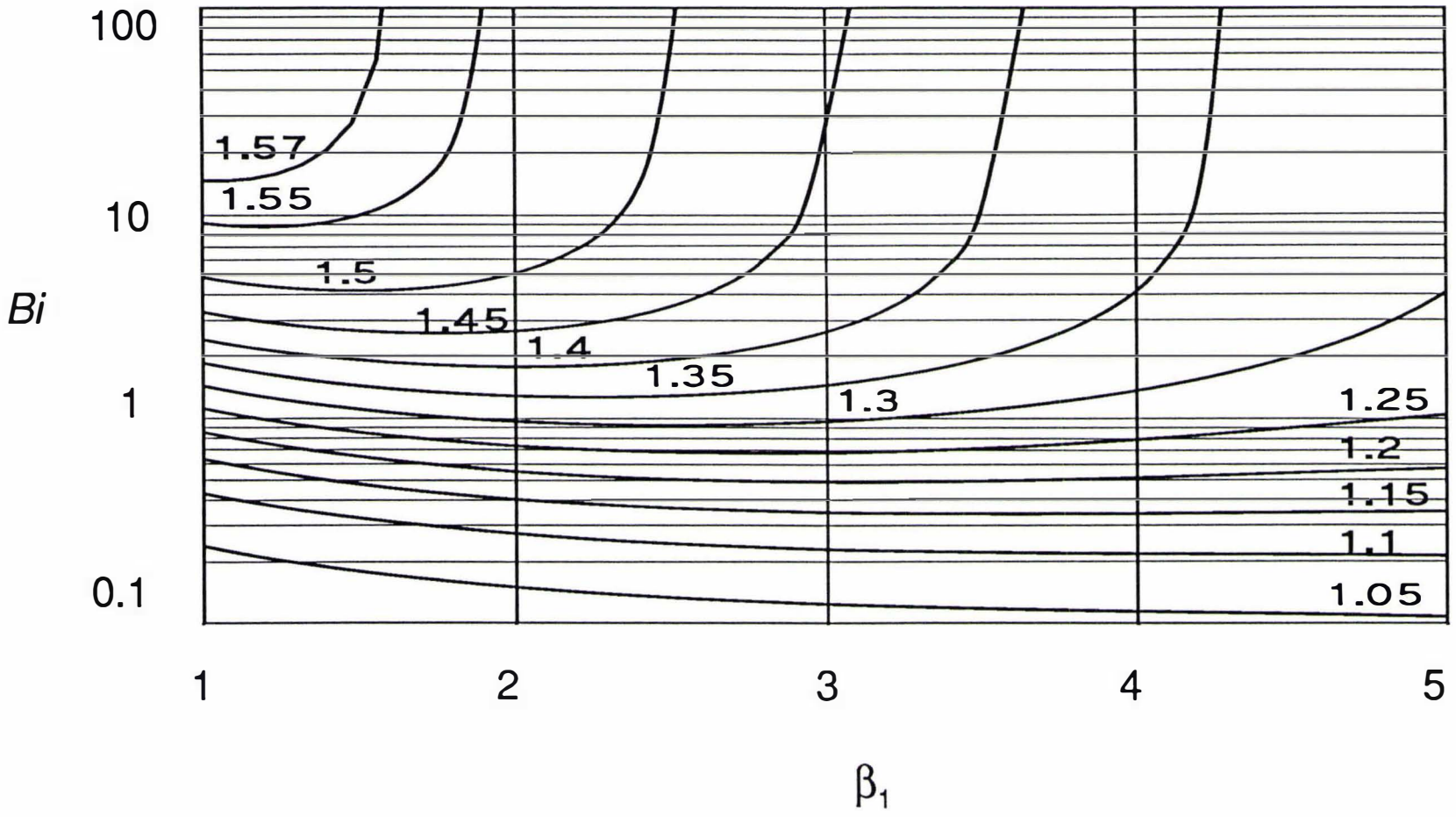

FIGURE 15 Values of L_c, the lag factor for thermal centre temperatures for infinite ellipses and 2-dimensional shapes as a function of *Bi* and β_1

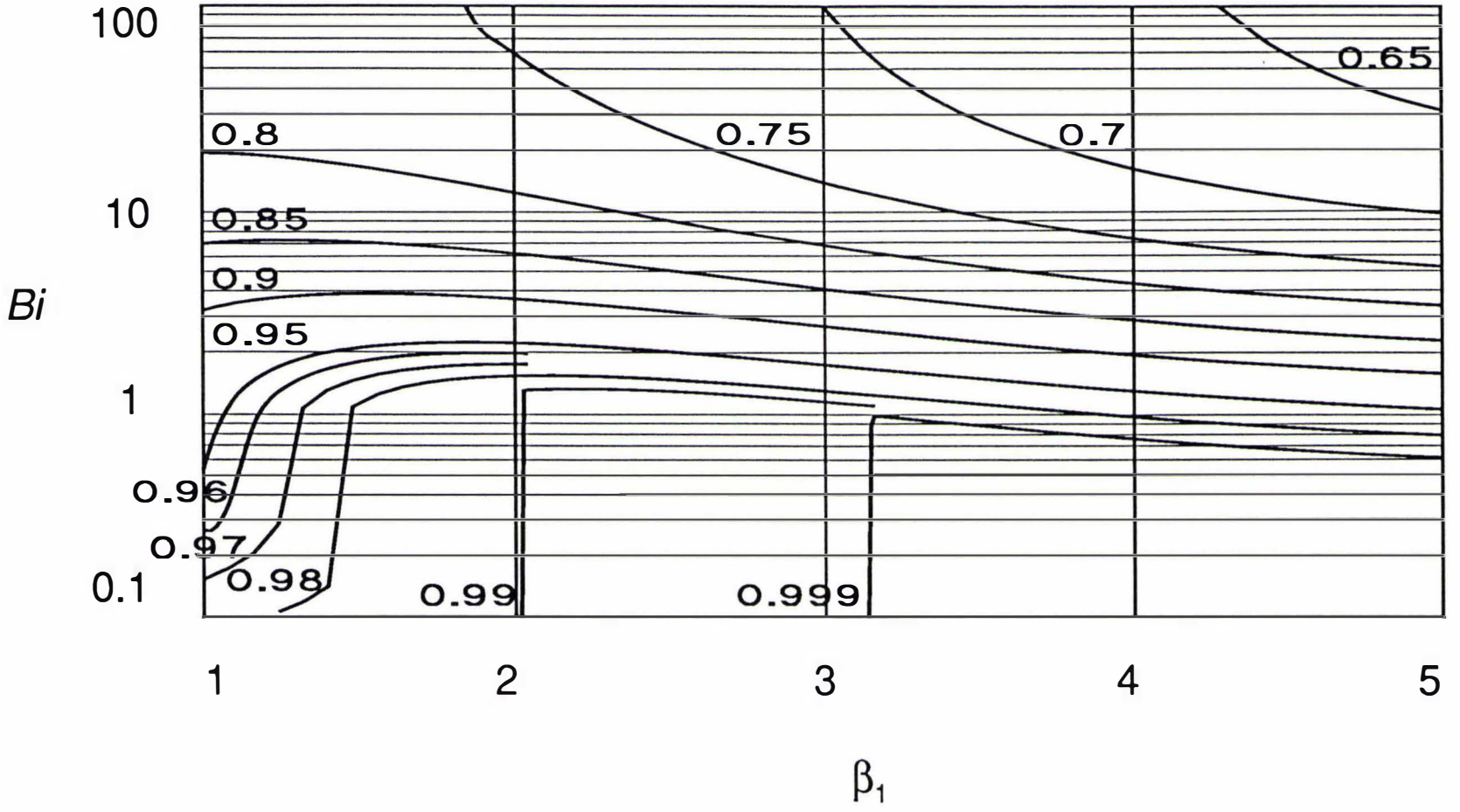

FIGURE 16 Values of L_m, the lag factor for mass-average temp. for infinite ellipses and 2-dimensional irregular shapes as a function of *Bi* and β_1

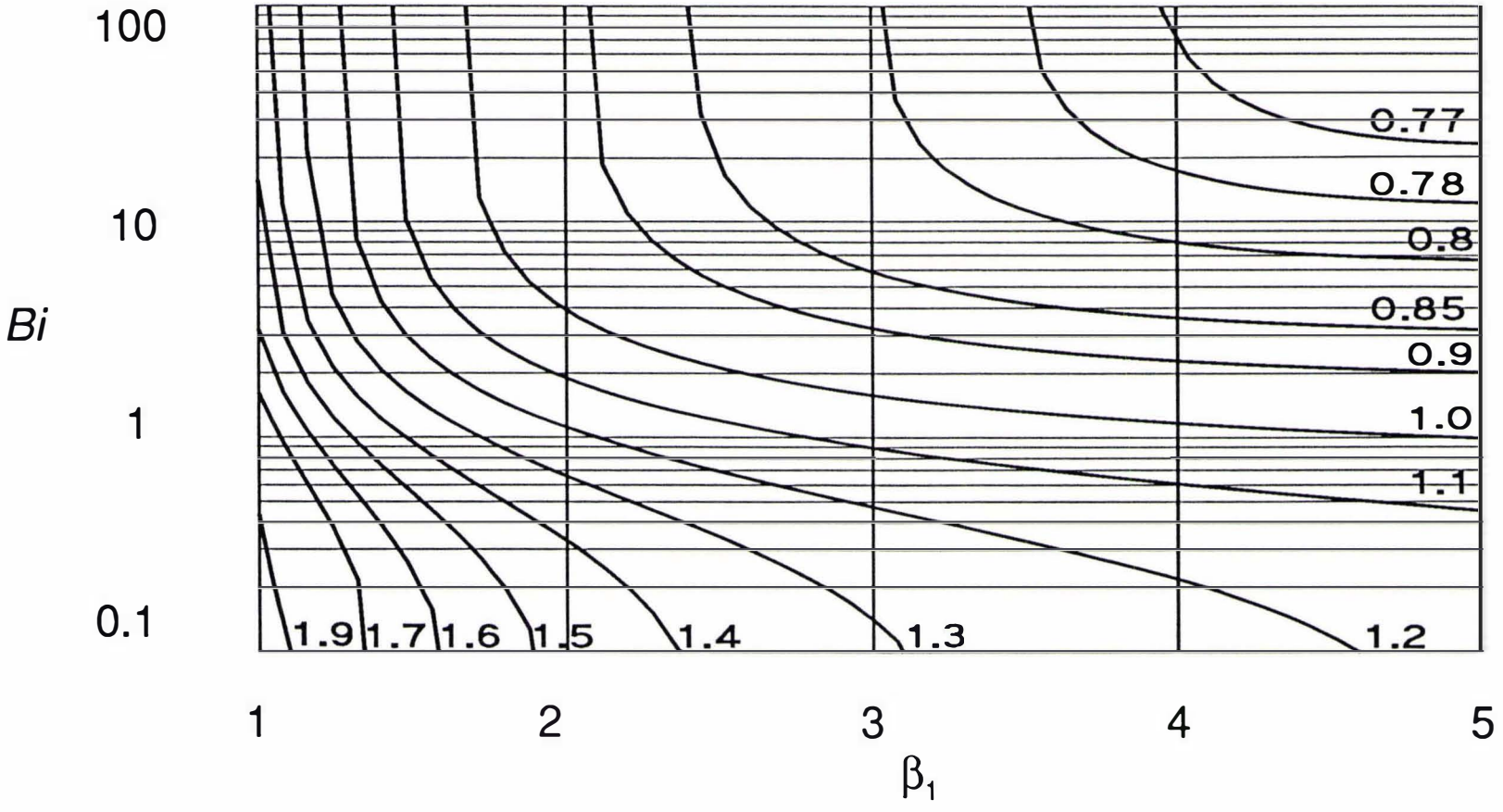

FIGURE 17 Values of E, the equivalent heat transfer dimensionality for infinite rectangular rods as a function of Bi and β_1

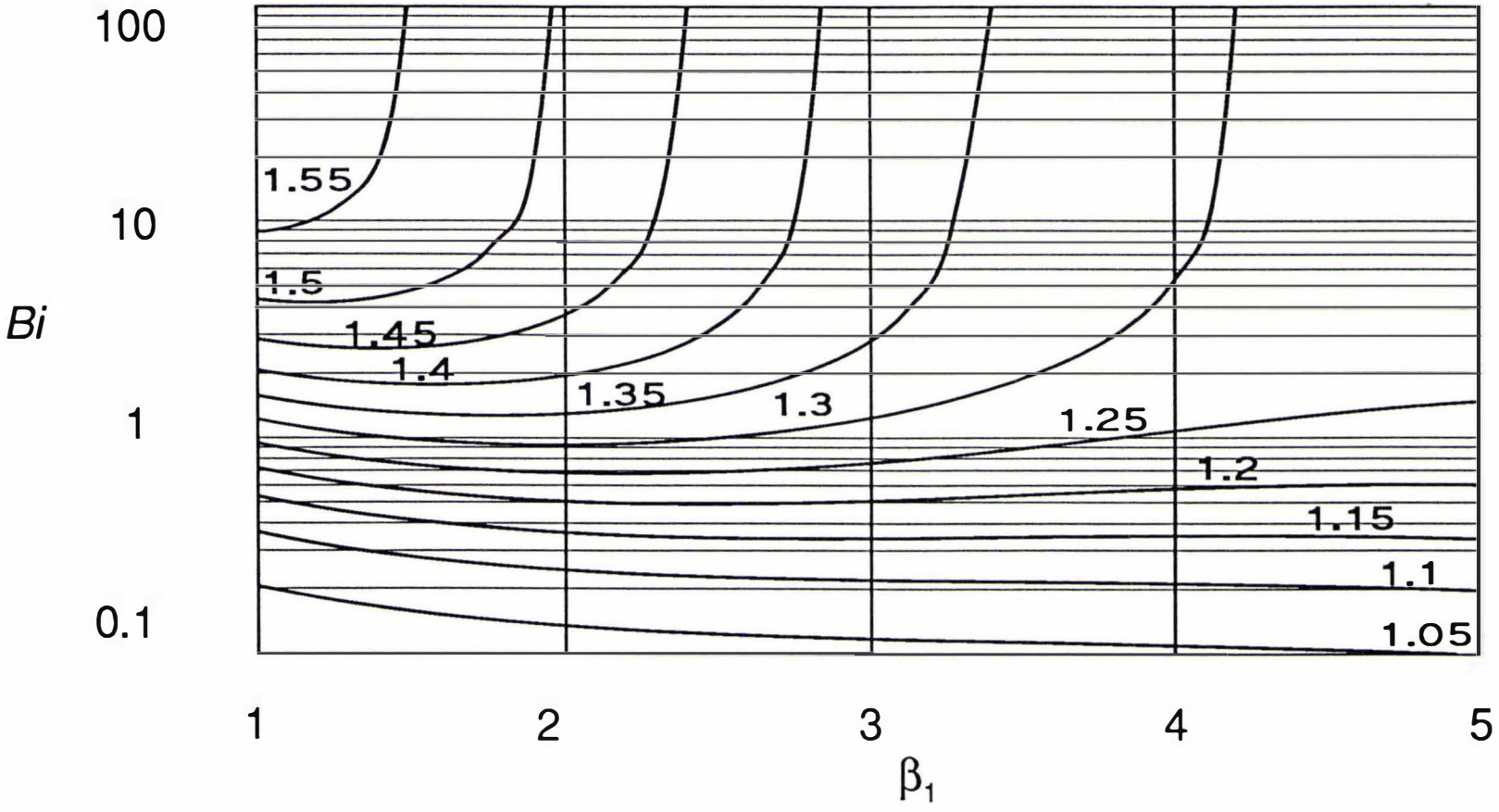

FIGURE 18 Values of L_c, the lag factor for thermal centre temperature for infinite rectangular rods as a function of *Bi* and β_1

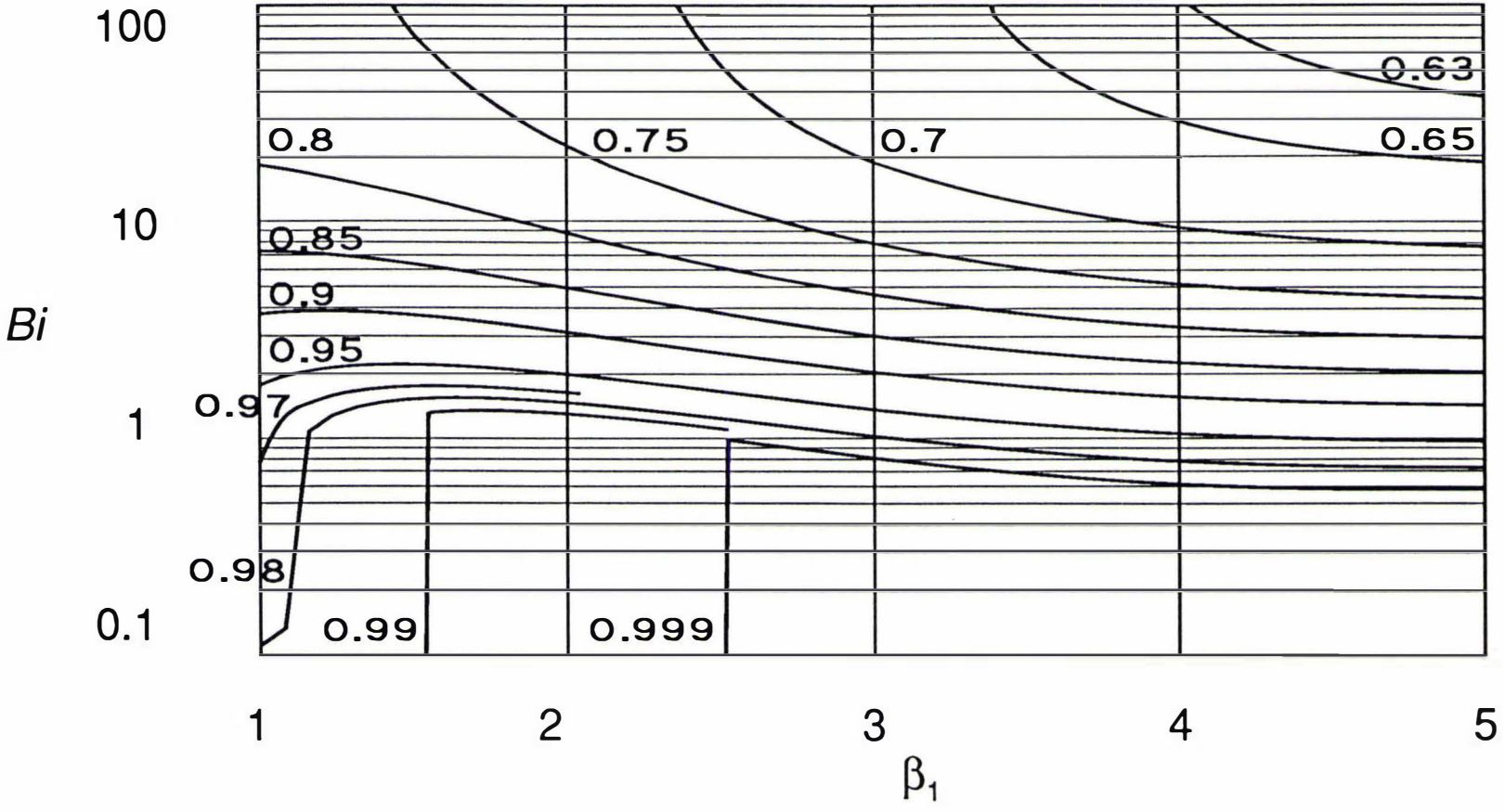

FIGURE 19 Values of L_m, the lag factor for mass-average temperature for infinite rectangular rods as a function of Bi and β_1

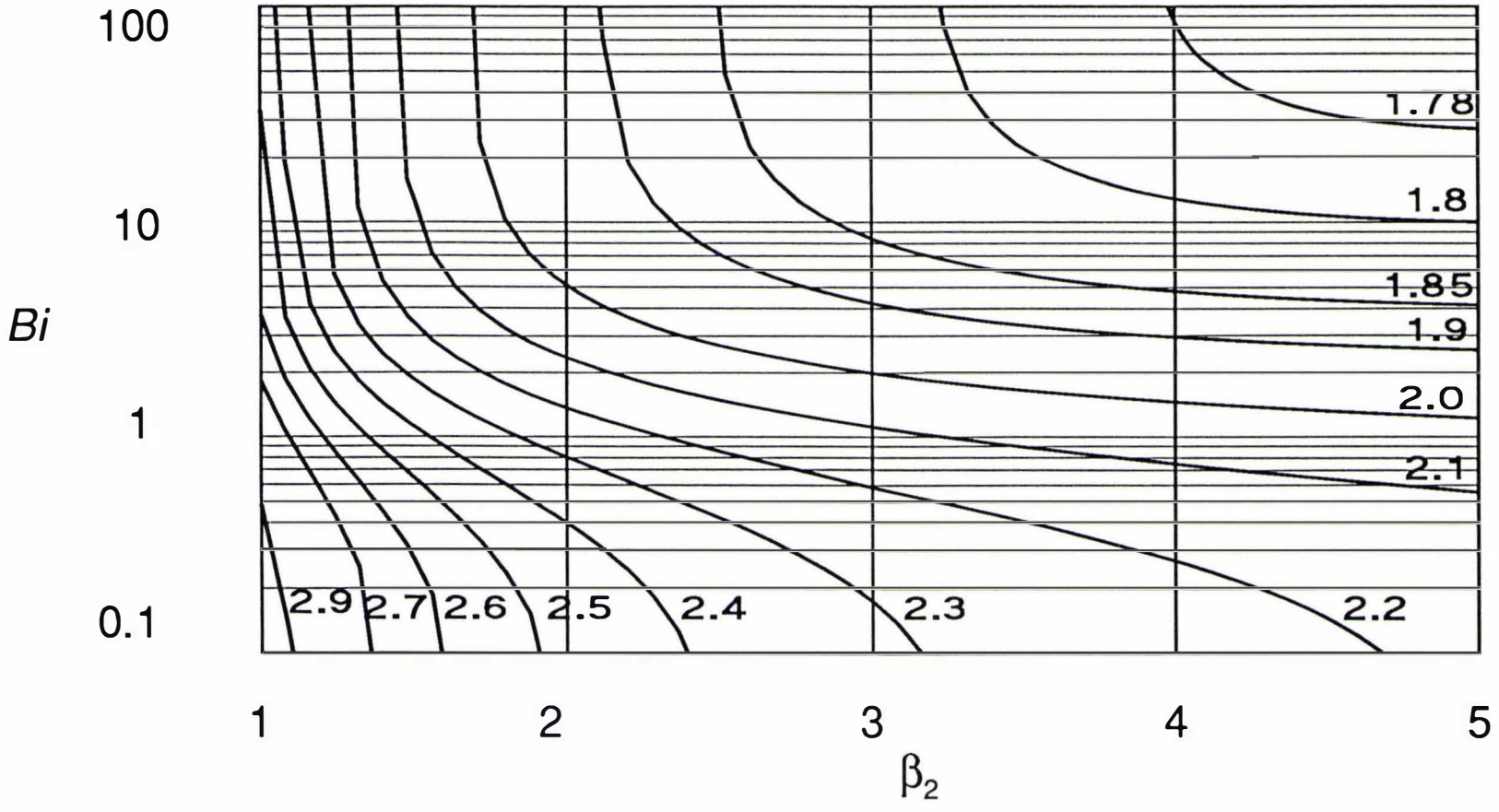

FIGURE 20 Values of E, the equivalent heat transfer dimensionality for short cylinders (height > diameter) as a function of Bi and β_2

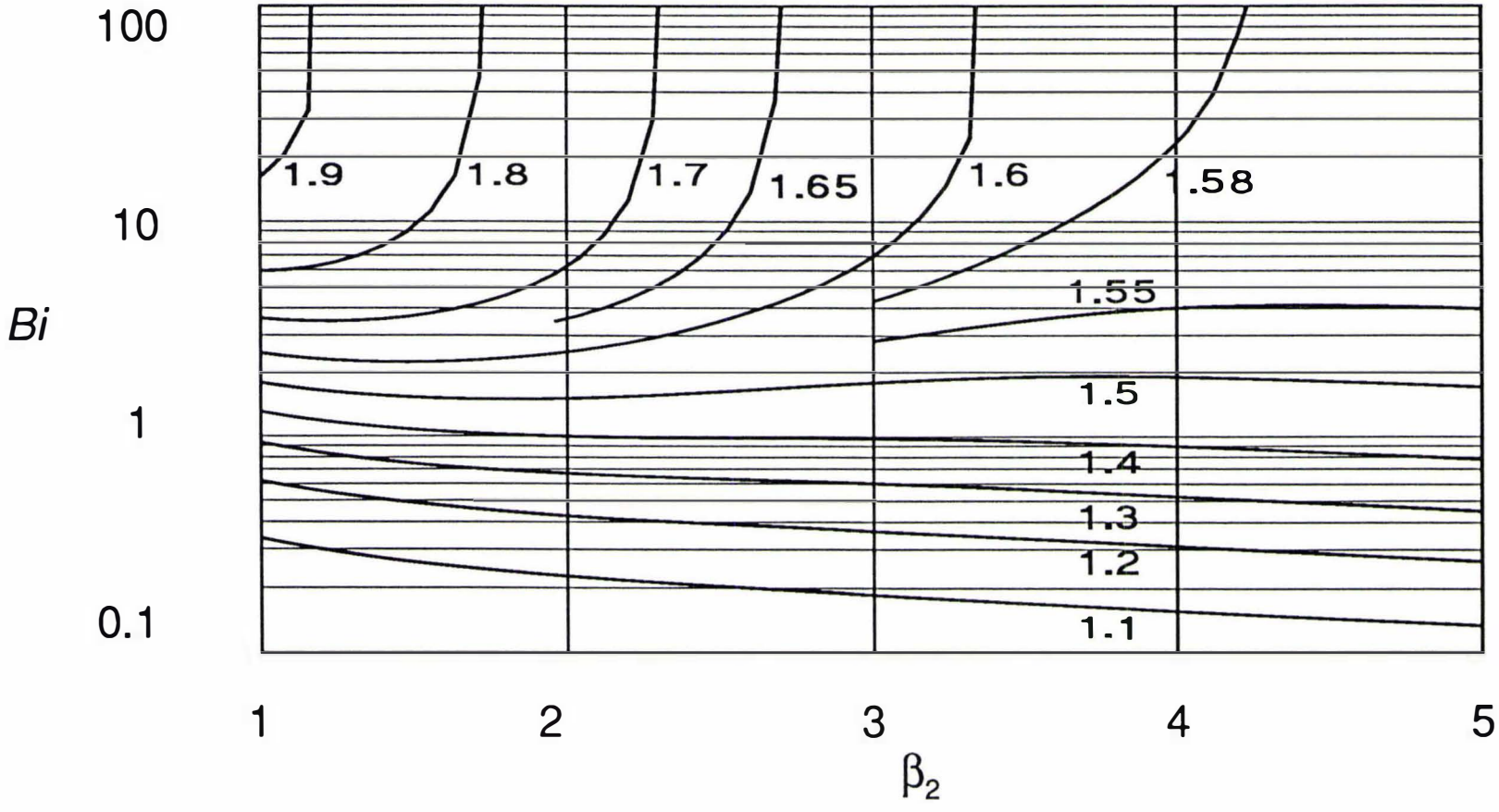

FIGURE 21 Values of L_c, the lag factor for thermal centre temperature for short cylinders (height > diameter) as a function of *Bi* and β_2

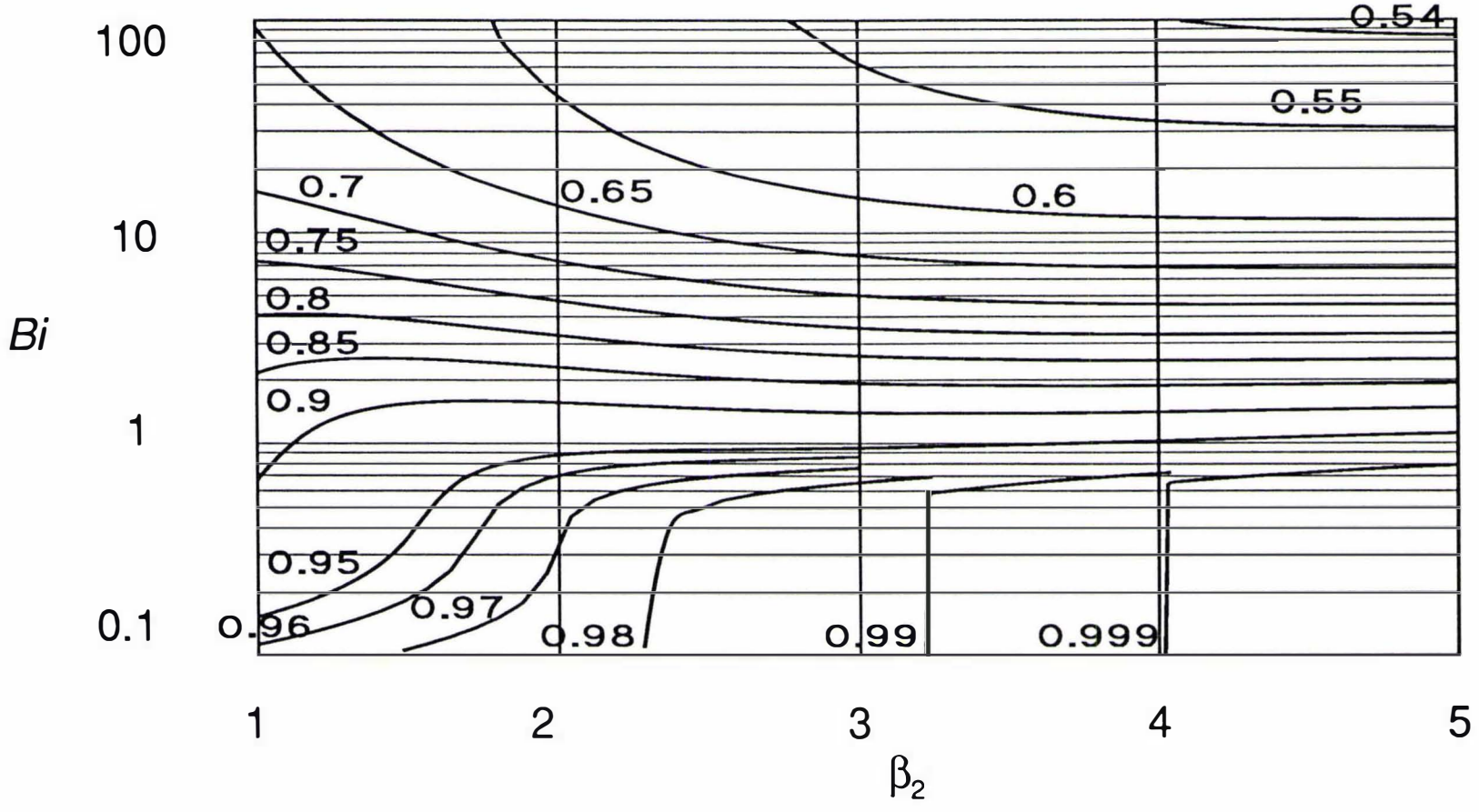

FIGURE 22 Values of L_m, the lag factor for mass-average temperature for short cylinders (height > diameter) as a function of *Bi* and β_2

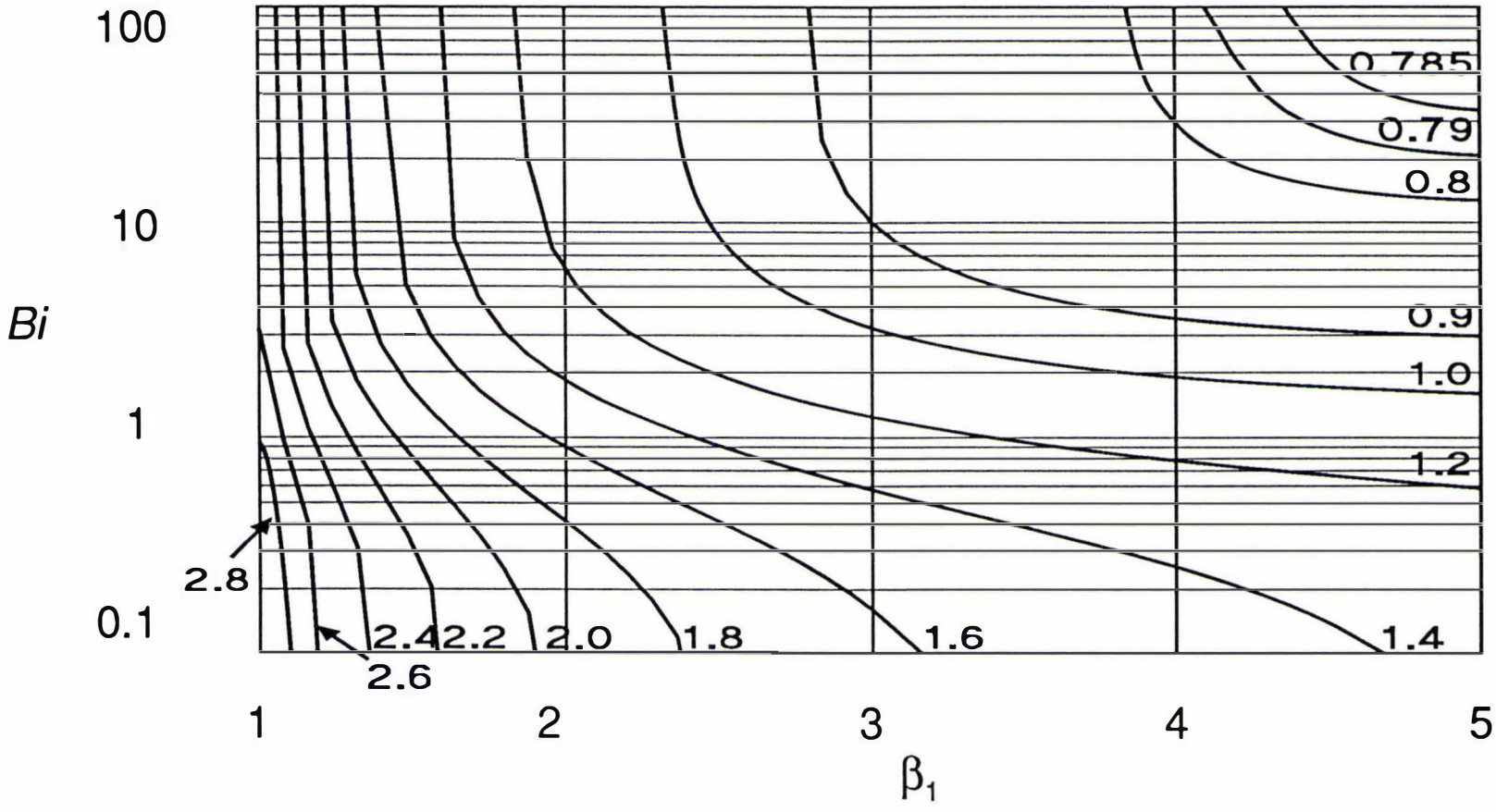

FIGURE 23 Values of E, the equivalent heat transfer dimensionality for squat cylinders (height ≤ diameter) as a function of Bi and β_1

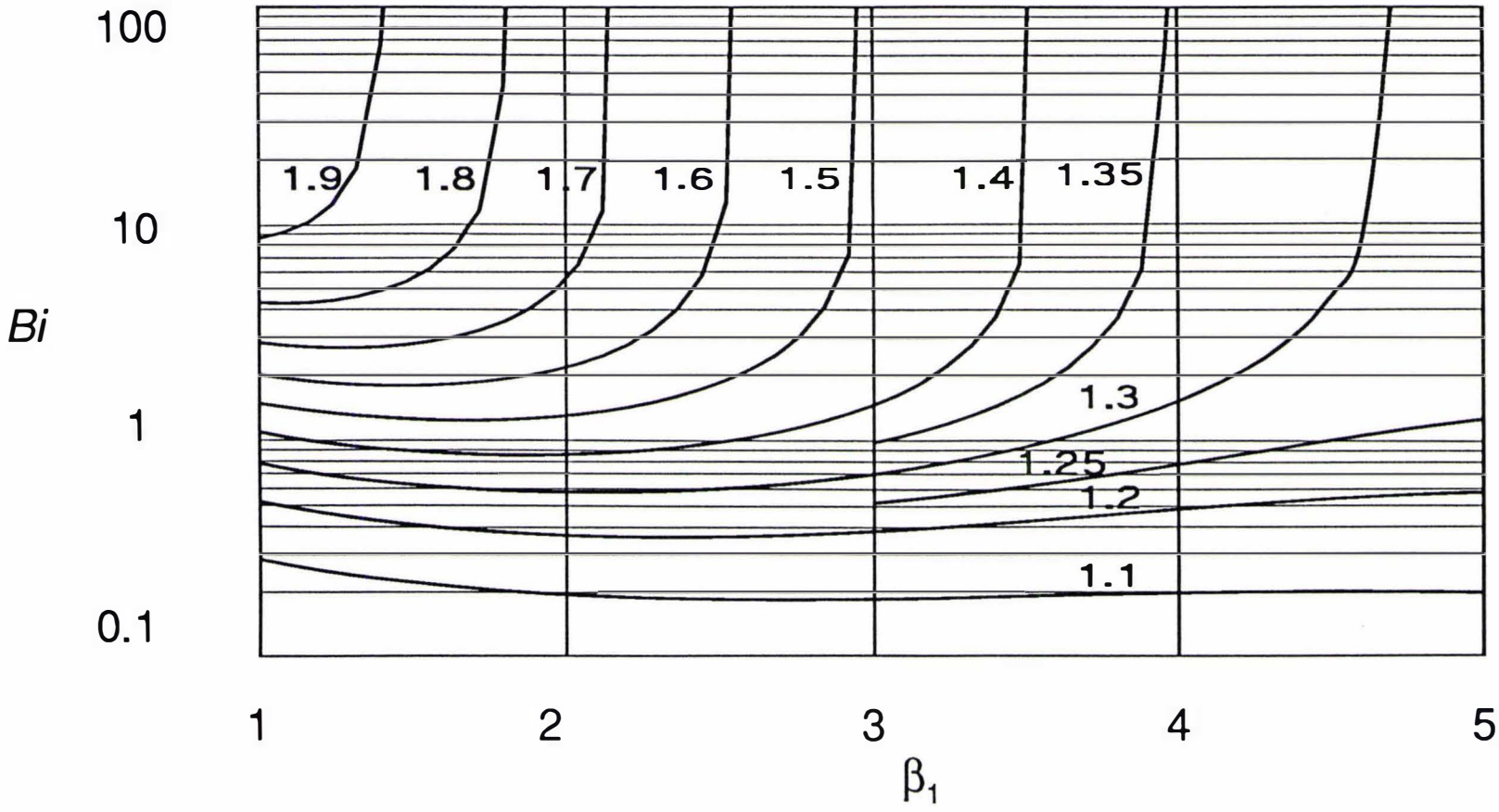

FIGURE 24 Values of L_c, the lag factor for thermal centre temperatures for squat cylinders (height ≤ diameter) as a function of *Bi* and β_1

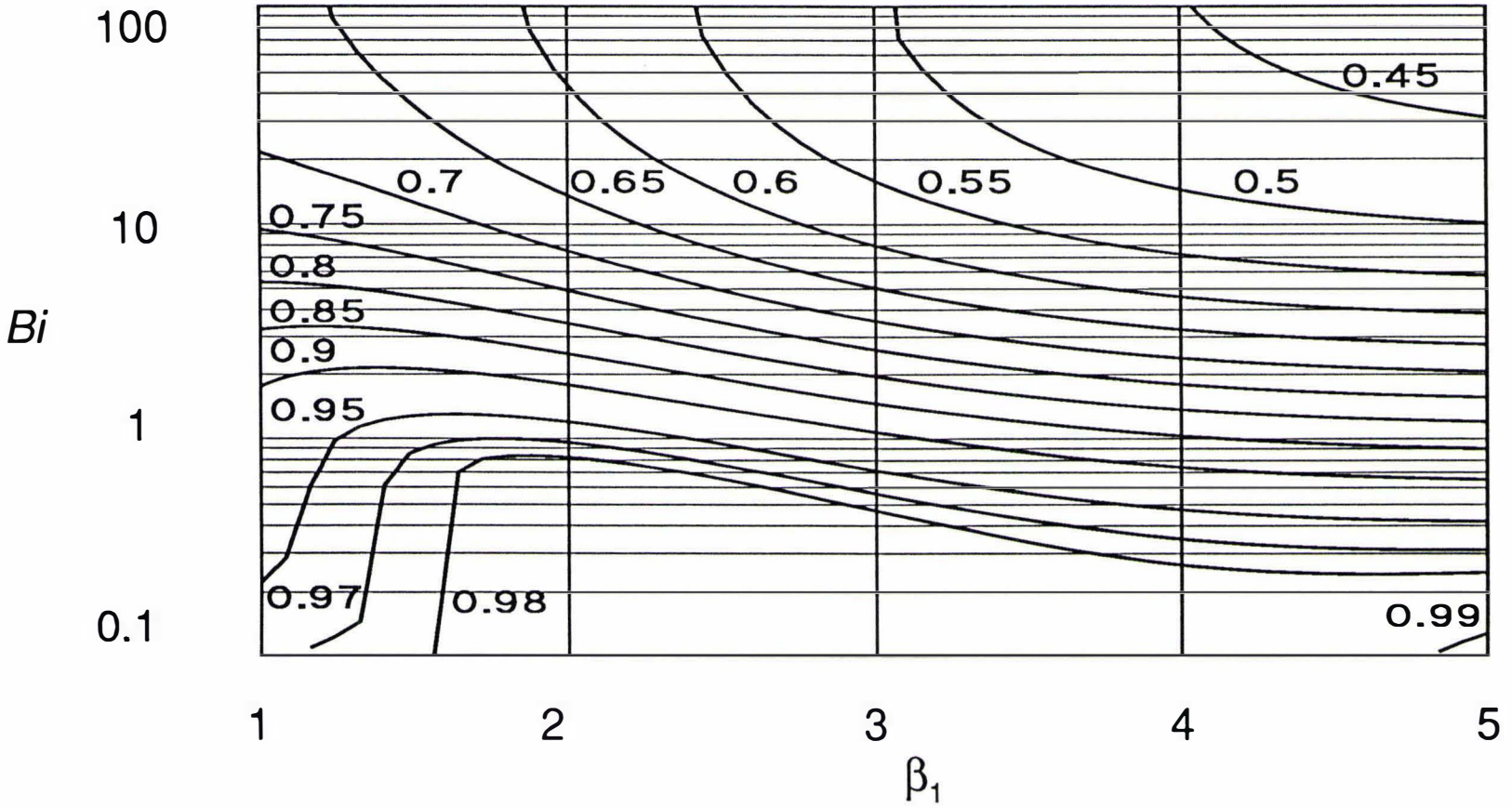

FIGURE 25 Values of L_m, the lag factor for mass-average temperatures for squat cylinders (height ≤ diameter) as a function of *Bi* and β_1